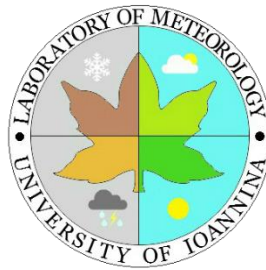# UNIVERSITY OF IOANNINA

DEPARTMENT OF PHYSICS
SECTION OF ASTRO-GEOPHYSICS
LABORATORY OF METEOROLOGY AND CLIMATOLOGY

POSTGRADUATE PROGRAM
«ATMOSHERIC SCIENCES AND ENVIRONMENT»

MASTER's THESIS

Climatology of polar stratospheric clouds and investigation of a possible relationship between their characteristics and solar activity

KOUTSOUGIANNIS KONSTANTINOS (physicist, postgraduate student)
Supervisor: HATZIANASTASSIOU NIKOS (professor)

IOANNINA 2024

1

THREE – MEMBER EXAMINATION COMMITTEE

1) Hatzianastassiou Nikos, Professor, Department of Physics, University of Ioannina, (Supervisor)
2) Patsourakos Spiros, Associate Professor, Department of Physics, University of Ioannina
3) Lolis Christos, Associate Professor, Department of Physics, University of Ioannina

Acknowledgements

Abstract

This thesis tries to combine atmospheric phenomena, such as the polar stratospheric clouds (PSCs) with solar radiation. Its first step was to create a climatology of PSCs and then investigate if there is any relationship between them and solar activity – specifically the 11-year sunspot cycle. Because the results were lacking in explanations, another parameter was added to the analysis, Stratospheric Temperatures, from which the relationship between solar activity and PSCs was examined. This step stood as a cornerstone in the study, through which valuable information and insights were unfolded.

The analysis of PSCs was based on the Cloud-Aerosol Lidar with Orthogonal Polarization (CALIOP) lidar Level-2 PSC Mask-Version-2.00 data products covering the 16-year period from 2006 to 2021. The primary Level-2 PSC data were converted to level-3 type data for 1°x1° latitude-longitude grid areas on a monthly mean basis, for 121 vertical layers extending from 8.4 to 30 km, with a resolution of 5 km horizontally and 180 m vertically. From the obtained statistics, the areal coverage and fractional cloud cover of PSCs were estimated. Ancillary parameters, such as stratospheric temperatures, were included in our dataset from the Modern-Era Retrospective analysis for Research and Applications, Version 2 (MERRA-2) while the data for solar activity were obtained from the World Data Center – Sunspot Index and Long-Term Solar Observations (WDC-SILSO), Royal Observatory of Belgium.

The monthly mean PSC areal coverage of the Northern Hemisphere (NH) ranges from about 2,000 to 510,000 km², whereas in the Southern Hemisphere (SH) it ranges from 500 to 1,200,000 km². PSCs most frequently form between 12 and 26 km above the Earth's surface, with their maximum frequency at 18-23 km. The global and annual mean areal coverage of PSCs varies from about 1,000 to 400,000 km², with minimum and maximum values in each hemisphere's local summer and winter, respectively. According to our analysis, the areal extent of PSCs—at the altitude of their maximum frequency of occurrence—has been found to have increased in the NH, while decreasing in the SH, though not statistically significantly. These trends of PSCs align with the recent reported literature on increasing and decreasing ozone trends in the SH and NH, respectively. Stratospheric hemispherical temperatures have been found to range between 198K and 232K for the Arctic, while 185K and 245K for the Antarctic, and they have been quite well correlated with the occurrence of PSCs in the altitude range of 12-26 km. Specifically, according to two different correlation approaches employed, the best correlation coefficients (r) between PSCs and temperatures vary from r = -0.47 to -0.44 for the NH and r = -0.78 to -0.7 for the SH. The vertical profiles of the correlation coefficient between solar activity with stratospheric temperatures, and PSCs have been developed, showing no strong evidence of a direct influence among these parameters in the low and middle stratosphere up to 30 km. The best r values for stratospheric temperatures and the number of sunspots were found to be 0.1 at 30 km over the NH (monthly mean values) and 0.155 at 30 km over the SH (yearly mean values). The best r values for PSCs and the number of sunspots were found to be -0.1 at 14 km over the NH and -0.18 at both 13.5 km and 26 km over the SH (yearly mean values).

Περίληψη

Η συγκεκριμένη μεταπτυχιακή διπλωματική εργασία προσπαθεί να συνδυάσει κάποια ατμοσφαιρικά φαινόμενα, συγκεκριμένα τα πολικά στρατοσφαιρικά νέφη (PSCs), με την ηλιακή ακτινοβολία. Το πρώτο βήμα ήταν να δημιουργηθεί μια κλιματολογία των PSCs και στη συνέχεια να διερευνηθεί εάν υπάρχει κάποια σχέση μεταξύ των χαρακτηριστικών τους και του 11ετούς κύκλου των ηλιακών κηλίδων. Ωστόσο, επειδή τα αρχικά αποτελέσματα χρειαζόντουσαν περισσότερο εμβάθυνση, επιλέχθηκε να ενταχθεί στη μελέτη μια ακόμη παράμετρος, οι στρατοσφαιρικές θερμοκρασίες και η πιθανή σχέση τους με την ηλιακή δραστηριότητα.

Η ανάλυση των πολικών στρατοσφαιρικών νεφών βασίστηκε στα προϊόντα δεδομένων του Lidar νεφών-αερολυμάτων με ορθογώνια πόλωση (CALIOP) lidar Level-2 PSC Mask-Version-2.00 κατά την 16ετή περίοδο από το 2006 έως το 2021. Τα αρχικά δεδομένα μετατράπηκαν σε πλεγματικά δεδομένα για περιοχές 1°x1° γεωγραφικού πλάτους-μήκους σε μηνιαία μέση βάση, για 121 κατακόρυφα στρώματα από τα 8,4 έως 30 km, με ανάλυση 5km οριζόντια και 180m κατακόρυφα. Από αυτά τα δεδομένα, υπολογίστηκε η περιοχική κάλυψη (km^2) και η νεφοκάλυψη. Βοηθητικές παράμετροι, όπως οι στρατοσφαιρικές θερμοκρασίες, συμπεριλήφθηκαν στο σύνολο δεδομένων μας από τη δεύτερη έκδοση του μοντέλου σύγχρονων αναλύσεων κλιματικών δεδομένων (MERRA-2 reanalysis), ενώ τα δεδομένα για την ηλιακή δραστηριότητα ελήφθησαν από το παγκόσμιο κέντρο ηλιακών δεδομένων (WDC-SILSO), του βασιλικού αστεροσκοπείου του Βελγίου.

Η μηνιαία μέση επιφανειακή κάλυψη των PSCs του βόρειου ημισφαιρίου κυμαίνεται από περίπου 2.000 έως 510.000 km², ενώ στο νότιο ημισφαίριο κυμαίνεται από 500 έως 1.200.000 km². Τα συγκεκριμένα νέφη σχηματίζονται συχνότερα μεταξύ 12 και 26 km πάνω από την επιφάνεια της Γης, με τη μέγιστη συχνότητα στα 18-23 km. Η πλανητική και ετήσια μέση επιφανειακή κάλυψη των νεφών ποικίλλει από περίπου 1.000 έως 400.000 km², με ελάχιστες και μέγιστες τιμές κατά τη διάρκεια του τοπικού θέρους και χειμώνα του κάθε ημισφαιρίου, αντίστοιχα. Σύμφωνα με την ανάλυσή μας, η έκταση των νεφών - στο υψόμετρο της μέγιστης συχνότητας εμφάνισής τους - έχει βρεθεί ότι έχει αυξηθεί στο βόρειο ημισφαίριο, ενώ μειώθηκε στο νότιο ημισφαίριο, αν και όχι στατιστικά σημαντικά. Αυτές οι τάσεις των νεφών βρίσκονται σε συμφωνία με την πρόσφατη αναφερόμενη βιβλιογραφία σχετικά με την αύξηση και τη μείωση των τάσεων του όζοντος στο νότιο ημισφαίριο και στο βόρειο ημισφαίριο, αντίστοιχα. Οι στρατοσφαιρικές θερμοκρασίες βρέθηκε ότι κυμαίνονται μεταξύ 198K και 232K πάνω από την Αρκτική, έναντι 185K και 245K για την Ανταρκτική, και συσχετίζονται αρκετά καλά με την εμφάνιση PSCs στα ύψη 12-26 km. Συγκεκριμένα, σύμφωνα με δύο διαφορετικές εφαρμοσθείσες προσεγγίσεις συσχέτισης, οι καλύτεροι συντελεστές συσχέτισης (r) μεταξύ των PSCs και των στρατοσφαιρικών θερμοκρασιών κυμαίνονται από r = -0,47 έως -0,44 για το βόρειο ημισφαίριο και r = -0,78 έως -0,7 για το νότιο ημισφαίριο από τη μια προσέγγιση στην άλλη. Αντιθέτως, δε βρέθηκαν τόσο καλές συσχετίσεις για τις άλλες παραμέτρους. Έτσι, οι καλύτερες τιμές r για τις στρατοσφαιρικές θερμοκρασίες και τον αριθμό των ηλιακών κηλίδων

βρέθηκαν να είναι 0,1 στα 30 km για την Αρκτική (μέσες μηνιαίες τιμές) και 0,155 στα 30 km για την Ανταρκτική (μέσες ετήσιες τιμές). Οι καλύτερες τιμές r μεταξύ των νεφών και του αριθμού των ηλιακών κηλίδων βρέθηκαν να είναι -0,1 στα 14 km πάνω από το NH και -0,18 σε αμφότερα τα 13,5 km και 26 km πάνω από το SH (μέσες ετήσιες τιμές).

List Of Acronyms

ACE: Atmospheric Chemistry Experiment

CALIOP: Cloud-Aerosol Lidar with Orthogonal Polarization

CALIPSO: Cloud-Aerosol Lidar and Infrared Pathfinder Satellite Observation

CFC: Chlorofluorocarbon

CME: Coronal Mass Ejection

MERRA-2: Modern-Era Retrospective analysis for Research and Applications, Version 2

MIPAS: Michelson Interferometer for Passive Atmospheric Sounding

MLS: Microwave Limb Sounder

NAT: Nitric Acid Trihydrate

PSC: Polar Stratospheric Cloud

SAD: Surface Area Density

SILSO: Sunspot Index and Long-term Solar Observations

TSI: Total Solar Irradiance

WDC: World Data Center

Table of Contents

1. Introduction

Earth's atmosphere is a complex system, comprising various layers and phenomena that are critical to the planet's climate and habitability (Seinfeld & Pandis, 2006). Throughout Earth's history, its climate has seen extensive variations across different time scales. Such fluctuations are partly attributed to the Sun's influence, through mechanisms such as the Earth's orbital variations around the Sun and changes in solar irradiance. Notably, since the year 1850, Earth has experienced considerable warming, sparking debates around its causation. The warming observed before 1950 is widely recognized to result from a combination of factors, including increased greenhouse gas concentrations, reduced volcanic activity, the internal variability of the atmosphere-ocean system, and heightened solar irradiance. This period's increasing sunspot number offers support for the solar irradiance's role (Lean and Rind, 1998; Folland and Karl, 2001). This contrasts with the 17th century's Little Ice Age, characterized by the Maunder Minimum, a period of notably low sunspot numbers (Eddy, 1976). Following 1950, a slight global temperature decline was observed until the mid-1970s, succeeded by a sharp increase, particularly pronounced post-1985. This recent warming has been predominantly attributed to human activities (Mitchell et al., 2001), though the Sun's exact role during this period remains to be fully elucidated. The sunspot number, considered a reliable proxy for solar irradiance, has slightly decreased during this time (Lean, et al., 1995).

The intricate dance between the atmospheric and celestial phenomena not only adds layers of complexity to our understanding of Earth's climate system, but also presents opportunities for breakthroughs in atmospheric physics. Among the actors in this complex system, Polar Stratospheric Clouds (PSCs), stratospheric temperatures, and solar activity emerge as pivotal elements. These components are not isolated; rather, they are linked through a variety of mechanisms and processes, grounded in principles of physics and chemistry, that can reverberate through the stratosphere and even influence tropospheric conditions (Solomon, 1999).

Solar radiation, which varies across different timescales—from seconds to decades or even centuries—due to solar activity, plays a crucial role as one of the natural driving forces of Earth's atmosphere. Given that this solar energy is not constant, it is logical to expect some level of climate response to its variations. Understanding this response is essential to enhance our knowledge of the climate system and assess the impact of anthropogenic activities on it. However, determining how subtle variations in solar radiation affect climate and weather remains a complex and unresolved issue.

A common approach to exploring this issue is examining the similarity in periodicities between various solar activity indices and different meteorological parameters. Historical data reveals both positive and negative correlations between solar activity cycles—such as the 27-day cycle, the well-known 11-year sunspot cycle, the 22-year Hale cycle, and the 80-90 year Gleissberg cycle—and climate parameters like temperature, rainfall, droughts, etc. This thesis includes correlative analyses between the 11-year sunspot cycles and two atmospheric parameters, PSCs and temperatures.

PSCs are not merely passive markers of stratospheric conditions but can significantly affect stratospheric temperatures via interaction with radiation and other microphysical processes (Peter & Grooß, 2012). Similarly, stratospheric temperatures can impact the formation and properties of PSCs (Newman & Nash, 2005). Meanwhile, variations in solar activity, e.g. sunspots - serving as good indicators of solar activity, can introduce perturbations that affect both stratospheric temperatures and cloud formation conditions, although the exact mechanisms and magnitudes of these interactions remain topics of intense investigation (Haigh, 1996; Frame & Gray, 2010).

Despite the extensive history of research into the influences of solar activity on Earth's climate, skepticism regarding these relationships will persist until a clear, indisputable physical mechanism is identified to explain the observed correlations. This search for definitive mechanisms continues to pose a significant challenge within the field of climate science, underscoring the complex interplay within Earth's climate system influenced by solar activity.

While numerous correlations and mechanisms linking solar activity to stratospheric phenomena have been identified, the causative relationships and the precise extent of their influence remain subjects for further investigation. This study aims to deepen our understanding of the interactions between solar activity and various atmospheric phenomena by exploring potential correlations, thereby addressing existing gaps in our current scientific knowledge. It is hoped that this thesis will lay the groundwork for further exploration of these complex dynamics, either by the broader scientific community or through subsequent research that builds on the findings presented here.

1.1. Stratosphere

The stratosphere is the second major atmospheric layer encountered when moving away from Earth's surface, extending from about 10 to 50 km above sea level. Within the range of interest for this study, up to 30 km, the stratosphere undergoes distinct temperature variations, which play a significant role in atmospheric dynamics and chemistry (Randel et al., 2009). Temperature in the stratosphere displays a distinct behavior compared to the underlying troposphere. Starting at the tropopause and moving upwards, temperatures begin to rise as one ventures further into the stratosphere, primarily driven by the ozone layer's absorption of ultraviolet (UV) radiation from the Sun (WMO, 2011), a phenomenon central to the formation and maintenance of the ozone layer (Seinfeld & Pandis, 2016).

Ozone formation within this layer is a natural, photochemical process, vital for life on Earth due to its capacity to absorb biologically detrimental UV radiation (Brusseau et al., 2018). Unlike its role in the troposphere, where it is considered a pollutant, ozone in the stratosphere forms a protective veil that filters out UV radiation with wavelengths shorter than approximately 300 nm (Liang, 2013). This filtration is crucial, as it protects humans and animals from the potential damages of solar UV radiation, which is significantly stronger at the top of the stratosphere than at its bottom.

The presence of water vapor in the stratosphere is scarce, mainly due to precipitation processes in the troposphere that diminish the water vapor amounts. The stratosphere's remote distance

from the primary sources of water vapor, lying on the Earth's surface, combined with the extensive temperature inversion in the lower stratosphere that inhibits water vapor transport, limits the presence of water vapor in the stratosphere. In this upper atmospheric layer, O_2 can be photolyzed by solar ultraviolet radiation to form ozone, thus establishing the "O_3 layer". This layer further absorbs solar ultraviolet radiation, completing the Chapman cycle of ozone formation in the natural stratosphere (Liang, 2013). The efficiency of this cycle ensures that the ozone layer persists, and that the majority of harmful solar UV radiation is absorbed before it can reach the Earth's surface.

Stratospheric temperatures are influenced by several factors. Radiative processes, particularly the absorption of solar radiation by ozone, are pivotal. Additionally, the dynamics of the Brewer-Dobson circulation, which transports heat from the tropics to the poles, have a notable impact on the stratospheric temperature distribution (Solomon et. al., 2010).

However, the stratosphere's delicate balance is threatened by human activities as well. Chemicals such as nitrous oxide (N_2O) and chlorofluorocarbons (CFCs), which decompose slowly in the troposphere, can accumulate and be transported into the stratosphere through stratosphere-troposphere exchange events. Once in the stratosphere, these chemicals are subjected to strong solar radiation, leading to their photolysis and the subsequent formation of NO and halogen radicals (Brusseau, 2019). These radicals can significantly disrupt the natural ozone formation process, affecting the thickness of the ozone layer. This disruption was starkly highlighted by the discovery of the "O_3 hole" over Antarctica in the early 1980s, a phenomenon that signified a dramatic decrease in ozone concentration, raising global concern over the "health" of the stratosphere.

Within the altitude range up to 30 km, the lower stratosphere is particularly sensitive to external forcings. Variations in solar radiation, volcanic eruptions introducing aerosols, and anthropogenic emissions of greenhouse gases, all have potential implications for temperature trends in this region (Waugh & Polvani, 2010). Moreover, stratospheric temperature anomalies can influence tropospheric weather patterns, potentially impacting surface weather over extended periods. Monitoring and understanding stratospheric temperatures is crucial for several reasons. It aids in understanding the "health of the ozone layer", provides insights into potential climate feedback mechanisms, and helps to predict certain long-term weather patterns.

Above the stratosphere, the mesosphere and thermosphere layers play minimal roles in affecting Earth's weather and pollutant transport processes. These layers are largely decoupled from the atmospheric dynamics of the stratosphere and troposphere, underscoring the stratosphere's unique importance in Earth's atmospheric composition and the critical role of the ozone layer in protecting life by filtering harmful solar radiation. The "health of the stratosphere", therefore, is not just a matter of scientific interest, but is essential for the sustenance of life and the "well-being" of the planet.

1.2. Polar Stratospheric Clouds (PSCs)

PSCs are icy cloud formations that predominantly occur within the polar regions' stratosphere during the winter and early spring months. These clouds play a significant role in atmospheric processes, especially concerning stratospheric ozone depletion in the Antarctic and Arctic regions (Solomon, 1999). The existence of PSCs is closely related to extremely cold temperatures in the lower stratosphere. Due to the harsh and specific conditions required, PSCs are predominantly seen in the polar regions during winter, when prolonged darkness leads to sustained cold conditions.

A historical review:

The narrative of PSCs has evolved significantly, transitioning from their initial sightings in the late 19th century to the advanced satellite observations of the 21st century. Initially viewed by the public as a captivating and perhaps enigmatic spectacle, and by scientists as a fascinating yet complex area of study, PSCs were considered meteorological anomalies without perceived detrimental effects.

This perspective shifted dramatically with the unexpected discovery of the Antarctic ozone hole in the 1980s, leading to the hypothesis that PSCs could be the critical intermediary between human-made chlorine emissions and the degradation of polar ozone. By the time the ozone hole was identified, the emission of chlorine-containing compounds, specifically CFCs, had significantly increased stratospheric chlorine levels to nearly six times those of the pre-industrial era, as reported by the World Meteorological Organization in 2018. Despite their stability and longevity in the troposphere, the ascent of CFCs into the stratosphere posed unforeseen risks to ozone integrity, highlighting the complex interplay between anthropogenic activities and atmospheric phenomena.

The mechanism through which CFCs lead to ozone depletion, first posited by Molina and Rowland in 1974, was understood to occur via photolysis in the stratosphere, releasing chlorine that could deplete ozone in gas-phase reactions. Initially, it was believed this depletion would primarily occur under sunlit conditions at lower latitudes, affecting the upper stratosphere (30–50 km) and resulting in an estimated overall ozone reduction of 5%–10%. This raised questions about how such reactions could account for the extensive ozone depletion observed in the Antarctic, characterized by minimal sunlight and significant ozone layer destruction. The theory that PSCs play a critical role in polar ozone depletion provided a two-pronged explanation: firstly, PSCs facilitate heterogeneous chemical reactions on their surfaces, converting chlorine from its inert forms to active, ozone-depleting forms; secondly, they scavenge reactive nitrogen compounds, preventing these compounds from neutralizing the chlorine. Since PSCs form within the altitudes where most of the ozone layer is concentrated, the activated chlorine has the potential to significantly deplete ozone.

The advent of spaceborne instruments such as the Michelson Interferometer for Passive Atmospheric Sounding (MIPAS), Microwave Limb Sounder (MLS), and CALIOP has

revolutionized our understanding of PSCs. These technologies have enabled comprehensive observations of PSCs across the polar vortex, elucidating their spatial and temporal distributions, existence conditions, and the intricate processes through which they contribute to polar ozone depletion.

Figure 1: Polar Stratospheric Clouds or nacreous clouds over Mawson. Photo: <u>Glenn Browning</u>.

There are two primary types of PSCs, classified based on their composition: Type I and Type II. Type I PSCs are further subdivided into Type Ia and Type Ib, based on the particular substances they contain and their method of formation. Type I clouds contain a mixture of water, nitric acid, and sulfuric acid, forming at slightly higher temperatures than their Type II counterparts. On the other hand, Type II PSCs are almost entirely consisted of water ice (Peter & Grooß, 2012). Delving a bit more into the types of PSCs, can reveal a range of complexities that certainly are of great significance to atmospheric science:

Type Ia PSCs

Information and Substances: These clouds are primarily composed of nitric acid trihydrate (NAT) (Voigt et al., 2005). They form at slightly higher temperatures compared to Type Ib and Type II PSCs, usually between 185K and 195K (Peter & Grooß, 2012).

Color and External Characteristics: Type Ia PSCs usually appear iridescent and have a "mother-of-pearl" appearance due to the scattering of sunlight. The particles in these clouds are typically larger than in Type Ib PSCs but smaller than in Type II PSCs (Carslaw et al., 1997).

Type Ib PSCs

Information and Substances: These clouds are generally composed of a binary mixture of sulfuric acid and water (H_2SO_4/H_2O). They tend to form at slightly lower temperatures compared to Type Ia PSCs (Peter & Grooß, 2012).

Color and External Characteristics: Type Ib PSCs are usually white or grayish and not iridescent. Their particles are small, often around a micron in diameter (Carslaw et al., 1997).

Type II PSCs

Information and Substances: Type II clouds are primarily made of water ice and form at much colder temperatures, usually below 185K (Peter & Grooß, 2012).

Color and External Characteristics: These clouds tend to be more diffuse and whiter than Type I clouds. The particles are larger, often exceeding 10 microns (Carslaw et al., 1997).

PSCs have garnered significant attention from the scientific community due to their relationship with the stratospheric ozone hole phenomenon. While they are not directly responsible for ozone destruction, they provide surfaces for chemical reactions that produce compounds capable of catalyzing ozone depletion when sunlight returns to the polar regions in the spring. The reactions that occur on PSC particles convert less reactive compounds into more reactive forms, which, upon exposure to sunlight, engage in processes that lead to the degradation of ozone molecules. In the most common process, the unreactive chemical compounds $CLONO_2$ and HCL react on the frozen surface of PSCs, under sunlit conditions, converting to active forms, which can destroy the ozone rapidly (Pitts et al., 2018).

Figure 2: Mother of Pearl Clouds as spotted in the Scottish Highlands near Invershin. Image Credit: Alan West.

Chemical reactions taking place on the surface of PSC particles transform the stable chlorine compounds, namely HCl and $ClONO_2$, into chlorine radicals that catalytically deplete ozone (Solomon et al., 1986; Crutzen et al., 1992; Solomon, 1999). The speed of these reactions is influenced by the Surface Area Density (SAD) and chemical makeup of the particles. These particles can consist of binary liquid droplets of sulfuric acid and water (H_2SO_4-H_2O), ternary liquid droplets of nitric acid, sulfuric acid, and water (HNO_3-H_2SO_4-H_2O, also known as STS or supercooled ternary solution), solid nitric acid trihydrate (NAT) particles, or water ice particles (Lowe and MacKenzie, 2008).

PSCs also impact polar ozone chemistry by temporarily absorbing gas-phase HNO_3 from the polar stratosphere during their formation and enlargement, a process known as denoxification. In addition to this, the sedimentation of sizable NAT particles can lead to the permanent removal of HNO_3, a phenomenon called denitrification (Fahey et al., 2001; Northway et al., 2002; Molleker et al., 2014). This denitrification extends the period of ozone depletion by postponing the re-establishment of stable chlorine compounds.
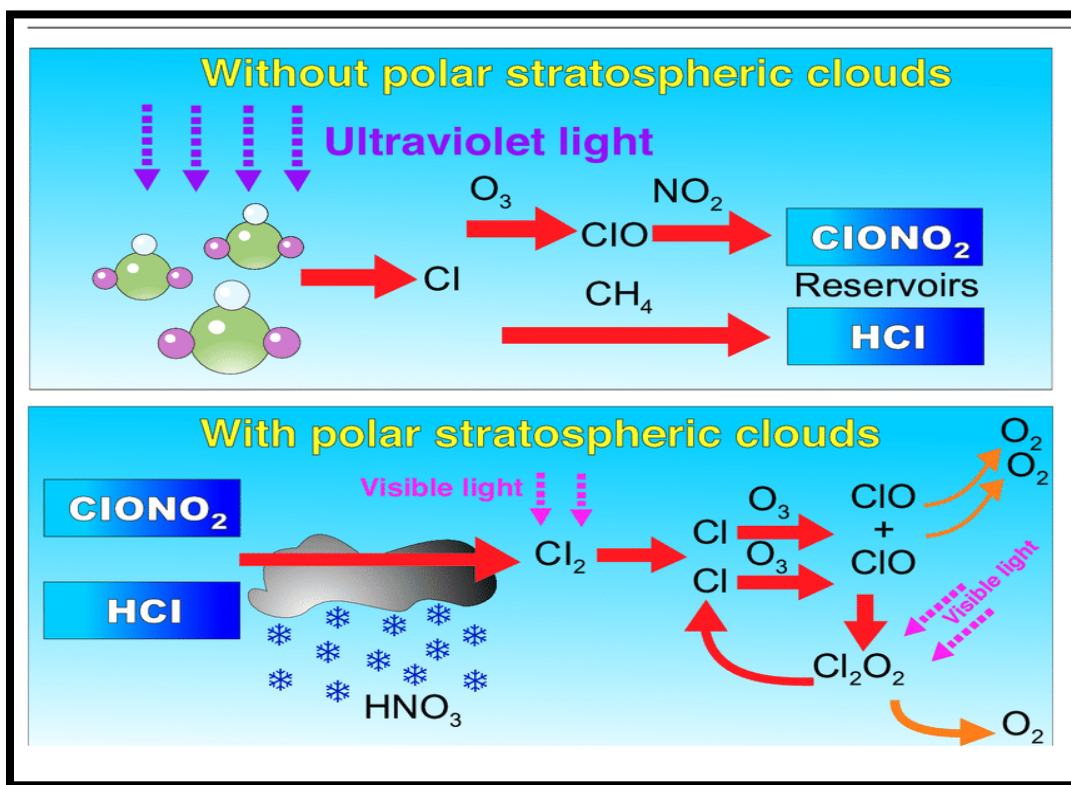
Figure 3: Diagram showing the effect of PSCs on ozone loss. The upper panel shows the situation when there are no PSCs and Ozone depletion takes place only in the gas phase (homogeneous chemistry). The lower panel shows the situation when there are PSCs present. The reservoir gases hydrochloric acid and chlorine nitrate react with each other on the surface of the PSC particles through a red-ox reaction and liberate elementary chlorine (Cl_2). Diagram made by Finn Bjørklid ([ResearchGate](#)).

Furthermore, PSCs influence the radiative balance of the Earth. Due to their interaction solar and terrestrial radiation, they might play a role in Earth's climate system, especially in polar regions

(Poole & Pitts, 1994). Moreover, the appearance of PSCs is often a spectacle. They can lead to vivid displays known as "nacreous clouds" (Fig. 1) or "mother-of-pearl clouds" (Fig. 2, as mentioned before, due to their iridescent colors. These clouds, catching the first or the last light of the day, can create shimmering displays of bright and pastel colors against the darker backdrop of the polar sky.

With the increasing awareness of global climate change, some studies have investigated how changes in the Earth's climate might impact PSCs. Rex and coworkers suggested that global warming, leading to colder stratospheric temperatures in polar regions could possibly increase the occurrence of PSCs, which could further influence ozone chemistry (Rex et al., 2004).
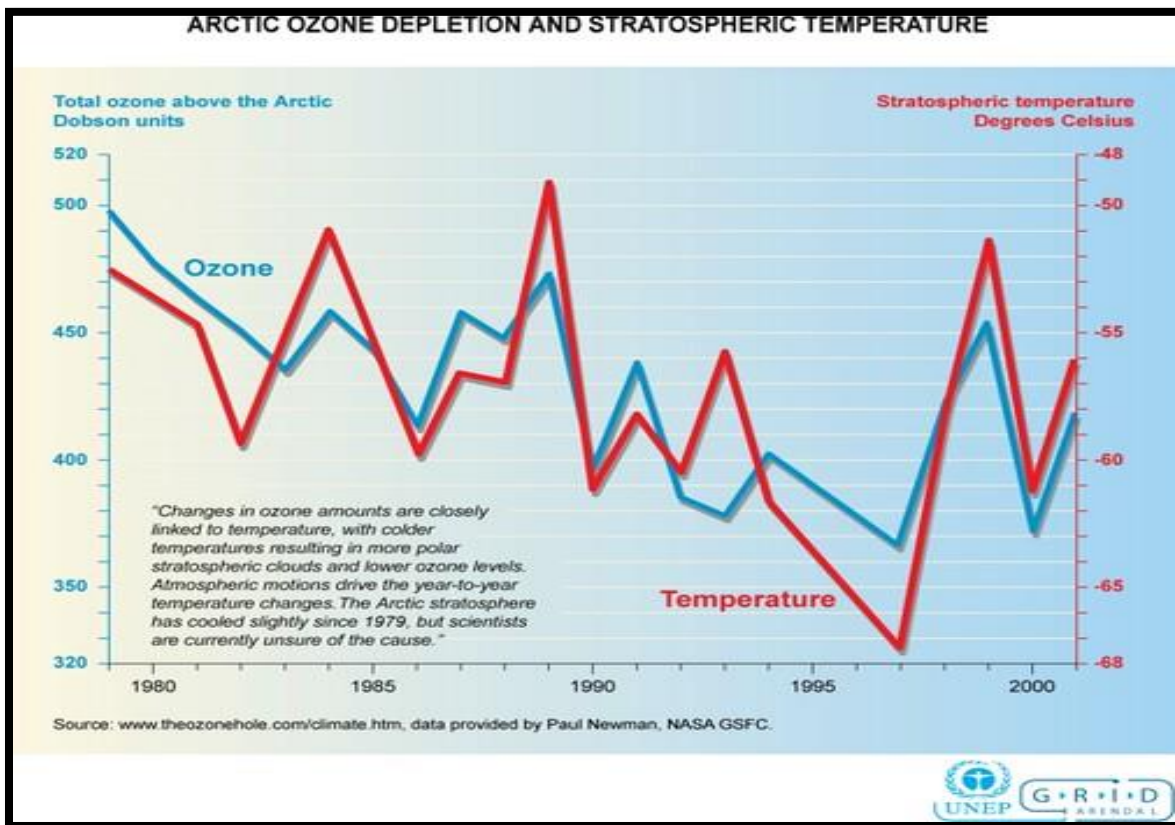
Figure 4: Graph showing the total ozone above the Arctic in Dobson Units and Stratospheric Temperatures for the same period of time starting from 1979 up to 2001. Data provided by Paul Newman, NASA GSFC.

Figure 4, featuring data from Paul Newman, elucidates the interaction between ozone levels and stratospheric temperatures in the Arctic. The graph demonstrates that fluctuations in ozone levels are intimately connected to variations in temperature. According to GRID-Arendal, variations in temperatures from year to year are propelled by atmospheric movements. It has been observed that the Arctic stratosphere has experienced a marginal cooling since 1979, a phenomenon that aligns with our findings as discussed in 4.2.1, but still remains under scientific scrutiny to pinpoint its underlying causes.

Research into PSCs is vital for understanding not only ozone depletion processes, but also broader climatic interactions. Their formation, composition, and interactions with other atmospheric components provide crucial insights into the complex interplay of atmospheric dynamics, chemistry, and even climatic changes. Their sensitivity to temperature changes also makes them potential indicators of broader atmospheric shifts, possibly driven by global warming and other large-scale climatic processes.

1.3. Solar Activity – Sunspots

Solar activity is a broad term that refers to the various phenomena originating from the Sun's energy output and magnetic activity, impacting both the Sun's surface and the broader solar system. One of the most visually observable and historically documented manifestations of this activity is the occurrence of sunspots (Hathaway, 2015).

Sunspots are temporary, dark regions on the Sun's surface (photosphere) characterized by magnetic activity and lower temperatures compared to the surrounding areas. Typically, they appear as dark spots because they are cooler – with temperatures around 3,500°C compared to the typical photospheric temperature of approximately 5,500°C (Thomas & Weiss, 2008).
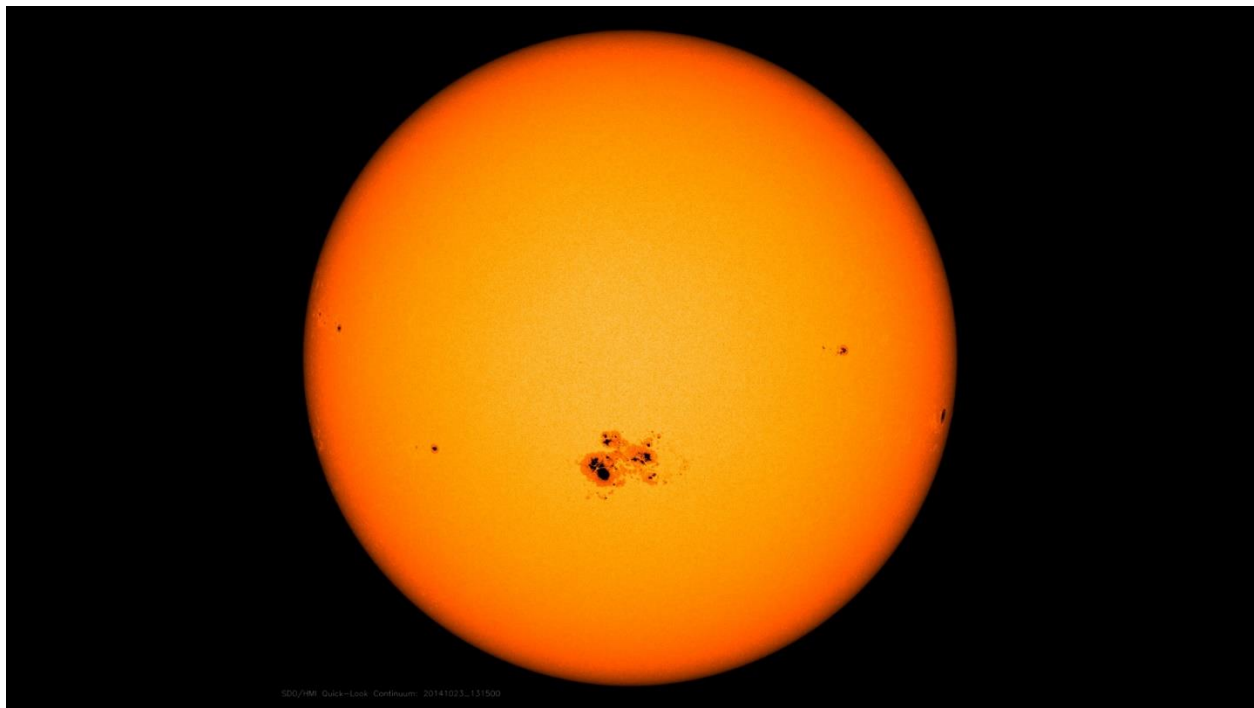
Figure 5: Sunspots. Image Credit: NASA/SDO.

The number of sunspots oscillates over approximately an 11-year cycle, known as the solar cycle. Periods with a high frequency of sunspots are termed 'solar maximum', while those with fewer sunspots are termed 'solar minimum'. This cycle is a manifestation of the underlying magnetic activity within the Sun, and the presence and number of sunspots serve as an indicator of this intrinsic solar activity (Charbonneau, 2010).

The Sun emits electromagnetic radiation across all wavelengths, from gamma rays to infrared, a spectrum collectively measured as the Total Solar Irradiance (TSI) and quantified in terms of power per unit area. Interestingly, TSI experiences an increase with a higher number and area of sunspots, despite these being darker features on the solar surface. This paradox is elucidated by understanding that the luminance of a flux tube is influenced by its diameter. Flux tubes, which carry magnetic fields and plasma from the Sun's interior to its surface, vary in size from the large, sunspot-containing active regions to smaller formations such as pores, faculae, and bipoles that constitute the quieter solar areas.

In larger flux tubes, like those encompassing sunspots and pores, the magnetic field restricts convective energy movement within the tube, diminishing the upward flow of heat and thus cooling and darkening these regions. Conversely, in smaller flux tubes found in faculae and the network, the radiative heat from the tube's hot walls significantly warms the middle and upper portions of the tube's photosphere. This heating process renders these areas brighter and hotter than their surroundings on the quiet Sun, as detailed by Fligge and Solanki in 2000. Due to the faculae and network features being more numerous and enduring than the darker sunspots, an increase in solar toroidal field or sunspot number leads to an overall rise in solar irradiance.
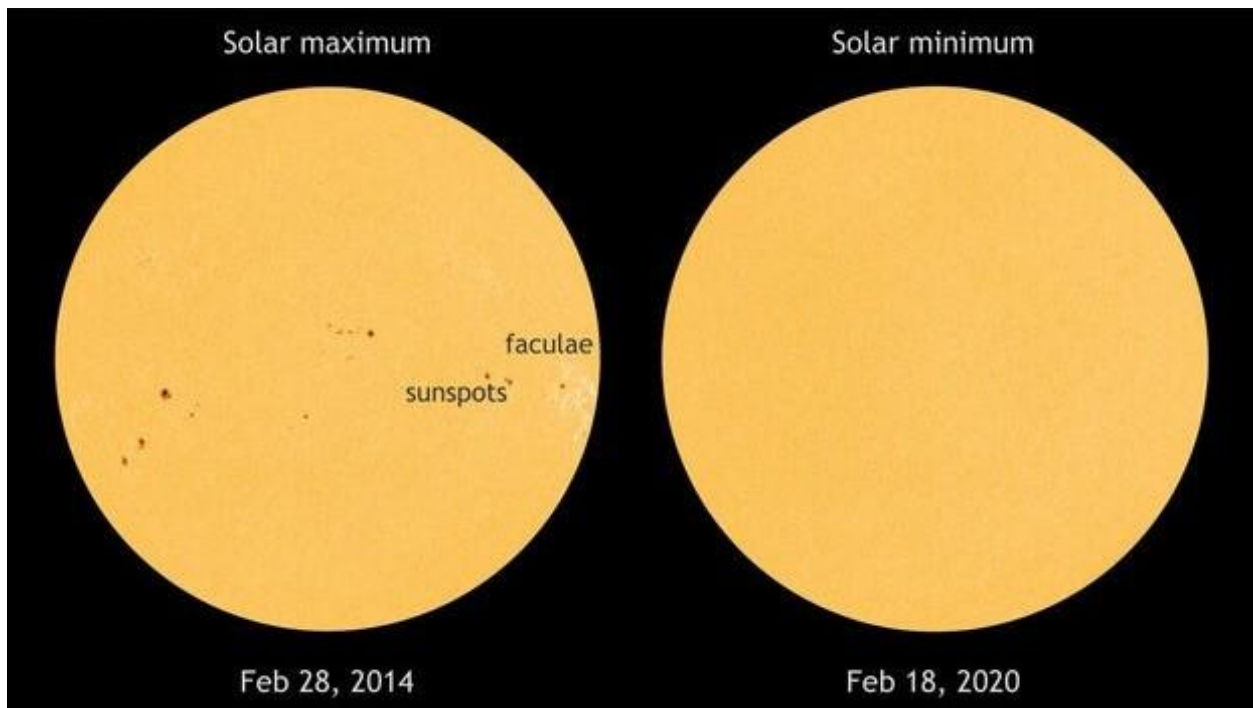
Figure 6: Images of the Sun in filtered visible light—based on data from NASA's Solar Dynamics Observatory telescope on February 28, 2014, (left), near the maximum of the last solar cycle, and on February 18, 2020 (right), near the solar minimum. Images from NASA/SDO.

Solar irradiance primarily consists of radiative output in the 400 to 800 nm wavelength range. Radiation exceeding 400 nm, encompassing visible and infrared light, can penetrate the troposphere and reach Earth's surface, directly influencing the planet's energy equilibrium. Conversely, radiation at shorter wavelengths is largely absorbed higher in the atmosphere,

playing a pivotal role in the chemical and dynamical integration of atmospheric layers, particularly through interactions with atmospheric ozone.

The significance of sunspots extends beyond mere solar observation. Sunspot activity and its cycles have been subjects of scientific investigations related to Earth's climate. These phenomena are associated with various other solar events like solar flares and coronal mass ejections (CMEs). Such events can have profound impacts on space weather, which in turn can influence the Earth's atmosphere (Eddy, 1976). On September 1, 1859, an unprecedented astronomical event was witnessed by Richard Carrington and, independently, by Hodgson, an English amateur astronomer. They observed a sudden and intense burst of light emanating from a cluster of large sunspots, an event that lasted approximately five minutes. Carrington would later term this phenomenon a "solar flare," marking the first recorded observation of such an event. Remarkably, this solar flare was followed, 17 hours later, by the most powerful geomagnetic storm ever documented, establishing a direct observational link between solar activity and terrestrial geomagnetic disturbances.

Solar flares and CMEs both stem from active regions on the Sun, characterized by their strong and chaotic magnetic fields. The abrupt liberation of stored magnetic energy within these regions can lead to the production of a solar flare, which is an intense emission of radiation across the entire electromagnetic spectrum accompanied by particle acceleration, or a CME, which involves a massive expulsion of plasma and magnetic fields from the solar corona. Occasionally, both phenomena can occur simultaneously. Research by Yashiro et al. (2004) indicates that with an increase in flare intensity, the occurrence of flares not accompanied by observed CMEs becomes less frequent.

Both flares and CMEs are expressions of the solar toroidal field, and their frequency and intensity are closely aligned with the sunspot cycle. Although solar flares themselves do not directly impact geomagnetic activity, CMEs, when interacting with Earth's magnetosphere, are responsible for triggering the most severe geomagnetic storms. This correlation peaks around the sunspot maximum (Smax), indicating a period of heightened geomagnetic activity driven by CMEs.

In the latter stages of the sunspot cycle, a fascinating transformation occurs. Leading sunspots, having neutralized their counterparts of opposite polarity from the other hemisphere, leave behind trailing polarity spots. These migrate poleward, coalescing into increasingly larger unipolar regions known as "coronal holes." Characterized by their unipolar magnetic fields, coronal holes have open field lines that extend into the heliosphere, enabling solar plasma to flow and accelerate freely along these pathways. This results in high-speed solar wind streams (HSSs) that, upon interacting with Earth's magnetosphere, can induce geomagnetic storms, as outlined by Tritscher et al. (2021).

Consequently, the relationship between geomagnetic activity and sunspot numbers is rather weak (figure 7A). The pattern of geomagnetic activity throughout the sunspot cycle features two distinct peaks: the first aligns with the sunspot maximum (Smax), driven by CMEs associated

with the solar toroidal field, while the second emerges during the declining phase of the sunspot cycle, instigated by HSSs linked to the solar poloidal field (figure 7B).
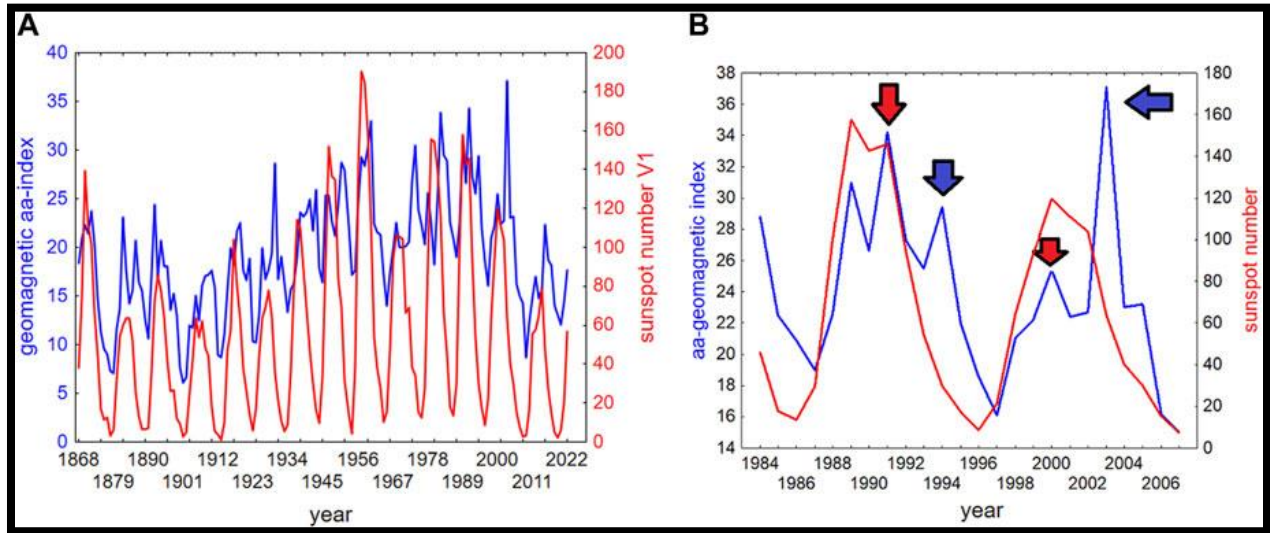
Figure 7: A) Sunspot (red line) and geomagnetic (blue line) activity since 1868. Here and further, the sunspot activity is presented by the international sunspot number, with the values from 2015 onward calculated during cycles 19 and 20. B) An illustration of the two peaks of the geomagnetic activity in the sunspot cycle: one caused by solar toroidal-field related CME's, and coinciding with Smax (red arrows), and a second one on the sunspot declining phase caused by solar poloidal field-related HSS's (blue arrows). Graph belongs to the work of Tritscher et al. (2021).

While the direct impact of sunspot variability on Earth's climate remains a topic of ongoing research, some studies (e.g. Eddy 1976, Hathaway 2015) have suggested correlations between prolonged periods of few sunspots, known as the Maunder Minimum, and colder climatic periods on Earth, such as the "Little Ice Age.

NASA has reported that extensive anomalies like the Maunder Minimum, also known as the Grand Solar Minimum (Fig. 8), highlight the fact that the Sun's magnetic activity and energy emissions can fluctuate significantly over decades. Recent space-based measurements over the last few cycles have observed relatively consistent total solar irradiance from one solar cycle to another. Solar Cycle 24, which spanned from December 2008 to December 2019, was noted to be less intense compared to its preceding cycles. Researchers have sporadically proposed that forthcoming solar cycles may experience prolonged phases of low solar activity. However, the forecasting models for such scenarios are not yet as refined as those for terrestrial weather and thus are not unanimously accepted.

Understanding solar activity, particularly sunspots, is crucial not just for solar physics but also for comprehending the broader interplay between the Sun and Earth. As our primary energy source, fluctuations in the Sun's activity can have a ripple effect on various Earthly systems, from technological infrastructures to climatic patterns (Lockwood, 2012).
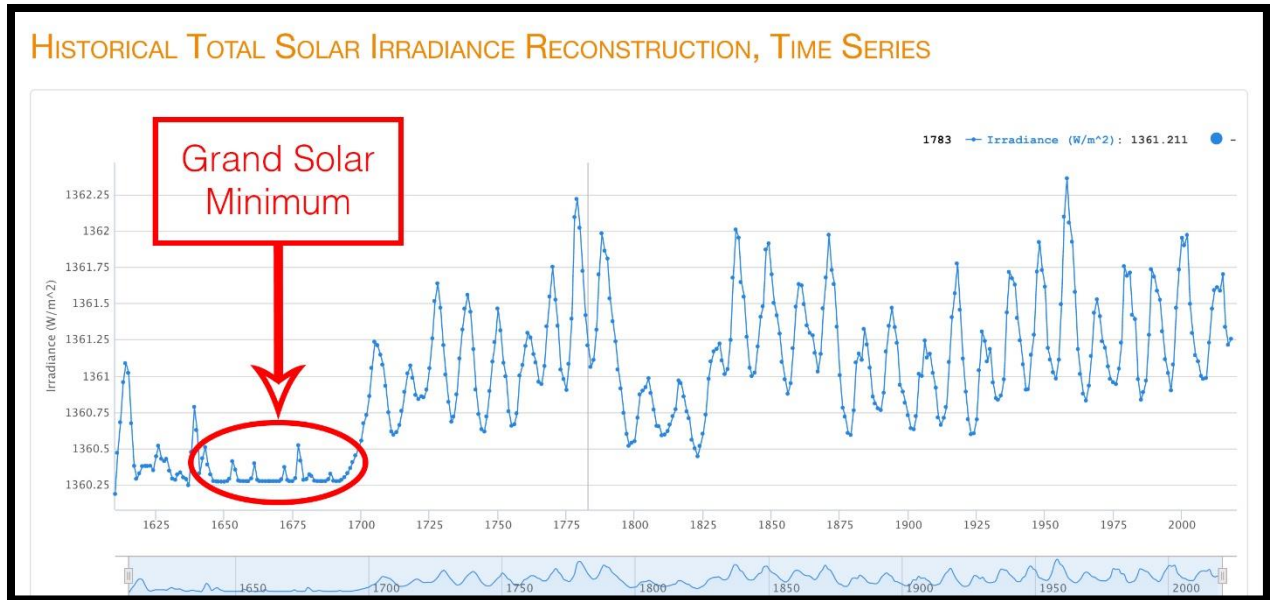
Figure 8: The Maunder Minimum (or, Grand Solar Minimum) period as predicted by NASA models. Source: The University of Colorado's LASP Interactive Solar Irradiance Datacenter

1.4. CALIPSO satellite and CALIOP lidar

Launched on April 28, 2006, the Cloud-Aerosol Lidar and Infrared Pathfinder Satellite Observation (CALIPSO) satellite was a collaborative mission between NASA and the French space agency, CNES. The satellite was developed to provide new insight into the roles that clouds and atmospheric aerosols play in regulating Earth's weather, climate, and air quality (Winker et al., 2010). NASA and CNES agreed to end the highly successful CALIPSO science mission on August 1. Designed for a lifetime of 3 years, CALIPSO delivered unprecedented measurements of the vertical structure of the Earth's atmosphere for 17 years.

CALIPSO was flying in a 98° inclination orbit at an altitude of 705 km as part of the NASA A-train satellite constellation (Stephens et al., 2002), along with the Aqua, Aura, CloudSat, and Orbiting Carbon Observatory 2 (OCO-2) satellites. Although PSC studies are not a primary mission objective, CALIPSO is an ideal platform for studying polar processes, collecting data along 14–15 orbits per day with coverage from 82° S to 82° N latitude on each orbit. CALIOP data collection began in mid-June 2006 and continued till the end of July 2023. However, the accessible data records on NASA's official portal, are covering a 16-year period, from mid-June 2006 to March 2021.

Central to CALIPSO's observational capabilities is the Cloud-Aerosol Lidar with Orthogonal Polarization (CALIOP), an innovative lidar instrument, which stands for Light Detection and Ranging, operates on a principle similar to radar but uses laser light instead of radio waves. CALIOP sends short pulses of laser light towards the Earth and then measures the light backscattered by clouds and atmospheric aerosols. The resulting data allows for detailed vertical

profiling of the atmosphere, offering a three-dimensional perspective on cloud and aerosol properties (Hunt et al., 2009).

Figure 9: CALISPO Satellite. Image Credit: NASA

One of the standout features of CALIOP is its ability to differentiate between aerosol and cloud particles, which can be particularly challenging for passive sensors. The lidar data from CALIOP, when combined with other satellite observations, provides a comprehensive view of atmospheric structures, helping to fill the gaps in our understanding of critical atmospheric processes and interactions (Omar et al., 2013).

Fortunately, the knowledge of the temporal and geographic distribution of PSCs and their particle composition has expanded greatly in the 21st century with the advent of three satellite instruments with extensive polar measurement coverage: the Michelson Interferometer for Passive Atmospheric Sounding (MIPAS) on Envisat (2002–2012), the Microwave Limb Sounder (MLS) on Aura (2004–present), and the Cloud-Aerosol Lidar with Orthogonal Polarization (CALIOP) on CALIPSO (2006–2023).

The data from CALIPSO and CALIOP has been instrumental in a wide range of atmospheric studies, from analyzing cloud-aerosol interactions, tracking long-range transport of aerosols, understanding cloud vertical structures, to studying phenomena like Polar Stratospheric Clouds (Pitts et al., 2018), which we analyze in this study.

2. Thesis Rationale and Literature Overview

2.1. Thesis Rationale

In recent decades, the study of the Earth's stratosphere has gained increased attention due to its essential role in climate regulation and ozone layer protection. One key phenomenon within this realm, as mentioned before, is the formation of PSCs, which have a noteworthy impact on ozone chemistry. According to the World Meteorological Organization (WMO), a substantial recovery of the ozone layer is expected by the middle of this century with reduced global production of ozone depleting substances in accordance with the Montreal Protocol and subsequent amendments and adjustments. But as climate changes, leading to a colder and perhaps wetter stratosphere and upper troposphere (e.g., Shindell, 2001), reliable model predictions of recovery of the Antarctic ozone hole and of potentially more severe ozone depletion in the Arctic are challenging because many global models use simple parameterizations that do not accurately represent PSC processes (e.g., Peter and Grooß, 2012; Morgenstern et al., 2017). Stratospheric temperatures also play a decisive role in the formation and persistence of PSCs, yet these temperatures themselves are susceptible to a plethora of factors including but not limited to solar activity. Specifically, the focus on sunspots as indicators of solar cycles opens a door to understanding potential links between solar radiation and stratospheric phenomena. Under these conditions, it is crucial to investigate and understand how well is correlated or not, the 11-year solar cycle with the stratospheric temperatures and formation of PSCs.

The study aims to synthesize 16 years of climatological data based on CALISPO and SILSO measurements, seeking correlations or patterns that might imply a relationship between PSCs, stratospheric temperatures, and solar sunspot activity—an approach not directly pursued before. However, this investigation represents the study's final phase. The primary objective is to create a global climatology of PSCs and stratospheric temperatures spanning from July 2006 to March 2021, both in spatial and temporal dimensions. This effort involves using CALIPSO data for PSC observations and MERRA-2 data for stratospheric temperatures. In doing so, the goal is to enrich the existing body of literature, which previously mapped a similar climatology using the same datasets, but only for the period 2006-2017. By extending this timeframe, the goal is to conduct a more thorough and essential analysis of PSC occurrences. This will allow for a comparison of the findings of this thesis with related studies and lay the groundwork for future research.

2.2. Literature Overview

Despite the wealth of research on each of these subjects individually – Stratosphere, PSCs, Sunspots – the triangular dynamics among them have not been extensively studied. The literature on PSCs is getting more extensive through time, marking significant milestones in our understanding of their chemical compositions and interactions. Notably, the studies by Solomon et al. (1986) provided a foundational analysis of the chemical processes involving PSCs that

contribute to ozone depletion. This was further expanded by Crutzen et al. (1992) and Solomon (1999), who delved into the kinetics of these reactions. Additionally, the work of Lowe and MacKenzie (2008) has been pivotal in dissecting the complex compositions of PSCs. Parallel to this, the study of stratospheric temperatures has benefited greatly from both models and observational data, which have been instrumental in assessing their variation and impact on PSC formation. Moreover, the influence of solar activity, especially sunspots, on stratospheric temperatures and potentially other related phenomena, has been acknowledged but still demands a more detailed investigation. The advent of CALIPSO satellite measurements has marked a significant advancement in stratospheric studies, providing unprecedented precision in observations. This technological leap has catalyzed a plethora of studies, enhancing our understanding of stratospheric phenomena, including PSCs.

By contextualizing this study within the broader scholarly discourse, it becomes clear that while substantial progress has been made in understanding the individual components of this tripartite relationship, a comprehensive analysis that integrates PSCs, stratospheric temperatures, and solar activity remains a critical need. This research endeavors to address this void, offering new insights into the mechanisms driving these complex interactions by examining how strong are any correlations between these parameters both in altitude and latitude.

More specifically:

2.2.1. PSCs and Stratospheric temperatures

The formation and behavior of PSCs are inextricably linked to stratospheric temperatures. As previously mentioned, they materialize under exceptionally cold conditions. But why does the stratosphere reach such frigid temperatures? This largely results from radiative processes and the limited mixing between the troposphere and stratosphere. In the polar winter, with the absence of sunlight, the stratosphere becomes particularly chilly, setting the stage for PSC formation.

But there's a twist. While PSCs might seem like mere byproducts of these cold conditions, they can, in fact, influence temperatures themselves. PSCs, especially the iridescent nacreous clouds, can scatter and reflect sunlight. This reflection can lead to localized warming events in the stratosphere. Though these events might be short-lived, they're vital for understanding the dynamism of stratospheric temperature fluctuations.

Research has been conducted on the relationship between PSCs and stratospheric temperatures. PSC formation is highly dependent on low stratospheric temperatures, and this relationship is often examined in the context of ozone depletion processes in polar regions. However, the specific datasets and timeframes used in these studies can vary widely, ranging from short-term observational campaigns to long-term satellite data analyses.

Some studies have employed satellite observations from platforms such as the Atmospheric Chemistry Experiment (ACE) or the Microwave Limb Sounder (MLS) to better understand PSC formation in relation to stratospheric temperature variations. Others have used reanalysis datasets

like ERA-Interim or ERA5 that provide comprehensive, gridded temperature data in the stratosphere.

It's less common to find studies that have specifically looked at a 16-year climatology of both PSCs and stratospheric temperatures up to 30 km. Many studies might focus on shorter timeframes, like Pitts et al., 2018, or specific events, like sudden stratospheric warmings, that have an immediate and dramatic impact on both PSCs and stratospheric temperatures. Therefore, while there is existing literature on the correlation between PSCs and stratospheric temperatures, this study's approach could provide new, comprehensive insights into this relationship.

2.2.2. Stratospheric temperatures and Sunspots

The relationship between stratospheric temperatures and sunspots has been a subject of ongoing debate and research. Some studies have suggested a link between solar activity, of which sunspots are a key indicator, and stratospheric temperatures. For example, solar maxima and minima (periods of high and low sunspot numbers, respectively) have been observed to coincide with variations in stratospheric temperatures. However, these relationships are not yet fully understood and are complicated by other factors, like volcanic activity and anthropogenic emissions.

The possibility that sunspots could exert an influence on stratospheric temperatures, directly or indirectly, opens the door to intriguing questions about how solar variability might impact Earth's climate system. If a relationship is proven, it could not only expand our understanding of Earth's climate but also enhance the accuracy of climate models.

Some studies have used satellite data or solar proxies to explore how solar irradiance variations over the solar cycle can affect stratospheric temperatures. However, it's important to note that solar effects are often considered secondary compared to other influences on stratospheric temperatures, such as greenhouse gases and volcanic activity.

The correlation between solar activity and stratospheric temperatures up to 30 km has not been as intensively studied as some other relationships involving the stratosphere. Focusing on a 16-year climatology and extending up to 30 km in altitude, could offer novel insights into this particular aspect of atmospheric science.

2.2.3. PSCs and Sunspots

When discussing sunspots, we're delving into the realm of solar activity and its potential impacts on Earth's atmosphere. Sunspots, dark patches on the sun's surface, are indicative of increased solar magnetic activity. They have been correlated with variations in solar radiation, which can influence Earth's climate and atmospheric conditions.

But, how does this tie into PSCs? Well, it's an area of active research, and while the connections are not entirely mapped out, there are some intriguing hypotheses. Increased solar radiation during periods of high sunspot activity can warm the stratosphere. This warming might reduce the prevalence or duration of the super-cold conditions needed for PSCs. On the flip side, during

periods of low sunspot activity, reduced solar radiation might promote conditions conducive to PSC formation.

Moreover, some studies suggest that solar activity can influence stratospheric wind patterns. These wind patterns can, in turn, modulate the temperatures in polar regions, potentially impacting PSC occurrence.

However, it's essential to note that while the connections between sunspots, stratospheric temperatures, and PSCs are tantalizing, they're also intricate. Many factors play into Earth's atmospheric processes, and it's a delicate balance. Teasing out the direct impacts of sunspots on something as specific as PSCs can be akin to listening for a whisper in a storm. Yet, the potential connections underscore the intricate interplay between Earth's atmosphere and our closest star.

Solar activity is generally considered to have a more indirect influence on stratospheric conditions through complex interactions that might affect temperature and circulation patterns. Given that PSCs are closely related to stratospheric temperatures, one could hypothesize that solar activity could have an indirect effect on PSCs, but proving this would require complex, multi-variable analyses. While solar activity has been examined in the context of its broader impacts on Earth's atmosphere and climate, its direct relationship with PSCs is less well understood or studied.

This thesis aims to fill a discernible gap in the current academic discourse on PSCs' global climatology and their direct relationship with stratospheric temperatures, by also investigating the presence (or absence) of any correlations between PSCs and Sunspot activity, within the timeframe of the dataset under consideration.

A comprehensive view:

The debate over the Sun's impact on Earth's atmosphere and climate has persisted intensely for over two centuries. Despite identifying correlations between sunspot numbers and various atmospheric phenomena, the underlying mechanisms remain elusive. Recent advancements have shed some light on these interactions, yet the inconsistency of these correlations—characterized by their tendency to strengthen, weaken, vanish, or even invert over different time frames— poses a significant challenge. No current theory fully accounts for this variability, which underscores the complexity of solar-terrestrial relationships. At the core of solar activity lies the solar magnetic field, which, alongside solar irradiance, plays a crucial role in influencing Earth's climate.

An interesting observation is the lagging of the tropospheric North Atlantic Oscillation's positive phase, indicative of a robust vortex, by a few years behind the peak in UV radiation during the sunspot maximum (Smax). However, it has been determined that this positive climatic response is not directly attributable to delayed UV effects but rather to the influx of precipitating energetic particles, which also reach their zenith a few years after Smax. Additionally, the solar wind and associated transient phenomena affect the influx of galactic cosmic rays, primary agents of atmospheric ionization below approximately 50 km. This modulation of cosmic rays influences

the generation of aerosols, which serve as cloud condensation nuclei, thereby affecting cloud cover. Increased cloudiness, in turn, reduces the amount of solar irradiance that penetrates the lower atmosphere and reaches the Earth's surface. Furthermore, fluctuations in galactic cosmic ray intensity can alter electric currents and the ionospheric potential over the polar caps, potentially amplifying microphysical processes within clouds and varying cloudiness.

This complex interplay of solar and terrestrial processes illustrates the intricate mechanisms through which the Sun can influence Earth's climate and atmospheric conditions, highlighting the need for continued investigation into the solar activity's multifaceted impact on our planet. Solar energetic particles (SEPs), released during solar eruptions, initiate a cascade of reactions in Earth's atmosphere with significant climatic implications. These particles generate reactive species of odd hydrogen (HOx) and nitrogen (NOx), which engage in catalytic reactions that deplete ozone in the mesosphere and upper stratosphere—a phenomenon known as the "direct effect." NOx, particularly stable in the absence of sunlight during the polar night, can migrate to lower stratospheric levels, where it continues to deplete ozone, leading to a "indirect effect" that manifests over a delayed timeframe. In conditions devoid of sunlight, ozone plays a critical role in absorbing the Earth and atmosphere's longwave outgoing radiation. Consequently, any increase in ionization that leads to ozone depletion can cool the polar middle atmosphere. This cooling accentuates the temperature gradient between the polar and mid-latitude regions, subsequently strengthening the stratospheric polar vortex.

While SEPs represent a potent but infrequent source of atmospheric disturbance, the Earth's magnetosphere harbors electrons that, during geomagnetic events, are accelerated and precipitated into the atmosphere. These electrons, though less energetic, are omnipresent and mimic the SEP's effects by producing additional HOx and NOx. This leads to ozone depletion, resulting in a strengthened polar vortex and a positive phase of the North Atlantic Oscillation (Georgieva K. and Veretenenko S., 2023).

Research indicates that the observed reversals in the correlation between solar activity and atmospheric parameters cycle approximately every 60 years. These shifts are closely linked to the evolution of large-scale atmospheric circulation patterns, which share a similar periodicity. The dynamics of these circulation forms are, in turn, influenced by the state of the polar vortex. The polar vortex can modify troposphere-stratosphere interactions through the propagation of planetary waves, highlighting the interconnectedness of solar activity, atmospheric chemistry, and Earth's climate system. This complex interplay underscores the profound impact of both solar and terrestrial energetic particles on our planet's atmospheric dynamics and climate.

Solar irradiance and sunspots, which are manifestations of the solar toroidal field, exhibit a direct relationship, with irradiance reaching its peak during the maximum of the sunspot cycle. Conversely, energetic particle precipitation, associated with the solar poloidal field, intensifies notably during the declining phase of the solar cycle. The toroidal and poloidal fields constitute the dual aspects of the Sun's large-scale magnetic field, intricately linked yet originating from

distinct domains within the solar interior. This distinction is further complicated by the stochastic nature of the process that converts the toroidal field into the poloidal field, leading to their variations over longer timescales.

Due to these differences in generation and the inherent randomness in the transformation from toroidal to poloidal fields, the dominance of solar influences on Earth's climate and magnetic environment can shift between those primarily associated with the poloidal field and those linked to the toroidal field. This cyclical variation results in periods where the effects of poloidal field-related solar drivers are more pronounced, and others where toroidal field-related influences take precedence. Such dynamism underscores the complexity of solar activity and its impact on Earth, highlighting a nuanced interplay between different components of the Sun's magnetic field over various phases of the solar cycle.

The impact of solar variability on Earth's atmosphere has been a persistent and challenging question in atmospheric sciences for decades, with a rich history of debate and investigation as highlighted by Pitrock's reviews in 1978 and 1983. Among the various aspects of solar-weather relationships that have sparked controversy, the connection between solar activity and ozone dynamics stands out as a notable exception. This relationship has gained recognition and has been considered in every international ozone trend assessment conducted by the World Meteorological in the years 1988, 1991, and 1994, reflecting its established significance in the scientific community.

The acknowledgment of the link between solar activity, stratospheric temperature, and ozone concentrations is backed by a wealth of theoretical and empirical research spanning the last two decades. Studies by scientists such as Zerefos and Crutzen (1975), Penner and Chang (1978), Brasseur and Simon (1981), Brasseur et al. (1987), Heath and Schlesinger (1986), Angell (1988, 1989, 1991), alongside the WMO's 1991 report, and works by Hood et al. (1993) and Chandra and McPeters (1994), have been pivotal. These investigations have unveiled the temporal dynamics of ozone's response to solar activity, capturing fluctuations over short timescales like the 27-day solar rotation, to longer cycles, including the 11-year solar cycle. The consensus from both modeling and observational data suggests a synchrony between ozone levels and solar activity, especially in the upper stratosphere where photochemical reactions occur rapidly, resulting in ozone variations by a few percentage points.

Angell's 1991 study, which investigates changes in stratospheric temperature as influenced by altitude and sunspot numbers from 1972 to 1989, utilizes data from rocketsonde and 12 radiosonde stations predominantly located in the western Northern Hemisphere. The research documents a significant cooling trend, with the low stratosphere experiencing a near $-0.5°C$ decrease per decade and the high stratosphere around $-1.6°C$ per decade. The analysis of the correlation between annual sunspot numbers and temperatures identified the most substantial connection (0.83) in the middle stratosphere, presenting a contrast to our data. However, it's important to note that this correlation did not reach statistical significance at the 5% level.

This body of research underscores the intricate relationship between solar activity and stratosphere but also emphasizes the critical role of observational satellite data, such as those from Nimbus 7 and NOAA 11, in advancing our understanding of these complex interactions. The elucidation of this solar activity-ozone linkage marks a significant stride in atmospheric sciences, offering insights into the mechanisms through which solar variability can influence Earth's climate and atmospheric chemistry.

The intricacies of the relationships above are compounded by several factors, making it an exceptionally complex issue to unravel. The cooling trend observed in the lower stratosphere, as documented by Zerefos and Mantis (1977) and further supported by Angell (1988) and Labitzke and van Loon (1995), is just the beginning. When one also considers the anthropogenic influences through heterogeneous processes, the complexity of the problem escalates, as highlighted in the World Meteorological Organization's 1994 report. This multifaceted issue combines natural variability with human-induced changes, creating a challenging puzzle for scientists to solve.

Over the past decade, the development and application of 2-D chemical-dynamical models have offered a new avenue for exploring the atmospheric responses to both long-term and short-term solar variability. Notable efforts in this domain include studies by Garcia et al. (1984) and Huang and Brasseur (1993), which have sought to simulate and understand the atmospheric dynamics influenced by solar activity. However, a consistent challenge has been the alignment of model simulations with observational data, particularly regarding the vertical distribution of solar cycle-induced ozone and temperature changes. Brasseur (1993) highlighted discrepancies between modeled predictions and empirical observations, underscoring the difficulty in accurately simulating the solar cycle's effects on the atmosphere.

In this study, we explore the relationship between solar activity and the stratosphere, utilizing the most comprehensive and recent dataset derived from lidar satellite observations spanning 2006 to 2021. This period is marked by considerable anthropogenic influences, such as fluctuations in greenhouse gas concentrations and levels of stratospheric aerosols. These factors, combined with the natural variations of solar cycles, contribute to complex interactions that significantly impact Earth's atmosphere, though the full extent of these effects remains partially understood.

3.   Data and Methodology

In the realm of any scientific research, the caliber of data used is paramount to the credibility and relevance of the study. For this master's thesis, which aims to explore the intricate relationships between polar stratospheric clouds, stratospheric temperatures, and solar activity, we turned to two established and reputable data sources: (i) the Cloud-Aerosol Lidar and Infrared Pathfinder Satellite Observation (CALIPSO) and the (ii) Royal Observatory of Belgium. These initiatives have been leading authorities in the collection of atmospheric and solar activity data, respectively. Their long-standing commitment to rigorous data collection and analysis provides a strong foundation for this research, ensuring that our conclusions are built on dependable and well-validated datasets.

3.1.   CALIPSO Data Products

The CALIPSO Lidar Level 2 Polar Stratospheric Cloud (PSC) data product ensemble, used for this study, describes the spatial distribution, optical properties, and composition of 121 PSC layers, from 8.4 to 30 kilometers above the earth's surface, observed by the CALIPSO lidar (CALIOP). This contained profiles of PSC presence, composition, optical properties, and meteorological information along CALIPSO orbit tracks. PSC detection was limited to nighttime CALIOP observations because higher levels of background light during daytime significantly reduce the signal-to-noise and, hence, the PSC detection sensitivity. Each file contained data from all nighttime orbit segments from a single day reported on a 5-km horizontal by 180-m vertical resolution. The Level 2 dataset for PSCs was extracted from CALIPSO Lidar Level 1B nighttime-only data, utilizing the V2 PSC identification and composition categorization algorithm as outlined in Pitts et al. (2018). For this research, the PSC data products were used as is, without additional processing through the V2 algorithm, as it had already been applied to the initial CALIPSO dataset.

Science Data Set (SDS)
Number_Of_LIDAR_L1_File
Number_Altitudes
Number_Profiles
L1_Input_Filenames
L1_Input_Start_Times
L1_Input_End_Times
Profile_Time
Profile_UTC_Time
Latitude
Longitude
Altitude
Orbit_Index
Temperature
Potential_Temperature
Pressure
Vortex_Edge_Outer
Vortex_Edge_Center
Equivalent_Latitude
Tropopause_Altitude_MERRA2

Figure 10: A sample of the science Dataset of CALIPSO data products.

The A-Train satellite network has provided a unique platform for scrutinizing PSCs, thanks to the amalgamation of data from CALIOP and almost simultaneous measurements of primary PSC condensable vapors—HNO_3 and H_2O—by the Aura MLS. Further contextual data is offered by ancillary meteorological information sourced from the Modern-Era Retrospective analysis for Research and Applications (MERRA-2) reanalysis products, including Tropopause Altitude (Gelaro et al., 2017) and Aura MLS-derived meteorological products (DMPs) (Manney et al., 2007, 2011a).

CALIOP

The main instrument aboard the CALIPSO satellite, CALIOP, is a dual-wavelength lidar with polarization sensitivity, offering detailed vertical profiles of backscatter coefficients at wavelengths of 532 and 1064 nm (Winker et al., 2009). Figure 1 shows a single day's typical orbital coverage by CALIPSO over the Antarctic polar area, dated 17 July 2008. Figure 2 displays a cross-section of CALIOP 532 nm total attenuated backscatter coefficient readings along one orbit for that particular day, highlighting CALIOP's unique capacity for high-resolution spatial analysis of clouds and aerosols. Though not explicitly engineered for stratospheric observation, PSCs generally result in noticeable increases in CALIOP backscatter profiles, evident at elevations greater than approximately 12 km in the orbital curtain shown in Figure 10.

The CALIOP measurements of the 532 nm perpendicular backscatter coefficient provide additional information on particle shape, from which PSC composition can be inferred. The v2 CALIOP PSC data products are derived from nighttime only CALIOP v4.10 level 1B 532 nm parallel and perpendicular backscatter coefficient measurements; daytime measurements contain elevated background noise due to scattered sunlight, which greatly inhibits the detection of PSCs. Ancillary meteorological data from MERRA-2, including temperature, pressure, ozone

number density, and tropopause height at the CALIOP measurement locations, are included in the CALIOP v4.10 level 1B data products and utilized in the PSC algorithm. Further details on the CALIPSO v4.10 level 1 data processing and calibration approach can be found in Kar et al. (2018).
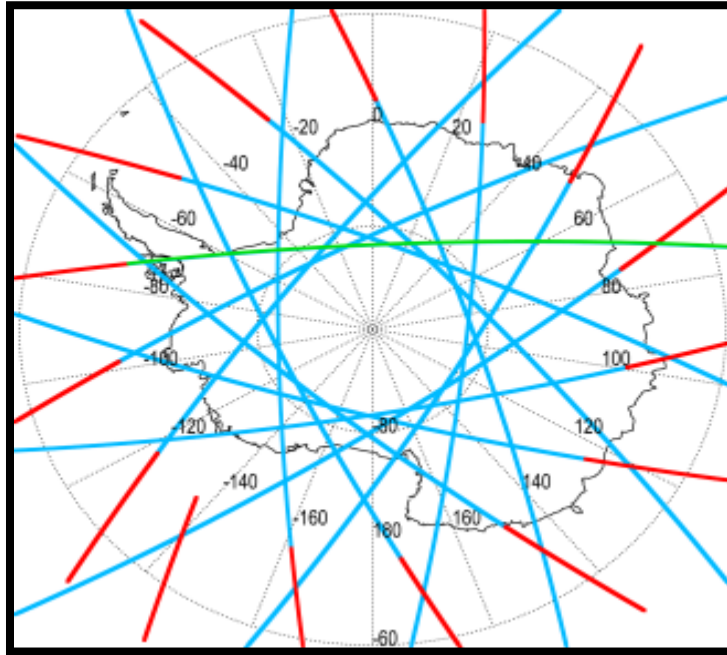
Figure 11: CALIPSO orbital coverage over the polar region of the Southern Hemisphere on 17 July 2008. Blue (red) lines depict nighttime (daytime) orbit segments. The CALIOP curtain along the orbit highlighted in green is shown in Fig.9.
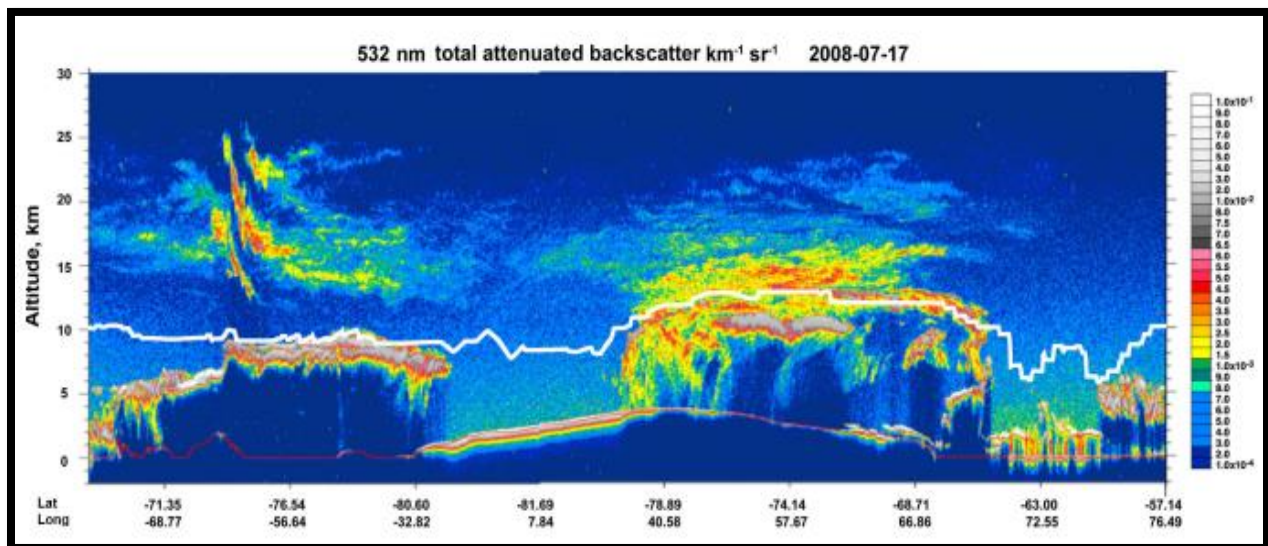

Figure 12: Orbital curtain of CALIOP 532 nm total attenuated backscatter coefficient (km−1 sr−1) along the single orbit highlighted in green in Fig. 1. The MERRA-2 tropopause height is indicated by the solid white line.

The data preprocessing approach was multi-step and aimed at correcting minimal crosstalk between CALIOP's two polarization channels and estimating uncertainties [u(x)] in both fundamental CALIOP measurements and derived values. Initially, nighttime-only profiles from CALIOP v4.10 lidar level 1B with 532 nm attenuated parallel and perpendicular backscatter coefficients were ingested, covering an altitude range of 8.4–30 km. To standardize the resolution, the data were smoothed to a uniform 5 km horizontal by 180 m vertical grid, thereby mitigating the altitude-related variability in the resolution of the CALIOP data initially received (Winker et al., 2007).

Subsequently, corrections were made for molecular and ozone attenuation using MERRA-2 molecular and ozone number density profiles, included in the CALIOP v4.10 level 1B data files. The theoretical relationship by Hostetler et al. (2006) was employed to calculate molecular backscatter (βmol) using the MERRA-2 molecular number density. This, in turn, facilitated the calculation of the 532 nm attenuated scattering ratio. Undertaking this step was crucial for identifying PSCs based on their backscattering characteristics, thereby aiding in the construction of the climatology and the subsequent analysis.

3.2. Methodology

In this study, we employed several key parameters to analyze PSCs. These included PSC areal coverage (km^2), PSC cloud fraction (%), stratospheric temperatures (K), and correlation coefficients. Initially, all raw data were transformed into monthly mean values to facilitate a comprehensive analysis over time.

A pivotal aspect of our methodological approach involved the restructuring of the original raw Level-2 data into a 1° x 1° latitude-longitude grid. This grid configuration, adhering to an equal angle area approach, was chosen to align with the Polar Stereographic Projection. This projection is well-suited for high-latitude studies, as it minimizes distortions near the poles, thereby providing a more accurate spatial representation for polar regions. The reformatting process encompassed 121 distinct vertical layers, ranging from an altitude of 8.5 km to 30 km, ensuring a detailed vertical profile of the atmospheric conditions.

Our dataset covered both the Northern and Southern Hemispheres, with a latitudinal and longitudinal span from 50° to 82°, converted to 50.5° to 81.5°. The decision to adjust the latitudinal and longitudinal degrees to 0.5° increments was strategic. This method was implemented to achieve a more precise representation of geographic areas. By adopting this half-degree increment system, we were able to delineate our study's spatial boundaries with greater specificity. This adjustment enhances the resolution of our analysis, allowing for a finer granularity in detecting and interpreting spatial variations in PSC occurrences. Researchers often employ such modifications in latitudinal and longitudinal degrees to improve the precision of spatial analyses, particularly when studying phenomena that exhibit significant variability over small geographical scales, as is the case with PSCs, where the precision in mapping can significantly impact the interpretation and conclusions drawn from the data.

3.2.1. PSC Detection

For the identification of PSCs, the PSC Composition Dataset was utilized. In the initial phase, PSCs were detected based on their composition values. During this process, entries with values of 0 or -9999 (indicative of missing data) were excluded, while the remaining data, as seen in figure 11, were aggregated. This approach enabled a comprehensive examination of PSCs without segmenting them into their various types.
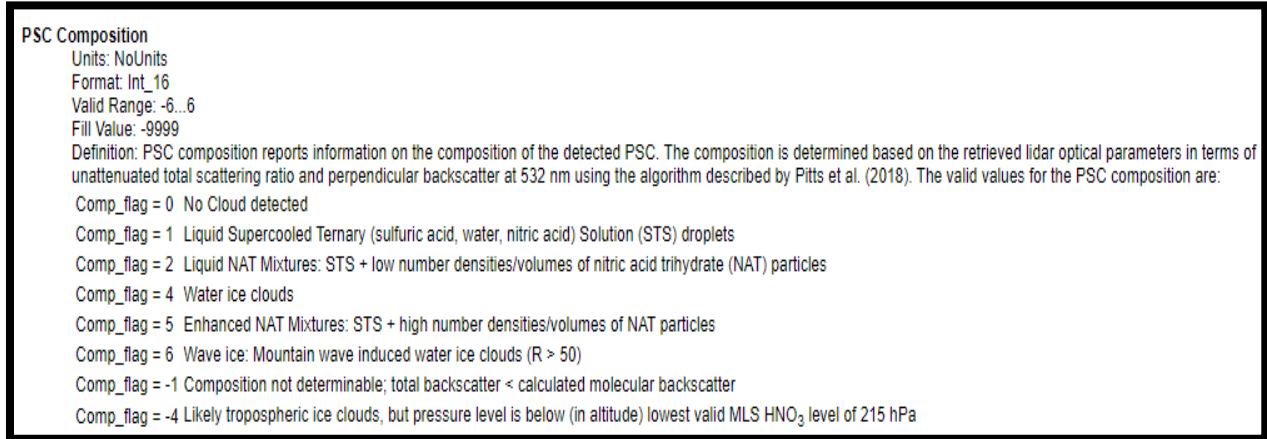
PSC Composition
    Units: NoUnits
    Format: Int_16
    Valid Range: -6...6
    Fill Value: -9999
    Definition: PSC composition reports information on the composition of the detected PSC. The composition is determined based on the retrieved lidar optical parameters in terms of unattenuated total scattering ratio and perpendicular backscatter at 532 nm using the algorithm described by Pitts et al. (2018). The valid values for the PSC composition are:
    Comp_flag = 0 No Cloud detected
    Comp_flag = 1 Liquid Supercooled Ternary (sulfuric acid, water, nitric acid) Solution (STS) droplets
    Comp_flag = 2 Liquid NAT Mixtures: STS + low number densities/volumes of nitric acid trihydrate (NAT) particles
    Comp_flag = 4 Water ice clouds
    Comp_flag = 5 Enhanced NAT Mixtures: STS + high number densities/volumes of NAT particles
    Comp_flag = 6 Wave ice: Mountain wave induced water ice clouds (R > 50)
    Comp_flag = -1 Composition not determinable; total backscatter < calculated molecular backscatter
    Comp_flag = -4 Likely tropospheric ice clouds, but pressure level is below (in altitude) lowest valid MLS HNO_3 level of 215 hPa

Figure 13: The detailed product of the PSC Composition dataset, from which the PSC areal coverage was estimated.

3.2.2. Tropopause height

Information on the height of the tropopause contained in the CALIOP v4.10 level 1b lidar data files originates from the MERRA-2 "blended" tropopause elevations. The MERRA-2 blended tropopause selects the lower of the two altitudes defined by temperature-based ("thermal") and potential vorticity-based ("dynamic") calculations (Bosilovich et al., 2016; Ott et al., 2016). Generally, the dynamic tropopause is the typical choice in mid- and high-latitude regions, whereas the thermal tropopause is more common in tropical areas. Identifying the tropopause in polar regions is often challenging, particularly during polar nights (e.g., Highwood et al., 2000), so caution is advised when using tropopause height data in these areas. Indeed, the shift from upper tropospheric cirrus clouds to polar stratospheric clouds (PSCs) frequently lacks a distinct boundary at the reported tropopause height. As a result, relying on the MERRA-2 tropopause as a strict division between tropospheric cirrus and PSCs could result in incorrect categorization.

Hence, using a criterion to distinguish tropospheric clouds from stratospheric clouds is quite essential. In the present study, according to Pitts et. al, 2018, the criterion for separating stratospheric from tropospheric clouds was that the location of stratospheric clouds needed to be 4 km above the reported tropopause. In Figures 11 and 12, one can observe variations in altitudes below approximately 13 km, where the presence of upper cirrus clouds is discernible. Without the applied criterion, these cirrus clouds could be misinterpreted as PSCs. Utilizing the specific criterion eliminates such ambiguity, ensuring the study is solely concentrated on PSCs, which is the principal focus of this thesis.
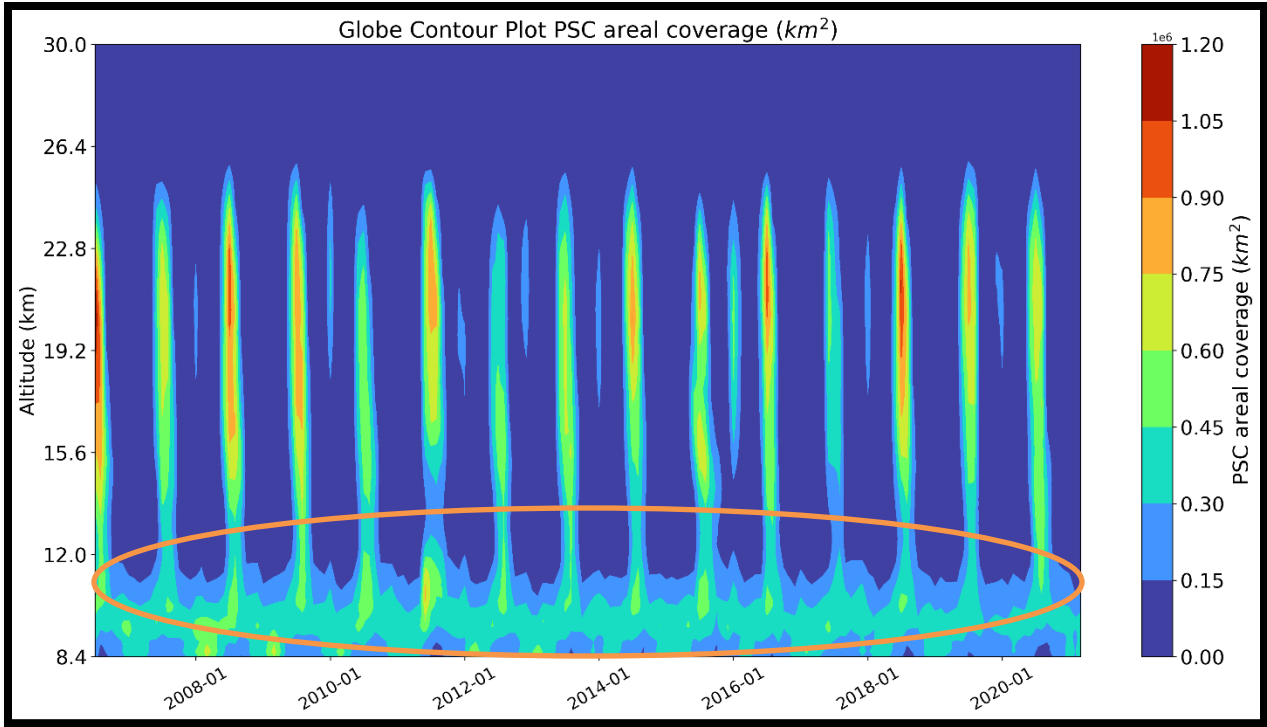
Figure 14: Monthly Hemispherical mean interannual variability of PSCs without the applied criterion.
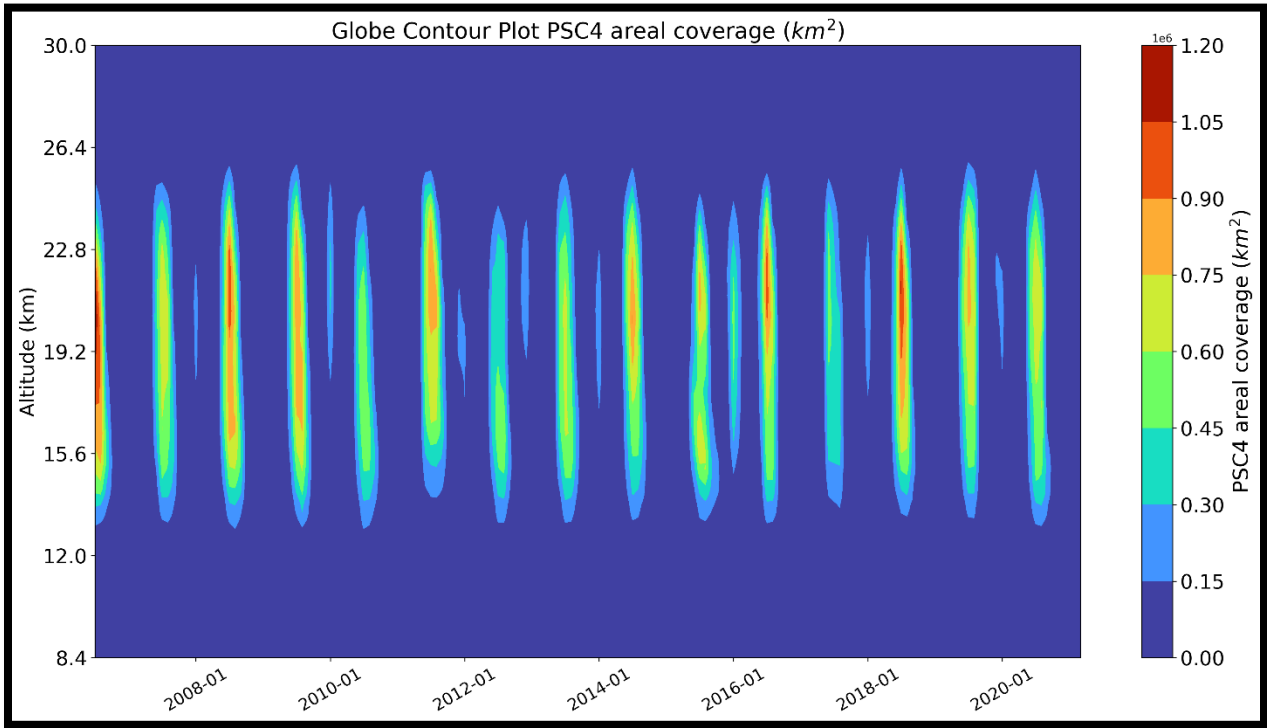

Figure 15: Monthly Hemispherical mean interannual variability of PSCs with the applied criterion.

The visual content presented in figs. 11 and 12 will be thoroughly dissected in the "Results and Discussion" section, as these images constitute the foundational elements of our study that warrant meticulous scrutiny. The reason for displaying them at this juncture is to elucidate the disparities that arise when the criterion is applied versus when it is not. In this context, 'PSC' refers to the detection of PSCs absent any criteria, while 'PSC4' designates the set of PSCs identified under the constraints of the applied criterion. Henceforth, the term 'PSC' within this document shall exclusively denote Polar Stratospheric Clouds as identified in accordance with the established criterion.

3.2.3. PSC areal coverage and cloud fraction

For computing the areal coverage of PSCs, the methodology was predicated on a horizontal resolution of 5 km. Hence, each detection point of a PSC was scaled by an area of 25 km², in alignment with the spatial resolution dimensions of 5 km by 5 km. Consequently, when these detection points were aggregated into a 1x1 degree latitude-longitude grid, all corresponding PSC detection values within that grid were summed. For temporal resolution on a monthly scale, the average of these daily aggregated values was calculated.

Subsequently, we computed another metric called the "Cloud Fraction," which was defined as the PSC areal coverage divided by the total scanned area (number of observations multiplied by the factor of 25 km^2). The number of observations (or counts) is the aggregate of all satellite observations for that grid cell. The factor of 25 km^2 accounts for the 5x5 km horizontal resolution of each observation, thereby converting the detection count into an area-based measure. This calculation provides a relative measure of PSC prevalence within each grid area, useful for understanding the distribution and frequency of these clouds.

This computation was rooted in the understanding that not every Lidar scan within a grid may result in PSC detection. For instance, if a particular grid had 300 Lidar scans in one day, but only 30 scans revealed PSCs, then the PSC areal coverage for that day would be 30 multiplied by 25 km^2. However, this information alone wouldn't offer insight into the Cloud Fraction for that grid. By incorporating the Cloud Fraction metric, we can gain a more nuanced understanding of the proportion of the grid actually covered by PSCs relative to the number of Lidar scans conducted.

This variation can be attributed to the inconsistent number of profiles generated by the Lidar at these specific altitudes. For instance, in a given month with 135 PSC detections at 11 km and 500 counts, the cloud fraction would be approximately 0.27. Conversely, in the subsequent month at the same altitude, with 140 PSC detections but 560 counts, the cloud fraction drops to about 0.25. Hence, even though the PSC areal coverage expands in the latter scenario, the cloud fraction actually decreases. The inconsistency in the number of profiles provided by the satellite on a daily basis in this altitude range contributes to this discrepancy.

This discrepancy will not have an impact on our research. As will be elaborated in the subsequent section, PSCs predominantly form at altitudes exceeding 11-12 km above the Earth's surface, which falls outside the altitude range in question for our study.
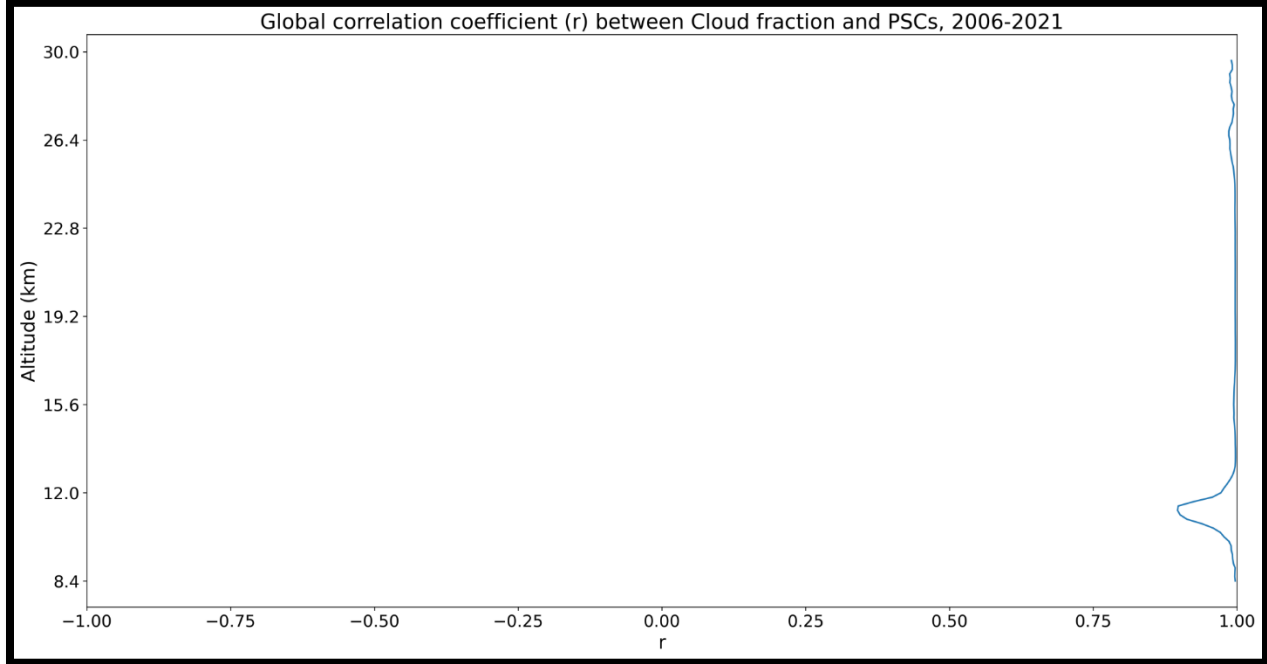
Figure 16: Correlation coefficient of monthly mean values between PSC areal coverage and Cloud fraction.

The lowest value of the correlation coefficient between PSC areal coverage and Cloud fraction is observed at approximately 11 kilometers altitude, with r = 0.9.

3.2.4. Polar Stereographic Projection

Using cloud fraction as our primary metric for graphing the spatial distribution of PSCs helps to mitigate the disparities caused by unequal satellite observation frequencies across different grids, leading to a more accurate and meaningful analysis of the PSC distribution. Thus, representing cloud fraction polar plots (instead of areal coverage) in our analysis of PSCs would indeed be the most appropriate approach. Here's a consolidated reasoning for this decision, considering the aspects of equal angle area grids and the Polar Stereographic projection:

<u>Visualization and Analysis</u>: Visualizing our data on the Polar Stereographic projection, the pole is at the center of the map, with latitudes represented as concentric circles and longitudes as straight lines radiating from the pole. This layout is particularly helpful for displaying the distribution of PSCs around the pole, which is a key area of interest in our study.

<u>Representation of Area and Shape</u>: While this projection does not perfectly preserve areas or shapes, it provides a reasonable compromise, especially near the poles. This means that although the grid cells won't represent equal areas (as would be the case in an equal-area projection), the distortion will be minimal in the polar regions, which are our primary area of interest.

Geographic Orientation: This projection allows for straightforward interpretation of latitudinal and longitudinal data. For our analysis, this means that the cloud fraction data can be accurately mapped to specific geographic locations, aiding in understanding the geographical distribution of PSCs.

Link with the cloud fraction parameter:

Normalization of Satellite Observations: The cloud fraction metric effectively normalizes the PSC detections based on the number of satellite observations in each grid cell. This is particularly important in our case, as not all grids have the same number of satellite observations. By using cloud fraction, we mitigate the impact of this variability, ensuring a more uniform and fair comparison across different grid cells.

Smoothing Spatial Data: When focusing on the spatial distribution, cloud fraction as a parameter can provide a more refined and smoothed representation of PSCs. By reducing the impact of random fluctuations in satellite passes and focusing on the proportion of area affected by PSCs, offers a clearer picture of their geographic spread. It also highlights the relative intensity of PSCs, offering consistent visualization of their spatial distribution.

Revealing Subtle Patterns: Cloud fraction can highlight subtle patterns in PSC distribution that might not be apparent from raw detection counts. For instance, a grid with fewer total observations but a high proportion of those being PSC detections (as previously discussed) might indicate a significant presence of PSCs, a detail that could be overlooked with raw counts.

3.2.5. Sunspots

The initial phase of the analysis entailed constructing a global climatology of PSCs at a monthly mean resolution. Subsequently, these figures were correlated with Stratospheric Temperatures. The final stage involved examining whether a relationship exists between these parameters and the recorded number of sunspots for the specified dataset. Given that sunspot numbers were available on a monthly and yearly mean resolution for a global scale, the correlation analysis was conducted at a monthly and yearly mean resolution for both a global and hemispherical scale.

To achieve this, the mean monthly grid values for PSC areal coverage were aggregated, either at the hemispheric or global level, while the monthly mean values for PSC cloud fraction were computed as the average across all relevant grids.

The monthly mean total sunspot number was obtained by taking a simple arithmetic mean of the daily total sunspot number over all days of each calendar month. Monthly means were available only since 1749 because the original observations compiled by Rudolph Wolf were too sparse before that year. (Only yearly means are available back to 1700). For the purposes of this study, the dataset of interest spanned from July 2006 to March 2021.
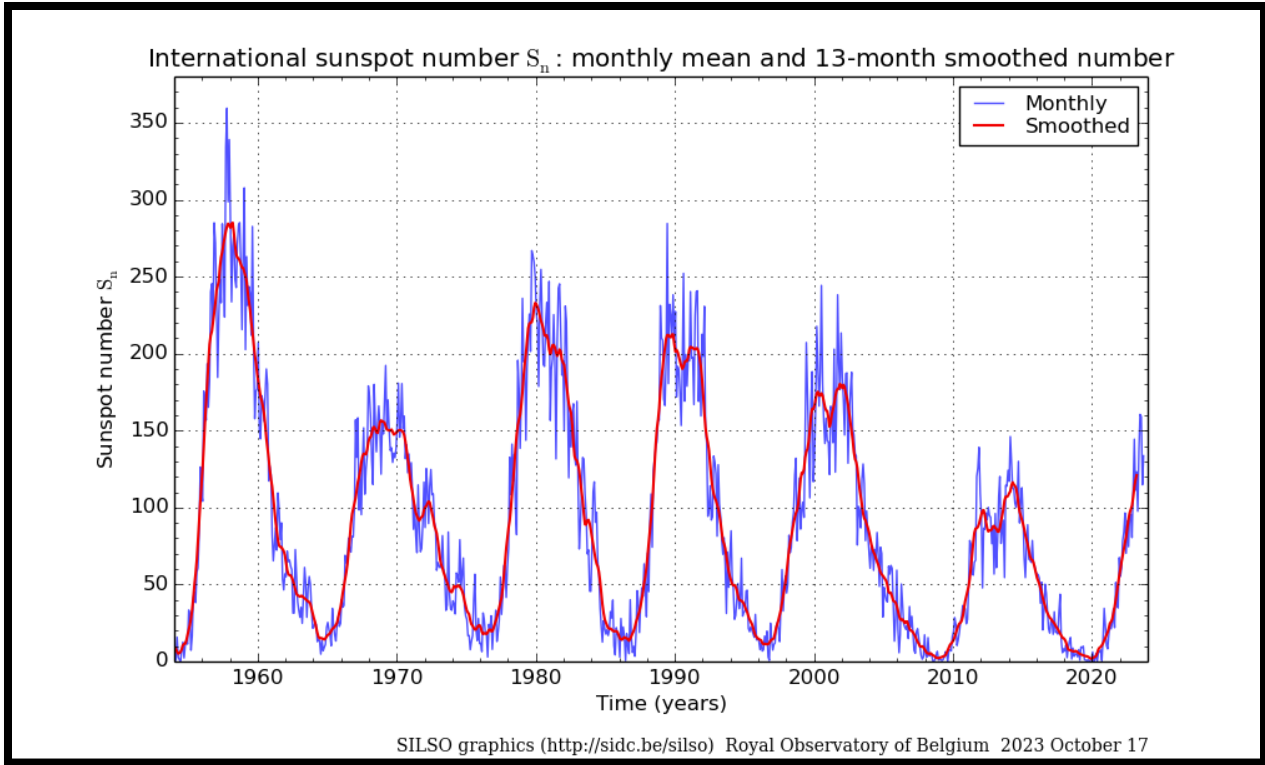
Figure 17: The monthly mean sunspot number (blue) and 13-month smoothed monthly sunspot number (red) for the last six solar cycles.

In Figure 14, the last six solar cycles are depicted. A noticeable trend of diminishing sunspots per solar cycle is evident upon examining the mean monthly global analysis. Within the timeframe of our CALIPSO dataset, starting in July 2006, the sunspot count was fewer than 50 and dipped to almost zero by 2009. The solar maximum peaked at approximately 120 sunspots in 2015, followed by a minimum in the cycle occurring in 2020. Therefore, the available CALIPSO dataset encompasses almost one and a half cycle with an entire solar cycle, starting in 2009 and concluding in 2020.

4. Results and Discussion

This section is divided into distinct subsections, each focusing on a different aspect of findings. We begin with an exploration of PSC climatology (Section 4.1), where we discuss the spatial distribution, seasonal and vertical variations, and the interannual trends observed in PSCs. This is followed by an analysis of stratospheric temperatures (Section 4.2), looking at their seasonal and vertical distribution and interannual variations. A significant aspect of this study is the investigation of correlations (Section 4.3), presenting an examination of the relationship between PSCs and stratospheric temperatures, alongside exploring the potential connections between stratospheric temperatures and sunspot activities, and finally assessing the correlation between sunspots and PSCs.
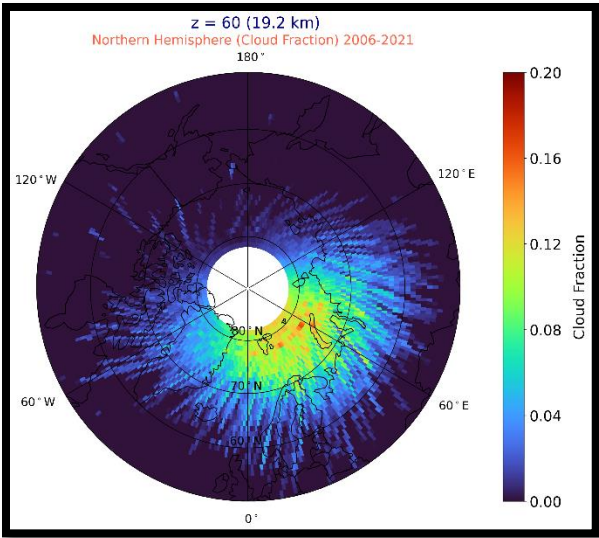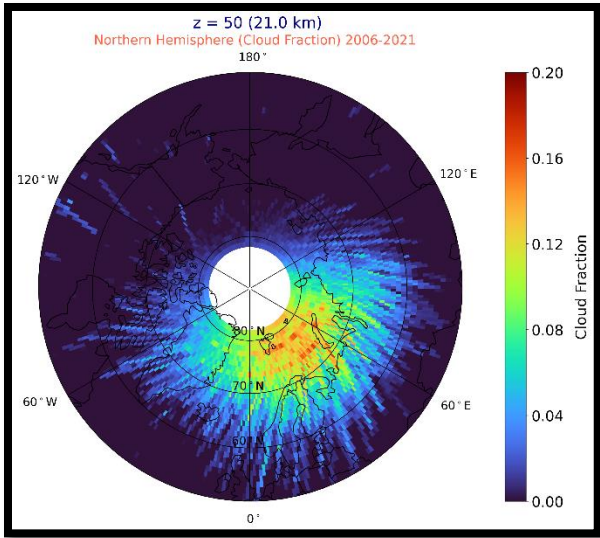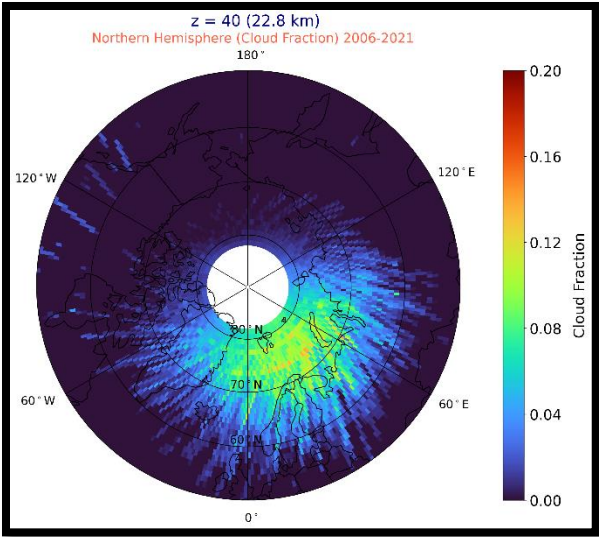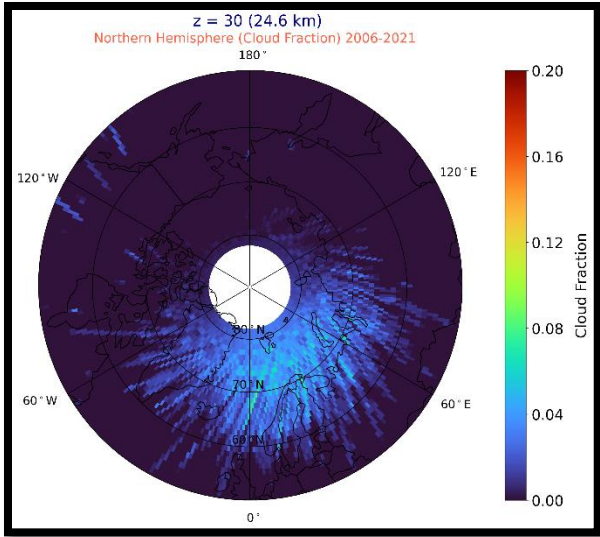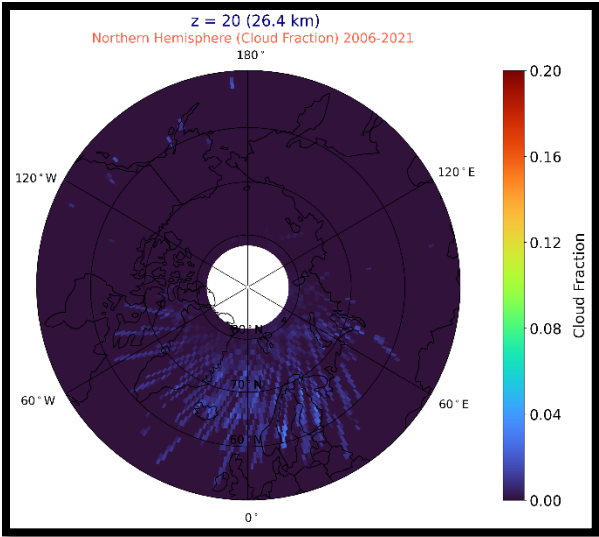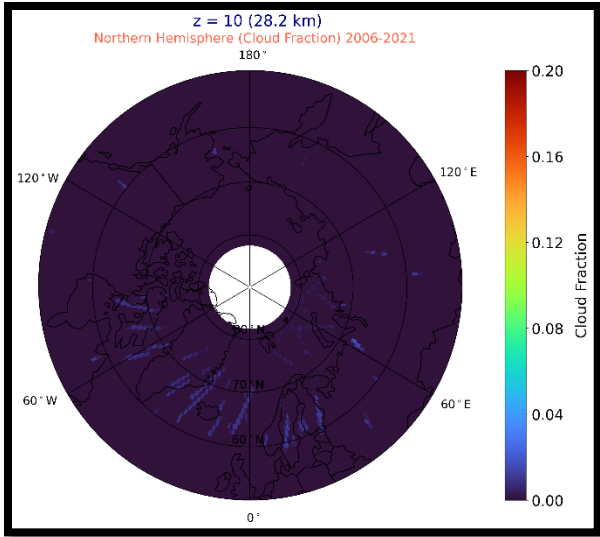
4.1. PSC Climatology

The climatological analysis of PSCs is structured into three distinct subsections: spatial, seasonal, and interannual. The spatial analysis primarily utilizes the cloud fraction (or occurrence frequency) parameter, which, as previously discussed, is the most effective metric for geographically pinpointing PSCs. Complementary to this, Appendix A includes figures illustrating the spatial distribution of PSCs, at the altitude of their maximum occurrence, based on their areal coverage in square kilometers. The remaining subsections concentrate on the areal coverage aspect of PSCs, encompassing both the Northern and Southern Hemispheres. These subsections delve into the vertical distribution and interannual variations of PSCs, offering a comprehensive view of their behavior and spread across different altitudes and over time.

4.1.1. Latitude-longitude distribution
NORTHERN HEMISPHERE

The spatial distribution of PSCs in the Arctic exhibits a quite consistent pattern from year to year, predominantly spanning longitudes from approximately 60° W to 120° E. This distribution is clearly depicted in the 16-year average Arctic PSC occurrence frequency maps presented in Figure 16. This region aligns with the climatologically preferred position of the Arctic vortex over recent decades, as noted in studies such as Zhang et al., 2016. The location of the vortex has been influenced by increased activity of zonal wavenumber 1, which displaces the vortex towards Eurasia from the North Pole.

According to Zhang et al., 2016, over the past three decades, the wintertime Arctic stratospheric polar vortex has weakened, leading to a greater likelihood of cold surface air from high latitudes moving into the middle latitudes. While this trend is established, it remains unclear if there has also been a persistent shift in the vortex's location due to Arctic climate change, and what implications such a shift might have for the climate system. The Arctic polar vortex has consistently moved towards the Eurasian continent and away from North America mainly during February over these three decades. This shift is closely linked to enhanced zonal wavenumber-1 waves, a response to the loss of Arctic sea ice, especially over the Barents–Kara seas.

z = 10 (28.2 km)
Northern Hemisphere (Cloud Fraction) 2006-2021

z = 20 (26.4 km)
Northern Hemisphere (Cloud Fraction) 2006-2021

z = 30 (24.6 km)
Northern Hemisphere (Cloud Fraction) 2006-2021

z = 40 (22.8 km)
Northern Hemisphere (Cloud Fraction) 2006-2021

z = 50 (21.0 km)
Northern Hemisphere (Cloud Fraction) 2006-2021

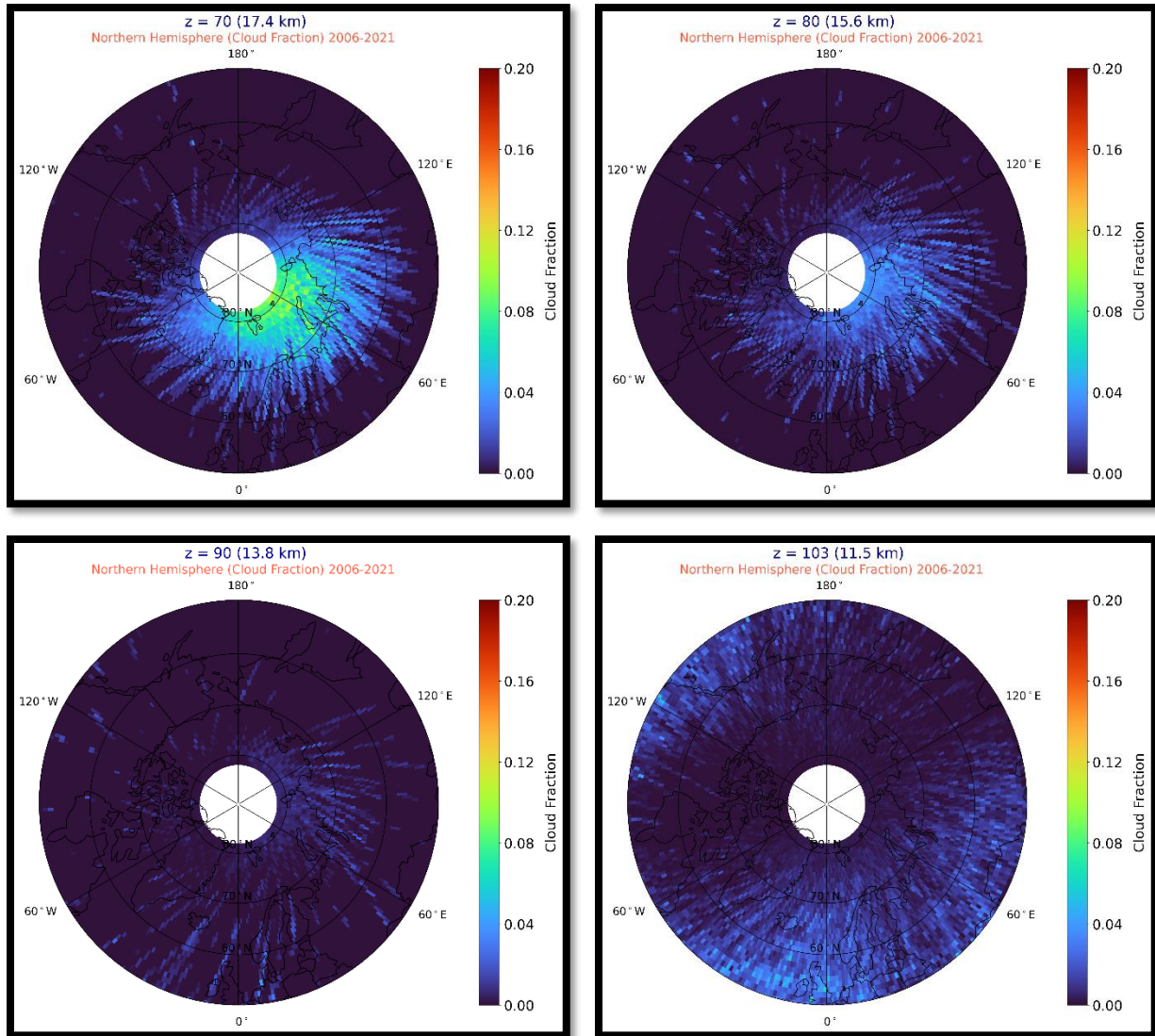z = 60 (19.2 km)
Northern Hemisphere (Cloud Fraction) 2006-2021

Figure 18: Sixteen-year average (2006-2021), polar maps of Arctic PSC occurrence frequency at: a) z=28.2 km, b) z=26.4 km, c) z= 24.6km, d) z= 22.8 km, e) z=21 km, f) z=19.2 km, g) z=17.4 km, h) z=15.6 km, i) z=13.8 km, j) z=11.5 km.

Additionally, increased Eurasian snow cover may have contributed to this shift. It has been found that this repositioning of the vortex leads to localized cooling in parts of the Eurasian continent and North America, partially counteracting the tropospheric warming observed in these regions over the last thirty years. The future implications of a potential vortex shift due to ongoing sea-ice loss, and its subsequent impact on climate, warrant further attention to refine predictions of future climate change.

The highest frequency of Arctic PSCs, averaged across the four key Arctic PSC months from December to March, peaks at the altitude of 21 km above sea level. This is followed by a secondary maximum at 11.5 km, after which the frequency gradually declines to nearly zero PSCs below 10 km. The PSC occurrences at these two altitudes, 21 km and 11.5 km, exhibit

distinct characteristics. At 21 km, the prime zone for PSC formation extends from 60ºW to 120ºE, with the highest concentration observed from 0º to 60ºE and above 70ºN. In contrast, at 11.5 km, the spatial distribution of PSCs is more diffuse, lacking a clearly defined longitudinal preference and tending to occur at lower latitudes. At the intermediate altitude of 13.8 km, PSCs are relatively scattered across the Northern Hemisphere, with the frequency of occurrence dropping to almost zero over a substantial portion of the Northern Hemisphere. In the region extending from 120° East to 120° West, at latitudes below 70° and altitudes above 13 km, PSCs are almost entirely absent. At altitudes above 28 km, as depicted in Figure 16, there is a notable absence of observed PSCs, reaching zero values at 28.5 km.

At this point, it is essential to highlight that the definition of PSCs can vary based on different criteria. Distinguishing PSCs from upper cirrus clouds is not always straightforward. As per studies like Polyakov et al. 2007, PSCs are often identified at altitudes above 15km. This study follows, as discussed in section 3.2, the approach of Pitts et al. 2018, adopting the +4km above the tropopause criterion. However, this does not imply that all observations at these altitudes are exclusively PSCs. The secondary maximum at 11.5km, for instance, likely represents a combination with upper cirrus clouds, as described in McCormick et al. 2007, who observed that cirrus clouds can vertically extend into the stratosphere quite often. Nonetheless, for this analysis, the findings are presented as they are analyzed with the 4km criterion, and it is up to the reader to apply their preferred interpretation of what constitutes PSCs.

Continuing, to gain a more comprehensive understanding of the spatial distribution of PSCs, monthly mean polar maps for the four key Arctic PSC months (Figures 17-20) are presented, focusing on two critical altitudes for each month:
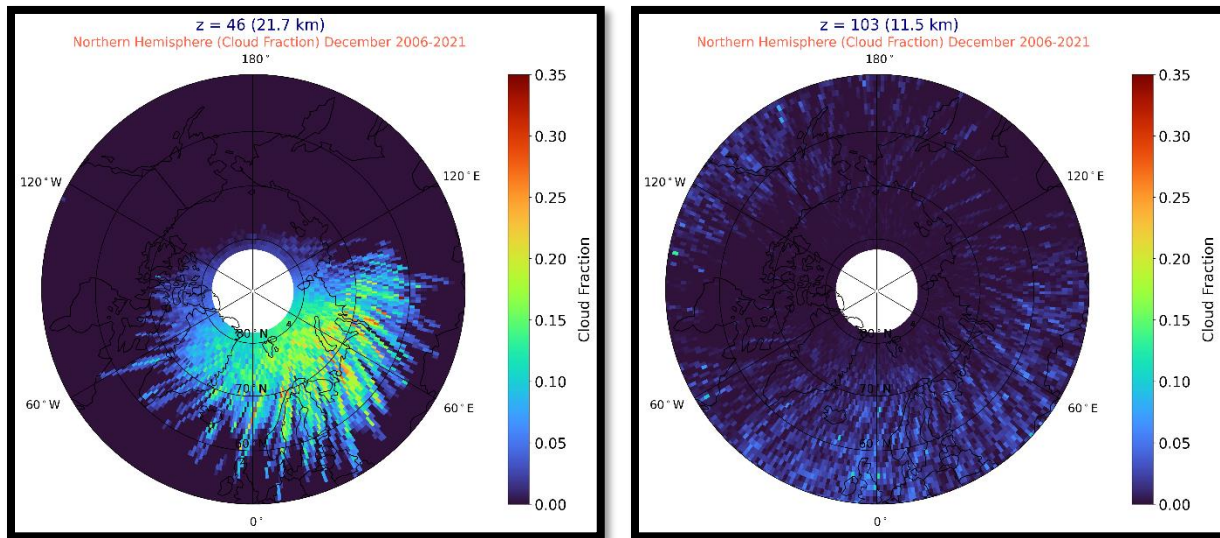

Figure 19: Fifteen-year average (2006-2020), monthly mean polar maps of December of Arctic PSC occurrence frequency at: a) z=21.7 km, b) z=11.5 km.

The distribution of PSCs over the Northern Hemisphere for the average December (2006-2020), as presented in Figure 17, aligns closely with their sixteen-year average distribution. At the altitude of 21.7 km, the highest occurrence frequency is observed for this month, particularly in regions above 70ºN and spanning longitudes from 60ºW to nearly 120ºE. Specifically, there are areas between 10ºW and 100ºE exhibiting an occurrence frequency of 0.35, the highest value noted for this parameter in average December. In contrast, the region extending from 120ºE to 60ºW, and at latitudes below 70ºN, shows an almost negligible frequency of PSC occurrence. For the secondary maximum, PSC distribution is more dispersed, with the highest occurrence frequencies reaching approximately 0.1 in several scattered areas, primarily at latitudes below 70º.
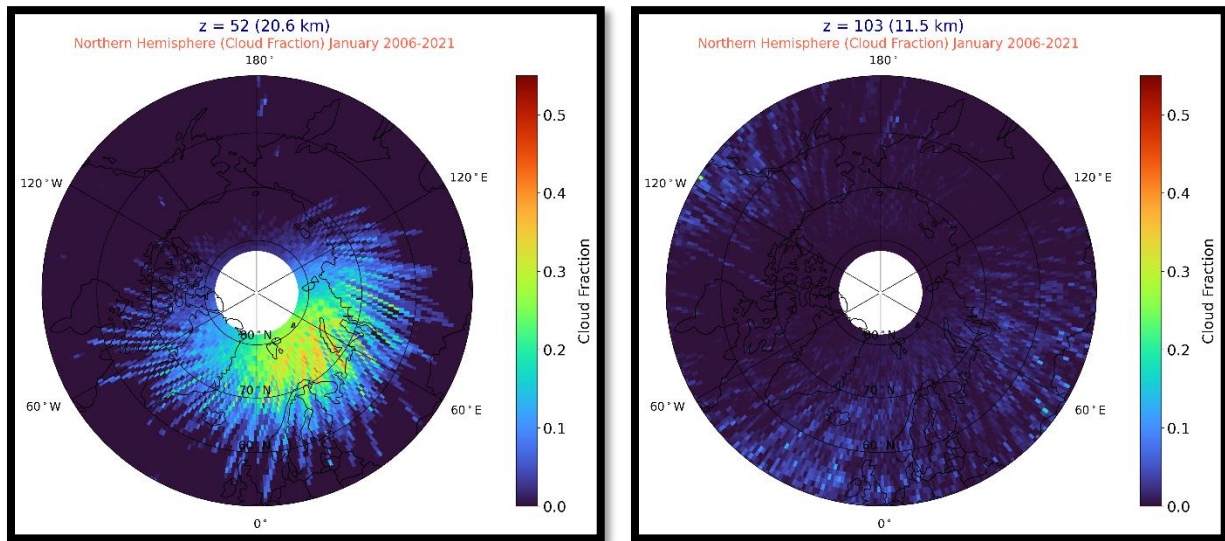

Figure 20: Fifteen-year average (2007-2021), monthly mean polar maps of January of Arctic PSC occurrence frequency at: a) z=20.6 km, b) z=11.5 km.

In average January (2007-2021) conditions, as shown in Figure 18, the distribution of PSCs exhibits its highest occurrence frequency at the altitude of 20.6 km above sea level, with a secondary peak at 11.5 km, as observed in the average December as well. At 20.6 km, a preferential area for PSC formation is observed, notably above the northernmost Norwegian Sea and the Barents-Kara Seas. The most significant concentrations are found in the region spanning 0° to 60° East, at latitudes above 70°, with occurrence frequency values to reach almost 0.52. For the 11.5 km altitude, the distribution aligns closely with the sixteen-year average, showing PSCs dispersed across various regions, with maximum values of PSC occurrence frequencies to be in the range of approximately 0.20 to 0.25. This pattern indicates certain areas with higher PSC densities, such as the region from 40° West to 20° East, and another from 140° to 100° West.

The peak in PSC frequency of occurrence at 20.6 km during January suggests that this altitude is quite conducive for PSC formation in this month, exhibiting the greatest areal coverage over the Northern Hemisphere. This finding will be further presented and discussed in the subsequent subsection.
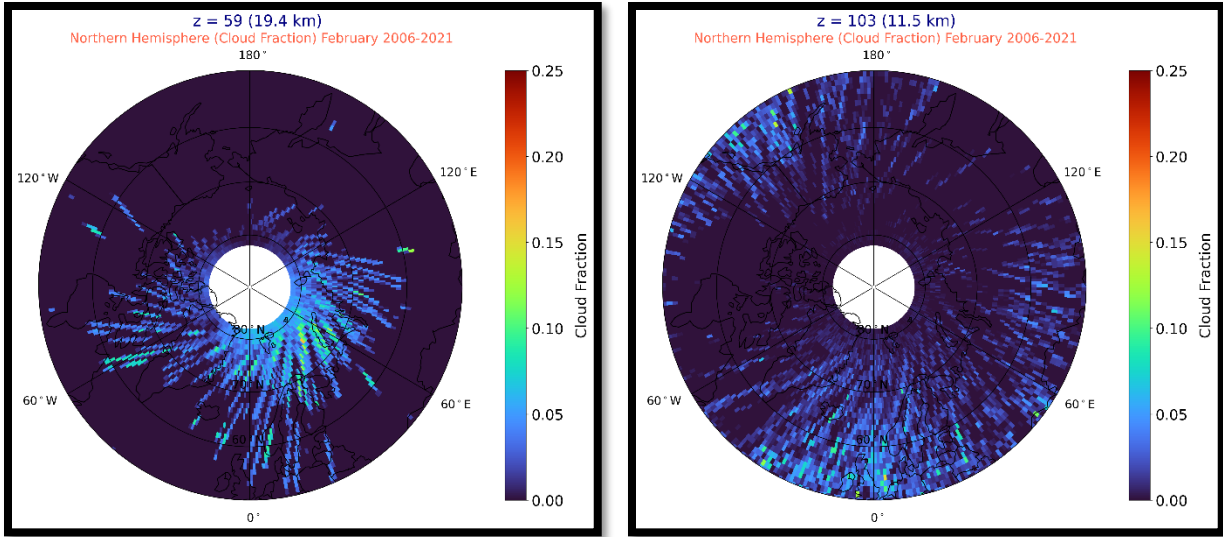
Figure 21: Fifteen-year average (2007-2021), monthly mean polar maps of February of Arctic PSC occurrence frequency at: a) z=19.4 km, b) z=11.5km.

The overall pattern for the average February indicates that the maximum PSC occurrence frequency is located at 19.4 km, with specific regions exhibiting a peak occurrence frequency of approximately 0.25 (e.g at 12.2 and 12.4km). These areas of heightened PSC activity are predominantly concentrated in the broader region north of 60°N latitude and span longitudes from 120°W to 110°E, and more specifically above the Barents-Kara seas. Regarding the secondary peak at 11.5 km, the general pattern mirrors that observed in average December and January. However, during this time, regions with high PSC occurrence frequency reach values ranging approximately from 0.13 to 0.18.
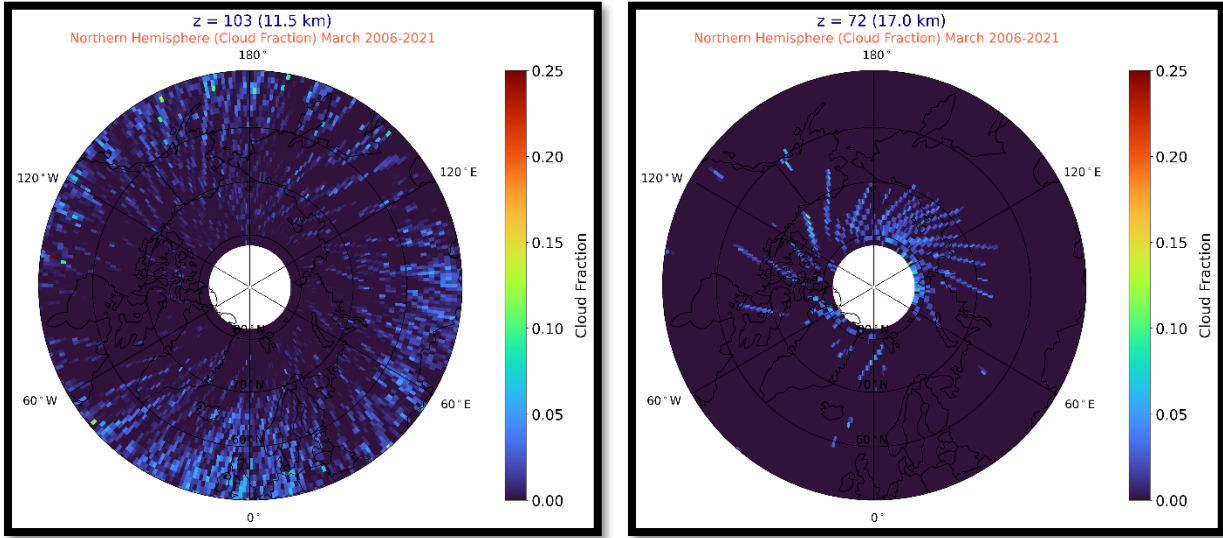

Figure 22: Fifteen-year average (2007-2021), monthly mean polar maps of March of Arctic PSC occurrence frequency at: a) z=11.5 km, b) z=17 km.

Concluding the latitude-longitude analysis of the Northern Hemisphere with the average for March, the results present intriguing points for discussion. In this month, the altitude exhibiting the maximum PSC occurrence frequency shifts to 11.5 km, which was previously identified as the secondary peak in earlier analyses, followed by a secondary peak at 17 km. The highest values of PSC occurrence frequency at 11.5 km reach approximately 0.25 for latitudes below 70°N, scattered in various regions of the map. Regarding the secondary peak at 17 km, the maximum PSC occurrence frequency is observed to be around 0.1. Over the Kara-Barents Seas, the PSC occurrence frequency is almost zero for both altitudes of 11.5 km and 17 km.

Delving deeper into the results, the average hemispherical values of PSC frequency of occurrence are detailed for the critical altitudes corresponding to the two peaks (the primary maximum and the secondary):

- December: At an altitude of 21.7 km, the average PSC frequency of occurrence for the entire hemisphere is 0.035, and at 11.5 km, it is 0.006.

- January: At 20.6 km, the average frequency is 0.055, and at 11.5 km, it is 0.006.

- February: At 19.4 km, the average frequency is 0.011, and at 11.5 km, it is 0.006.

- March: At 11.5 km, the average frequency is 0.004, and interestingly, at the altitude of 17 km, it drops to 0.002.

The purpose of this analysis is to statistically evaluate the likelihood of encountering PSCs at any location in the Northern Hemisphere, given a specific altitude and month. This approach provides a measure of understanding regarding the frequency of PSC occurrences. For example, in January at an altitude of 21.7 km, there is a 3.5% chance of observing a PSC. Conversely, in March at an altitude of 17 km, the probability of spotting a PSC in any location drops to 0.2%.
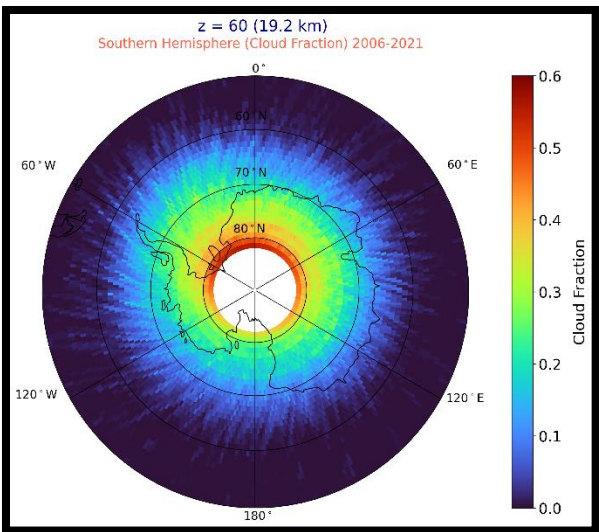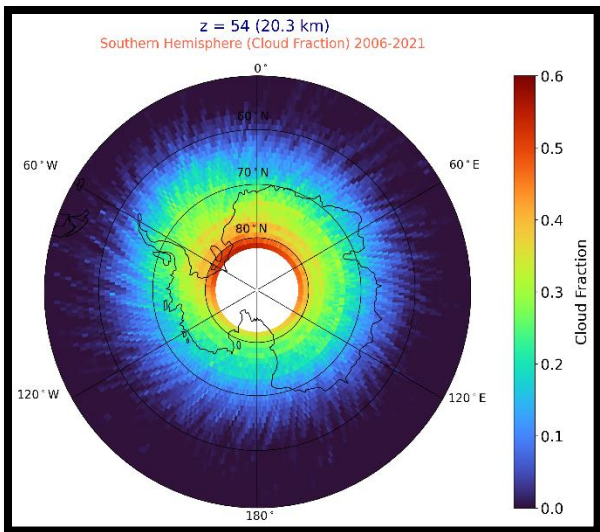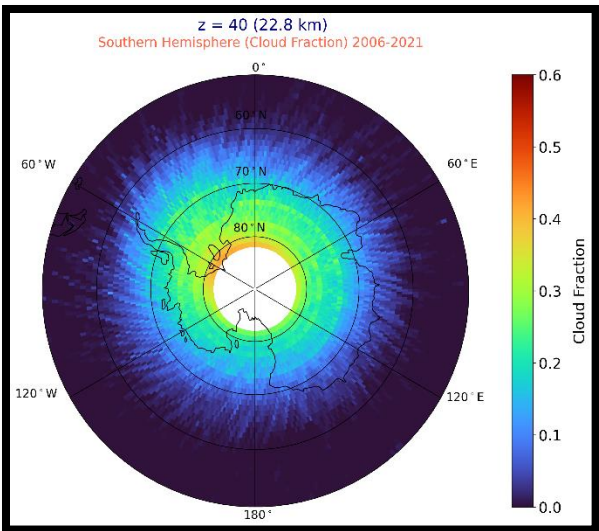
Our findings largely come to an agreement with the existing literature on the spatial distribution of PSCs. For instance, Polyakov et al. 2007, who analyzed data from SAGE III covering the period from 2002 to 2005, concluded that PSCs are generally observed within the longitudinal zone from 120°W to 100°E, though they did not delve further into these results. This area is quite large and corresponds to the latitudinal zone 65º – 80º N. More significantly, our results align more closely with the detailed and recent analysis by Pitts et al. 2018. This study suggests that PSCs are primarily confined to the region from 60°W to 120°E, analyzing data from CALIPSO for the period 2006 to 2017. This area corresponds to the climatologically favored location of the Arctic vortex in recent years, further validating our findings. In their paper, they also examined the eleven-year monthly mean average for December and January. Their analysis revealed that in the approximate range from 120°E to 120°W, at around 20 km altitude, PSCs are almost absent. This finding aligns with our analysis for the same months over the extended period from 2006 to 2021, indicating a consistent pattern of PSC scarcity in this specific region and altitude range.

SOUTHERN HEMISPHERE

Figure 21 displays the frequency of PSC occurrences over a 16-year period, as compiled from the CALIOP Antarctic data record, averaged for the six key Antarctic PSC months from May to October. According to Pitts et al. 2018, the highest frequency of PSCs is typically found at latitudes near the vortex edge, where there is an ideal mix of adequate condensable materials and cold temperatures. PSC occurrences are not uniformly distributed across either geographic or equivalent latitude coordinate systems; rather, they show distinct longitudinal patterns. The distribution of PSC occurrence frequency and the associated cold pool is not uniformly centered around the pole. Instead, it is displaced slightly off the pole towards the Greenwich Meridian (GM) longitude quadrant. The analysis conducted on the distribution and frequency of occurrence of Southern Hemisphere PSCs over the period from 2006 to 2021 indicates that PSCs tend to form preferentially in a specific region of Antarctica, resembling a curtain-like area. The core area of PSC activity is typically located in a sector near the base of the Antarctic Peninsula.

The increased PSC activity in the vicinity of the Antarctic Peninsula can be attributed to frequent mountain wave events in the region, as noted by Alexander et al. (2011) and Hoffmann et al. (2017b), along with prevalent large-scale upper tropospheric forcing events at these longitudes, as identified by Kohma and Sato (2013). According to Wu and Jiang (2002), it is well-established that gravity waves frequently occur in this region and are closely associated with the formation of PSCs. While gravity waves may play a significant role in the formation of the observed PSCs, it is also probable that synoptic-scale tropospheric disturbances contribute to this process by impacting stratospheric temperatures, thereby influencing PSC development. These disturbances can alter atmospheric dynamics, leading to conditions conducive for PSC formation, such as temperature drops in the stratosphere.

The highest frequency of Antarctic PSCs, averaged over the six key Antarctic PSC months from May to October, reaches its peak at the altitude of 20.3 km above sea level, just 0.7 km below the Northern Hemisphere's maximum. A secondary maximum is observed at 11.5 km, beyond which the frequency steadily decreases to almost zero below approximately 10 km. The PSCs at these two altitudes, 20.3 km and 11.5 km, demonstrate unique characteristics. In analyzing PSC distribution over the Southern Hemisphere, the altitude of 11.5 km will not be further explored due to the lack of significant aspects for analysis. Only the values of PSC occurrence frequency will be provided, without an extensive analysis of their horizontal distribution. At this altitude, PSCs appear to be dispersed across the hemisphere, showing no significant variations or noteworthy patterns. PSCs become noticeably present below 26 km, with frequency values reaching approximately 0.1 to 0.15, just before they start increasing at lower altitudes. At 24.6 km, PSCs begin to establish a distribution over the Southern Hemisphere, attaining their highest frequencies within the latitudinal "ring" of 80°N, ranging from 0.15 to 0.25. Concentrating on the altitude of maximum frequency at 20.3 km, the preferred area for PSC formation spans from 120°E to 120°W. The most intense concentration is found between 90°E and 90°W, and latitudes greater than 70ºS.

z = 10 (28.2 km)
Southern Hemisphere (Cloud Fraction) 2006-2021

z = 20 (26.4 km)
Southern Hemisphere (Cloud Fraction) 2006-2021

z = 30 (24.6 km)
Southern Hemisphere (Cloud Fraction) 2006-2021

z = 40 (22.8 km)
Southern Hemisphere (Cloud Fraction) 2006-2021

z = 54 (20.3 km)
Southern Hemisphere (Cloud Fraction) 2006-2021

z = 60 (19.2 km)
Southern Hemisphere (Cloud Fraction) 2006-2021
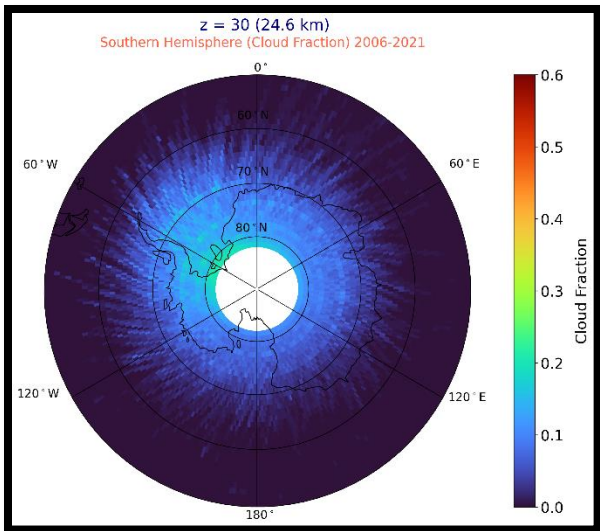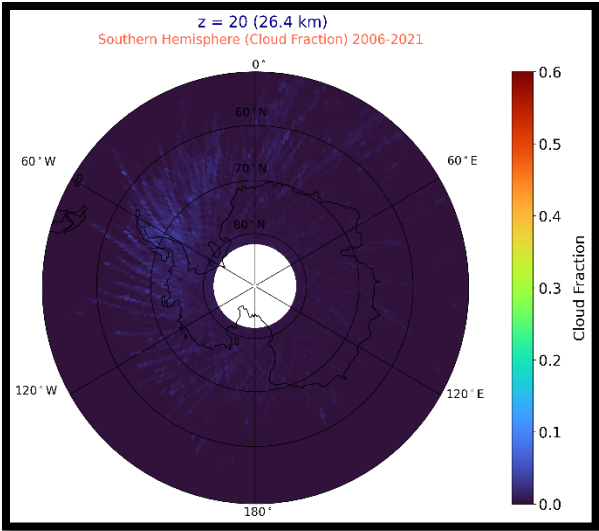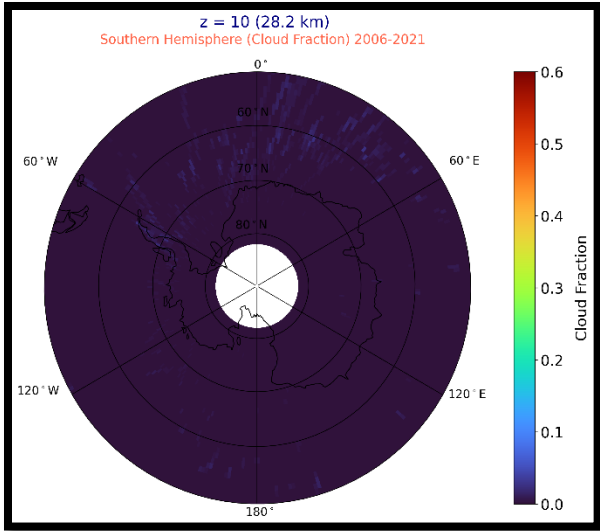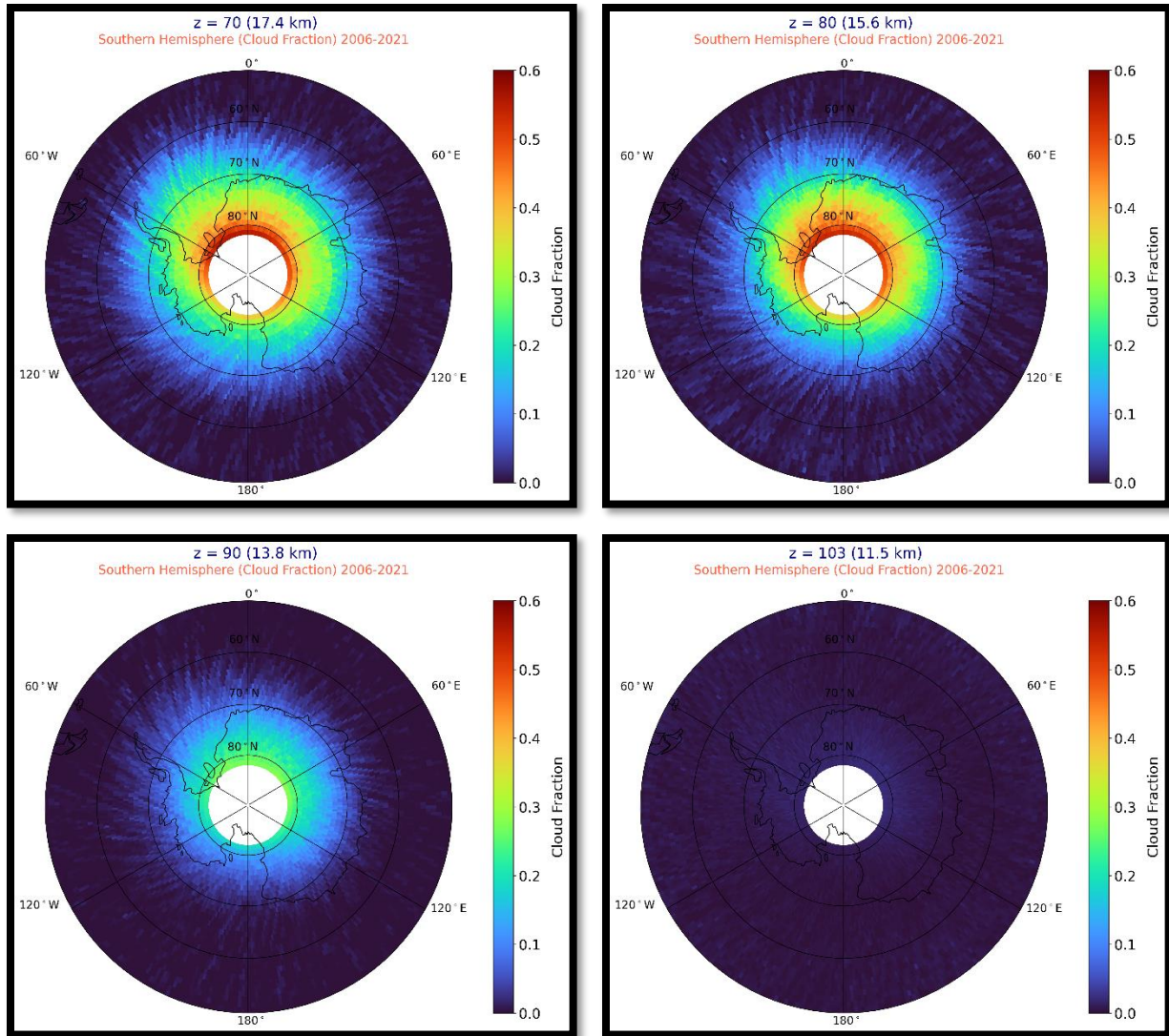
Figure 23: Sixteen-year average (2006-2021), polar maps of Antarctic PSC occurrence frequency at: a) z=28.2 km, b) z=26.4 km, c) z= 24.6km, d) z= 22.8 km, e) z=20.3 km, f) z=19.2 km, g) z=17.4 km, h) z=15.6 km, i) z=13.8 km, j) z=11.5 km.

At altitudes of 19.2 km, 17.4 km, and 15.6 km, PSCs consistently appear in the same area across the Southern Hemisphere. A notable difference is observed between the altitude with the maximum PSC occurrence frequency and the region around 17 km. At this altitude, PSCs exhibit higher occurrence frequencies at latitudes above 75°S, while showing lower frequencies below 70°S. As altitude decreases below 13 km, PSCs gradually become less frequent, dwindling to almost zero at altitudes lower than 11 km. It is important to highlight that at altitudes above 18 km, the region extending from 120°W to 120°E within the latitudinal zone of 50°S to 60°S exhibits nearly zero occurrence frequency of PSCs.
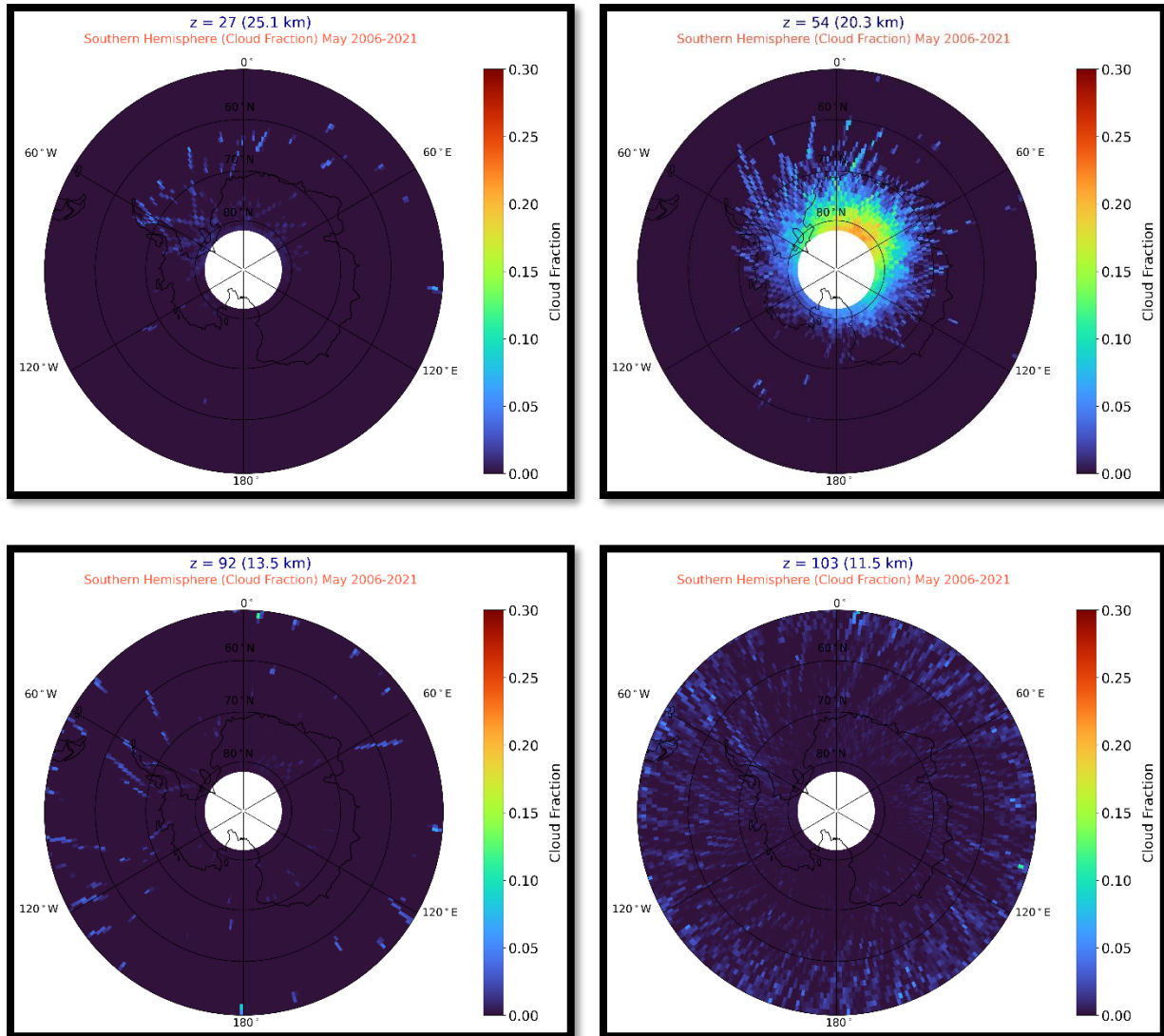
Figure 24: Fourteen-year average (2007-2020), monthly mean polar maps of May of Antarctic PSC occurrence frequency at: a) z=25.1 km, b) z=20.3 km, c) z=13.5 km, d) z=11.5 km.

In May, Figure 22, PSCs are primarily observed at latitudes south of approximately 70°S. Their altitude range extends from 11 km to almost 25 km, with the peak frequency of occurrence at about 20.5 km. The highest frequency of occurrence, approximately 25%, is noted at the most extreme latitudes, particularly in regions spanning from the Greenwich Meridian to 60°E. The epicenter of PSC formation is centrally located within this region, around 30°E. May marks the onset of the PSC season in the Southern Hemisphere, and it is observed that at 20.3 km, the altitude of their highest occurrence, PSCs do not form at latitudes below 70°S across a broad 240° region from 60°E to 60°W. The most favorable altitude range for PSC formation lies between 19 and 21 km, where their occurrence frequency values exceed 20%. Regarding the average hemispheric frequency of PSC occurrence at 20.3 km, it stands at approximately 2%. However, this frequency diminishes to 0.1% at 25 km and further decreases to 0.04% at 13.5 km.

Figure 25: Fourteen-year average (2007-2020), monthly mean polar maps of June of Antarctic PSC occurrence frequency at: a) z=26.7 km, b) z=20.5 km, c) z=18.1 km, d) z=11.5km.

In June, Figure 23, PSCs are observed at latitudes southward of approximately 60°-65°S, extending from near the tropopause to altitudes of about 26-27 km. The highest mean occurrence frequency, surpassing 80%, is recorded near 18 km at the highest latitudes. Specifically, frequencies reach approximately 83% within the latitudinal ring from 78°S to 82°S. These high occurrence frequencies persist at around 80% for altitudes between 17 and 20 km. An intriguing aspect of PSC spatial distribution is observed at two different altitudes: 18.1 km and 20.5 km. At 18.1 km, PSCs tend to form more easterly compared to their formation at 20.5 km. The epicenter of PSC formation at 18.1 km is approximately around the Greenwich Meridian, while at 20.5 km, it shifts to around 15°W. At 18.1 km, where the highest frequency exceeds 80%, the average hemispheric frequency is about 17.5%, whereas at 20.5 km, it exceeds 18.5%. At an altitude of 26.7 km, the average hemispheric occurrence frequency dramatically reduces to 0.2%.
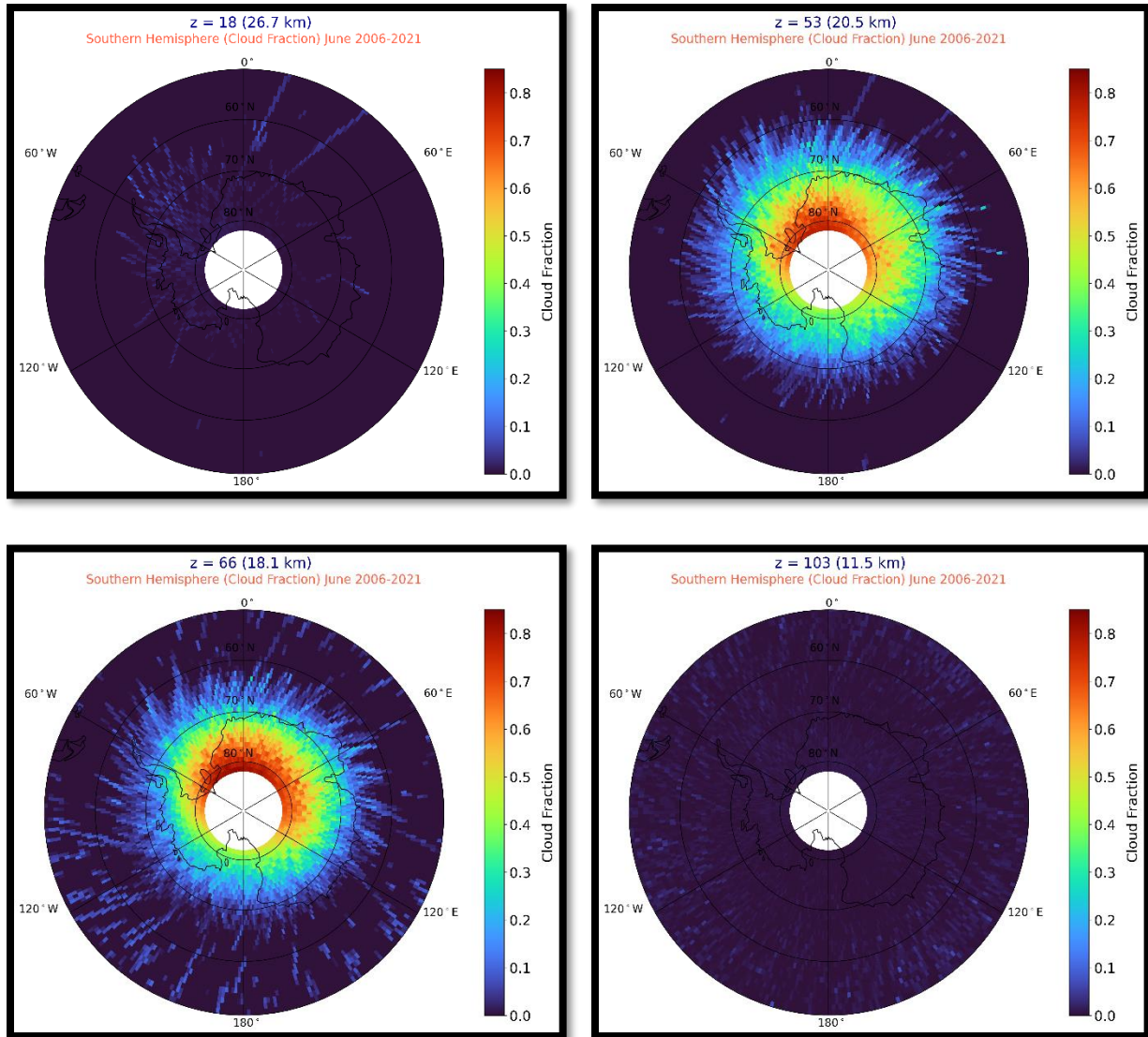
Figure 26: Fifteen-year average (2006-2020), monthly mean polar maps of July of Antarctic PSC occurrence frequency at: a) z=27.1 km, b) z=21.2 km, c) z=16.3 km, d) z=11.5km.

During July (Figure 24) and August (Figure 25), the occurrence of PSCs reaches its peak, with the region of highest frequency expanding both in altitude and latitude. This expansion is attributed to the progressive cooling of the polar vortex, as detailed by Pitts et al. (2018). July, in particular, displays a potential double peak in occurrence frequency at different altitudes: a primary peak near 16 km and a secondary one at 21 km. At the altitude of 16.3 km, the highest frequency of PSC occurrence, nearing 85%, is observed at extremely high latitudes (greater than 78°S), while the average hemispherical frequency of occurrence at this altitude is around 25%. Conversely, at 21.2 km, the highest frequency of occurrence, approximately 82.5%, spans a much broader area compared to that at 16.3 km. The average hemispherical frequency of occurrence at this altitude is about 30.5%, suggesting that 21.2 km might be the altitude with the maximum PSC areal coverage (analyzed in section 4.1.2.).

In terms of spatial distribution, there are notable differences between these two altitudes. At 16.3 km, most PSCs are concentrated at latitudes above 70°S, particularly over Queen Maud Land, while at 21.2 km, PSCs are distributed over a wider area, extending from the pole to around 60°-65°S, with the epicenter above the Weddell Sea, near the southernmost point of the Antarctic Peninsula. The optimal altitude range for PSC occurrence in these months is broader than in previous months, spanning from around 15 km (with an average hemispherical occurrence frequency of about 20%) to 24 km (where the average hemispherical frequency again reaches 20%), with the highest PSC occurrence ranging from 70% to 85%. Above 27 km, PSCs start to diminish, with the average hemispherical occurrence frequency dropping to 0.2%, till they reach almost zero at 28 km. This pattern underlines the dynamic nature of PSC distribution in response to atmospheric conditions over the Southern Hemisphere's winter months.
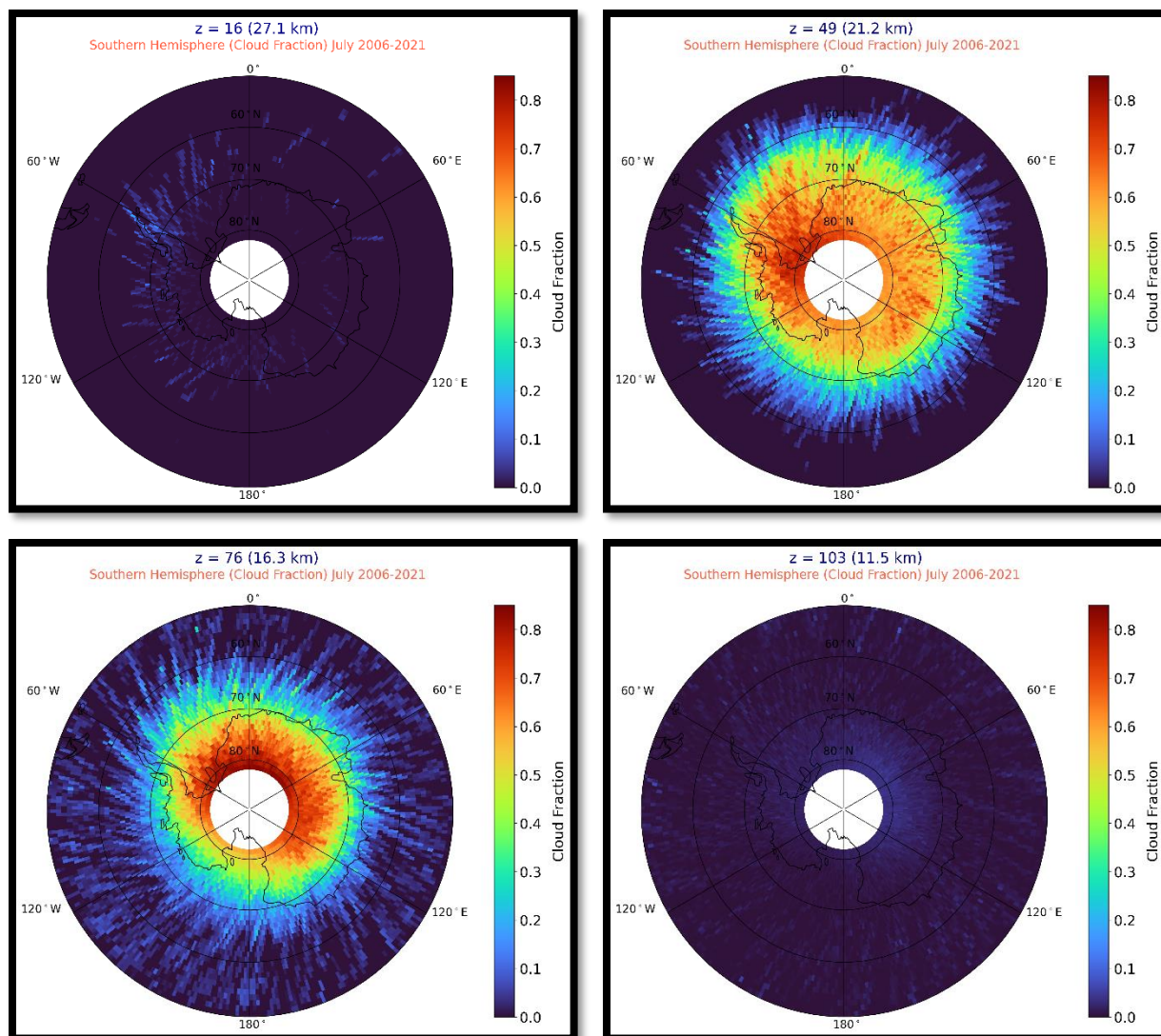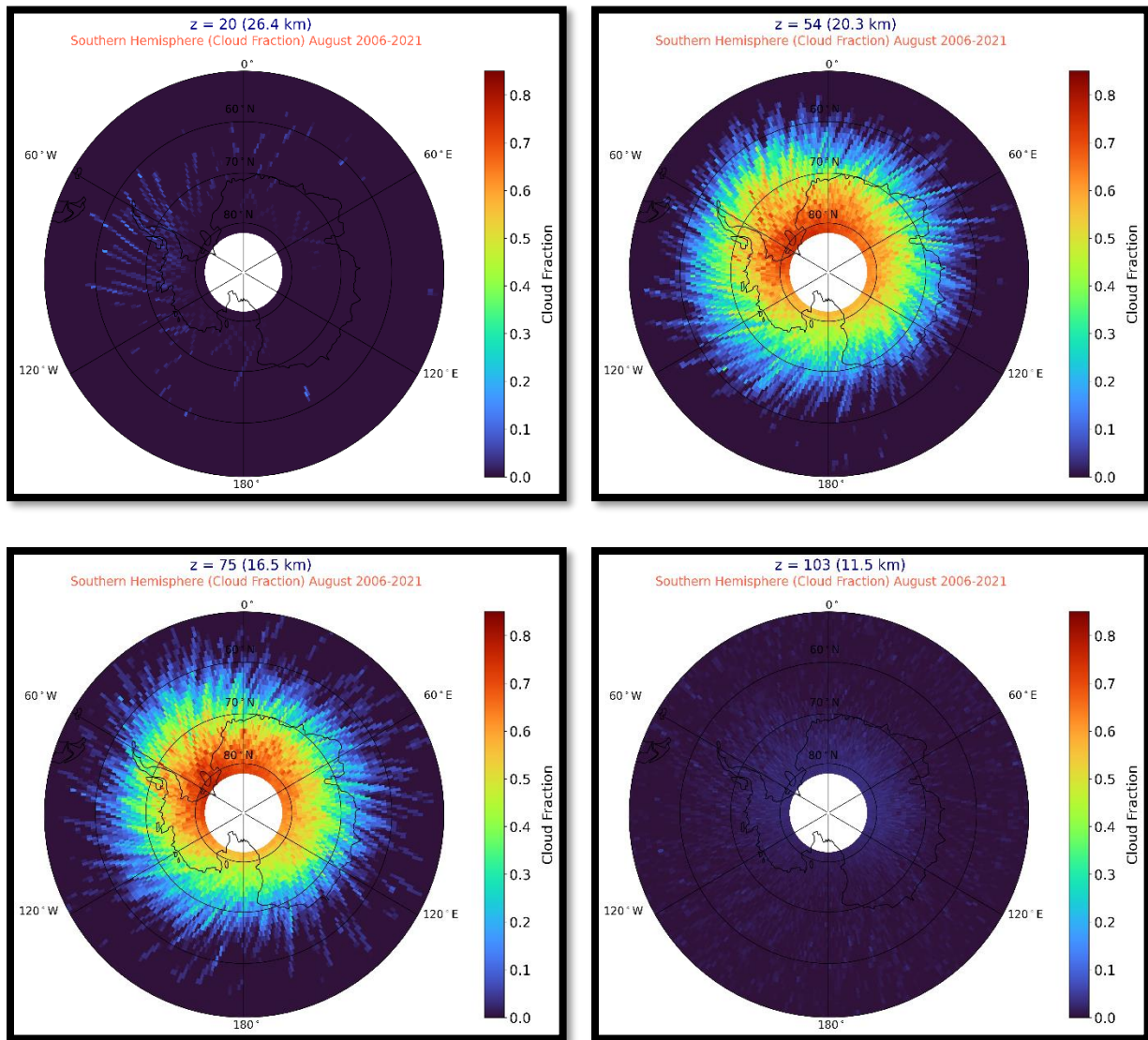

Figure 27: Fifteen-year average (2006-2020), monthly mean polar maps of August of Antarctic PSC occurrence frequency at: a) z=26.4 km, b) z=20.3 km, c) z=16.5 km, d) z=11.5 km.

In August, as shown in Figure 25, the spatial distribution of PSCs exhibits a more uniform pattern at altitudes with the highest occurrence frequency. The epicenter of this distribution is located above the Weddell Sea, near the southernmost point of the Antarctic Peninsula, similar to observations made in July. The majority of PSCs appear to form at latitudes south of 65°S, with the most favorable longitudinal region spanning from 60°E to 120°W. This region is centered above the southernmost part of Graham Land on the Antarctic Peninsula

Additionally, there is a notable double peak in occurrence frequency with altitude: the primary peak for high latitudes is at 16.5 km, with a secondary peak observed at 20.3 km. At 16.5 km, the highest frequency of PSCs reaches 80%, while at 20.3 km, it attains 76%. The average hemispherical frequency at 16.5 km is approximately 24%, and at 20.3 km, it increases slightly to 25%. The most favorable altitude range for PSC formation is identified as being from 15 km to 22 km, where the average hemispherical frequency is around 20%, with the highest occurrences ranging from 70% to 75%. However, at 26.4 km, the average hemispherical frequency significantly decreases to 0.02%, and it approaches nearly zero at an altitude of 27 km. This pattern highlights the varied nature of PSC distribution in August, with specific altitudinal ranges demonstrating particularly high frequencies of occurrence.

Figure 28: Fifteen-year average (2006-2020), monthly mean polar maps of September of Antarctic PSC occurrence frequency at: a) z=15.4 km, b) z=11.5 km.

In September, Figure 26, there is a noticeable decrease in PSC occurrence, evident in both frequency and spatial extent. A significant concentration of PSCs, with frequency surpassing 60%, is observed only at 15.4 km in the latitude range of 78°-82°S. During this month, PSC occurrences are largely restricted to altitudes below 24 km. As noted by Pitts et al. (2018), this pattern is due to warming in the vortex at higher altitudes. Observations confirm a systematic downward shift in the altitude of the peak zonal mean PSC occurrence, descending from approximately 18–20 km in June to below 16 km by September.

The spatial distribution of PSCs in September typically favors latitudes south of 60°S, particularly in the longitudinal range from 45°E to 120°W. Outside this zone, PSCs can be found at latitudes below 60°S. The average occurrence frequency of PSCs at 15.4 km is around 12%, but this frequency drops to 0.2% at approximately 24 km. Frequencies approach zero at altitudes above 25-26 km, highlighting the altitudinal and latitudinal limitations of PSC formation as the Southern Hemisphere transitions from winter to spring.

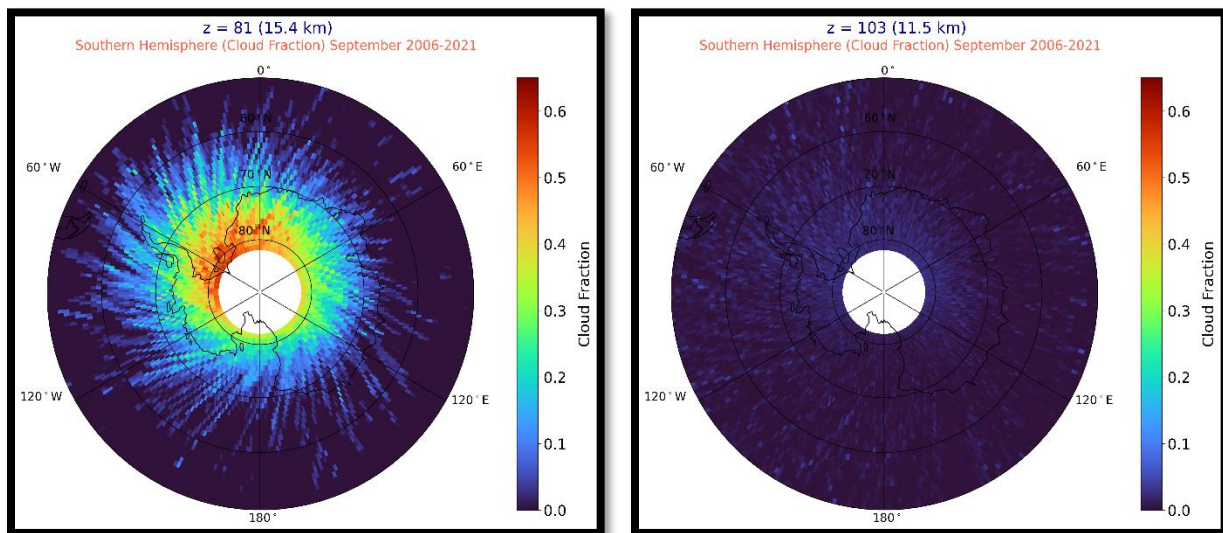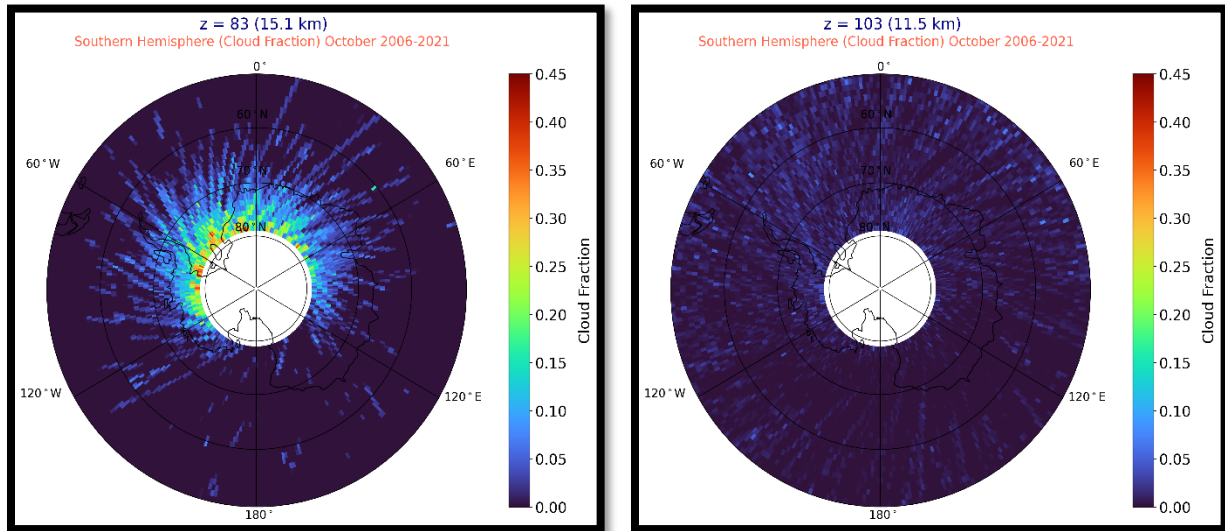*Figure 29: Fifteen-year average (2006-2020), monthly mean polar maps of October of Antarctic PSC occurrence frequency at: a) z=15.1 km, b) z=11.5 km.*

October, Figure 27, marks the end of the Southern Hemisphere's PSC season. During this month, the most favorable altitude range for PSC occurrence is between 14 and 17 km, with the peak occurrence frequency observed at 15.1 km. However, the frequency values do not exceed 45%, and such high occurrences are limited to just a few scattered grids at latitudes above 75°S, within the longitudinal zone stretching from the Greenwich meridian to 100°W. Typically, high frequencies of PSC occurrence, ranging between 15-20%, are located in the southernmost part of the Antarctic Peninsula, barring a few exceptions, such as the previously mentioned maximum of 45%. The maximum average hemispherical frequency of PSC occurrence at 15.1 km is approximately 2.5%, but this frequency declines to almost zero for altitudes above 20 km and below 10 km. A comparison between May, the initial month of the Southern Hemisphere PSC season, and October, the closing month, reveals a notable shift. PSCs have moved significantly westward in their spatial distribution by October compared to their positioning in May, indicating a seasonal shift in their geographic occurrence within the Southern Hemisphere.

As noted by Pitts et al. (2018), the frequency of upper tropospheric cirrus cloud occurrence exceeds 10-15% throughout the season at all latitudes, making it particularly challenging to distinguish upper cirrus clouds from PSCs at lower altitudes, where their characteristics can overlap, leading to potential ambiguities in their identification and analysis.

Compiling the statistical data on the frequency of occurrence for the Southern Hemisphere's PSC season yields the following results:

- **May**: The highest frequency of occurrence is at 20.6 km altitude, reaching 23%. The maximum average hemispherical occurrence at 20.3 km is 2%.

- **June**: The peak frequency is observed at 18.1 km, registering 83.3%. The maximum average hemispherical occurrence at 20.5 km is 18.5%.

- **July**: The highest frequency is noted at 16.3 km with a value of 85%. The maximum average hemispherical occurrence at 21.2 km is 30.5%.

- **August**: The peak frequency occurs at 16.5 km, with a value of 80%. The maximum average hemispherical occurrence at 20.3 km is 24.5%.

- **September**: The highest frequency of occurrence is at 15.4 km, reaching 61%. The maximum average hemispherical occurrence at the same altitude is 12%.

- **October**: The peak frequency is observed at 15.1 km, with a value of 45%. The maximum average hemispherical occurrence at 15.2 km is 2.5%.

Starting with an earlier study by Polyakov et al. (2007), which analyzed data from SAGE III for 2002-2005, they suggested that in the Southern Hemisphere, PSCs were typically observed within a 120° longitudinal sector centered at 40°W. Palm et al. (2005), focusing on PSC distribution during September and October, found most PSCs concentrated over central Antarctica and the Weddell Sea, reaching latitudes around 60°S.

Our results particularly resonate with the detailed and recent study by Pitts et al. (2018). They observed that in June, PSCs were mainly seen poleward of about 65°S, peaking at 18 km with frequencies exceeding 60% (compared to our finding of over 80%). They also noted peak PSC occurrences in July and August, expanding in both altitude and latitude, which our study corroborates. Their study hinted at a potential double peak in occurrence frequency in July and August, which we have further investigated and confirmed in our research. For September, Pitts et al.'s findings align with those of Polyakov and Palm, indicating a significant decline in PSC occurrence, consistent with our observations of PSCs being primarily confined to high latitudes and altitudes below 23-24 km. Our study extends this observation, noting PSC persistence at altitudes up to 24 km and the last occurrences up to 26 km.

Crucially, Pitts et al. did not include analyses for May and October, the beginning and end of the Southern Hemisphere PSC season, which our study addresses. The differences between our work and previous studies can be attributed to various factors, including: (i) Use of different satellite data, (ii) Different study periods and (iii) Different resolution of results (monthly mean versus daily mean values).

4.1.2. Vertical distribution

Compiling the data from PSC detection, this section focuses on analyzing the vertical distribution of PSCs in both the Southern and Northern Hemispheres. The analysis spans a 16-year mean and average monthly data from December through March and from May through October. Moving forward, the discussion will shift from the frequency of PSC occurrence to the spatial coverage of PSCs in square kilometers (km^2), assessed for each atmospheric layer, beginning at 8.4km extending up to 30km in altitude, as indicated by the satellite data products. Notable differences in PSC areal coverage between the two hemispheres are highlighted, providing a clearer picture of their hemispherical spread. The mean seasonal evolution of Arctic and Antarctic PSC areal coverage from 2006 to 2021 is illustrated in Figures 29 and 35.

The method for distinguishing between PSCs and cirrus clouds, as previously discussed, follows the criterion of being +4 km above the tropopause, in line with Pitts et al. (2018), noting that upper cirrus clouds typically exist at altitudes below about 12 km. Therefore, any reference to PSCs below this altitude should be approached with caution to avoid potential misidentification. The challenge in differentiating these cloud types necessitates presenting our findings based on the established filtering criterion. It is left to the discretion of the reader to interpret whether clouds at altitudes below 12km, e.g. at 11.5km, can be considered as PSCs or cirrus clouds, or a combination of them. However, it is reasonably certain that at altitudes above 13 km, most detected clouds can be classified as PSCs. This approach to cloud identification allows for a more enhanced understanding of their areal coverage climatology impact.
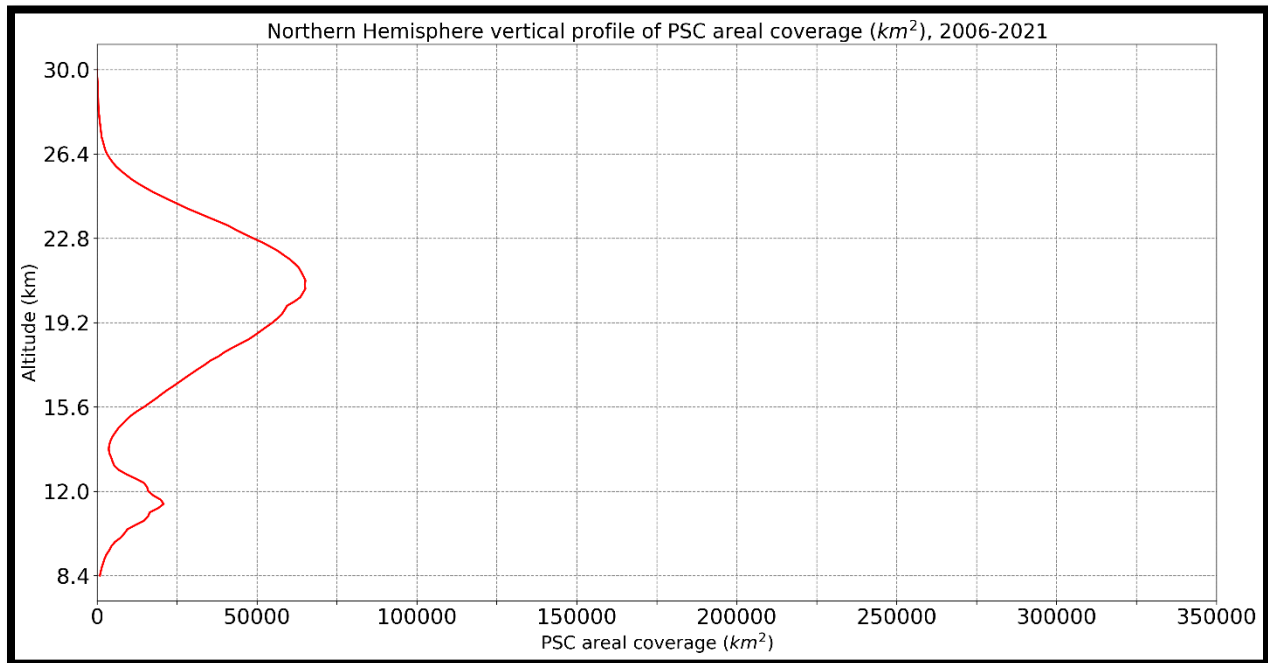
NORTHERN HEMISPHERE

Figure 30: Vertical Profile of the Average PSC areal coverage of the Northern Hemisphere for the period 2006-2021.

As depicted in Figure 28, the average spatial coverage of PSCs in the Northern Hemisphere for the period 2006-2021 reveals two distinct peaks. The primary maximum is observed at the altitude of 21 km, where the spatial coverage of PSCs is approximately 65,000 km². The secondary peak occurs at 11.5 km, covering an area of around 21,000 km² of the Northern Hemisphere's surface. Notably, the spatial coverage dips to its minimum value of about 3,500 km² at the intermediate altitude of around 14 km. Above 25 km, PSC coverage starts to decrease to less than 10,000 km², and this value further reduces to around 1,000 km² at altitudes exceeding 27 km. This overview of PSC spatial coverage provides an initial insight into their distribution pattern across various altitudes in the Northern Hemisphere, highlighting the altitudinal zones where PSCs are most and least prevalent.
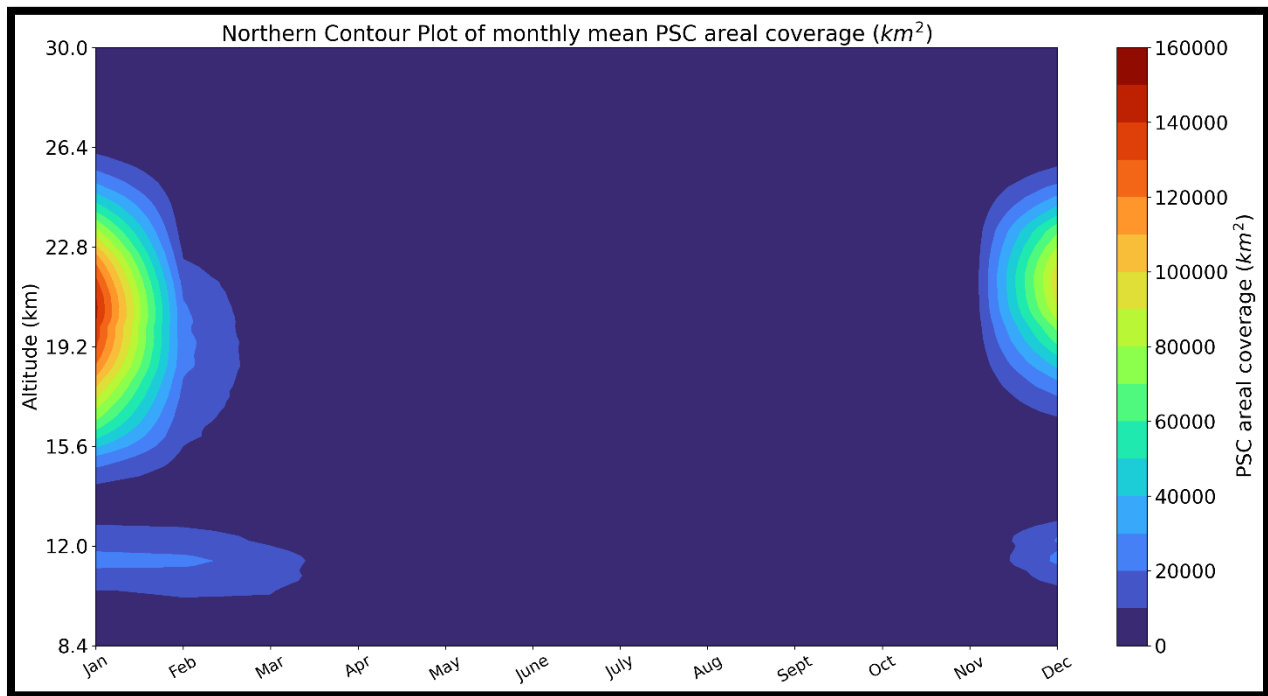
Figure 31: Sixteen-year mean monthly PSC areal coverage over the Arctic, as a function of altitude.

As we examine the sixteen-year mean monthly areal coverage of PSCs over the Arctic during the key months from December to March, a clear seasonal pattern emerges. PSC formation begins in early December, reaching peak values in January. Subsequently, there is a gradual decline to lower coverage values in late February, leading to a significant diminishment by March. This trend is evident in Figure 29, particularly at the altitude range of 13-14 km, where the presence of PSCs is minimal, indicating a notable gap in their vertical distribution. This observation allows for a distinction between lower altitude PSCs and those at higher altitudes. Such a separation is crucial for our analysis, as it aids in understanding the vertical stratification of PSC occurrence and provides insights into the dynamics of PSC formation and dissipation throughout the Arctic winter and early spring, which will be further discussed in the subsection 4.1.3.

Figure 30 presents the vertical profile of the average December, illustrating the dual peak pattern characteristic of the Northern Hemisphere's PSC vertical distribution. In this depiction, the primary peak is observed at an altitude of 21.7 km, where the spatial coverage of PSCs reaches nearly 100,000 km². Meanwhile, a secondary peak is noted at 11.5 km, with spatial coverage approximating 22,000 km². A particularly noteworthy aspect is the marked decrease in PSC spatial coverage within the 14-15 km altitude range, where values plummet to less than 1,000 km². This dramatic drop highlights a distinct gap in PSC presence at these mid-range altitudes. Additionally, similarly low values are observed at higher altitudes, particularly beyond 26-27 km, suggesting that PSCs start to become scarce or vanish altogether at these elevations. This pattern provides valuable insights into the altitudinal limits of PSC occurrence during the early winter month of December in the Northern Hemisphere.

Figure 32: Vertical Profile of the Average December PSC areal coverage of the Northern Hemisphere for the period 2006-2020.

In January, as illustrated in Figure 31, a two-peak pattern of PSC distribution, similar to that observed in the average December and the general spatial coverage profile of the Northern Hemisphere, is again evident. The primary peak occurs at 20.6 km with an impressive spatial coverage exceeding 140,000 km². In contrast, the secondary peak at 11.5 km has a significantly smaller coverage, not exceeding 23,500 km². Notably, the lowest spatial coverage values between these two peaks are found in the altitude range of 13-14 km, where they do not exceed 7,000 km². This value is starkly lower than the top maximum, representing less than 5% of the primary peak's spatial coverage. Spatial coverage values below 7,000 km² are also observed at altitudes from 26.5 km upwards, and there is a dramatic drop in coverage at 28 km, with values falling below 1,500 km².

Regarding the secondary peak at 11.5 km, it is noted that there are no significant changes in spatial coverage compared to the average December. This consistency suggests a degree of stability in PSC formation at this altitude. However, in contrast, the primary peak at 20.6 km exhibits a notable increase in spatial coverage in January, surpassing the December peak by over 40,000 km². This substantial growth in the area covered by PSCs at the higher altitude underscores the pronounced variability in PSC distribution and intensity as the Northern Hemisphere progresses from early to mid-winter.

The marked increase in the spatial coverage of PSCs at the primary peak in January highlights this month as a period of peak PSC activity. This significant rise in PSC occurrence and extent at 20.6 km reflects the dynamic nature of atmospheric conditions during this time, emphasizing January as a key month for the most remarkable occurrences of PSCs in the Northern Hemisphere's winter season.
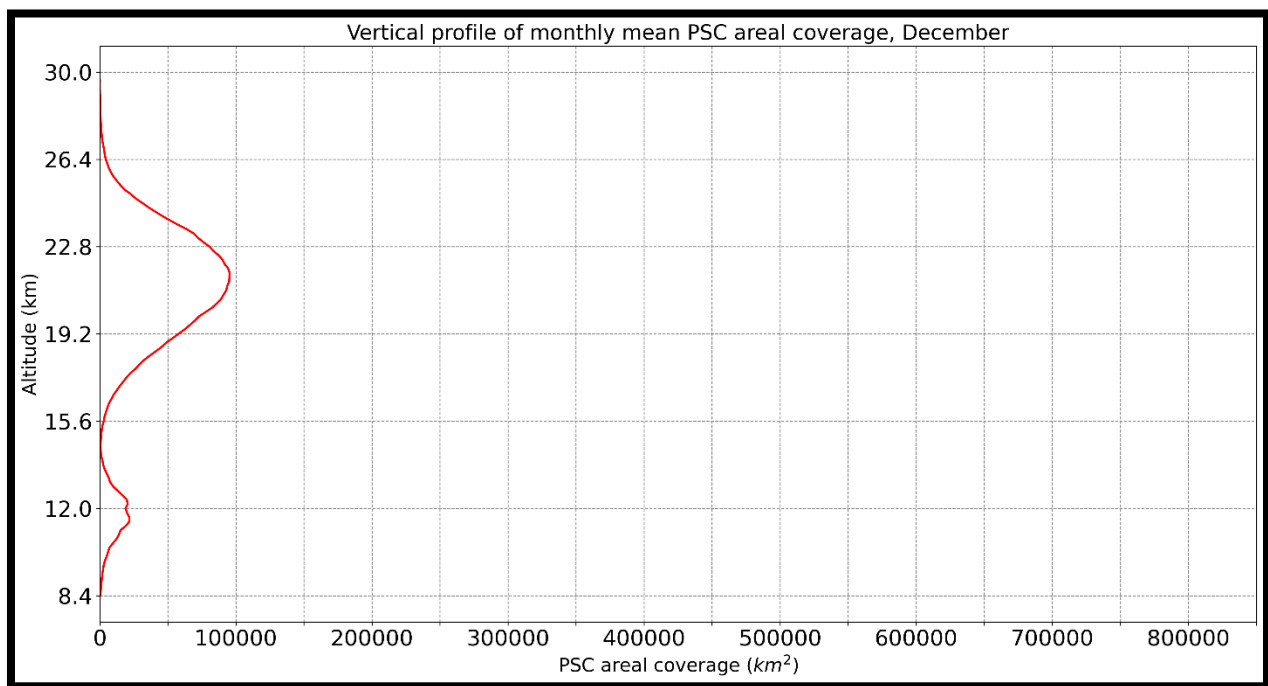

Figure 33: Vertical Profile of the Average January PSC areal coverage of the Northern Hemisphere for the period 2007-2021.

In February, as depicted in Figure 32, the characteristic dual peak pattern of PSCs persists, though the difference in spatial coverage between the primary and secondary peaks is less distinct. The top peak is observed at 19.4 km with PSC spatial coverage reaching around 23,000 km², closely followed by the secondary peak at 11.5 km, which has a coverage of nearly 22,000 km². This month's data illustrate that the peak of maximum spatial coverage shifts to lower latitudes as the Northern Hemisphere's PSC season progresses.

Between the two peaks, specifically in the 13-14 km altitude range, the spatial coverage remains relatively low, not exceeding 4,500 km². This indicates a substantial reduction in PSC prevalence

within these mid-altitude ranges. At altitudes above 25 km, there is a noticeable decrease in spatial coverage to about 2,000 km². This decline becomes more pronounced at higher altitudes, where spatial coverage dramatically falls to less than 500 km² at around 26 km. This pattern highlights the diminishing prevalence of PSCs at higher altitudes towards the end of the Northern Hemisphere's winter season.
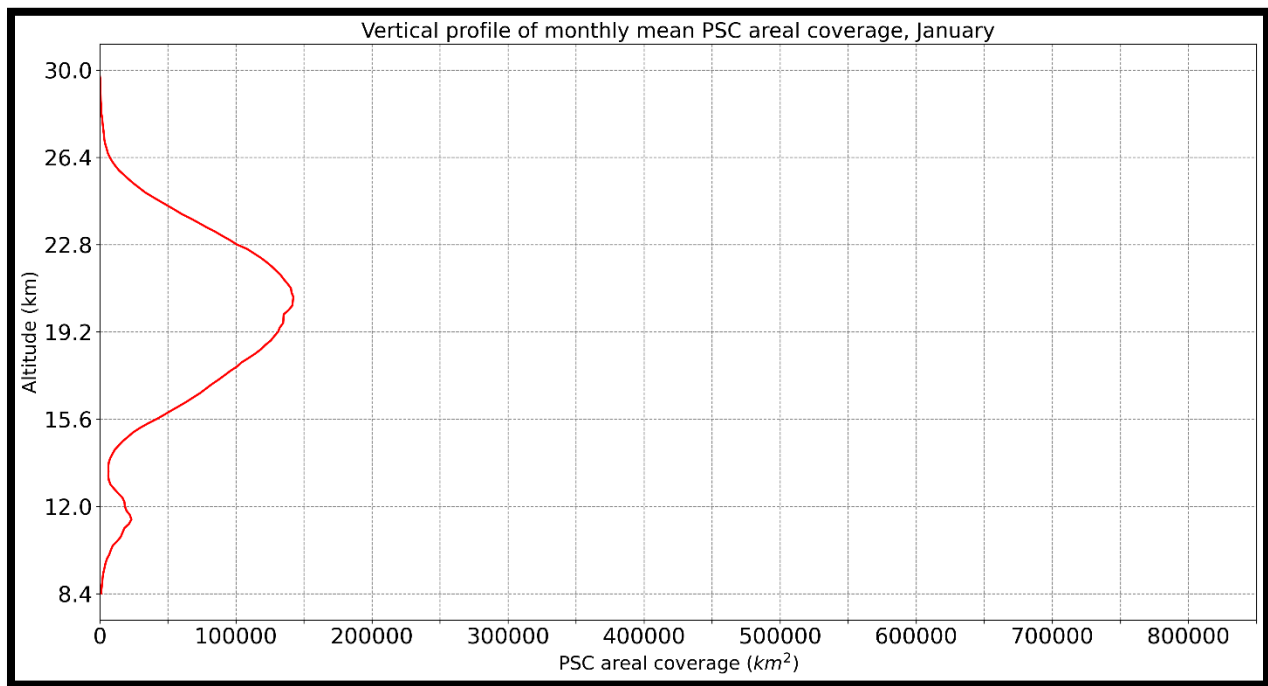

Figure 34: Vertical Profile of the Average February PSC areal coverage of the Northern Hemisphere for the period 2007-2021.

The dual peak pattern of PSCs is still present in March, Figure 33, but there is a noticeable shift in the prominence of the peaks. The primary peak, which previously occurred at higher altitudes, is now observed at a lower altitude. Specifically, the top peak is at 11.5 km with an areal coverage of approximately 17,000 km², overtaking the previously dominant higher altitude PSCs. The secondary peak is found at 17 km, with an areal coverage not exceeding 4,500 km². A notable minimum in areal coverage, reaching only up to 1,500 km², occurs at around 13.5 km, situated between these two peaks. Furthermore, areal coverage values lower than this minimum are observed for altitudes above 20.5 km. It is particularly evident in March that PSCs do not extend vertically beyond 21 km, where the spatial coverage diminishes to 500 km².

In this month, the total areal coverage of PSCs does not exceed 5,000 km² for altitudes above 12.5 km. This trend indicates that PSCs in March are not commonly found in the middle stratosphere but are predominantly located in the lower stratosphere/upper troposphere. This shift highlights the seasonal progression of PSCs, with their vertical extent and distribution changing significantly as the Northern Hemisphere transitions from winter into spring.

This variation is likely attributable to the weakening of the Arctic polar vortex and the concurrent increase in temperatures at higher altitudes, further discussed in section 4.1.3. The diminishing strength of the vortex and the warming of the stratosphere seem to be pivotal factors contributing to the reduced presence and altered distribution of PSCs during this transitional period. This trend can possibly reflect the dynamic nature of atmospheric conditions in the polar regions and their impact on the formation and persistence of PSCs.
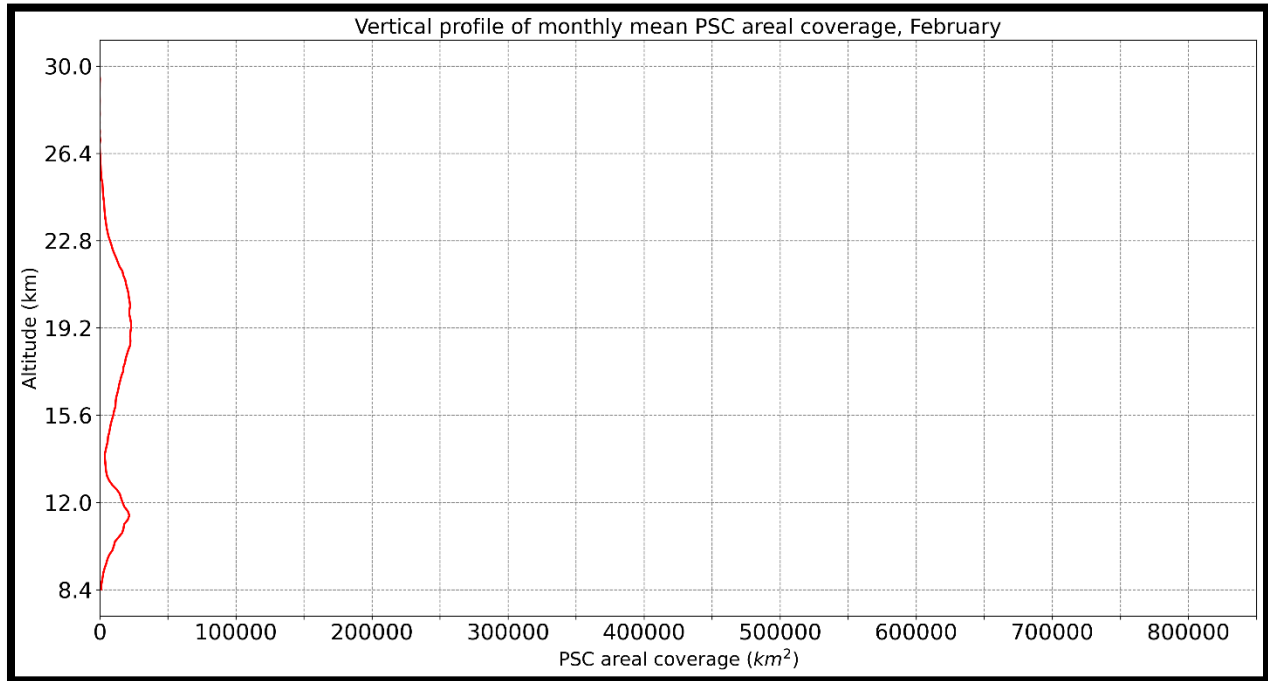

Figure 35: Vertical Profile of the Average March PSC areal coverage of the Northern Hemisphere for the period 2007-2021.

Focusing on the high-altitude peaks of PSCs for our study and providing more precise values, we observe the following trends:

- In December, the high-altitude peak is at 21.7 km with an areal coverage of 95,500 km².

- In January, this peak shifts to 20.6 km, with the areal coverage increasing to 142,500 km².

- By February, the peak occurs at 19.4 km with a reduced coverage of 23,000 km².

- In March, the peak further descends to 17 km, with areal coverage dwindling to 4,500 km².

Conversely, at the lower altitude of 11.5 km, the spatial coverage of PSCs displays a different pattern:

- In December, the spatial coverage is 21,850 km².

- In January, it slightly increases to 23,250 km².

- In February, it remains relatively stable at 21,750 km².

- By March, it decreases to 16,750 km².

These results indicate that the rate of change in areal extent of PSCs is more rapid at higher altitudes compared to lower ones. This variance can be attributed to several factors, including the dynamics of the polar vortex. The impact of these factors and their role in the observed altitudinal shifts of PSCs will be further discussed in the next subsection. This detailed analysis elucidates the complex nature of PSC distribution and the factors influencing their seasonal variability in the Northern Hemisphere.

SOUTHERN HEMISPHERE

The Southern Hemisphere (Figure 34) exhibits a distinct pattern in the distribution of PSCs that sets it apart from the Northern Hemisphere. Like its northern counterpart, it too shows a dual peak pattern in PSC distribution. However, a striking difference lies in the proximity of the secondary peak to the primary peak. Unlike the Northern Hemisphere, where a significant gap between the high and low altitude PSCs was noted – particularly with the secondary peak at 11.5 km – the Southern Hemisphere's peaks are much closer in altitude.

In detail, the top peak in the Southern Hemisphere, is at 20.3 km, characterized by an extensive spatial coverage of approximately 340,000 km². Remarkably close to this, the secondary peak is observed at 16.9 km, with a spatial coverage nearing 320,000 km². This closeness in altitude suggests a different dynamic in PSC formation in the Southern Hemisphere, where high spatial coverage is maintained within a relatively narrow altitudinal range (from 16 km to 22 km).

Comparing these findings with those of the Northern Hemisphere reveals stark contrasts. The top peak in the Southern Hemisphere not only occurs at a slightly lower altitude (0.7 km lower) but also exhibits a spatial coverage that is almost five times larger than that observed in the Northern Hemisphere. This substantial difference in spatial coverage highlights the unique atmospheric conditions of the Southern Hemisphere, associated with the extremely low temperatures there, according to McCormick et al.1989, particularly in relation to PSC formation and distribution.

The intricacies of these differences become even more evident when delving into the vertical profiles for each average month of the Antarctic PSC season. These monthly analyses are poised to provide deeper insights into the behavior and characteristics of PSCs in the Southern Hemisphere, further emphasizing the distinct climatic and environmental factors that influence PSC formation in this region. The upcoming examination of each month's vertical profile is expected to shed more light on the unique aspects of PSC distribution in the Southern Hemisphere, contributing to a more comprehensive understanding of global PSC dynamics, which will be further discussed and analyzed in the next subsection (4.1.3).
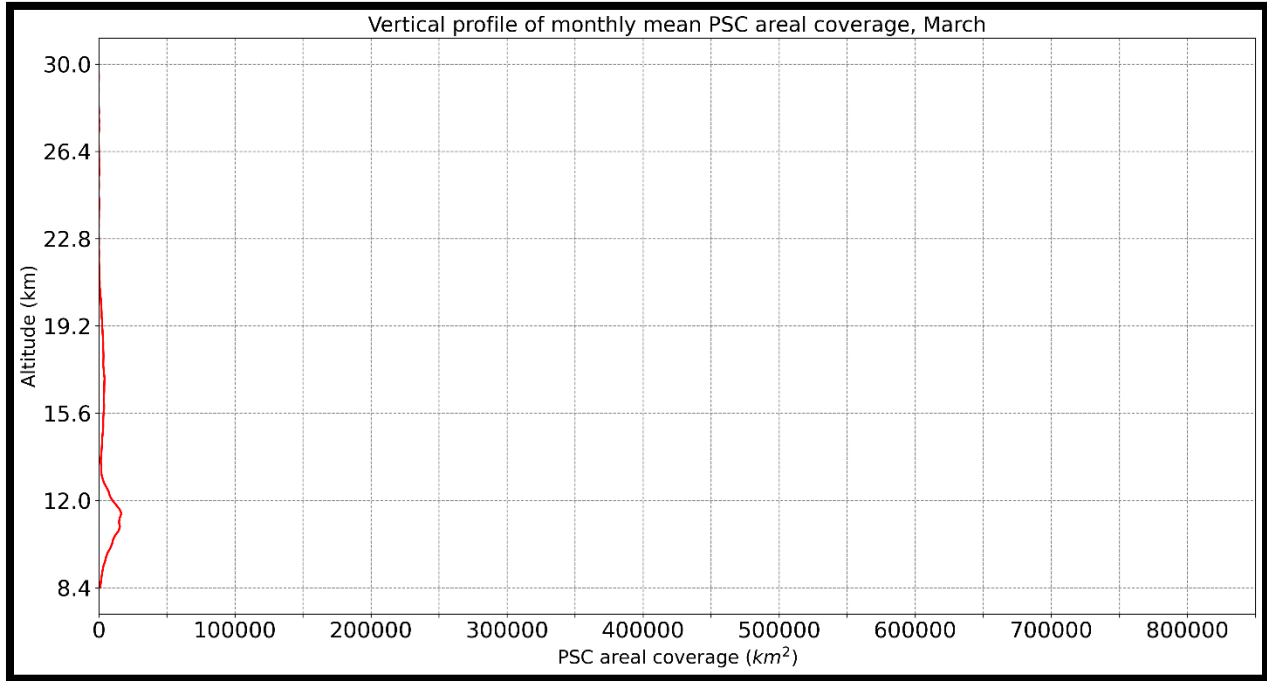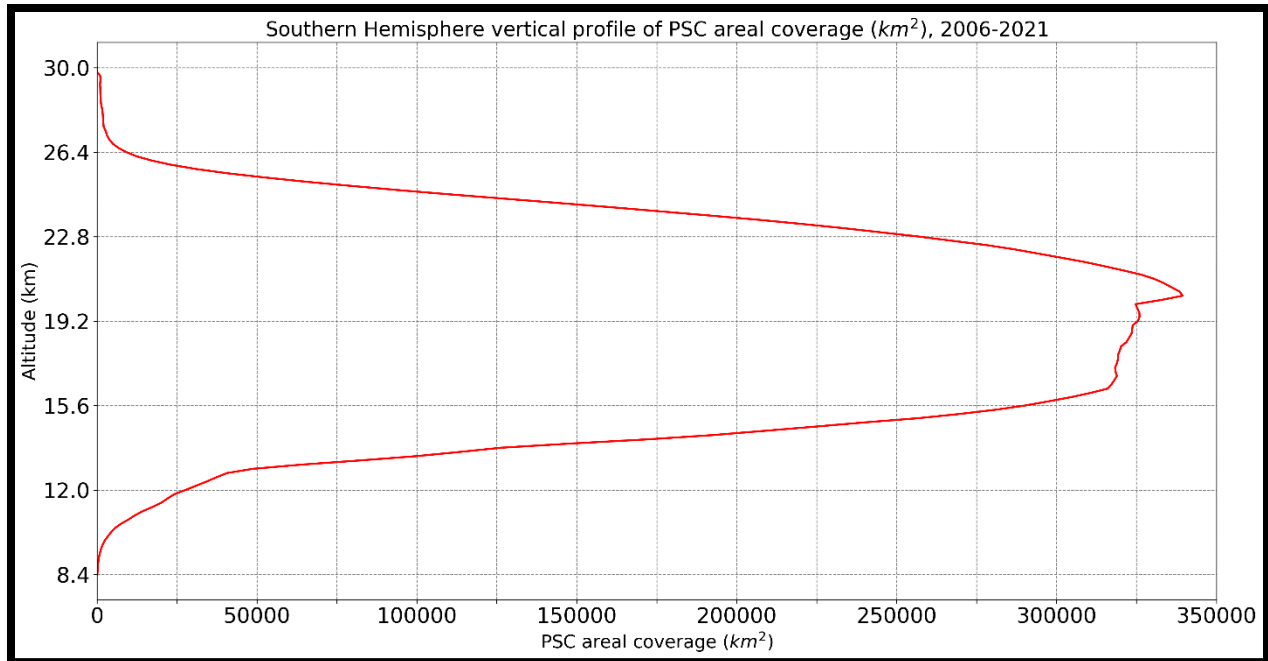
Figure 36: Vertical Profile of the Average PSC areal coverage of the Southern Hemisphere for the period 2006-2021.

The analysis of the sixteen-year mean monthly areal coverage of PSCs over the Antarctic during the key months from May to October reveals a distinct seasonal pattern. This pattern, clearly depicted in Figure 35, shows that PSC formation in the Antarctic begins in early May, with coverage reaching its greatest peak in July. Following this peak, there is a noticeable gradual decline in coverage that starts in mid-late September and leads to a significant reduction by October.

In comparison to the Northern Hemisphere, the Southern Hemisphere displays considerably lower values of low altitude PSCs, in contrast to the high altitude ones. This disparity suggests that the focus for the Southern Hemisphere should primarily be on high altitude PSCs, with only a brief mention of the low altitude PSCs. This approach is reinforced by the evident differences in the duration and intensity of PSC seasons between the two hemispheres.

It becomes clear that the Antarctic PSC season spans a longer period, lasting six months, in contrast to the four-month duration of the Arctic PSC season. Moreover, the average monthly values of areal coverage in the Southern Hemisphere are significantly larger than those in the Northern Hemisphere. This extended duration and greater coverage in the Southern Hemisphere can potentially underscore the differing climatic conditions, sufficient condensables and atmospheric dynamics that govern PSC formation and persistence in each hemisphere. The analysis thus highlights the unique characteristics of the PSC seasons in both hemispheres, with the Southern Hemisphere exhibiting a more prolonged and expansive PSC presence.

The transitions between the months within the Antarctic PSC season, particularly from May to June and from September to October, exhibit significantly more intensity compared to the

analogous transitions in the Northern Hemisphere, namely December to January and February to March. This increased intensity in the Southern Hemisphere is marked by a rapid escalation or decline in the areal coverage of PSCs.

During the shift from May to June in the Antarctic, there is a notable and rapid increase in PSC coverage, signaling a swift onset of the PSC season. This rapid change contrasts with the more gradual increase observed in the Arctic from December to January. Similarly, the transition from September to October in the Antarctic is characterized by a sharp decrease in PSCs, indicating a swift conclusion to the PSC season. This is in stark contrast to the more gradual diminishment observed from February to March in the Arctic.
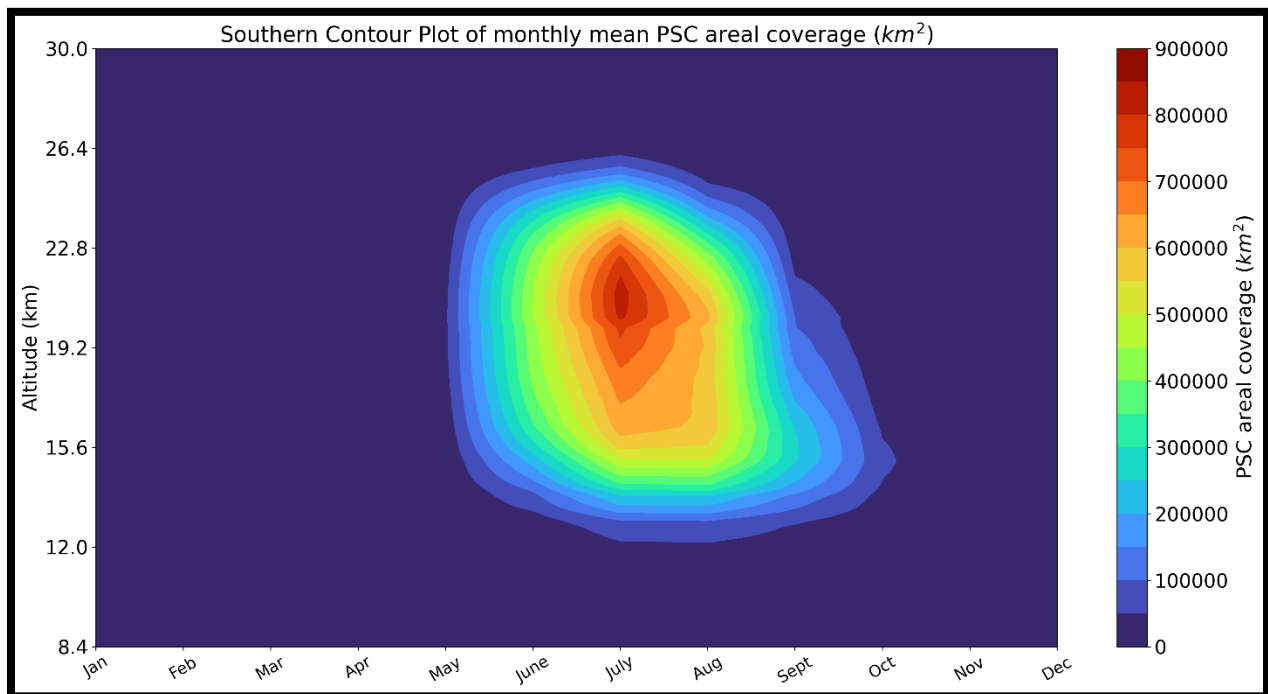
Figure 37: Sixteen-year mean monthly PSC areal coverage over the Antarctic, as a function of altitude.

Commencing the Antarctic season in May, as shown in Figure 36, a distinct vertical pattern in the spatial coverage of PSCs is quite evident. The primary peak in spatial coverage is observed at 20.3 km, with an area exceeding 40,000 km². In contrast, the secondary peak occurs at a lower altitude of 11.5 km, with a spatial coverage not surpassing 12,000 km². Within the altitudinal range of 13-14 km, there is a notable dip in PSC coverage, with the values being less than 2,000 km², indicating a significant decrease in PSC presence at these mid-range altitudes. Similarly, altitudes above 25 km also exhibit low PSC coverage values.

When comparing these findings to the start of the Arctic PSC season in December, where the peak occurs at 21.7 km with a spatial coverage of approximately 95,000 km², notable differences emerge. The peak in the Southern Hemisphere occurs at a slightly lower altitude and with less than half the spatial coverage of the Northern Hemisphere's peak. Furthermore, the range of

altitudes over which PSCs are found in May is somewhat narrower (by about 1 km) compared to December. This suggests that in May, PSCs in the Antarctic are typically found at altitudes ranging from just over 14 km to 25 km, where their spatial coverage exceeds the 2000km^2.

Figure 38: Vertical Profile of the Average May PSC areal coverage of the Southern Hemisphere for the period 2007-2020.

In June, as illustrated in Figure 37, there is a significant increase in the spatial coverage of PSCs compared to May. The primary peak occurs at 20.5 km, encompassing an extensive area of approximately 450,000 km², which is around 11 times greater than the peak observed in May. A less pronounced secondary peak is evident at around 11.5 km, with spatial coverage not surpassing 18,000 km².

Notably, substantial spatial coverage values, exceeding 100,000 km², are observed within the altitude range of 14 km to around 25 km. The maximum coverage values, surpassing 400,000 km², are found within a narrower altitude band from 17.5 to 22.5 km, spanning an approximate 5 km range. This indicates a concentrated area of intense PSC activity at these altitudes.

The presence of PSCs begins to decline rapidly above 25 km. At this altitude, the spatial coverage is approximately 135,000 km², but it sharply decreases to 25,000 km² at 26 km. Beyond this point, PSCs become increasingly sparse, with spatial coverage dropping below 2,000 km² at altitudes greater than 27 km. This trend demonstrates the diminishing extent of PSCs in the higher altitudes of the stratosphere during June, offering insights into the vertical limits of their presence during the Antarctic winter.
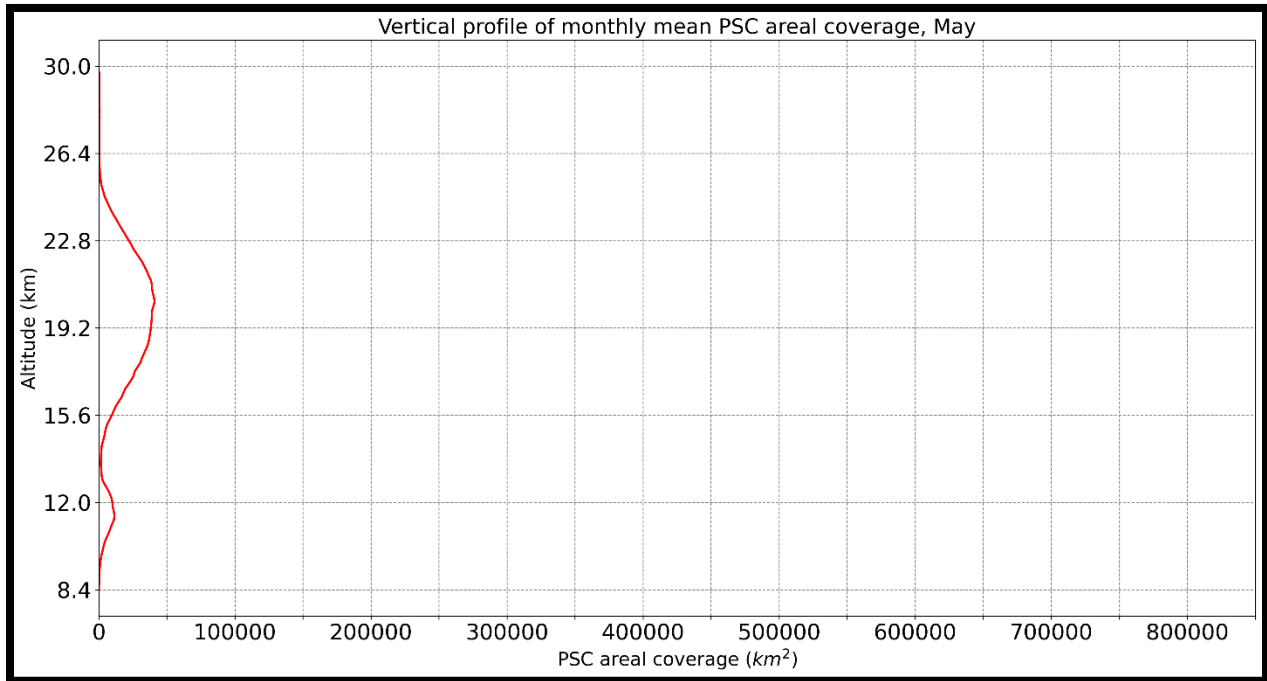
Figure 39: Vertical Profile of the Average June PSC areal coverage of the Southern Hemisphere for the period 2007-2020.

In July, as depicted in Figure 38, there is a dominant increase in the spatial coverage of PSCs, with a primary peak reaching exceptionally high values and a potential secondary peak at a slightly lower altitude. The primary peak takes center stage, located at 21.2 km, where the PSC spatial coverage soars to 825,000 km². This is nearly double the coverage observed in June and almost twenty times larger than the peak in May.

Significant spatial coverage values, exceeding 100,000 km², are present across a broad altitude range from 13 km to 25.5 km. The highest coverage values, surpassing 700,000 km², are found within an altitude range of 18.5 to 23 km. Particularly, the most extreme coverage values, exceeding 800,000 km², are concentrated in a narrow band between 20.3 and 21.7 km, spanning an area of no more than 1.5 km.

PSCs begin to exhibit a significant decrease in occurrence at altitudes above 25 km, while between the altitude band from 25 to 26km, their spatial coverage loses about 205000km². This decline becomes more pronounced at altitudes exceeding 28 km, where the spatial coverage falls below 2,000 km², indicating the onset of PSC dissipation in these higher stratospheric regions. This trend in July highlights the peak of the PSC season in the Southern Hemisphere, with the substantial spatial coverage reflecting the extensive presence of these clouds during the Antarctic winter.

In the case of PSCs for the period under study, there is not a distinct separation between low and high-altitude PSCs in terms of spatial coverage. Unlike some typical patterns where such

separation is evident, here we observe a continuous increasing trend in spatial coverage starting from the initial altitude captured by satellite data.

This trend suggests that while there isn't a stark separation, a potential demarcation could be considered at altitudes above 13 km. Beyond this altitude and up to 15 km, the increase in spatial coverage is quite significant, with values rising by more than 15,000 km² for every 100 meters of altitude. In contrast, below 13 km, the rate of increase in spatial coverage is more gradual, with an increment of approximately 3,000 to 4,000 km² per 100 meters.

This pattern indicates that the denser concentration of PSCs begins to intensify notably above 13 km, marking a transitional zone into a region of more substantial cloud formation. This analysis provides insights into the vertical distribution of PSCs, highlighting the altitudes at which these clouds become more prevalent, suggesting that high altitude PSCs form from altitudes above 13km.
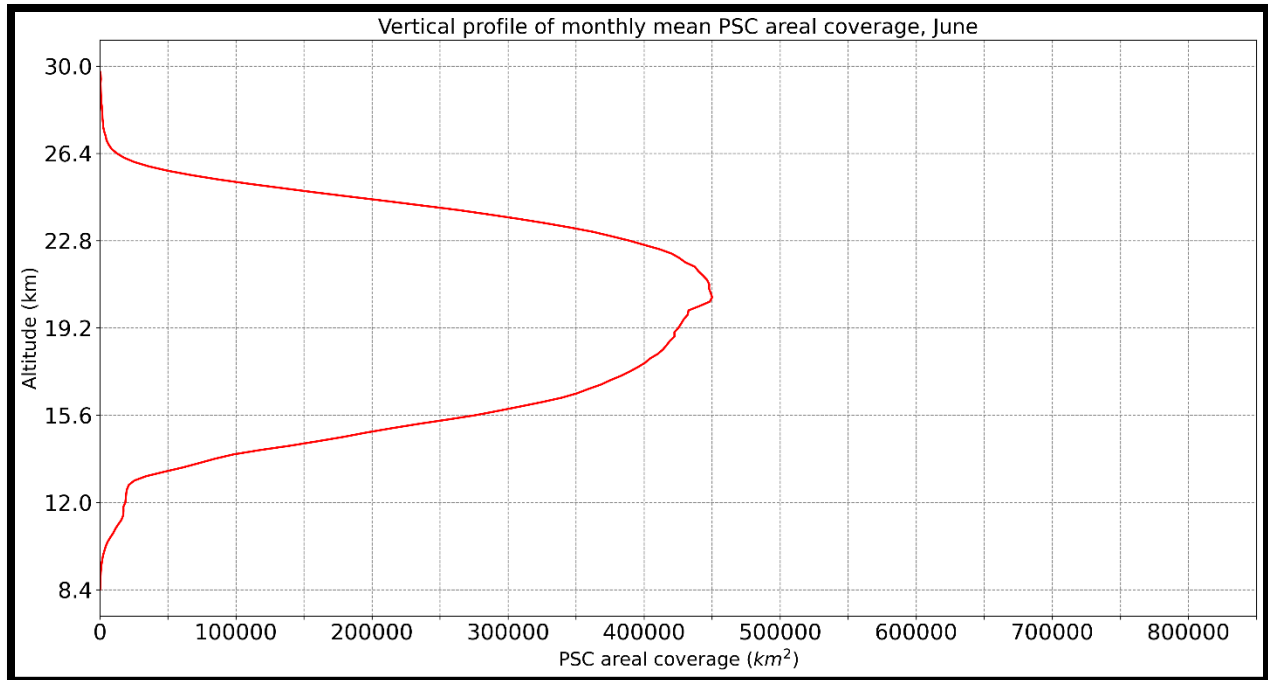

Figure 40: Vertical Profile of the Average July PSC areal coverage of the Southern Hemisphere for the period 2006-2020.

August, as shown in Figure 39, follows the peak month of July in the Antarctic PSC season. This month continues to exhibit high areal coverage values, albeit not to the same extent as July, and is characterized by a notably multi-peak profile. The primary peak is observed at 20.3 km, similar to May, with an areal extent exceeding 600,000 km². Close to this, a secondary peak occurs at 19.2 km, covering an area of approximately 595,000 km², and a third peak appears at 16.9 km with about 590,000 km². A particularly interesting aspect of August is the stability in areal extent of PSCs across a range of altitudes. From 16.3 km to 20.8 km, the areal extent

fluctuates between approximately 590,000 km² and 610,000 km². This indicates that within this altitudinal band, the coverage of PSCs remains exceptionally high with only minor variations.

Overall, in August, PSCs exceed an areal coverage of 100,000 km² for altitudes ranging from 13 km to 24.5 km. However, the values drop significantly for altitudes above 27 km, reaching exceptionally low levels (lower than 2,000 km²).

When considering the separation of low altitude and high-altitude PSCs, it is observed that high altitude PSCs could be considered for altitudes above 13 km. This is suggested by the ratio of areal coverage increase, which is greater than 15,000 km² for every 100 meters of altitude increase. This distinction helps in understanding the vertical stratification of PSCs during this phase of the Antarctic winter, indicating the presence of PSCs predominantly at higher altitudes with significant areal coverage.
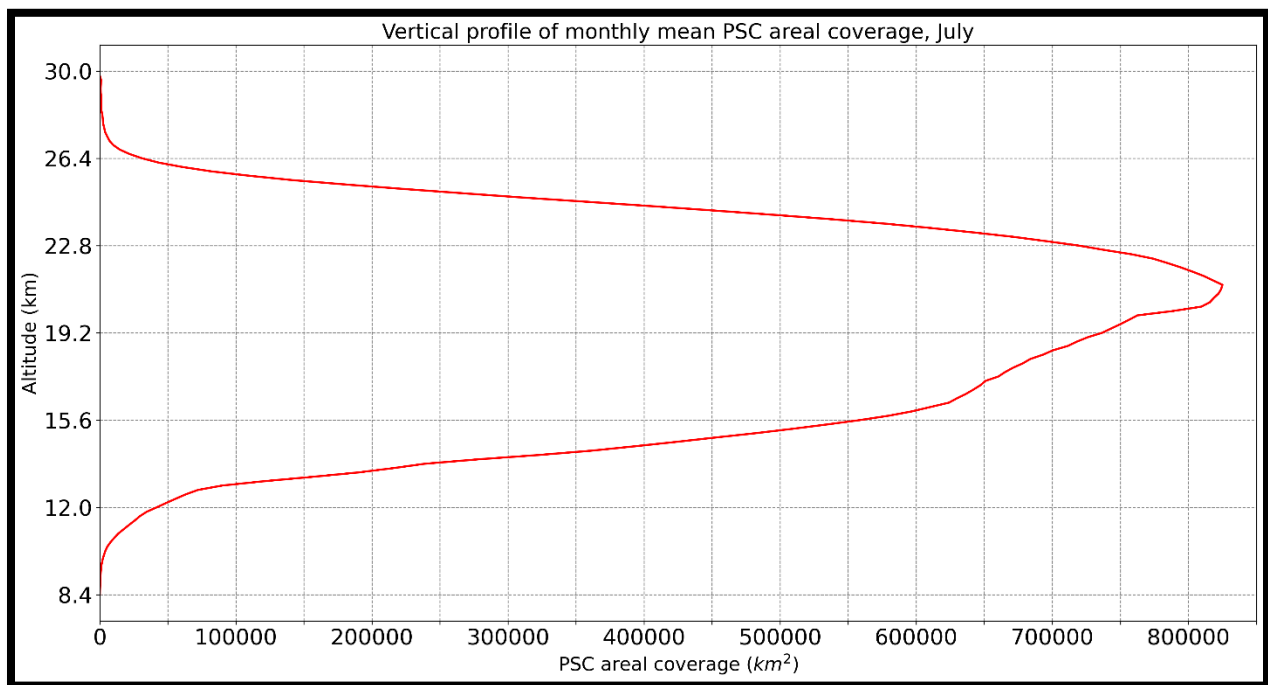

Figure 41: Vertical Profile of the Average August PSC areal coverage of the Southern Hemisphere for the period 2006-2020.

September, as illustrated in Figure 40, signals the approaching end of the Antarctic PSC season. This month is characterized by a primary peak in PSC areal coverage at 15.4 km, where it reaches approximately 260,000 km², more than twice lower than the Augusts' primary peak, along with two potential peaks at higher altitudes.

During this month, PSCs maintain an areal coverage greater than 100,000 km² across a range of altitudes from 13.5 km to 20 km. The most densely populated altitude band is observed from 14.5 km to approximately 17 km, where the areal coverage values range from 200,000 km² to 260,000 km². This indicates a concentration of PSCs within this specific altitude range.

73

However, there is a marked decrease in PSC coverage at higher altitudes. The areal coverage drops dramatically to values below 10,000 km² for altitudes above 24 km. At altitudes exceeding 27.5 km, the areal coverage reaches extremely low levels, indicating the substantial reduction in PSC presence in these upper stratospheric regions. This trend in September reflects the gradual reduction in PSC activity as the Antarctic winter progresses towards spring, with a significant decline in the extent and density of PSCs at higher altitudes.
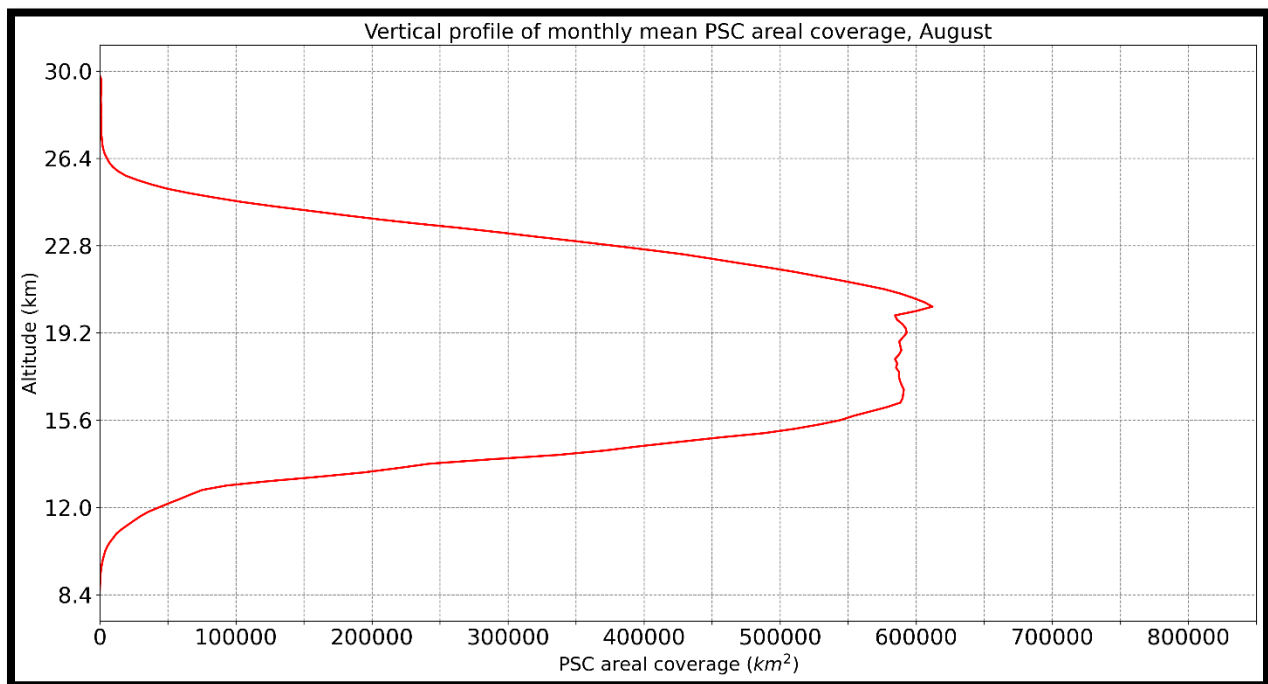

Figure 42: Vertical Profile of the Average September PSC areal coverage of the Southern Hemisphere for the period 2006-2020.

As the Antarctic PSC season draws to a close in October, as depicted in Figure 41, the familiar two-peak pattern observed in many months of the Arctic PSC season becomes apparent. In this month, the primary peak is situated at a relatively lower altitude compared to earlier months. This primary peak occurs at 15.1 km, covering an area of approximately 60,000 km². Accompanying this, a secondary peak is observed at around 11.5 km, where the areal coverage does not exceed 20,000 km².

In terms of PSC distribution at higher altitudes, there is a significant reduction in coverage. Above 21 km, the areal extent of PSCs is limited to less than 3,000 km². Within the altitude range of 21 to 26 km, there are minor fluctuations in areal coverage, oscillating between 2,000 km² and 3,000 km². This pattern indicates a notable decrease in the presence of PSCs at these higher altitudes as the season transitions from the cold Antarctic winter into spring.

The shift in the primary peak to a lower altitude in October and the decrease in areal coverage at higher altitudes underscore the seasonal dynamics of PSCs in the Southern Hemisphere. This

trend reflects the gradual winding down of the PSC season, with a significant reduction in the extent and density of these clouds as the Antarctic region moves towards warmer temperatures.
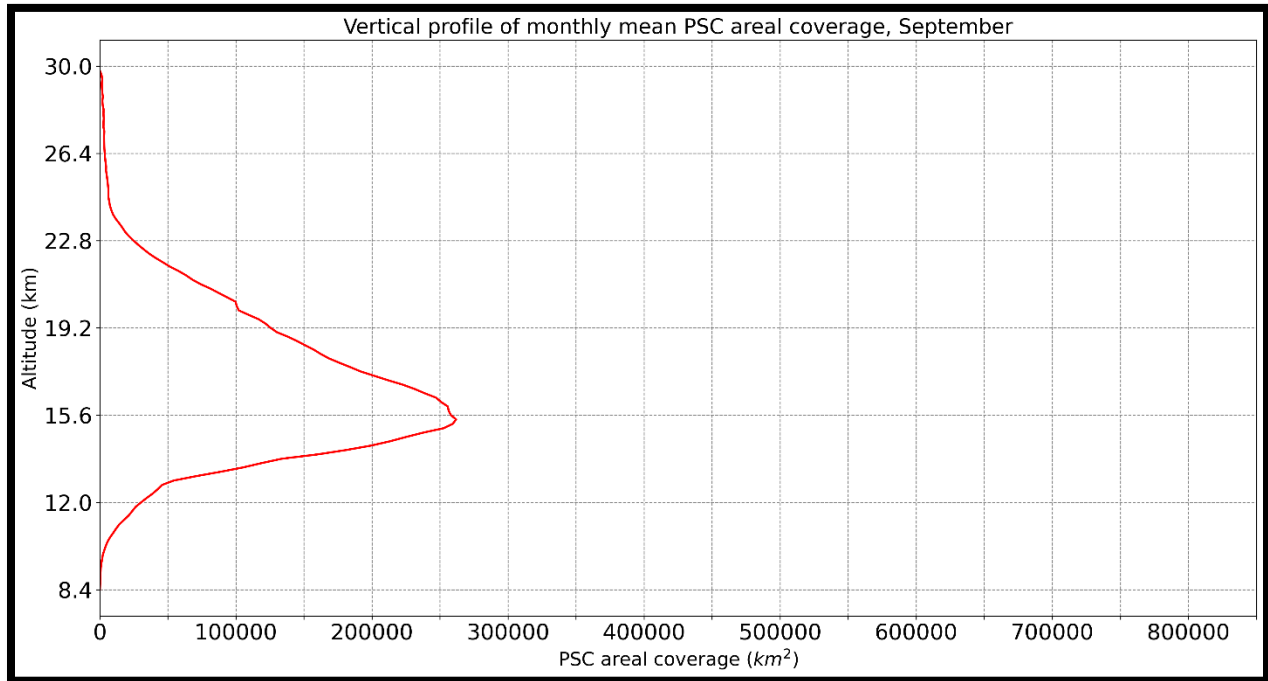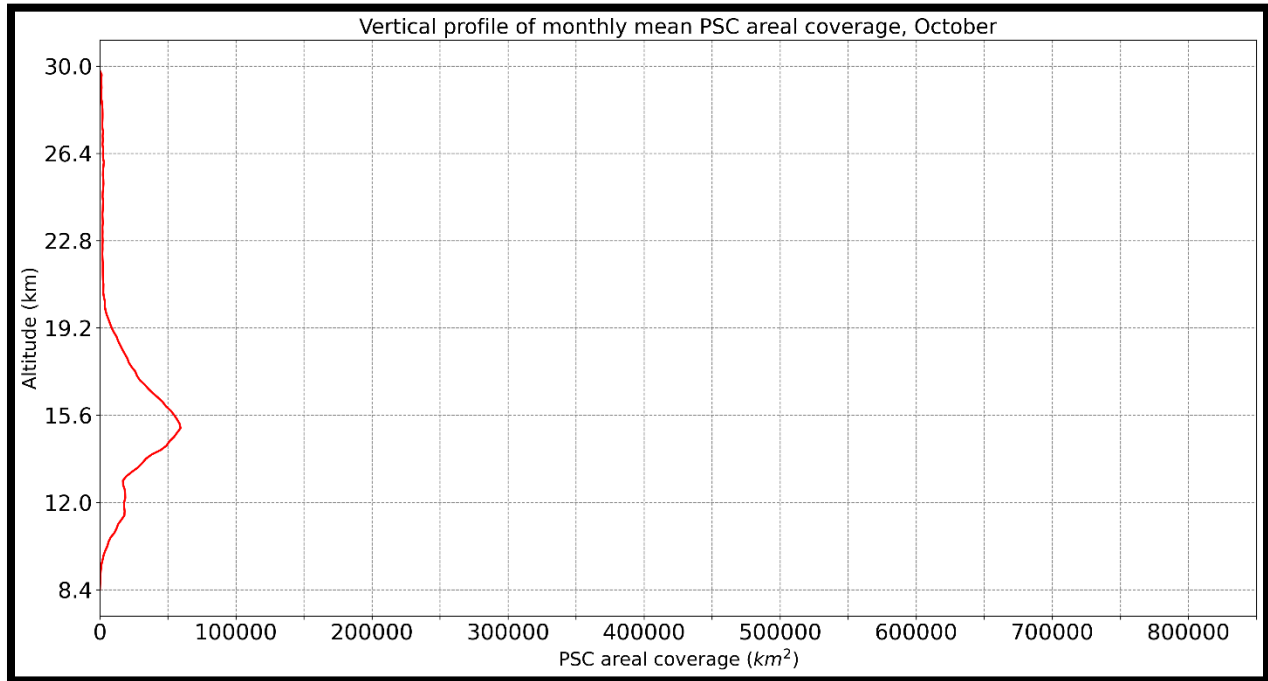

Figure 43: Vertical Profile of the Average October PSC areal coverage of the Southern Hemisphere for the period 2006-2020.

Continuing with the discussion on the vertical profiles of PSCs in both the Northern and Southern Hemispheres, let's examine a summary of the top peaks of Southern Hemisphere PSC areal coverage. This summary includes the altitude at which maximum spatial coverage occurs for each month from May to October:

May: The season in the Southern Hemisphere begins with the top peak at 20.3 km, showing an areal coverage of approximately 41,100 km², marking the onset of the PSC season in the Antarctic.

June: There's a significant increase in areal coverage, with the highest peak at 20.5 km covering an extensive area of about 450,000 km², reflecting the intensification of the PSC season.

July: This month exhibits the highest areal coverage of the season, with the primary peak at 21.2 km encompassing an impressive 825,000 km², representing the peak of the PSC season in terms of spatial extent.

August: While still high, the areal coverage decreases slightly compared to July, with the primary peak at 20.3 km covering approximately 612,000 km², indicating the beginning of the gradual decline of the PSC season.

September: The areal coverage continues to decrease, with the primary peak at 15.4 km covering about 262,000 km², signaling the nearing end of the PSC season.

October: Marking the end of the Antarctic PSC season, the primary peak is at 15.1 km with a significantly reduced areal coverage of around 60,000 km².

Key conclusions and insights

Combining the initial insights with the additional conclusions from the analysis of PSCs in both the Southern and Northern Hemispheres, we can develop a comprehensive understanding of their behavior, distribution, and impact:

Seasonal variability and altitude shifts: There is a notable seasonal variability in PSC areal coverage, with shifts in the altitude of maximum coverage as the season progresses in both hemispheres. In the Southern Hemisphere, the peak altitudes for PSCs fluctuate between 15.1 km to 21.2 km, with the highest spatial coverage observed in July, steadily decreasing till October, indicating a downward shift as the season advances and that the PSCs in the Southern Hemisphere reach their maximum extent mid-season. The Northern Hemisphere shows a consistent downward trend in peak altitudes as the season progresses from December to March, starting from 21.7 km in December and descending to 17 km in March. This descending trend indicates a gradual lowering of PSCs' vertical extent as the Arctic winter progresses.

Magnitude of areal coverage: The Southern Hemisphere's PSCs exhibit significantly larger areal coverage compared to the Northern Hemisphere. July's coverage of 825,000 km² at peak altitude in the Southern Hemisphere is markedly higher than any month in the Northern Hemisphere. In the Northern Hemisphere, the highest PSC coverage is 142,500 km² in January, considerably less than in the Southern Hemisphere despite similar or slightly higher peak altitudes in some months.

Duration of PSC Season: The PSC season in the Southern Hemisphere spans six months (May to October), which is longer than the four-month season (December to March) in the Northern Hemisphere. This extended duration in the Southern Hemisphere could be attributed to different atmospheric and climatic conditions conducive to PSC formation.

Impact of atmospheric conditions: The differences in peak altitudes and areal coverage between the hemispheres suggest variations in atmospheric conditions, such as temperature and the strength of the polar vortices. The Southern Hemisphere's more robust PSC presence could be influenced by colder temperatures, further discussed in section 4.2, and a stronger polar vortex, further discussed in subsection 4.1.3.

Implications for climate and ozone layer: The extensive coverage of PSCs, particularly in the Southern Hemisphere, has significant implications for ozone depletion as PSCs play a crucial role in the chemistry of ozone destruction, especially in the Antarctic where the ozone hole forms.

Link with bibliography

Our findings align with the broader research in the field of PSC climatology. More specifically:

Seasonal Variation and Peak Altitudes: The fluctuating peak altitudes in the Southern Hemisphere are consistent with the findings in 'Polar Ozone and Aerosol Measurement (POAM) III' observations, which document the variability in stratospheric conditions over Antarctica (Lucke et al., 1999). The pattern of decreasing peak altitudes over the Arctic aligns with research by D. E. Siskind et al. (2000), who studied the vertical distribution of PSCs in the Northern Hemisphere and observed similar trends. Additionally, the downward trend in peak altitudes from December to March correlates with research by Solomon et al. (1986) and other studies that highlight the seasonal dynamics of the Arctic stratosphere and its impact on PSC formation.

Areal Coverage Extent: The extensive coverage in the Southern Hemisphere aligns with research by Shettle et al. (2002), which discusses the atmospheric conditions conducive to widespread PSC formation over Antarctica, while the smaller areal coverage of the Northern Hemisphere is in line with studies by Alfred Wegener Institute for Polar and Marine Research, which highlights the differences in stratospheric moisture and temperature between the poles affecting PSC formation. The smaller areal coverage compared to the Southern Hemisphere, despite similar peak altitudes, aligns with discussions in the scientific literature (e.g., McCormick et al., 2007) on the role of the Arctic polar vortex and its lesser extent compared to the Antarctic vortex.

Hemispherical Differences: The longer and more extensive PSC season in the Southern Hemisphere can be related to studies by Hervig et al. (2002), which analyze the differences in stratospheric temperature and water vapor content between the Arctic and Antarctic. The longer duration and larger coverage area in the Southern Hemisphere can be compared with studies like those by Palm et al. (2005), which examine the differences in polar vortex strength and size between the hemispheres and their effects on PSC formation.

Impact of Atmospheric Conditions: The impact of varying climatic conditions on PSC formation correlates with the research by Voigt et al. (2005), which examines the influence of atmospheric dynamics on PSC characteristics in both hemispheres. The different atmospheric dynamics suggested by the variations in PSC behavior find support in literature such as Wu and Jiang (2002), which explores how differences in temperature and polar vortex characteristics influence PSC formation in each hemisphere.

Implications for Climate and Ozone Layer: The role of PSCs in ozone depletion, particularly in the Southern Hemisphere, is supported by the findings of Drdla and Müller (2002), who investigate the chemistry of PSCs and their impact on polar ozone depletion. The role of PSCs in ozone depletion, particularly in the Southern Hemisphere, correlates with foundational research by Solomon et al. (1986) on the Antarctic ozone hole and the role of PSCs in ozone-depleting processes.

4.1.3. Interannual variability

The results presented in this section, Figure 44, are pivotal to this thesis. They encapsulate a comprehensive analysis of the seasonal evolution of PSCs areal coverage across 15 seasons in both the Arctic and Antarctic. This analysis helps in understanding the seasonal dynamics of PSCs in the Northern and Southern Hemispheres, highlighting the month-to-month variability and their altitude-dependent distribution. Additional detailed graphs supporting these findings are included in the Appendix B section.

General findings

Our study, and according to the available CALIPSO data, indicates that the Antarctic PSC season consistently extends from May to October, in contrast to the Arctic, where the PSC season shows more variability, typically ranging from December to March. This highlights a longer and more stable presence of PSCs in the Southern Hemisphere. Notably, the areal coverage of PSCs significantly varies both regionally and seasonally.
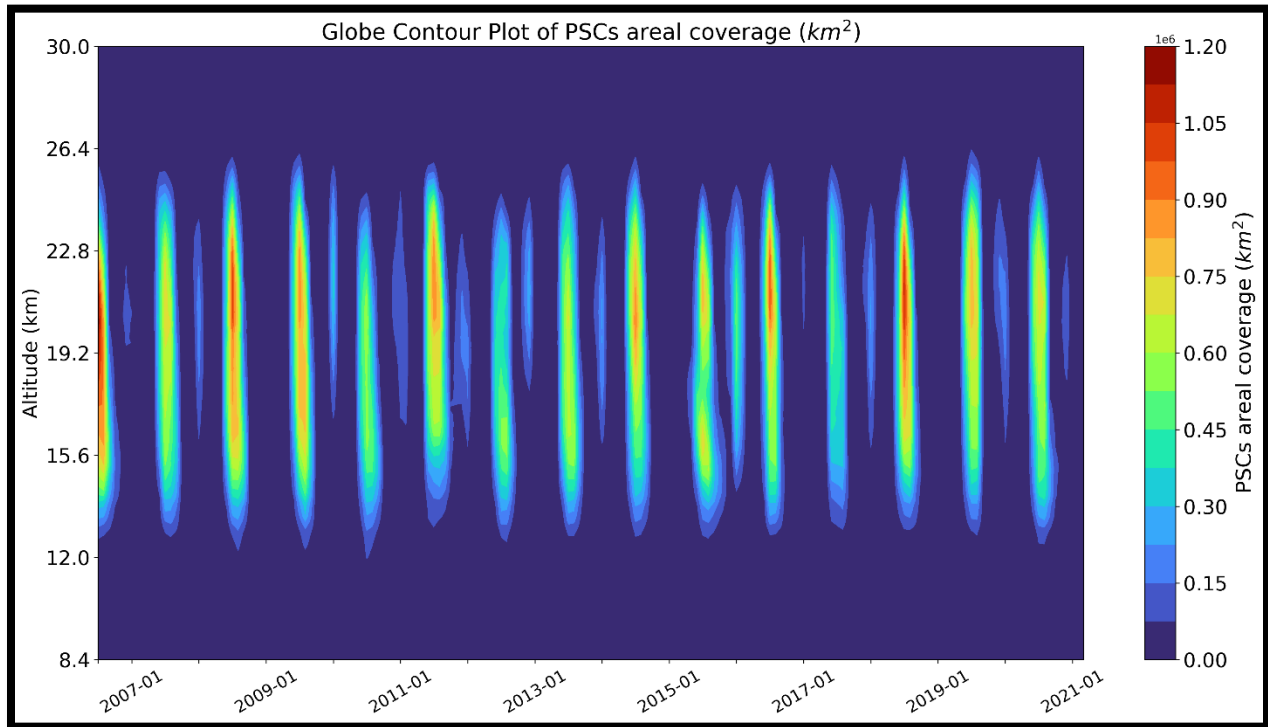
Figure 44: Mean monthly interannual variability and vertical distribution of PSC areal coverage (km²) for the period 2006–2021. Results are shown for the period May–October for the Southern Hemisphere and December–March for the Northern Hemisphere, for each PSC season of the dataset.

The NH's PSC coverage is considerably smaller compared to the SH, with the monthly mean PSC areal coverage ranging between 1,984 km² and 510,184 km². This is in stark contrast to the SH, particularly the Antarctic, where coverage spans from 462 km² to an extensive 1,196,110 km². The extremities of these ranges are vividly illustrated in Figure 42, with the SH's coverage

highlighted in greenish, yellowish, and reddish hues, particularly noticeable in July 2006, where the absolute monthly mean maximum reached around 1.2 million km².

The SH typically experiences its peak PSC areal extent in July, occasionally extending into August, followed by a marked decrease in September and a near disappearance by October. This pattern exhibits a consistent yearly trend, albeit with minor annual variations. These fluctuations are primarily influenced by dynamical factors like the stability and size of the polar vortex and the frequency and intensity of upper tropospheric and orographic forcing events, as outlined in various studies, such as Pitts et al. 2018. Notably, during the peak months of July and August, there is an increase in the area of highest PSC occurrence, expanding both in latitude and altitude, correlating with the ongoing cooling of the polar vortex.

Conversely, PSC occurrence in the NH shows significant seasonal variability. The most extensive areal coverage during the 16-year study was recorded in the years 2015 and 2016, as indicated in Figure 42. This period stands in stark contrast to earlier seasons, such as 2014–2015, which witnessed minimal PSC activity. The NH's PSCs typically reach their areal extent peak in December or January, followed by a rapid decrease in February and almost complete dissipation by March. This variability underscores the complex interplay of atmospheric conditions that govern PSC formation and persistence in the Arctic, reflecting the unique environmental and climatic factors at play in the Northern Hemisphere.

Now, let us delve deeper into the results presented in Figure 42. The accompanying graphs, located in the Appendix B section, detail the peaks and maximum areal coverage of each month, spanning from December through October, for all the dataset, from July 2006 – March 2021.

The initial observations regarding the vertical distribution of PSCs areal coverage for the month of **December** begin in 2006. During this year, the preferred altitude range for PSC occurrence was approximately 19.5-21.5km, with an areal coverage around 100,000 km². From 2006 to 2008, the altitude of PSC occurrence shifted to higher altitudes, but this trend reversed towards lower altitudes again until 2011. In 2012, the December data recorded the most significant peak in areal coverage for the study period, exceeding 250,000 km² and approaching 280,000 km² within an altitude range of 20.5-22.5km. Subsequent years, up to the end of the dataset, generally saw areal coverage not exceeding 160,000 km², except for December 2019, which observed PSC areal coverage surpassing 160,000 km² within the 21-22.5km altitude range. Noteworthy is the remarkably low areal coverage of PSCs in December for the years 2009, 2014, 2016, and 2018, characterized not only by their reduced areal extent, values lower than 80000km^2 for 2009 and 2016, and even lower (<40000km^2) for 2014 and 2018, but also by their limited vertical distribution.

In **January**, the dynamics of PSCs areal coverage become particularly intriguing. The highest areal coverage recorded for this month was in 2016, where it approached an impressive 560,000 km² within the altitudinal range of 19.5-21.5km. This peak stands out as a significant deviation

from the norm observed in other years. Specifically, during the years 2007, 2009, 2013, 2015, 2019, and 2021, the PSC areal coverage remained notably low, not exceeding 90,000 km². The years 2015 and 2019 were especially remarkable for their minimal PSC presence, almost reaching a point where PSCs were virtually absent.

Focusing on high-altitude PSCs and their areal coverage trends between December and January it is observed that in six Northern Hemisphere seasons (2006-2007, 2008-2009, 2012-2013, 2014-2015, 2018-2019, and 2020-2021), the areal coverage peaks were more pronounced in December. This observation is particularly interesting as it coincides with the years where January's areal coverage was significantly lower than usual. However, in the other nine seasons analyzed, January emerged as the month with higher peaks. Despite these variations, January consistently emerges as the more dominant month in terms of Arctic PSC areal coverage. This dominance is not just because January surpassed December in nine out of the fifteen seasons analyzed but also because the highest peak observed in January was approximately double the size of the largest peak in December. Additionally, it's important to note that in the seasons where December had greater areal coverage than January, the margin of difference was smaller compared to the seasons where January's coverage exceeded December's. This pattern underscores the pivotal role of January in the annual cycle of Arctic PSC areal coverage, both in terms of its propensity for higher areal coverage values and its overall influence on the seasonal behavior of PSCs.

In **February** and **March**, two trends become evident regarding PSCs. Firstly, PSCs are generally found at lower altitudes compared to December and January. Secondly, the areal coverage of PSCs during these months is markedly smaller, with February typically showing larger coverage than March. A notable exception to this pattern occurred in 2011 when February's peak areal coverage reached approximately 120,000 km² within an altitude range of 18.5-20.5km. March's highest peak was observed in 2020, with an areal coverage not exceeding 50,000 km², situated within the altitude range of 15.5-18.5km.

February presents a clearer distinction between high- and low-altitude PSCs compared to March, where most PSCs are concentrated between 10.5-12.5km. Particularly noteworthy is the 2014-2015 and 2018-2019 Arctic seasons, where the peaks in PSC areal coverage were observed at lower altitudes, around 11.5km, and occurred in February, not in December or January. This observation suggests a deviation from the typical pattern seen in other months.

Overall, the general pattern in the Northern Hemisphere indicates that January has higher PSC areal coverage values than other months in 9 out of 15 analyzed Arctic seasons. In contrast, December exhibited higher values in 4 Arctic seasons, and February was dominant in 2 seasons, albeit with relatively low altitude peaks and notably lower coverage values (not exceeding 35,000 km² in 2018-2019 and 30,000 km² in 2014-2015). Therefore, it can be confidently stated that in periods where February is the dominant month, these periods also tend to have a scarcity of PSCs, indicating a substantial reduction in their presence during these periods.

Transitioning our focus to the Southern Hemisphere, we begin with **May**, the inaugural month of the Antarctic PSC season, based on the CALIPSO dataset. Characteristically, May displays relatively modest values of PSC areal coverage compared to the later months of the season. A notable peak in coverage was observed in the 2015 season, reaching around 120,000 km². Interestingly, this peak occurred within the altitudinal range of 17-18.5km, which stands out as surprisingly low, considering the average altitude for peak PSC areal coverage in May is generally around 20.3km. For most other seasons, May demonstrates its most favorable altitudinal range for PSC formation at higher altitudes, approximately around 20-21km. However, the consecutive years of 2008 and 2009 present a contrasting scenario. In 2008, May records its lowest values in terms of both areal coverage and vertical distribution, suggesting a significant reduction in PSC presence. Conversely, in 2009, there is a marked increase in the areal coverage of low-altitude PSCs during May. This increase highlights the interannual variability and underscores the complexity of PSC observations, particularly at the onset of the season.

As we progress into **June**, and subsequently July and August, the Southern Hemisphere's PSC season evolves, showcasing a stark contrast in seasonal variability compared to the Northern Hemisphere and underscoring the Southern Hemisphere's relative smoothness. In June, there is a notable escalation in PSC areal coverage, with values soaring to exceed 600,000 km². This significant peak was recorded in 2011 within an altitudinal range of 20-22.5km, a season where July's peak reached around 1.05 million km². Consistent with earlier observations, the average altitude for peak areal coverage in June hovers around 20.5km, which aligns with the seasonal vertical distribution patterns of PSCs observed in the Southern Hemisphere.

During June, there are few remarkable deviations from this trend, except for the year 2015. In this year, the highest peak of PSC areal coverage is observed at a comparatively lower altitude of around 16km, with coverage reaching approximately 500,000 km². Notably, this peak is distinct from the season's maximum in July, which reached around 800,000 km². This anomaly in 2015, where the peak shifts to a lower altitude than typically observed in June, adds an intriguing dimension to the understanding of PSC distribution and behavior during the Antarctic winter. It exemplifies the interannual variability and the intricate dynamics governing PSC formation and distribution in the Southern Hemisphere, particularly during the mid-season months when PSC activity intensifies.

July, undeniably, stands out as the most pivotal month in the Antarctic PSC season. The data analysis reveals that July consistently dominates the season, with the highest peak in PSC areal coverage recorded in 2006. This peak astonishingly reaches 1.2 million km², spanning an altitude range of 19-22km, centering around 20.5km, which is marginally below the average maximum PSC areal coverage altitude for July. Equally noteworthy is the year 2018, where July also exhibits exceptionally high PSC areal coverage, nearly mirroring the 2006 peak at approximately 1.1 million km². However, this coverage in 2018 is confined to a narrower vertical range of 21-

22km, centering closer to 21.5km. Such observations highlight the variability in the vertical extent of PSCs across different years.

Throughout the 15 analyzed Antarctic seasons, July consistently surpasses the areal coverage of other months in all seasons, with the sole exception being 2012, where August takes the lead. Remarkably, July's areal coverage exceeds 1 million km² in six distinct seasons (2006, 2008, 2011, 2014, 2016, and 2018), underscoring its significant role in the Antarctic PSC season. The only instances where July's areal coverage remains relatively "low" occur in 2010, with a peak near 640,000 km², and in 2012, where it reaches about 560,000 km². Notably, the peak altitude in 2012 is observed to be around 3km lower than that of 2010, illustrating the dynamic nature of PSC distribution and the variability inherent in their vertical extent during the Antarctic winter.

In the analysis of **August**, another crucial month in the Antarctic PSC season, it's observed that the top peak of areal coverage never surpasses 1 million km², yet it consistently maintains significantly high values across the seasons. The year 2006, following July's record maximum, sees August reaching its peak coverage at around 900,000 km², spanning an altitude range of 17-21km. The central altitude of this peak is approximately 18.5km, slightly lower than the average maximum areal coverage altitude typically observed in August. In the subsequent year, the peak of August's PSC areal coverage is approximately 700,000 km², with the central altitude around 19km. The year 2009 presents a scenario where August almost rivals the high values of July, nearing 850,000 km², but with a smaller vertical extent compared to July's distribution. The year 2012 stands out distinctly, as August not only competes with but also surpasses the PSC areal coverage of July, exceeding 560,000 km² within a relatively small vertical range, while July's values fluctuate between 480,000 and 560,000 km² for a similar vertical extent.

Overall, August firmly holds its position as the second most significant month in terms of PSC areal coverage over the Southern Hemisphere. It marks the beginning of a rapid decline in PSC coverage that becomes more pronounced in September and leads to considerably lower values by October. This trend underlines the seasonality of the Antarctic PSC cycle, where August serves as a transitional month, signaling the gradual reduction in PSC activity as the Antarctic winter progresses towards its end.

September, in its role within the Antarctic PSC season, tries to exhibit quite a stable seasonal variability. It is evident that during this month, PSCs predominantly form at lower altitudes compared to other months, and there is a noticeable decline in their areal coverage. A key characteristic of September is the concentration of PSCs within an altitudinal range of 14.5-16.5km. The most significant peaks of PSC areal coverage in September are observed in the years 2006, 2008, and 2011. During these years, the coverage peaks do not exceed 500,000 km² but tend to fluctuate between 400,000 and 480,000 km². This indicates a consistent, yet reduced presence of PSCs compared to the earlier months of the season. The year 2017 is particularly notable for recording the lowest PSC areal coverage in September, falling below 80,000 km². Similarly, 2019 also witnesses relatively low levels of PSC areal coverage, with values not

surpassing 100,000 km². These observations highlight the variability within the month of September, marking it as a period of transition towards the end of the Antarctic PSC season, characterized by lower altitudes and diminishing areal coverage of PSCs.

October, as the concluding month in our analysis based on CALIPSO data, displays a notable variability in PSC areal coverage compared to other months of the Antarctic season. This variability is characterized by some years exhibiting relatively high areal coverage, while others show significantly lower levels of PSC presence. Delving into the specifics, we find that the highest peak of PSC areal coverage in October was recorded in 2015. During this year, PSCs nearly spanned an area of approximately 200,000 km², primarily within an altitude range of 14-16km. The center of this peak is around 15km, aligning closely with the altitude of maximum PSC areal coverage typically observed for October. However, apart from the year 2015, the majority of the other years show PSC areal coverage not even surpassing 50,000 km², with PSCs occupying a more confined altitude range. An exception to this trend was noted in 2016, where PSC areal coverage in October remained high, nearing 150,000 km², but only within a narrow altitudinal span of 0.5km. Other years such as 2009, 2012, 2014, and 2019, witnessed October PSC areal coverage fluctuating around 25,000 km². This pattern in October, marked by its higher variability and often reduced PSC presence, signals the tail end of the Antarctic PSC season, indicating a transition towards the polar stratospheric conditions of the Southern Hemisphere's spring.

Linking our results with existing bibliography, it is noted that:

Southern Hemisphere

In the Southern Hemisphere, temperatures conducive to PSC formation typically occur within the stratospheric polar vortex. The Antarctic vortex is large, relatively axisymmetric, and exhibits consistency from year to year, as noted by Waugh and Randel (1999). Consequently, the Antarctic PSC season displays a regular pattern annually, beginning in mid to late May and extending into October. The total areal extent of PSCs usually reaches its peak during July and August, coinciding with the largest and coldest conditions of the vortex, and then markedly decreases in September, approaching near-zero levels by October.

The altitude range of PSCs spans from near the tropopause to above 25 km. However, there is an observable downward trend over time in the altitude of maximum areal coverage—from above 20 km early in the season to near 15 km by September. This trend aligns with the downward shift in the coldest temperatures axis as the vortex warms at higher altitudes, a phenomenon also documented by Poole and Pitts (1994).

Most years, as per Pitts et al. (2018), display a notable merging of the upper tropospheric and lower stratospheric cloud layers in July and August. This is often associated with CALIOP observations of deep synoptic-scale clouds extending from the troposphere into the stratosphere, reaching well above 20 km. These episodic events are likely the result of large-scale adiabatic

cooling along upwardly displaced isentropic surfaces above upper tropospheric anticyclones, as discussed in studies by Teitelbaum and Sadourny (1998), Teitelbaum et al. (2001), and Kohma and Sato (2013). Additionally, distinctive tilted cloud layers, often formed during the cold phases of strong orographic gravity waves, occasionally extend from the troposphere into the stratosphere, especially over the Antarctic Peninsula. These phenomena have been observed in various studies, including those by Cariolle et al. (1989), Höpfner et al. (2006), and Orr et al. (2015), and are visible in CALIOP orbit curtains like the one shown in Figure 10.

While the general seasonal evolution is consistent annually, moderate year-to-year variability in PSC coverage does occur, influenced primarily by dynamical processes that affect the vortex's size, thermal structure, and stability, as well as the strength and frequency of orographic and upper tropospheric forcing events. For example, the year 2006, characterized by an unusually large and cold vortex as reported by the World Meteorological Organization (2007), exhibited the largest PSC areas observed by CALIOP to date. Conversely, years like 2010 and 2012 had relatively warm vortices, resulting in significantly smaller PSC areas. The climatological mean seasonal evolution of Antarctic PSC areal coverage compiled for the 2006–2021 period, presented in Figure 35, serves as a reasonable approximation of the seasonal evolution in any given year. However, dynamic variability of the vortex, along with orographic and upper tropospheric forcing, can lead to significant deviations from this mean pattern, as emphasized by Pitts et al. (2018).

Northern Hemisphere

In the Northern Hemisphere, the irregular topography contributes to stronger upward-propagating wave activity than in the Southern Hemisphere, leading to a weaker and more distorted Arctic vortex compared to the Antarctic, as detailed by Waugh et al. (2017). Consequently, the Arctic polar vortex is generally warmer and displays greater temporal variability, including sudden stratospheric warmings. These warmings, as Charlton and Polvani (2007) observed, can disrupt or even completely break down the vortex in midwinter.

This variability is reflected in the year-to-year differences in Arctic PSC occurrence, as illustrated in Figure 42. The figure shows the monthly mean PSC areal coverage for each of the 15 Arctic seasons in the CALIOP data record. Notable seasons include 2010–2011, marked by persistent PSCs from December to March, leading to record ozone depletion over the Arctic (Manney et al., 2011b). The 2015–2016 season, as observed by Pitts et al. (2018), saw the largest areal coverage of PSCs over the Arctic to date, including rare synoptic ice PSCs, previously observed only in the 2009–2010 season.

Contrastingly, the warm winter of 2014–2015 was almost devoid of PSCs, highlighting the influence of varying atmospheric conditions on PSC formation. Additionally, similar to the Antarctic, the Arctic also experiences merging of upper tropospheric and lower stratospheric cloud layers during some winters. This phenomenon, indicative of upper tropospheric forcing

events (Fromm et al., 2003; Achtert et al., 2012), results in deep synoptic-scale cloud layers extending from the troposphere into the stratosphere.

These observations underscore the complexity of PSC dynamics in the Arctic, driven by unique atmospheric conditions and topographical influences that differentiate it from the Antarctic. This variability has significant implications for understanding the stratospheric processes that contribute to polar ozone depletion and atmospheric chemistry in the Northern Hemisphere.

Trends

From 2006 to 2021, our study reveals nuanced trends in the areal extent of PSCs. In the Southern Hemisphere, there's been an observed, albeit statistically insignificant, downward trend in PSC areal extent. This decline, as discussed in the work of Stone et al. (2018), could be contributing to the recovery of ozone depletion noted since the year 2000. The significance of this trend lies in its potential link to global climatic changes and atmospheric recovery processes. In contrast, the Northern Hemisphere, demonstrates a slight upward trend in PSC areal coverage during the same period. Although this trend does not reach statistical significance, it remains critical for understanding the dynamic nature of PSCs and their influence on the Arctic atmosphere. This upward trend may be linked to increased stratospheric temperature fluctuations and variability in the Arctic, as compared to the Antarctic. Such variability might result in more frequent conditions that are favorable for PSC formation. Studies, including those by Manney et al., have delved into the dynamics of the Arctic stratosphere, particularly examining phenomena like sudden stratospheric warmings and their impact on PSC formation. Notably, existing literature has not extensively examined the trend of PSC areal coverage over the years for each specific altitudinal layer across the stratosphere, an aspect that our current chapter aims to address comprehensively.

The observed variability in PSCs can generally be attributed to a range of factors including alterations in atmospheric circulation patterns, volcanic activity, fluctuations in greenhouse gas concentrations, and notably, variations in condensation nuclei. This multifaceted nature of variability plays a significant role in the formation and extent of PSCs. Studies conducted by Rex et al., among others, have delved into the analysis of these year-to-year changes in PSCs, exploring their profound implications for stratospheric chemistry and climate. Such research sheds light on the complex interactions within the stratosphere, emphasizing how these varied factors collectively influence the behavior and impact of PSCs in both hemispheres.

In this study, our primary focus is not to delve into the myriad factors influencing PSCs, a task that would entail extensive additional research. Instead, our objective is to highlight and present the existing trends in PSC behavior. By identifying and documenting these trends, we aim to contribute a foundational understanding of PSC variability, which could serve as a basis for future studies exploring the complex influences and mechanisms driving these trends. This approach allows us to concentrate on the patterns observed in PSC areal coverage, providing

valuable insights into their temporal dynamics without venturing into the detailed analysis of the underlying causative factors.

Monthly Trends

NORTHERN HEMISPHERE

Upon examining the trend of monthly mean values of PSC areal coverage over the Northern Hemisphere from December 2006 through March 2021, we can state with considerable confidence that there is a general, albeit slight, upward trend. This assertion is firmly grounded in our examination of the dataset for each atmospheric layer, as provided by CALIPSO. Central to our analysis is the criterion that PSC detection should occur at least 4km above the reported tropopause. It's crucial to note that, within our dataset, trends were observed at altitudes below 9km. However, we have chosen to exclude these trends from our analysis due to the relatively minor areal coverage of clouds at these lower altitudes. Moreover, it is evident from prior discussions that in these lower altitudes, the clouds observed are more likely to be upper cirrus.

To ensure clarity and precision in our analysis, we have limited our focus to clouds situated above 10km. This decision has not complicated our results; rather, it has enhanced the specificity and accuracy of our findings. In the Northern Hemisphere, we have observed both upward and downward trends in PSC areal coverage. Downward trends are specifically noted at altitudes of 10.4km, between 12-13.1km, across all layers from 24-29km and at 29.6km. On the other hand, upward trends are evident from 10.6-11.8km, 13.3-23.7km, and from 29.1-29.4km. It's important to highlight that none of these trends reached statistical significance. When considering the entire scope of our analysis, which encompassed 108 distinct altitudinal layers from 10.4km to 29.6km, we found that a downward trend appears in 38 layers, whereas a dominant upward trend is observed in 70 layers. This distribution clearly indicates an overall increasing tendency in PSC areal coverage in the Northern Hemisphere based on monthly mean values.

Delving deeper into the results, as discussed in section 4.1.2, we find that the peak of average PSC areal coverage for the Northern Hemisphere is located at 21km, indicating that this layer, where the densest concentration of PSCs is found, is part of the upward trend. Moreover, the layers corresponding to the peaks of average PSC areal coverage for each Arctic month—specifically 21.7km, 20.6km, 19.4km, 17km, and 11.5km—are also included in these upward trending layers. This further bolsters the suggestion of an upward trend in the Northern Hemisphere. Thus, the conclusion of an upward trend in PSC areal coverage in the Northern Hemisphere is supported not just by the fact that 70 out of 108 layers exhibit an increasing trend, but also because all layers representing the highest PSC areal coverage fall within this category of upward trends.

Indicatively, are presented four graphs to illustrate the trends in PSC areal coverage. Of these, two graphs depict the most significant positive trends, while the other two illustrate negative trends. The rationale behind choosing these specific graphs lies in their representation of the altitudes where these trends are most pronounced.

For the positive trends, we focused on altitudes where the increase in PSC areal coverage is most notable. One of these graphs specifically highlights the altitude corresponding to the top peak of PSC areal coverage observed for the Northern Hemisphere (which happens to be the same for the Southern Hemisphere, at 20.3km), showcasing where the upward trend is most prominent. This choice provides a clear visualization of the layers where PSCs are most densely concentrated and where the upward trend is most evident. Conversely, for the negative trends, one of the graphs was selected to represent a low altitude, despite the significant downward trend being more apparent in higher altitudes. This was done intentionally to demonstrate that the behavior of a downward trend in PSC areal coverage is not confined to specific altitudes but is also observable in different strata of the atmosphere. Indeed, the selection of these four representative graphs is a decision, primarily influenced by the space constraints within this master thesis. By focusing on these examples, we think that effectively encapsulate the primary positive and negative trends in PSC areal coverage. This approach allows us to provide a concise yet comprehensive overview of the trend patterns without the need to present all the data for all layers.
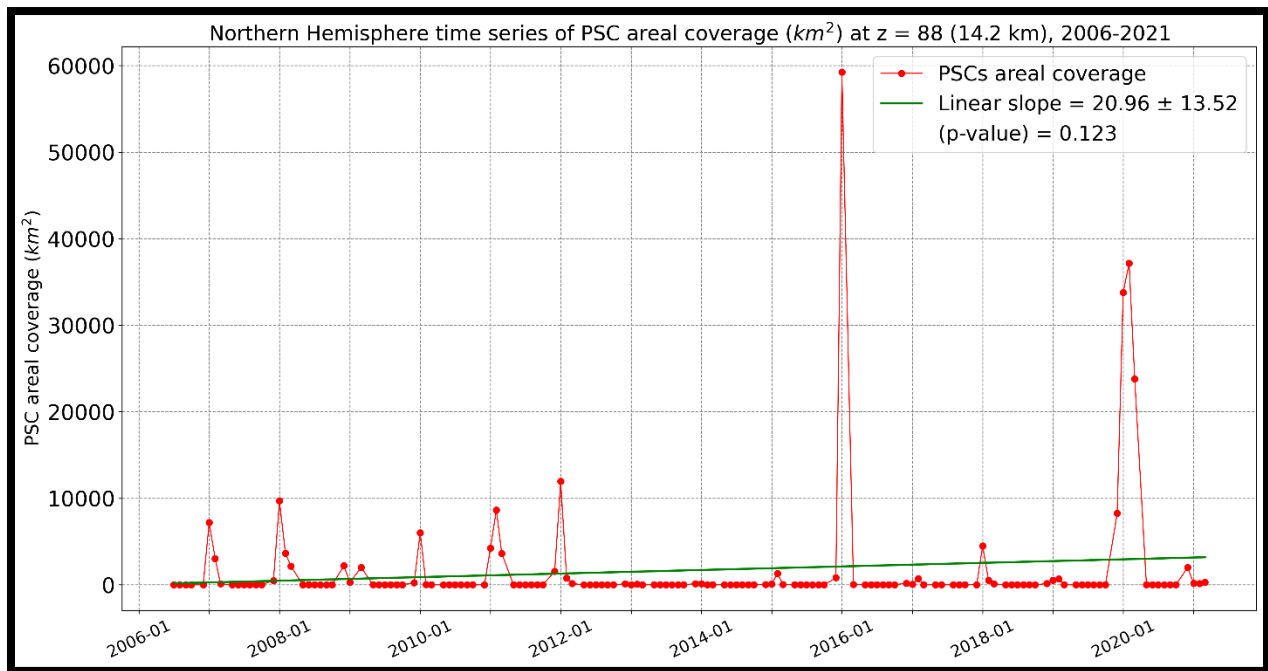

Figure 45: Interannual positive trend of monthly mean values of PSC areal coverage over the Northern Hemisphere, for the altitude with the most significant trend, at 14.2km.

In Figure 43, we observe a notable aspect of the PSC areal coverage at an altitude of 14.2km. The p-value, reaches its lowest at 0.123 among all the positive trends we've examined. However,

this result must be contextualized with the exceptional peaks observed in January 2016 and 2020. In these years, the PSC areal coverage at this altitude surged to levels 4 times (in 2020) and 6 times (in 2016) higher than the highest peak recorded prior to 2016.

Such significant peaks play a crucial role in influencing the overall trend. Without these extraordinary peaks, it is plausible to suggest that the trend at this altitude would have demonstrated a negative inclination rather than a positive one. Therefore, while the trend at 14.2km initially appears positive, this observation is heavily swayed by the anomalous peaks in 2016 and 2020. This raises questions about the stability and consistency of this trend, suggesting that it may not be as robust or indicative of a general upward trend as it initially appears.
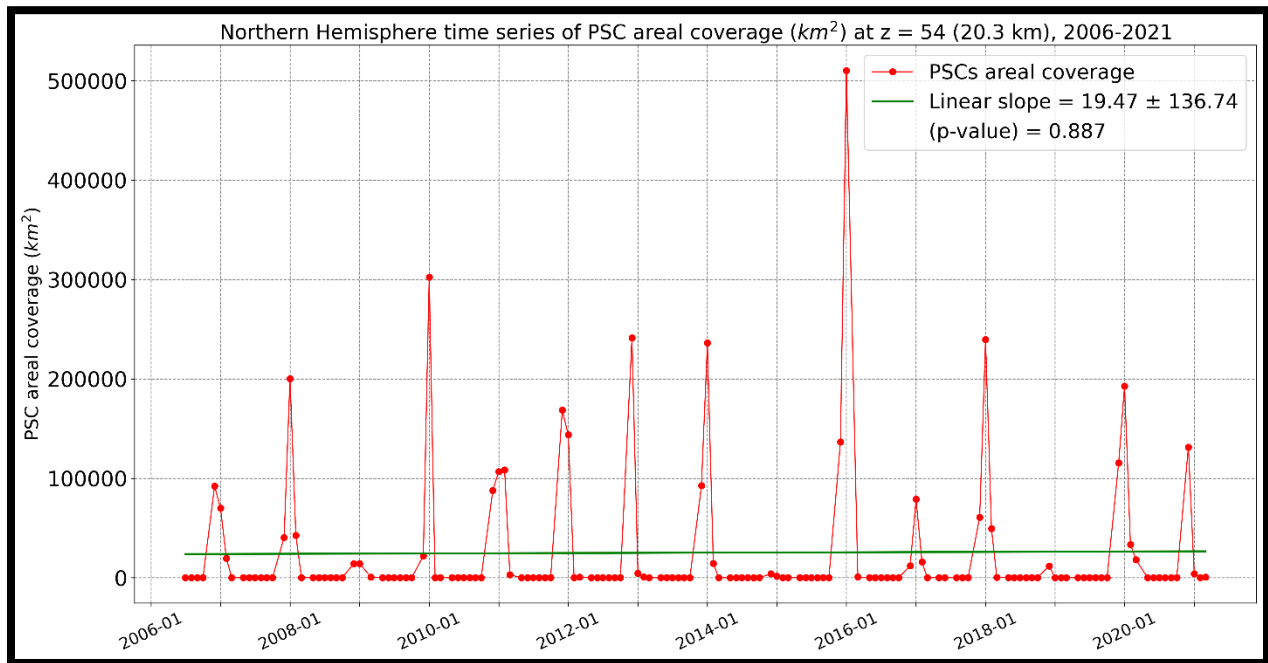

Figure 46: Interannual positive trend of monthly mean values of PSC areal coverage over the Northern Hemisphere, for the altitude with the greatest PSC areal coverage observed, at 20.3km.

The data at 20.3km (Figure 44), the altitude of the greatest peak of Northern Hemisphere's monthly mean PSC dataset, presents a striking scenario. This altitude marks the site of the greatest peak in the entire dataset, in terms of areal coverage in km^2, occurring in January 2016. Here, the PSC areal coverage notably surpassed 500,000 km², representing a substantial increase, especially when contrasted with the exceptionally low areal coverage observed in 2015. Subsequent peaks at this altitude, though significant, were comparatively lower, with the second-highest peak reaching approximately 300,000 km² and the third just about 250,000 km². This pattern at 20.3km underscores the dramatic rise in PSC areal coverage in 2016. It's noteworthy that this extreme peak was not isolated to the 20.3 km altitude but was also evident across a broad altitudinal range from 13-23km (not in the same extent as observed at 20.3km).

However, the magnitude of the peak's deviation from the second or third highest peaks varied across these altitudes. An additional dimension of our analysis focuses on the subsequent peaks that followed the 2016 surge. Until January 2011, the second peak at 20.3km was predominant within the altitudinal range of 23-26km. Post this period, the dominance shifted to higher altitudes, extending up to 29.5km. This shift in the location of the peak within the stratosphere is indicative of dynamic changes in PSC distribution over time and altitude.
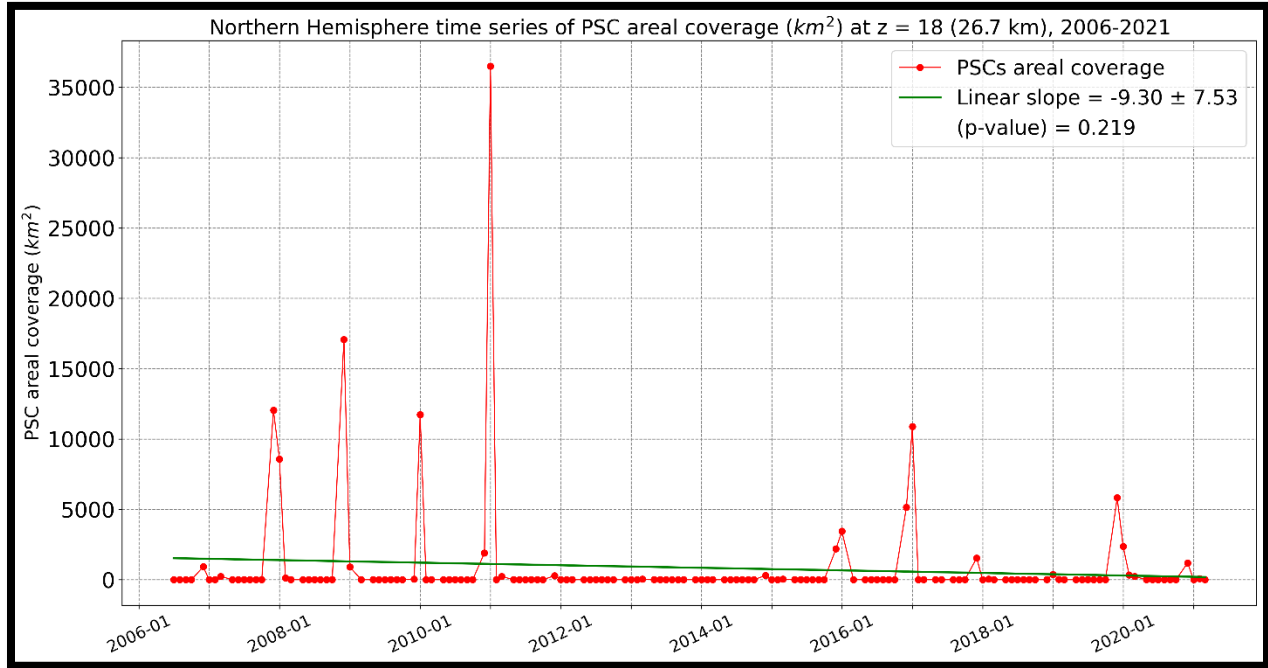

Figure 47: Interannual negative trend of monthly mean values of PSC areal coverage over the Northern Hemisphere, for the altitude with the most significant trend, at 26.7km.

As seen in Figure 45, at 26.7km the peak of areal coverage has been shifted in 2011. At this altitude, the most significant negative trend is indicated by a p-value of 0.219. Although this value is not statistically significant, it is important to consider the context in which this trend is observed. The pronounced increase in PSC areal coverage in 2011 is a key factor complicating the interpretation of this trend. The peak in 2011 is approximately twice as large as the second-highest peak, which occurred in 2009. Following this peak in 2011, the areal coverage of PSCs at 26.7km in the Northern Hemisphere remained at exceptionally low levels until there was a noticeable increase in 2017, surpassing 10,000 km², and again in 2020, exceeding 5,000 km².

Comparing the Figures 43 and 45, which are representing trends at 14.2km and 26.7km respectively, a consistent pattern of extremely low PSC areal coverage at both altitudes in the years 2013, 2014, 2015, and 2019 appears. This observation suggests a broader trend across different altitudes in the Northern Hemisphere, indicating years where PSCs are notably scarce.

Figure 46, depicting the PSC areal coverage at 12.7km, presents a scenario that is simultaneously more intricate yet smoother than other altitudes. In this case, the fluctuations in areal coverage

from year to year are not as drastically pronounced. Despite a p-value of 0.54, which typically suggests a lack of statistical significance, there is a discernible and seemingly stable downward trend in areal coverage at this altitude. This trend suggests a consistent decrease over time, hinting at a more persistent downward trajectory in PSC coverage at 12.7km.

A notable observation at this altitude is the peak in PSC areal coverage recorded in December of 2009, where it exceeded 30,000 km². Interestingly, the second-highest peak occurred in February of the same year, reaching approximately 27,000 km². This pattern is somewhat atypical given the general trend observed in the Northern Hemisphere, where January is more likely to witness the highest values of PSC coverage. Upon closer examination of the data presented in these graphs, it becomes apparent that significant peaks in PSC coverage can indeed occur in both December and February. However, it is also clear that such peaks are not typically observed in March.
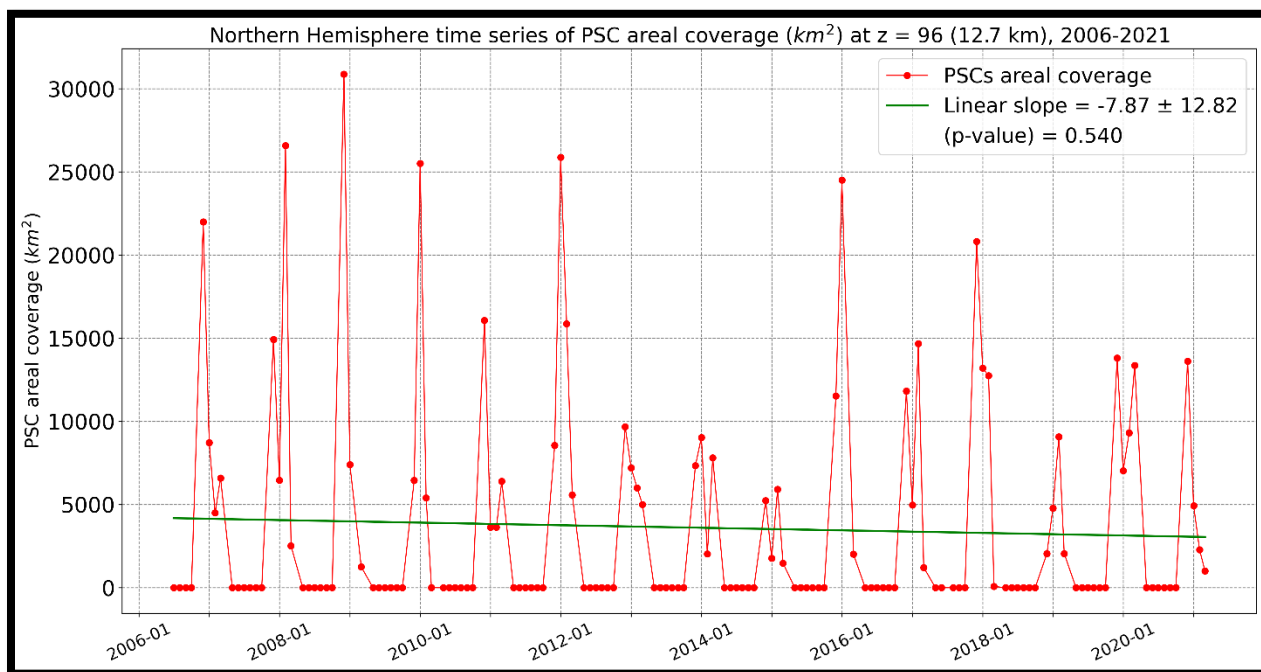

Figure 48: Interannual positive trend of monthly mean values of PSC areal coverage over the Northern Hemisphere, at 12.7km.

Continuing with this logic, we extend our analysis to the Southern Hemisphere, applying a similar methodology to select representative trends that effectively illustrate the overarching patterns in PSC areal coverage. This selection will be guided by the most significant trends observed in the Southern Hemisphere, ensuring that the chosen examples are reflective of the broader climatic and atmospheric dynamics in this region. Subsequently, we will delve into the analysis of yearly trends, adopting the same approach as this one used for the monthly trends.

SOUTHERN HEMISPHERE

In the Southern Hemisphere, the overall trend in PSC areal coverage is more discernible than in the Northern Hemisphere, with a distinct downward tendency. Similar to the Northern Hemisphere, both positive and negative trends are observed across different atmospheric layers. However, the Southern Hemisphere is characterized predominantly by negative trends, which are observed in 92 out of 108 layers. The remaining 16 layers exhibit an upward trend.

As with the Northern Hemisphere analysis, these trends have been analyzed across 108 distinct layers, beginning from an altitude above 10km. A striking feature of the Southern Hemisphere trends is the uniformity in the direction of the trends across a wide range of altitudes. All layers from 10.4km up to 26.7km exhibit a negative trend, while the higher altitudes, specifically those above 26.7km, display positive trends. This contrast with the Northern Hemisphere, where trends varied across six different altitudinal zones, suggests a more pronounced and consistent downward trend in the Southern Hemisphere until the 26.7km mark, where there appears to be a transition in trend direction. However, this transition and its underlying causes have not been extensively documented or referenced in existing literature.

It's noteworthy that, although none of these trends reach statistical significance at the 95% confidence level (indicated by p-values lower than 0.05), many of the p-values in the Southern Hemisphere are smaller than 0.1, a pattern not as prevalent in the Northern Hemisphere. This observation implies a stronger trend signal in the Southern Hemisphere, albeit not strong enough to be considered statistically significant by conventional standards.

When we correlate our findings from Section 4.1.2 regarding the vertical distribution of PSC areal coverage with the observed trends, an intriguing pattern emerges in the Southern Hemisphere, just like with the Northern Hemisphere as well. In Section 4.1.2, it was established that the altitude with the highest average maximum areal coverage of PSCs in the Southern Hemisphere is at 20.3 km. This altitude is notably where the top peak of the dataset was observed, with an impressive areal coverage of approximately 1.2 million km² in July 2006. Additionally, the altitudes corresponding to the maximum areal coverage for the average months, spanning from May through October, were identified at 20.3, 20.5, 21.2, 20.3, 15.4, and 15.1 km. All these identified altitudes fall within the range that exhibits a downward trend. This is a critical observation, as it confirms that the dominant downward trend in the Southern Hemisphere is not only substantiated by the fact that 92 out of the 108 layers exhibit this trend, but also because all layers that represent the maximum average areal coverage for each month are located within this downward trending altitudinal range.

This alignment of the layers with the maximum average areal coverage for the Southern Hemisphere and the altitudinal zones of the downward trend provides a compelling argument for the predominance of this downward trend. It underscores that the downward trend is pervasive across the key layers that contribute significantly to the overall PSC areal coverage.

To effectively convey the results of our study, we have selected eight layers out of the 108 analyzed to showcase the general behavior of monthly PSC areal coverage across the Southern Hemisphere. This selection has been made to provide a broad perspective on the vertical distribution of PSCs, ensuring that a wide range of altitudes is represented. The chosen layers aim to shed light on the behavior of PSCs not only at low altitudes but also at mid and high altitudes. By doing so, a more holistic view of the stratospheric dynamics at play can be offered, allowing us to highlight trends and patterns that might be prevalent at different altitudinal levels.

At the lower altitude of 11.3km, as seen in Figure 47, the analysis of PSC areal coverage reveals some intriguing patterns. The highest peak in areal coverage at this altitude is observed in 2011, slightly surpassing 40,000 km², followed by another significant peak in the subsequent year, only about 2,500 km² lower. This altitude marks a notable increase in PSC areal coverage compared to just 0.9km below, at 10.4km, where the peak barely exceeds 12,000 km². This increase at 11.3km can stand as an indication of the altitude's significance in terms of PSC formation and distribution. However, a downward trend is apparent at 11.3km, particularly after 2016, with peaks in areal coverage gradually decreasing over time. This trend suggests a diminishing presence of PSCs at this altitude in recent years. Additionally, the year 2006 stands out for its consistency in PSC coverage across three consecutive months - July, August, and September - all showing similar areal coverage. This pattern of consistency is also evident in 2007, from June through October, with areal coverage fluctuating within the range of 16,500 to 18,000 km².
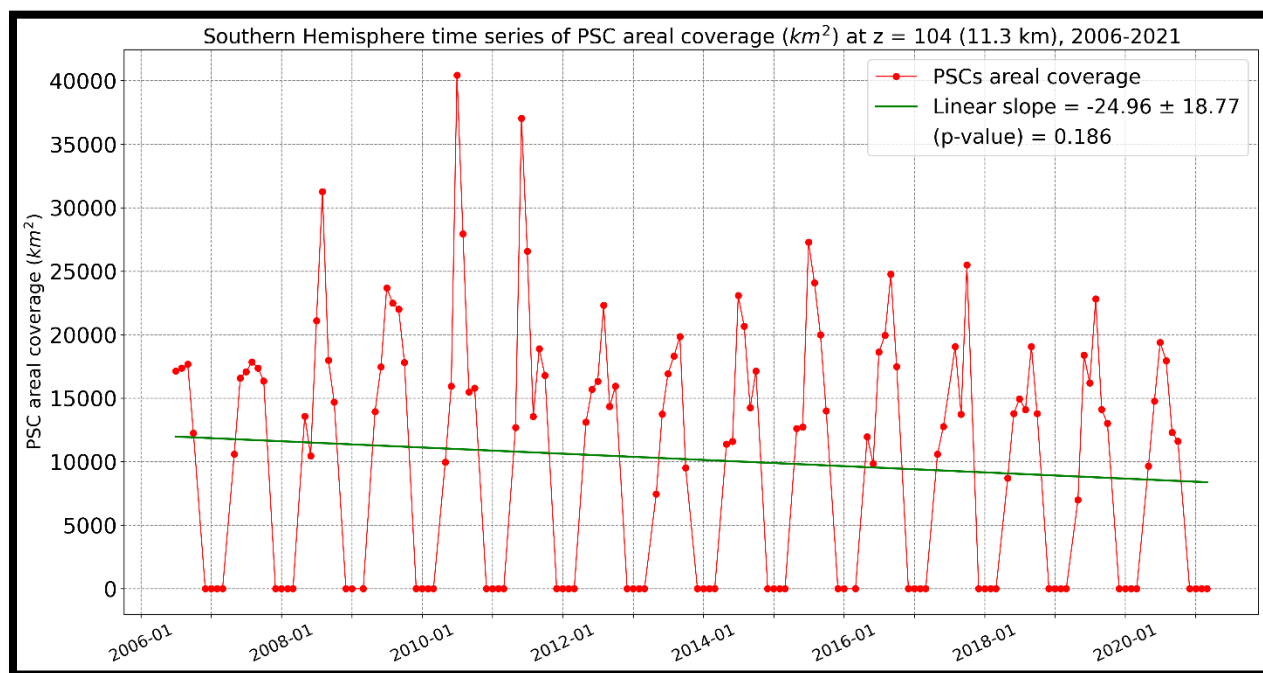

Figure 49: Interannual negative trend of monthly mean values of PSC areal coverage over the Southern Hemisphere, at 11.3 km.

Another notable observation at 11.3km is the variability in the timing of the main peak during a seasonal period. For instance, in 2008, the peak in PSC coverage occurs in August, whereas in 2011, it is observed in June. This variability in the timing of peak coverage across different years can possibly highlight the dynamic nature of PSC distribution and the influence of various atmospheric factors that can affect their formation and extent at this altitude.
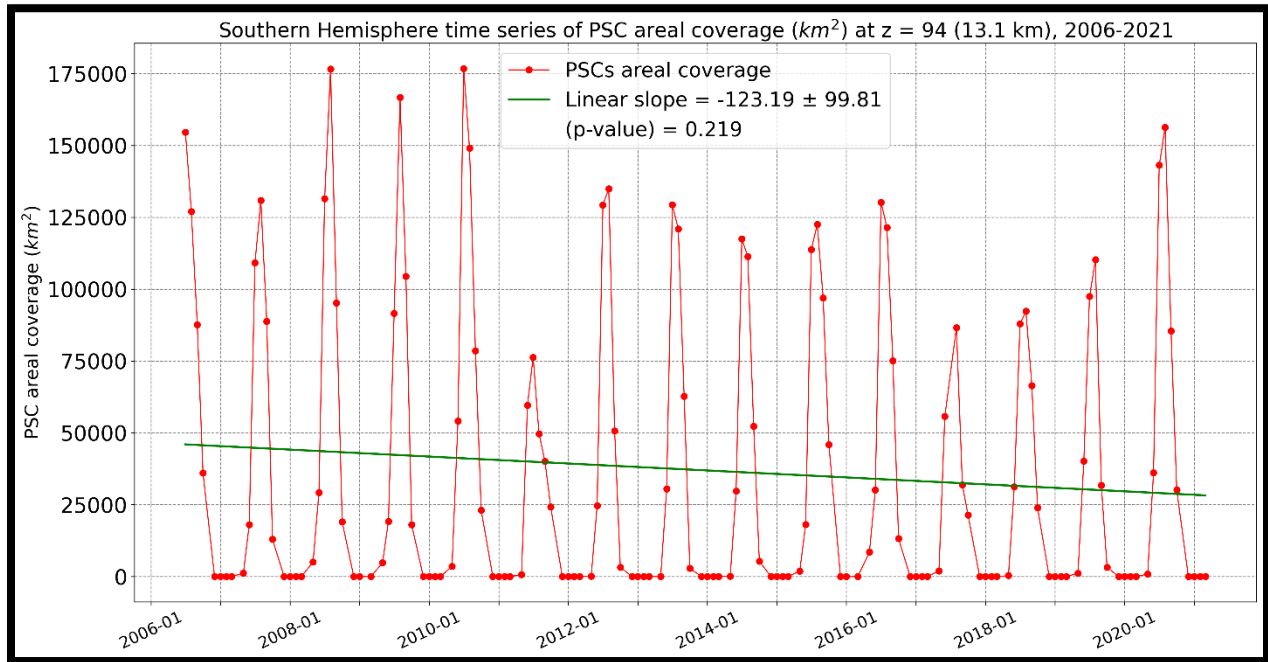

Figure 50: Interannual negative trend of monthly mean values of PSC areal coverage over the Southern Hemisphere, at 13.1 km.

Moving at the altitude of 13.1km, Figure 48, the highest peaks have just exceeded an area of 175,000 km², while the lowest, observed in 2011, reached approximately 75,000 km². Notably, two top peaks are observed with roughly similar areal coverage, each nearing 175,000 km². Sandwiched between these, in 2009, lies another significant peak, at around 170,000 km². This indicates that the period from 2008 to 2010 was marked by the highest values of PSC areal coverage observed at this altitude. A particularly interesting aspect at 13.1km is the timing of these peak occurrences. Contrary to what might be expected, most peaks, if not all, occur in August rather than July, which is generally considered the most favorable month for high PSC areal coverage. This shift in peak timing to August is an intriguing deviation from the norm.

Another point of note is the consistently low mean values of PSC areal coverage in May across the dataset, typically not surpassing 5,000 km². An exception to this trend is May 2016, where coverage reached 10,000 km². This outlier suggests variability in the onset of the PSC season. Additionally, a noteworthy difference is observed in 2009 between July and August, where the latter exceeds the former's areal coverage by about 75,000 km². This significant gap between the two months in that year underscores the month-to-month variability in PSC distribution.

Lastly, an analysis of the more recent years from 2017 to 2020 at this altitude suggests an upward trend in PSC areal coverage. This observation could point to a possible shift in PSC dynamics in the Southern Hemisphere, indicating changes in atmospheric conditions conducive to PSC formation at this altitude. This upward trend, while needing further observation and analysis, marks an interesting development in the behavior of PSCs at 13.1km.
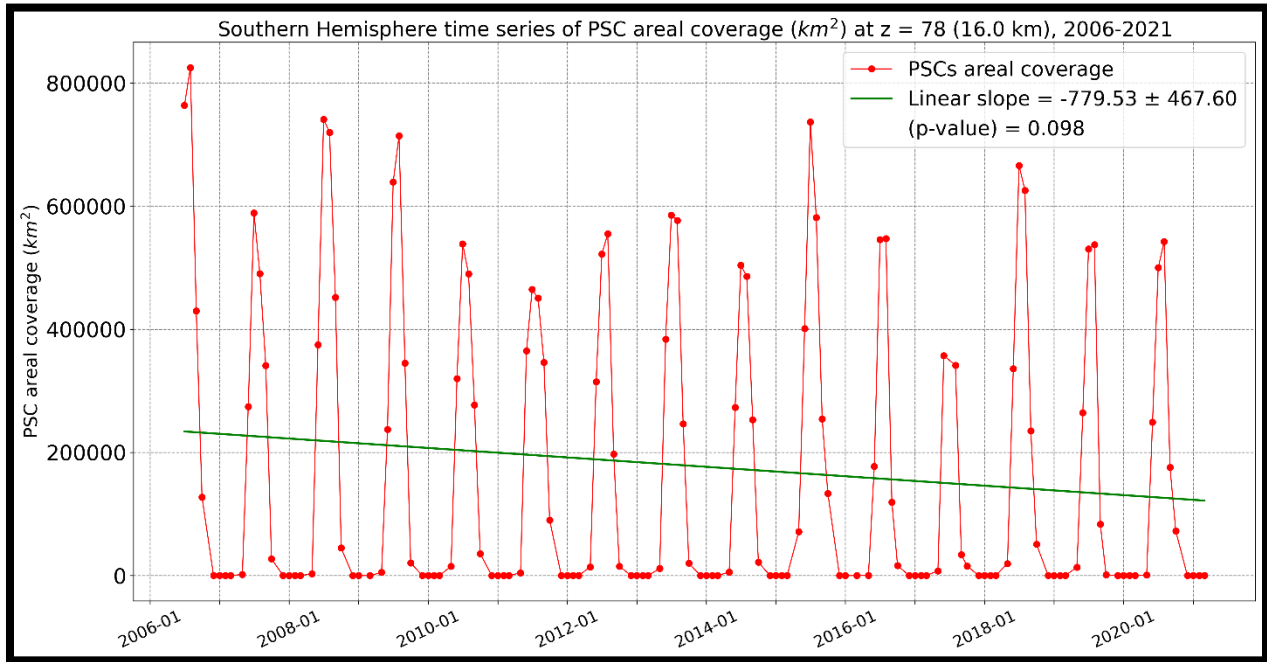

Figure 51: Interannual negative trend of monthly mean values of PSC areal coverage over the Southern Hemisphere, for the altitude with the most significant trend, at 16 km.

At 16km, as depicted in Figure 49, we encounter significant values in PSC areal coverage, with a notable peak surpassing 800,000 km². This peak, recorded in August 2006, stands as the highest until the altitude reaches 17.2km, at which point July begins to emerge as the dominant month for PSC areal coverage. Delving deeper into the data at 16km, we observe the most pronounced negative trend seen in our analysis at this altitude, with a p-value of 0.098. This is particularly noteworthy as it's the lowest p-value encountered in our upward journey through the stratosphere, starting from 10km. The top peak of August 2006 is closely followed by a significant peak in July 2008, which shows an areal coverage of roughly 750,000 km², a value closely mirrored by July 2015.

At this altitude, both July and August emerge as dominant months, often displaying closely matched areal coverage values within the same seasons. For instance, the seasons of 2013, 2016, and 2019 exhibit only minor differences in coverage (not exceeding 10,000 km²) between these months. This pattern suggests a relatively even distribution of PSCs during the mid-winter months in the Southern Hemisphere at this specific altitude, which can be also observed inside the altitudinal zone 15-17km (not depicted). Additionally, the PSC areal coverage values for May at this altitude remain notably low, generally not surpassing 10,000 km² across all observed

seasons. A remarkable exception is May 2015, where the coverage escalates to approximately 75,000 km². This anomaly indicates variability in the early onset of the PSC season, suggesting that certain atmospheric conditions can lead to earlier and more extensive PSC formation at this altitude.
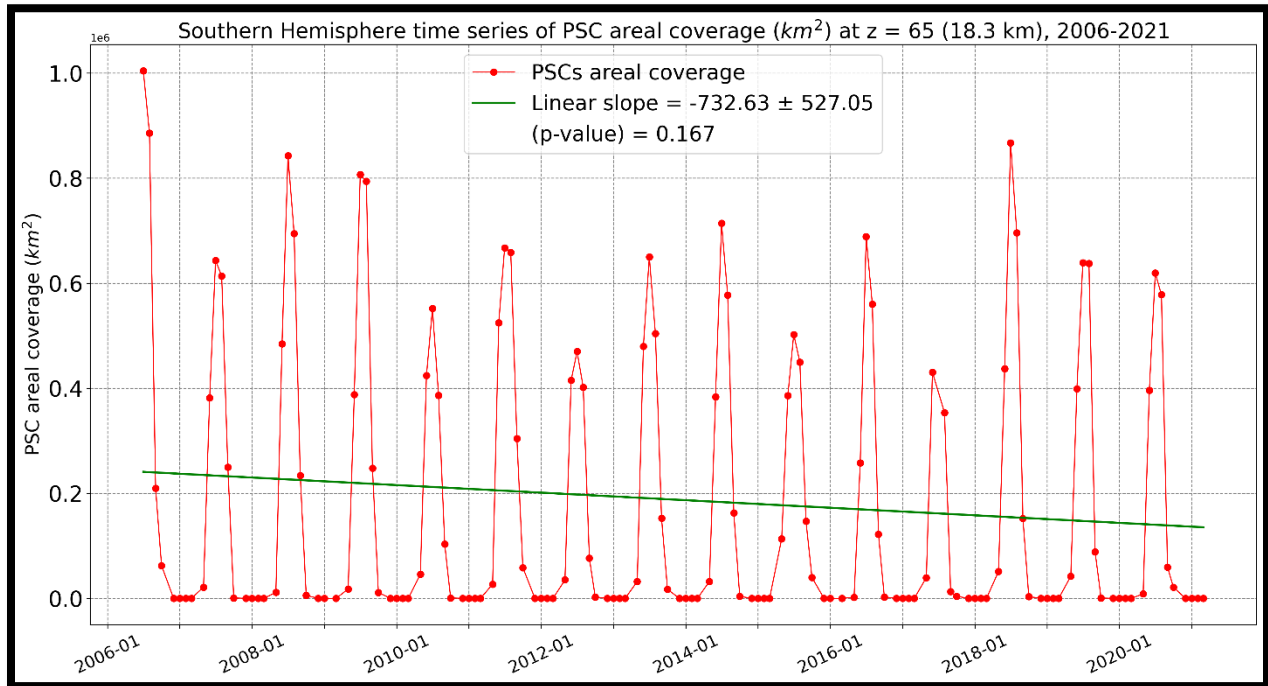

Figure 52: Interannual negative trend of monthly mean values of PSC areal coverage over the Southern Hemisphere, at 18.3 km.

Reaching the altitude of 18.3km, as illustrated in Figure 50, we encounter a significant milestone in our study: for the first time, a peak in PSC areal coverage surpasses the 1 million km² mark. This remarkable peak is recorded in July 2006 and remains the highest observed peak, surpassing 1 million km², up to an altitude of 21.9km. At 18.3km, July clearly emerges as the predominant month for PSC areal coverage, consistently holding the record for the seasonal peak across all observed years. Following the record-setting peak in 2006, the second highest peak in PSC areal coverage at this altitude occurs in 2018, with an impressive coverage exceeding 850,000 km². The third highest peak is observed in 2008, surpassing 825,000 km². An interesting dynamic is noted in the 2019 season, where August nearly rivals the areal coverage of July, falling short by just about 5,000 km². This close competition between July and August in the same season is a recurrent theme, although June and July sometimes show significant differences, with the largest disparity observed in 2018, reaching 175,000 km².

Another notable aspect at this altitude is the behavior of PSC coverage in May. Although the monthly mean values of PSC areal coverage in May generally remain low, not exceeding 25,000 km², May 2015 stands out with coverage exceeding 125,000 km². This marks a departure from the trend observed at lower altitudes, where May's coverage was consistently lower than that of

October. At 18.3km, we observe a reversal of this trend, with May's PSC areal coverage surpassing that of October.
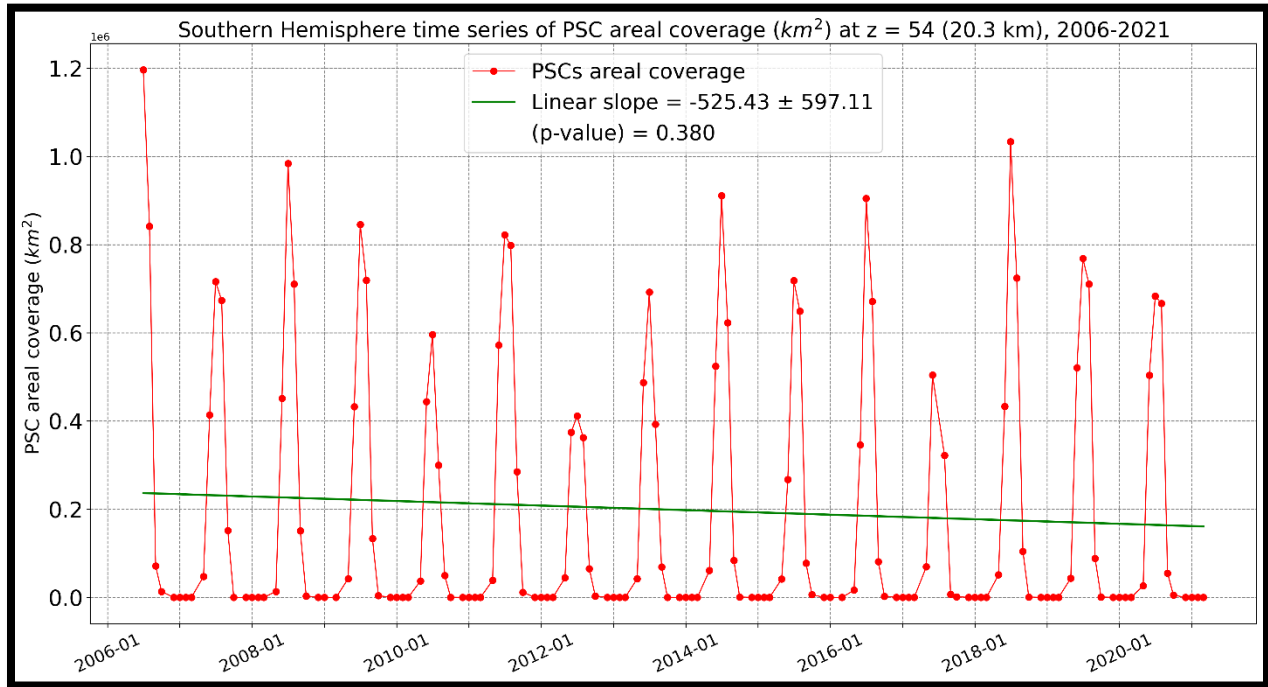

Figure 53: Interannual negative trend of monthly mean values of PSC areal coverage over the Southern Hemisphere, for the altitude with the greatest PSC areal coverage observed, at 20.3 km.

At the altitude of 20.3km, Figure 51, we observe the most significant peak in PSC areal coverage within the entire dataset. This remarkable peak is part of the monthly mean value for July 2006 and stands out as the only instance where the areal coverage escalates to an extraordinary extent, reaching 1.2 million km². This represents the absolute zenith of PSC areal coverage observed in our study. Following this unprecedented peak, the next highest peak in terms of areal coverage surfaces in July 2018, surpassing the 1 million km² mark. The third highest peak, observed in 2008, approaches this 1 million km² threshold. A unique characteristic of the 20.3km altitude is that, across all seasons, July consistently hosts the highest peaks in PSC areal coverage. The most pronounced difference between July and August within the same season is recorded in 2006. In this year, July's areal coverage surpasses August's by about 375,000 km², underscoring the significant disparity in PSC presence between these two months. This difference highlights the prominence of July in terms of PSC distribution at this altitude.

The lowest peak in our dataset is observed in July 2012, with an areal coverage of 400,000 km². This value sets a notable benchmark, as it helps to underscore the immense disparity between the highest and lowest peaks in PSC coverage at this altitude. The highest peak, as previously mentioned, reaches an astonishing 1.2 million km². This means that the gap between the highest and lowest peaks is a staggering 800,000 km², or put differently, the highest peak is three times larger than the lowest. This threefold difference is a first in our observations, highlighting the

significant variability in PSC coverage at this altitude. A closer look at consecutive seasonal peaks reveals that the maximum difference occurs between the 2006 and 2007 seasons. In this case, the areal coverage in 2007 is about 37.5% less than that of 2006, with a difference exceeding 400,000 km². This substantial decrease from one year to the next illustrates the dynamic nature of PSC distribution and the factors influencing their formation and extent.

Another noteworthy observation at 20.3km is the trend in May's monthly mean values, which substantially exceed those of October. While most of October's values hover around 10,000 km², May's figures are considerably higher. However, despite these intriguing findings and the marked variability in PSC areal coverage at 20.3km, the statistical analysis yields a p-value of 0.380. This value indicates that the trend observed at this altitude, while notable, is not statistically significant. The lack of statistical significance suggests that the observed variations in PSC coverage might be strongly influenced by short-term atmospheric dynamics as well, or other transient factors, rather than long-term climatic trends only, as mostly discussed before.

According to what has been discussed so far, the formation of PSCs is quite closely related to the dynamics of the polar vortex over the Arctic and the Antarctic. Moreover, according to recent studies such as Waugh et. al 2018, Pitts et. al 2018, Stone et al. 2018 and Charlton Polvani 2007, the formation of PSCs is supported to be a multifactored event. These suggest that the polar vortex dynamics, stratospheric warming events – and in general temperature fluctuations, even El Niño's Influence can contribute to the formation or destruction of PSCs. Many studies of Rex et al. have been focused on the short-term variability in the polar regions, suggesting that PSC trends can be influenced not only by atmospheric circulation patterns, but also volcanic activity, and variations in greenhouse gas concentrations. Thus, not a clear explanation can be attributed to these no statistically significant trends and fluctuations, focused on each specific layer in the earth's atmosphere.

In our trend analysis, we have concentrated on identifying and elucidating the most salient observations derived from examining the temporal behavior of PSC areal coverage. This includes a detailed commentary on the observed peaks, the variations between consecutive years, and other notable aspects. The goal of this approach is to furnish a comprehensive overview of the interannual behavior of PSCs, highlighting patterns and deviations that emerge over time.

Continuing our discussion, we now turn our attention to the 25km layer, as depicted in Figure 52, where the trend of decreasing PSC areal coverage persists. At this elevation, no peak in PSC coverage surpasses 400,000 km². Four distinct peaks are observed, all in July, where PSC areal coverage exceeds 375,000 km². The smallest of the peaks, covering approximately 65,000 km², is recorded in July 2012. The variability in areal coverage year-on-year at this altitude is pronounced; for instance, the 2009 peak is more than five times larger than that in 2010, and similarly, the peak in 2011 is around five times greater than in 2012. This observation suggests that at higher altitudes, where PSC concentrations diminish, the variations in areal coverage become increasingly pronounced, exhibiting significant disparities between annual peaks.
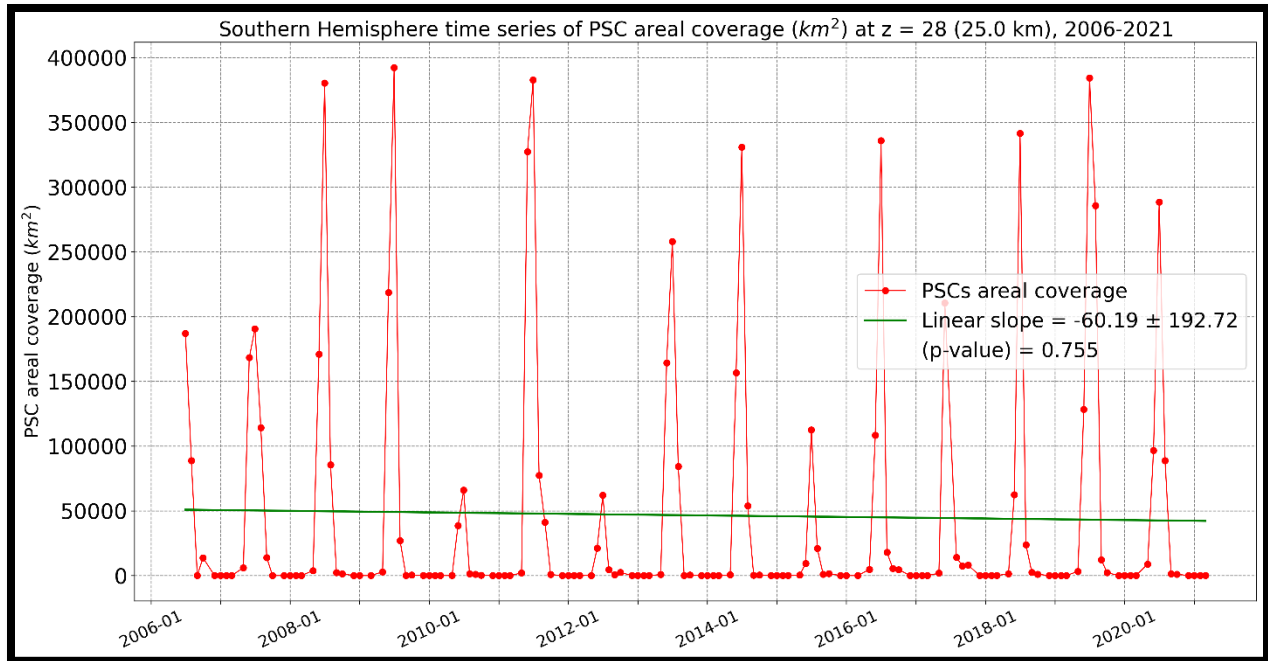
Figure 54: Interannual negative trend of monthly mean values of PSC areal coverage over the Southern Hemisphere, at 25 km.

Despite these noticeable fluctuations, the p-value at this altitude is relatively high (0.755), indicating that the trend observed here lacks statistical significance. Another point of interest at this altitude is that the average monthly values of PSC coverage for May and October remain quite low, with September now also showing marginally higher values.

At the altitude of 26.9km, Figure 53, we observe a marginal upward trend in PSC areal coverage, though it is not statistically significant (p-value = 0.755). The areal coverage of PSCs at this elevation exhibits considerable fluctuations, with the highest peak in 2011 reaching approximately 25,000 km², while the lowest peak, observed in 2010, barely attains 2,000 km². This variability presents a challenge in establishing a definitive pattern for PSC areal coverage at this altitude. Nevertheless, a closer inspection of the data from 2015 to 2020 suggests a more discernible upward trend in PSC areal coverage.

At 29.3km, as illustrated in Figure 54, we encounter the most significant p-value across all examined layers. This value, though marginally above the standard threshold for statistical significance (0.053), signifies a noteworthy trend at this high altitude. However, it's important to recognize that the highest peak in PSC areal coverage at this altitude modestly surpasses just 5,000 km², indicating that PSC occurrences are relatively scarce at these elevated stratospheric levels compared to lower altitudes. The lowest recorded peak, in 2009, barely reaches 500 km² — almost an order of magnitude smaller than the peak observed in 2017. A particularly interesting aspect of PSC behavior at this altitude is the variability in the timing of peak occurrences. Unlike lower altitudes where peaks predominantly occur in specific months, here we observe peaks in June, July, August, September, and even October. This variation might be

indicative of the complex dynamics governing PSC formation at these higher stratospheric regions, suggesting that a range of factors could be influencing PSC behavior above 27-28km.
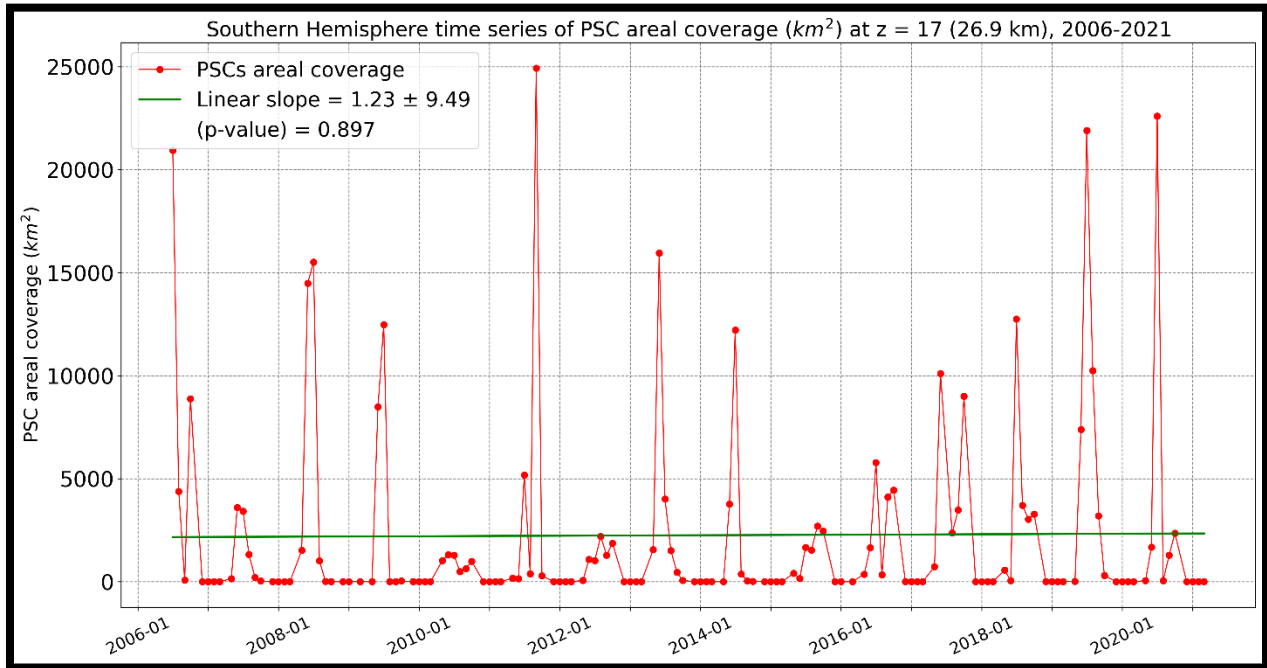

Figure 55: Interannual positive trend of monthly mean values of PSC areal coverage over the Southern Hemisphere, for the transitory altitude of negative to positive trends, at 26.9 km.
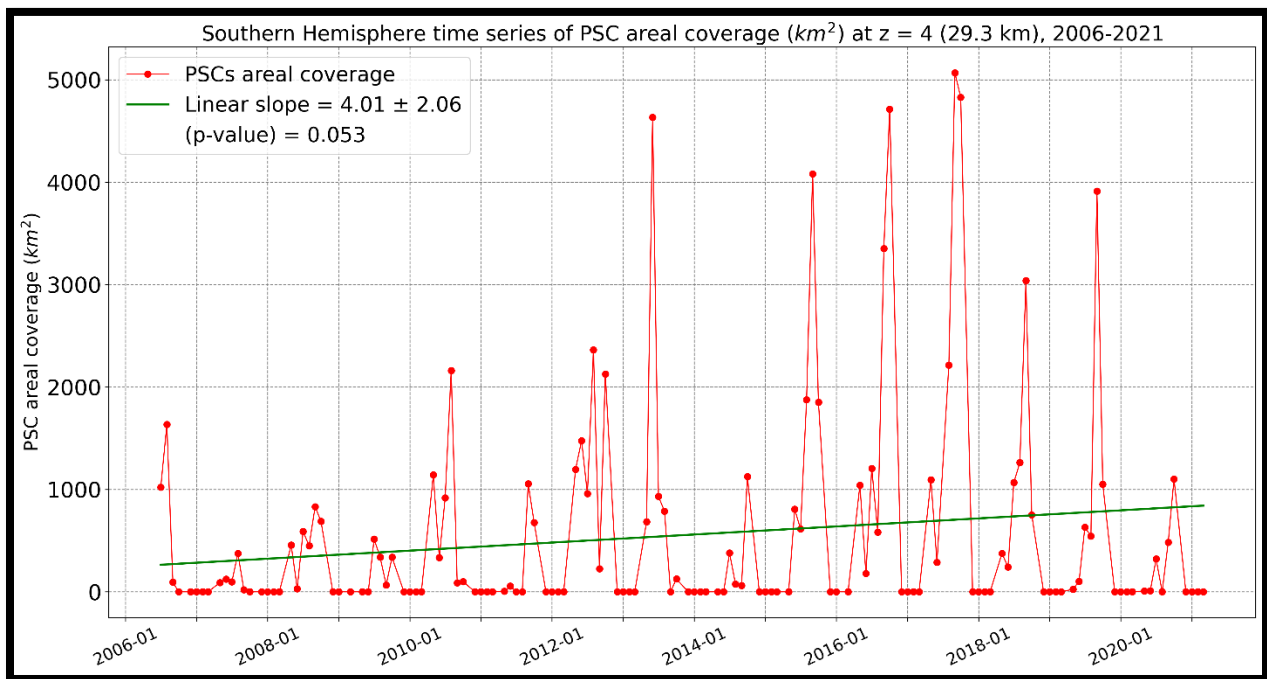

Figure 56: Interannual positive trend of monthly mean values of PSC areal coverage over the Southern Hemisphere, for the altitude of the most significant trend, at 29.3 km.

Summarizing some key findings before progressing to the next facet of our trend analysis, it's noted that several stratospheric layers exhibit a consistent trend, either positive or negative, in both hemispheres. However, as previously discussed, these trends are statistically insignificant. Specifically, the layers at 10.4km, from 12 to 13.1km, 23.9 to 26.6km, and from 29.1 to 29.4km exhibit common trends across both hemispheres. In contrast, the remaining altitudinal layers display divergent trends between the two hemispheres.

From these observations, it's challenging to derive extensive insights into the behavior of PSCs. The existing literature primarily focuses on overarching trends in each hemisphere rather than specific layers. There appears to be a lack of comprehensive studies that delve into why certain stratospheric layers exhibit specific trends, whether positive or negative. Our research aligns with existing literature in terms of the general trend behaviors observed in each hemisphere. However, the nuanced findings from our study underscore the complexity and variability inherent in PSC dynamics, highlighting the need for further in-depth investigations into layer-specific behaviors and their potential implications for understanding atmospheric phenomena.

Yearly Trends

To gain a more comprehensive understanding and to identify any significant trends over a longer time frame, our analysis extends to examining yearly mean values of PSCs areal coverage from 2007 to 2020. The years 2006 and 2021 have been excluded from this aspect of the analysis due to incomplete data coverage; 2006 offers data from only July to October, and 2021 from January to March. In this year-to-year trend analysis, our approach differs slightly from the previous monthly analysis. Rather than delving into the intricacies of each stratospheric layer, examining them in detail, the focus here is on highlighting key findings and significant trends that emerge from the yearly data. This approach allows for a broader overview, capturing the overarching patterns and tendencies in PSC areal coverage over an extended period. This method is particularly useful for identifying underlying trends that may not be immediately apparent in shorter-term, month-to-month analyses, thereby contributing to a more holistic understanding of PSC dynamics.

NORTHERN HEMISPHERE

In the analysis of yearly mean values for PSC areal coverage, spanning altitudinal layers from 10.4 to 29.6 km, our findings indicate an overall upward trend in PSC areal coverage. Of the 108 layers examined, 69 exhibit a positive trend, while the remaining layers demonstrate a negative trend. This pattern broadly aligns with the monthly mean values observed in the Northern Hemisphere, where 70 layers showed positive trends and 38 layers showed negative trends.

However, this parallel does not necessarily mean that each specific layer consistently exhibits the same trend direction (positive or negative) in both monthly and yearly analyses. Our data reveals several layers where trends observed in the yearly mean values diverge from those in the monthly mean values. For instance, layers from 10.6 to 11.8 km, which showed a positive trend

in the monthly mean values, display a downward trend in the yearly mean values. Similarly, at altitudes of 13.1 km, 23.9 to 24.6 km, and 29.6 km, the trends shift to the opposite direction compared to the monthly trends.

Despite these variances, it is crucial to note that none of the trends reached statistical significance. The lowest p-values recorded were 0.16 at two different altitudes, 26.6 km and 14.2 km, a considerable distance from the 0.05 threshold required to suggest a statistically significant trend at a 95% confidence level. This lack of statistical significance underscores the complexity of PSC behavior and the influence of various atmospheric factors over time in the Northern Hemisphere. Consequently, while our study sheds light on potential trends in PSC areal coverage, further research and extended data analysis are needed to confirm these findings and understand the underlying mechanisms driving these trends.

SOUTHERN HEMISPHERE

Upon delving into the analysis of yearly mean PSC areal coverage trends within the Southern Hemisphere, our study uncovers some distinctive patterns. Unlike the Northern Hemisphere, where trends across various layers didn't show statistical significance, the Southern Hemisphere presents a more defined trend landscape. In this region, ten layers specifically, spanning from 10.4 to 11.8 km and at 12.2 km, exhibit trends that are statistically significant, with p-values under 0.05. The layer at 10.9 km stands out, showcasing the most notable p-value at 0.023, really close to the second significant p-value of 0.027 at 10.8km. These layers uniformly demonstrate a downward trend, aligning with the overarching decline in PSC areal extent observed in the Southern Hemisphere. Broadening our scope to encompass all 108 layers analyzed for the Southern Hemisphere, it's evident that the majority, totaling 85 layers, follow a negative trend. Within this subset, ten layers are statistically significant. The remaining 23 layers show an upward trend. This contrasts slightly with the monthly mean values, particularly in the layers from 25.7 to 26.7 km, where we notice a shift in the trend's direction from negative in the monthly analysis to positive in the yearly.

Comparing these findings between the two hemispheres, the Southern Hemisphere's trend dynamics are more starkly defined than those in the Northern Hemisphere. The Southern Hemisphere not only shows a larger number of negative trends but also includes layers where these trends reach statistical significance in the yearly mean analysis. In contrast, while the Northern Hemisphere displays an overall upward trend across more than 69 out of 108 layers, none of these trends achieve statistical significance. This divergence in trend behavior between the hemispheres is a pivotal aspect of our findings. These results underscore the need for ongoing study of PSCs to further unravel their complex behavior. A key part of this "puzzle" is the role of stratospheric temperatures. As we've touched on before, these temperatures could give us some useful clues about how PSCs behave. So, up next in this thesis, we're going to dive into stratospheric temperatures and see what they can tell us about a significant part of PSCs' story.

4.2. Stratospheric Temperatures

In our study, moving from PSCs to examining stratospheric temperatures marks a key transition. It highlights how these two areas are connected. Stratospheric temperatures play a significant role in the behavior and formation of PSCs, making this aspect an important part of our research. It is within this context that the significance of stratospheric temperature trends becomes evident. The latter part of the 20th century and the onset of the 21st century have been marked by a discernible cooling of the stratosphere; a phenomenon meticulously outlined by Randel et al. in their 2009 study. This cooling trend, especially pronounced in the polar lower stratosphere, has largely been attributed to two main factors: an increase in greenhouse gas concentrations (Ramaswamy et al., 2001 and 2006) and, in the polar regions, to ozone depletion (Manzini et al., 2003; Ramaswamy et al., 2001). Specifically, in the Antarctic, the late winter and spring periods have seen the most significant stratospheric cooling, which in turn has led to a delay in the breakup of the Southern Hemisphere's polar vortex (Akiyoshi et al., 2009). This is thought to be a direct result of the radiative cooling that accompanies springtime ozone depletion.

Previous research, such as the work by Rex et al. 2004 and 2006, has delved into the relationship between polar stratospheric temperatures and polar ozone. They established a linear relationship between chemical ozone loss and VPSC (Volume of Polar Stratospheric Clouds), particularly in Arctic winters. However, as Braesicke et al. 2006 pointed out, this linear relationship might not hold true indefinitely, suggesting that polar stratospheric temperature will continue to be a crucial factor in understanding and predicting chemical ozone loss. This notion was further supported by Newman et al. 2004, who predicted that while reductions in halogens might shrink the Antarctic ozone hole size, this could be offset by an expansion due to the cooling effect of increasing greenhouse gases.

Our analysis in this section won't go into as much depth as previously discussed in section 4.1. However, we aim to present a succinct yet comprehensive overview of the stratospheric temperatures, firstly looking at how stratospheric temperatures have changed from year to year, identifying any notable trends. Next, we'll examine how these temperatures vary across different regions and finally, we'll explore how temperatures differ at various heights in the stratosphere and what this means for atmospheric processes and PSCs.
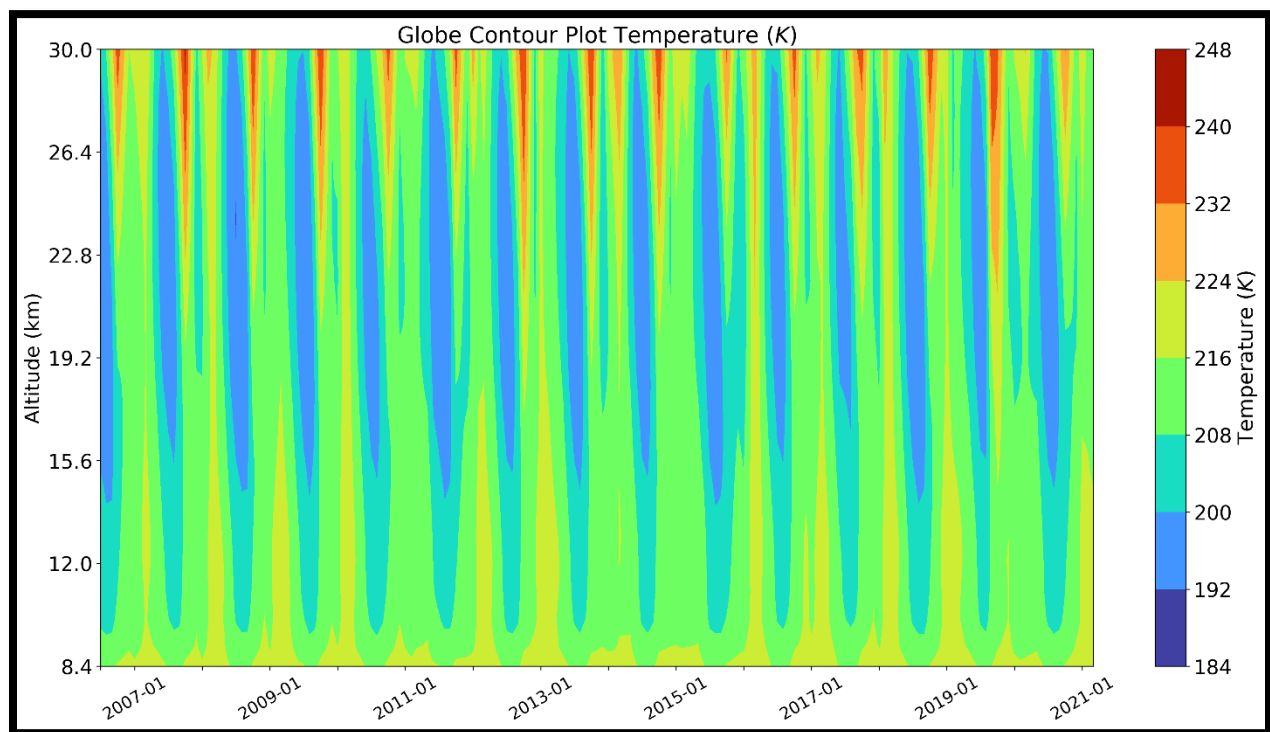
4.2.1. Interannual

In Figure 55, we delve into the analysis of the interannual variability of mean monthly stratospheric temperatures over the substantial 16-year period (July 2006 – March 2021), categorized by altitude. This depiction uncovers a striking pattern of seasonal variability. Most notably, the lowest temperatures align with the altitudes at which PSCs are predominantly observed, a phenomenon that is particularly pronounced in the Southern Hemisphere.

In the Northern Hemisphere, a pattern emerges, with the coldest temperatures typically manifesting from December through mid-January. This finding is intriguing as it may suggest a

linkage to atmospheric circulation patterns specific to the NH winter. Furthermore, the figure sheds light on the stark contrast in stratospheric temperatures between the periods of 2014–2015 and 2015–2016. The former period is warmer, a variation that intriguingly correlates with the fluctuating areal coverage of PSCs observed in these respective periods. This correlation might hint at the sensitivity of PSC formation to even minor temperature shifts.

The SH presents its own unique patterns. July consistently shows the lowest temperatures, succeeded by a subtle warming trend in the upper stratosphere (above 23 km) come August. Above 26 km, the SH temperatures hover near 200 K, a stark contrast to the higher temperatures at similar altitudes in the NH. This difference is not just a numerical variance but could signify fundamental atmospheric differences between the hemispheres. The broader blue areas in the SH in the polar stratosphere visually emphasize this distinction, suggesting more persistent and extensive lower temperatures in the SH.

Figure 57: Mean monthly interannual variability and vertical distribution of stratospheric temperatures (in K) averaged over the areas with PSC occurrence, for each hemisphere, for the period 2006–2021. Results are shown for the period May–October for the Southern Hemisphere and December-March for the Northern Hemisphere, for each year.

A comparative analysis of Figures 44 and 57 reveals a compelling correlation across both hemispheres: the occurrence of PSCs is intricately linked with stratospheric temperatures. This relationship is more than just a coincidental overlap; it underscores the critical role of temperature in the genesis and morphological characteristics of PSCs. It suggests that temperature is not merely a backdrop but a dynamic and influential factor in the life cycle of

PSCs. Delving into a season-to-season analysis for each hemisphere, based on the vertical distribution of stratospheric temperatures, reveals several intriguing findings on how the temperatures are distributed:

Northern Hemisphere:

In the Northern Hemisphere, our analysis defines the Arctic season as spanning from December 2006 to March 2021, covering a total of 15 seasons. During this period, there were observed temperature fluctuations in the range of 198K to 232K. Notably, the lowest temperatures predominantly occurred at mid to high altitudes, primarily in the months of December and mid-January. In contrast, the highest temperatures were observed at both lower altitudes and at high altitudes during the latter part of the season, specifically in February and March.

It's important to note that these temperatures represent average values across the hemisphere for each Arctic month of each season, within the latitude range of 50.5 to 82.5 degrees. Diving deeper, as will be expounded in Section 4.2.3 with an analysis of mean zonal data, notable discrepancies in these temperatures become apparent. For example, average temperatures in December are observed to dip marginally below 200K, in mid-high altitudes.

Further, in examining the interannual aspects of this study, we note the variance in seasonal temperature extremes. The smallest observed difference stands at 14K, as recorded in the 2018-2019 season, and the largest difference reaches 32K during the seasons 2013-2014 and 2015-2016. Notably, the 2015-2016 season also coincided with the highest recorded PSC areal coverage in the Northern Hemisphere. Thus, the calculated average span between the lowest and highest recorded temperatures across the Northern Hemisphere is approximately 18K.

Upon a closer analysis of the graphical data, several distinct patterns emerge, offering valuable insights into the interplay between temperatures and PSCs. It becomes evident that the seasons with the lowest temperatures often align with the seasons experiencing the most frequent occurrences of PSCs. This observation, while indicative of a relationship, stops short of implying a direct causation. Instead, it points to a potentially strong correlation between these two atmospheric phenomena.

For instance, during the seasons of 2006-2007, 2010-2011, 2015-2016, and 2019-2020, a noteworthy alignment is observed. In these periods, not only do the prolonged periods of cold temperatures correlate with increased PSC activity, but there is also a remarkable concurrence in their altitudinal distribution and temporal patterns. Additionally, the seasons of 2014-2015 and 2018-2019 present an intriguing contrast. These seasons are marked by comparatively higher temperature averages, which interestingly coincide with a noticeable decrease in PSC areal coverage. This inverse relationship is consistent both in terms of the altitude at which these clouds are found and the duration over which they are present. Such observations hint at a nuanced and intricate relationship between the thermal dynamics of the stratosphere and the physical characteristics of PSCs.

Southern Hemisphere:

In the Southern Hemisphere, temperature distributions exhibit a more uniform pattern, both month-to-month and season-to-season. This uniformity extends to the distribution of temperatures across different altitudes and over time. Notably, the altitudinal range of low temperatures remains relatively stable as one moves higher in the atmosphere. Additionally, the coldest temperatures are consistently observed in July, suggesting a seasonal regularity. A significant observation is that the lowest temperatures for each month of the Antarctic season tend to occur at increasingly higher altitudes as the season progresses from May to October. This trend in temperature altitude corresponds intriguingly with the downward shift in the maximum areal coverage of PSCs, particularly noticeable from July to October.

Delving further into the data, it's evident that the lowest temperatures of the Antarctic season are typically found at the lower altitudes in May and ascend to the highest altitudes by October. Remarkably, these high altitudes in October can exhibit temperatures exceeding 230K, approaching 240K. In terms of temperature range, the Southern Hemisphere contrasts with the Northern Hemisphere by displaying a wider gap between its lowest and highest temperatures, spanning approximately 185K to 245K. However, when analyzing the highest minus the lowest temperatures across all seasons, we find that the seasonal temperature differences vary between 45K and 54K. This implies that the average maximum temperature differences between different Antarctic seasons could reach up to 9 to 10K.

When correlating temperature data with PSC areal coverage, it becomes evident that there is a stronger correlation between these two factors in the Southern Hemisphere compared to the Northern Hemisphere. This observation, although notable, is not extensively discussed in the main text of this section but is supported by the graphical data presented in the subsection 4.3.1. A key observation from these graphs pertains to the Antarctic season of 2008. During this period, we noted that the low temperatures did not persist for an extended duration. This short-lived nature of low temperatures is reflected in the PSC areal coverage for the same season. Specifically, the most significant concentration of PSCs was observed only for a brief period towards the end of June and the beginning of July. This temporal alignment between the brief period of low temperatures and the concentrated occurrence of PSCs provides a compelling example of the interplay between these atmospheric phenomena.

A consistent observation across both hemispheres is that the lowest temperatures do not precisely align with the altitudes where PSCs occur most frequently. This intriguing detail, although not exact in its occurrence, provides a nuanced perspective on the interplay between atmospheric temperatures and PSC formation, triggering that stratospheric temperatures, are not the only factor contributing to PSC formation/dissolution. A more detailed analysis and discussion of this phenomenon will be presented in Section 4.2.3.

Upon further processing of our data, the study has uncovered certain trends in stratospheric temperatures. These trends are discerned using a similar analytical approach as applied to the

observable trends in PSC areal coverage. This approach, combining our parallel analysis with insights gleaned from the bibliography, has the potential to provide a cohesive understanding of the interplay between temperature variations in the stratosphere and the dynamics of PSC distribution. This perspective could become increasingly attainable as the analyzed data encompass a more extensive time period under study, allowing for a more robust exploration of long-term trends and their implications.

Trends:

Temperature trends are insignificant both for the 5% and 10% significance level and, at the same time, weakly negative for the Northern Hemisphere and positive for the Southern Hemisphere. To clarify, it has been observed that out of 121 layers in the Northern Hemisphere, 76 exhibit a weakly negative slope within the altitudinal range of 16-30km. Conversely, the layers spanning from 8.4 to 16km show a marginal positive trend. In the Southern Hemisphere, every layer analyzed, covering altitudes from 8.4 to 30km, displays a positive trend, though this is deemed statistically insignificant. More than 95% of total variance is explained by the short-term variability in polar regions. Among the global maximums in the temperature of the lower stratosphere, based on the work of Jakovlev et al. (2019) one can note the maximums of 1991–1992, 1998, 2009, 2012–2013, and 2016, which are manifested in both hemispheres and the maximums of 1998 and 2013 in the polar zone of the Northern Hemisphere and the maximum of 2002 in the Southern Hemisphere. Compared with the phases of the El Niño phenomenon, according to Jakovlev, its most pronounced manifestation in 1998 is characterized by the presence of a temperature maximum in the lower stratosphere of the Arctic and a minimum in the lower stratosphere of the Antarctic. A similar picture is observed in 2010, and in 2016, the maximum temperature of the lower stratosphere appears in the polar lower stratosphere of both hemispheres. In general, it can be noted that, despite the fact that the temperature of the lower stratosphere of the polar regions is characterized by a well-pronounced interannual variability determined by dynamic processes affecting the stability of the polar vortex, such as wave activity and sudden stratospheric warming events, global variability, largely determined by processes in the tropical zone, also manifests itself in polar regions.

4.2.2. Spatial

This subsection serves as a critical foundation in our data analysis, offering an initial yet insightful glimpse into the potential correlation between stratospheric temperatures and PSC formation. The observation that lower temperatures are prevalent at altitudes where PSCs occur most frequently was a key preliminary finding. By focusing on data from these specific altitudes and summarizing the average conditions in both hemispheres, we aim to present a clear picture of the significant role temperatures play in this context. This groundwork sets the stage for the more detailed analysis in Section 4.3, where we will quantitatively establish this relationship through exact correlation coefficients.

The short-term variability in the polar regions is largely determined by the dynamics of the polar vortex, the stable state of which leads to a cooling of the polar stratosphere due to the isolation of the polar region from warmer middle latitudes, and the unstable polar vortex leads to a warmer stratosphere, as proposed by Smyshlyaev et al. (2016). The polar vortex is stable almost every year throughout the entire winter in Antarctica and unstable in the Arctic, which is caused by the higher wave activity in the Arctic, leading to the rapid destruction of the polar vortex that forms at the beginning of winter. Sudden stratospheric warming events (SSW), which regularly occur in the Arctic and rarely in the Antarctic, can also lead to the destruction of the polar vortex.

NORTHERN HEMISPHERE
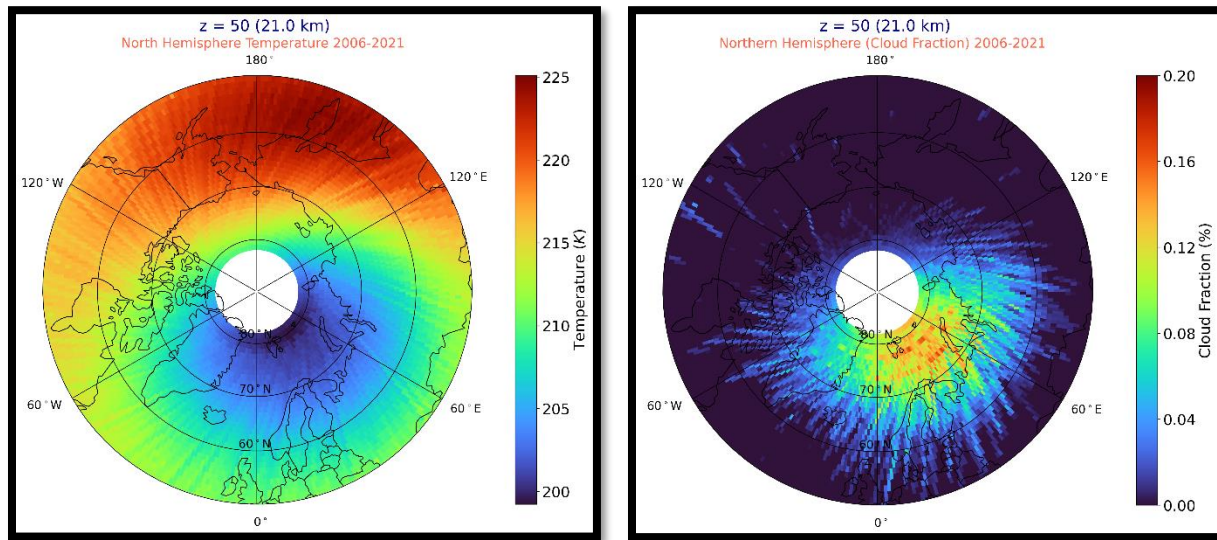
Figure 58: Left: Sixteen-year average (2006-2021), polar maps of Arctic PSC Stratospheric Temperatures at 21km – Right: Sixteen-year average (2006-2021), polar maps of Arctic PSC occurrence frequency at 21km.

For the analysis presented, the critical altitude selected was 21 km, which aligns with the peak average frequency of PSCs observed across the Northern Hemisphere. It is evident that the highest PSC occurrence rates span from 30°W to 90°E, specifically at latitudes above 60°N, peaking between 0° and 70°E for latitudes exceeding 70°N. This pattern concurs with the distribution of stratospheric temperatures at 21 km over the Northern Hemisphere, where the coldest temperatures—and consequently, the highest PSC frequencies—are found. Furthermore, in areas stretching from 120°E to 120°W at latitudes below 70°N, where stratospheric temperatures are warmer, PSC occurrences are markedly lower, evidenced by only a few isolated grids indicating PSC presence. This suggests that the majority of this region remains free of PSCs. Overall, the general pattern of PSC frequency of occurrence and stratospheric temperatures over the Northern Hemisphere appears to correlate closely, with only a few deviations across different latitudes-longitudes.
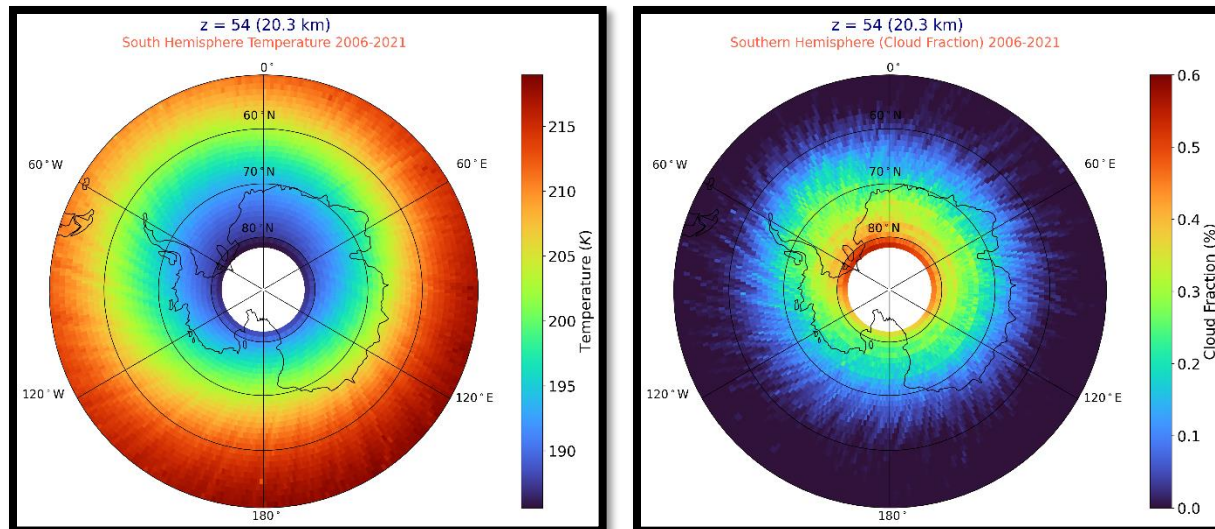
Figure 59: Left: Fifteen-year average (2006-2020), polar maps of Antarctic PSC Stratospheric Temperatures at 20.3km – Right: Sixteen-year average (2006-2020), polar maps of Antarctic PSC occurrence frequency at 20.3km.

In the Southern Hemisphere, the altitude of 20.3 km was identified as the level where the highest average frequency of PSCs occurs. The lowest temperatures are observed in the latitudinal zone from 60°E to 90°W for latitudes above 65°, and from 120°W to 30°E for latitudes above 70°. Unlike the Northern Hemisphere, the distribution of the coldest temperatures across latitudes in the Southern Hemisphere is more uniform. Both hemispheres exhibit their coldest temperatures between 30°W and 90°E; however, the notable difference is that the lowest temperatures in the Southern Hemisphere are approximately 15 degrees lower than those in the Northern Hemisphere (around 200K in the North compared to approximately 185K in the South).

When comparing the PSC frequency of occurrence at 20.3 km, it becomes apparent that regions with the coldest temperatures also have a higher frequency of PSC occurrence compared to areas with warmer atmospheric conditions. In the latitudinal zone of 50°-60°, where temperatures rise above 205K, reaching nearly 220K, only a few PSCs are observed, specifically from 60°E to 120°W. The maximum frequency of occurrence illustrates a distinct correlation, forming a "ring" around the pole, which is consistent with both the stratospheric temperature and PSC occurrence graphs. These observations suggest a strong correlation between stratospheric temperatures and PSC occurrences, with only minor deviations, as would be expected.

4.2.3. Vertical

As observed, stratospheric temperatures exhibit significant variations across latitude and longitude zones, with the changes in latitude being considerably more pronounced than those in longitude. To provide a more detailed representation of the vertical distribution of stratospheric temperatures, a latitudinal segregation has been conducted. The primary latitudinal zones are defined as follows: from 50 to 60 degrees (represented by an orange line), 60 to 70 degrees

(green line), 70 to 75 degrees (blue line), and greater than 75 degrees (purple line). Additionally, a mean value was calculated encompassing all these latitudinal zones (depicted by a red line).

A few clarifications regarding the latitudes involved in our analysis are pertinent. The latitudes corresponding to greater than 75 degrees extend up to a maximum of 82.5 degrees, rather than reaching all the way to 90 degrees, which is the geographical North Pole. This means that the calculations represented by the purple line encompass latitudes up to 82.5 degrees. As for the red line, its calculations start from 50 degrees and extend to 82.5 degrees, not covering the entire range from 0 to 90 degrees as might be inferred from the diagrams. This specific range selection for display purposes stems from considerations regarding data interpretation and analysis methodology. Therefore, when examining these vertical profiles (represented by the red and purple lines), it is important to bear in mind the aforementioned details about the latitude ranges being analyzed.

NORTHERN HEMISPHERE
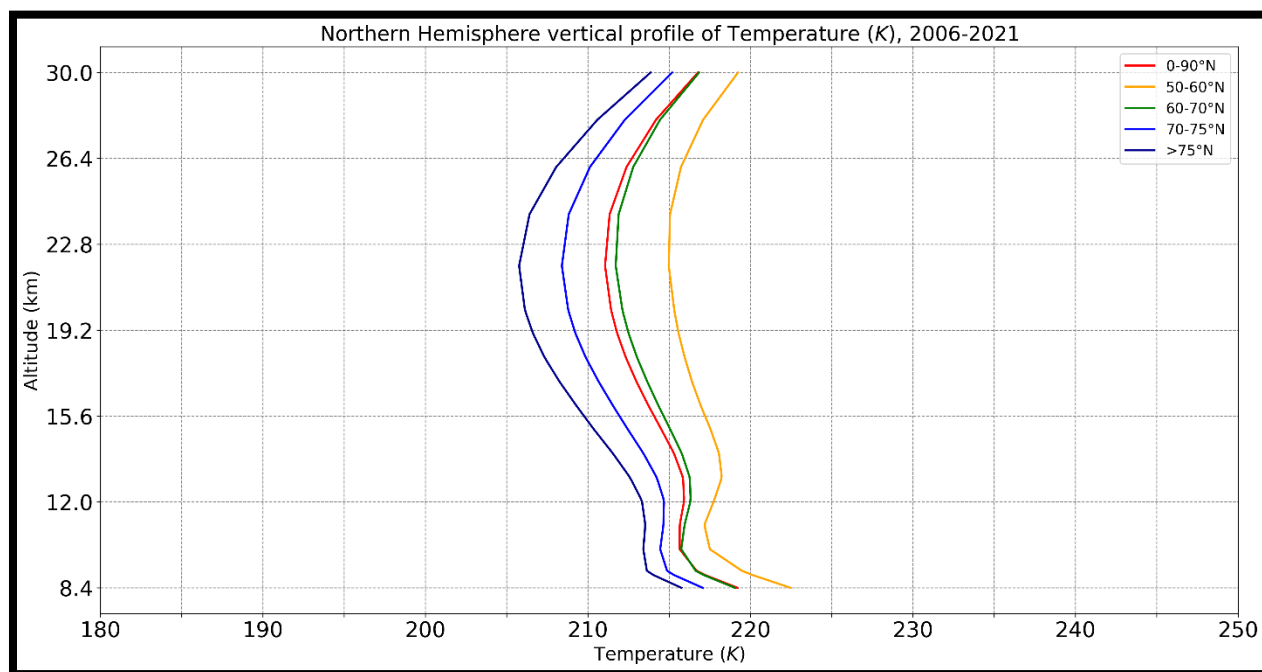
Figure 60: Vertical Profile of the Average Temperature of the Northern Hemisphere for the period 2006-2021.

Our analysis begins by examining the average temperatures of the Northern Hemisphere across the entire dataset, ranging from December 2006 to March 2021. This period encompasses only the months of December, January, February, and March, corresponding to the Northern Hemisphere's PSC season, as indicated by CALIPSO data products.

Notably, Figure 58 reveals three significant turning points. The warmer, lower latitudinal zones—which exhibit higher temperatures—display these turning points at slightly higher altitudes compared to others. For instance, the first turning point for the purple line is observed at

approximately 9 km, whereas for the orange line, it occurs around 11 km. The third and highest turning point for the purple line is noted at approximately 22 km, while for the orange line, it spans from 22.5 to 30 km.

Analyzing the diagram's results, we find that the general trend of stratospheric temperatures across the altitude range of 8.4 to 30 km above sea level aligns closely with the 60-70 degrees latitudinal zone, where the lowest recorded temperatures reach 212K at 22 km. However, significant variations emerge upon examining the remaining latitudinal zones. Near the pole (greater than 75 degrees, purple line), the lowest temperatures dip to 206K, whereas those within the 50-60 degrees latitudinal zone reach 215K. These discrepancies are highlighted further when analyzing the vertical distribution from season to season, offering deeper insights into the distinct differences among these latitudinal zones.
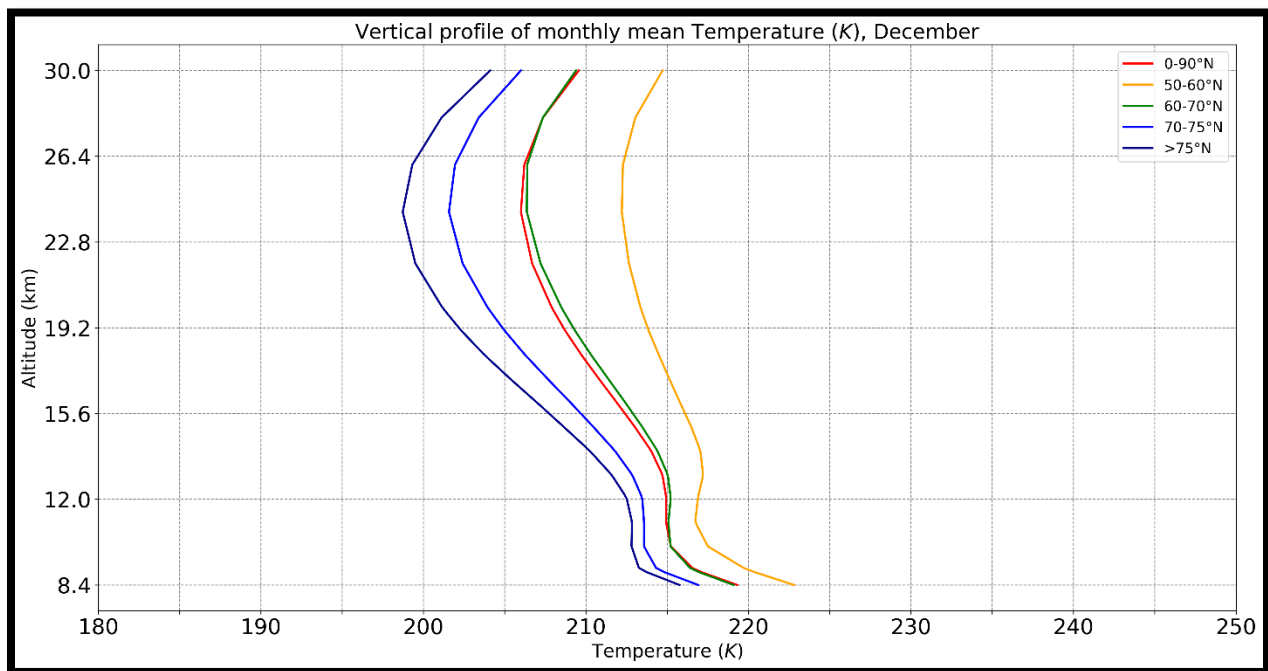
Figure 61: Vertical Profile of the Average December Temperature for the Northern Hemisphere for the period 2006-2021.

The vertical distribution of stratospheric temperatures for the average December is illustrated in Figure 59. Here, the pattern of three turning points persists, exhibiting a behavior consistent with the overall trends observed over the Northern Hemisphere. Notably, the latitudinal zone of 60-70 degrees closely matches the red line, with the lowest temperatures reaching approximately 206K. However, the lowest temperature within the 60-70 degrees latitudinal zone occurs at a slightly higher altitude compared to the average latitudinal temperature.

It is particularly noteworthy that these two lines display nearly identical behavior at both the lowest (8.4 to 10.5 km) and highest altitudes (26 to 30 km) of the dataset. This similarity was also observed in the average temperatures during the Arctic PSC season, as depicted in Figure

58. A critical observation is that the lowest temperatures near the North Pole are approximately 198K at 23.5-24 km, while the lowest temperatures for the latitudinal zone of 50-60 degrees reach approximately 212.5K.

What was previously the lowest average temperature for the North Pole region during the average PSC season (Figure 58) now, in average December, appears to apply to both the latitudinal zone of 60-70 degrees (green line) and the average value across all latitudes. This indicates that temperatures in December shift towards lower (colder) values.
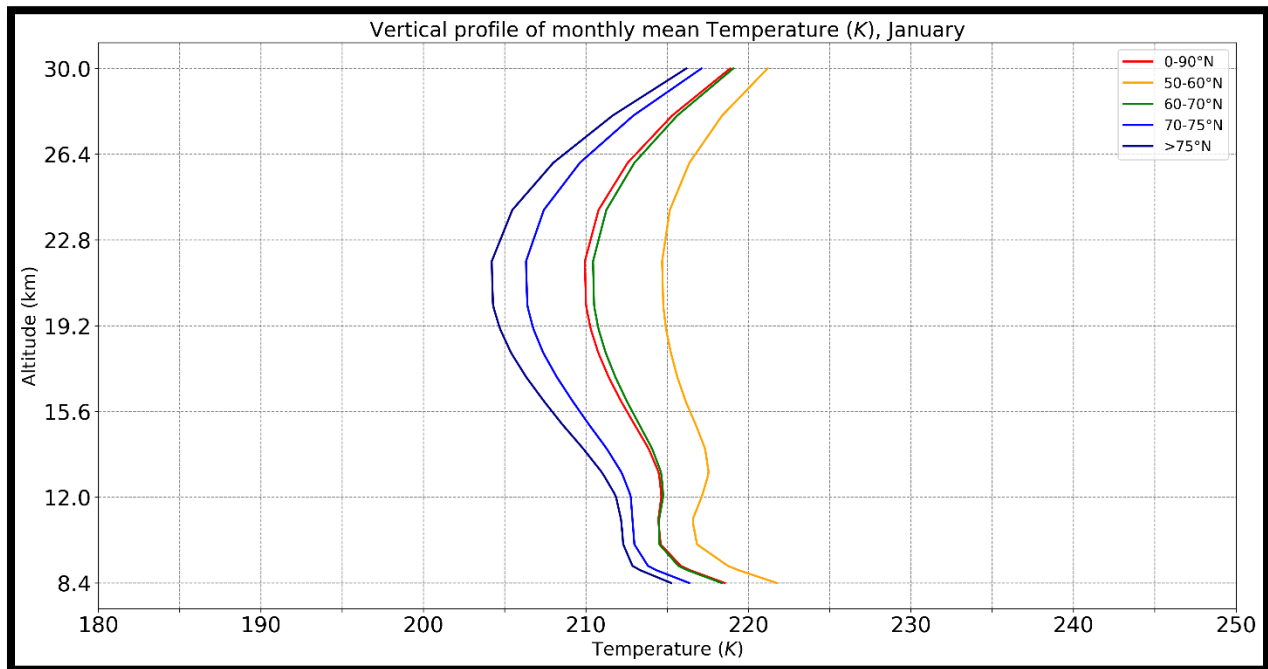
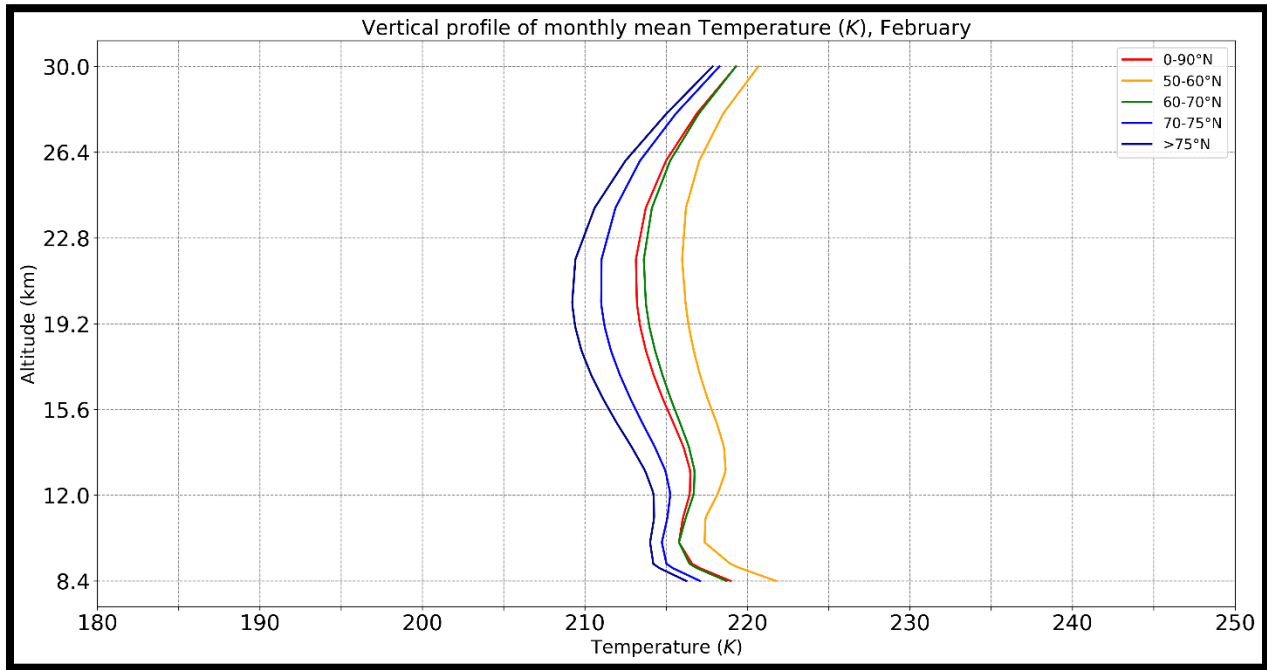*Figure 62: Vertical Profile of the Average January Temperature for the Northern Hemisphere for the period 2007-2021.*

Transitioning into January (Figure 60), the vertical profiles of stratospheric temperature continue to display the three turning point pattern observed in previous diagrams. A significant observation for January is that the lowest temperatures are found at lower altitudes compared to December. This trend is consistent with the behavior of the altitude at which PSCs form the most. Specifically, for average December, the altitude of maximum PSC formation was identified at 21.7 km, with the lowest temperatures (below 200K) occurring within the altitude range of greater than 21 to 26.5 km. In contrast, for average January, the altitude of maximum PSC formation shifts to 20.6 km, with the lowest temperatures (below 205K) found within the altitude range of 19 to 23 km. This indicates that the vertical extent of low temperatures in average December (approximately 6.5 km) is larger than that in average January (approximately 4 km). Most important though is that December seems to be cooler than January.

Despite December having a larger vertical area with the coldest temperatures, January is considered the most favorable month for PSC formation. This highlights the importance of the

altitudinal range covered by these temperatures, as PSC formation is influenced by multiple factors beyond just temperature. Given the complexity of PSC formation and its dependency on various atmospheric parameters, it's clear that the formation of PSCs is not solely determined by temperature but also by the availability of water vapors, nitric acid, sulfuric acid, and other condensation nuclei at specific altitudes. The condensation of stratospheric water vapor and nitric acid vapor onto available stratospheric aerosol particles under low temperatures is a key process in PSC formation, as mentioned by M. Tesche et al. (2021).

Figure 63: Vertical Profile of the Average February Temperature for the Northern Hemisphere for the period 2007-2021.

In February, Figure 61 demonstrates the persistence of the three turning point pattern, with the red line more closely mirroring the vertical profile of the 60-70 degrees latitudinal zone. This month is characterized by a noticeable rise in temperatures across different latitudinal zones, resulting in a convergence of the vertical profiles of these zones closer than what is observed in December and January. The distinctions in temperature across latitudes diminish, highlighting a crucial transitional period in the Arctic atmosphere.

Specifically, the peak for the latitudinal zone above 75 degrees is found at approximately 20 km with an average temperature of around 209K. In contrast, for the 50-60 degrees zone, the peak is at about 22.5 km with an average temperature of 216K. This February scenario shows a narrower temperature gap across latitudes compared to December (approximately 14.5K) and January (9K), with February's gap being around 7K. According to Pitts et al. (2018), February signifies a significant phase in the cessation of the Arctic PSC season, with the maximum area coverage of PSCs in February exceeding that of January by more than sixfold.

This phase of the season could signify not only a physical transformation within the stratosphere but also a critical window for studying the processes governing PSC lifecycle and their impact on polar chemistry, particularly ozone depletion. The PSC coverage peak in February, despite rising temperatures, suggests that conditions remain conducive to PSC formation over a substantial area, enhancing the idea behind that PSC formation is complex and it's not exclusively dependent on the atmospheric temperatures.
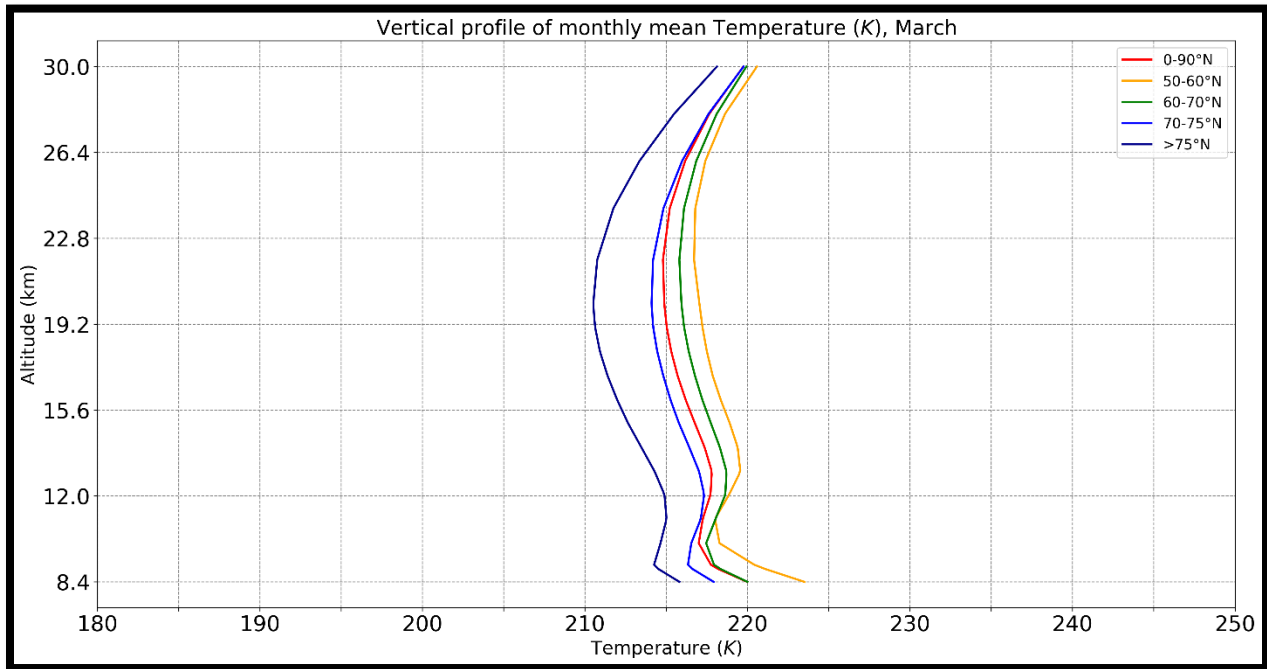

Figure 64: Vertical Profile of the Average March Temperature for the Northern Hemisphere for the period 2007-2021.

March marks the last month of the Arctic PSC season according to our data. As observed in Figure 62, the three turning point pattern continues to be evident. The lowest temperatures for the northernmost latitudinal zone have been recorded at approximately 210K at 20 km, with the coldest temperatures for other latitudinal zones occurring at slightly higher altitudes. For the 50-60 degrees latitudinal zone, the lowest temperatures reach around 217K at an altitude of 22.5 km. Therefore, the temperature difference between the coldest regions of the northernmost and southernmost latitudinal zones remains approximately 7K, similar to the average for February. The alignment of the red and green lines is restricted to very low or very high altitudes, with an average temperature difference between them of approximately 0.85K.

What is much clearer now is that the altitude at which PSCs most frequently occur does not closely correspond with the altitude of the lowest temperatures observed. Moreover, it is observed that December generally records lower temperatures over the Arctic than January. This observation underscores the complexity of PSC formation, demonstrating that stratospheric temperatures alone are not the sole factor influencing the development of PSCs. For a better and

more comprehensive analysis other atmospheric conditions, including moisture content, atmospheric circulation, and the presence of condensation nuclei, should be considered as the play significant roles in PSC formation and variability.

Transitioning from the Northern to the Southern Hemisphere reveals distinct climatic patterns regarding temperature variations. In the Northern Hemisphere, the coldest mean temperatures occur in the northernmost latitudinal zones, averaging 198K in December. By contrast, March typically experiences the highest temperatures, with the lowest of them averaging 217K. Upon moving to the Southern Hemisphere, the situation becomes markedly different, exhibiting even colder temperatures and larger temperature differentials between higher and lower latitudinal zones for any given month.
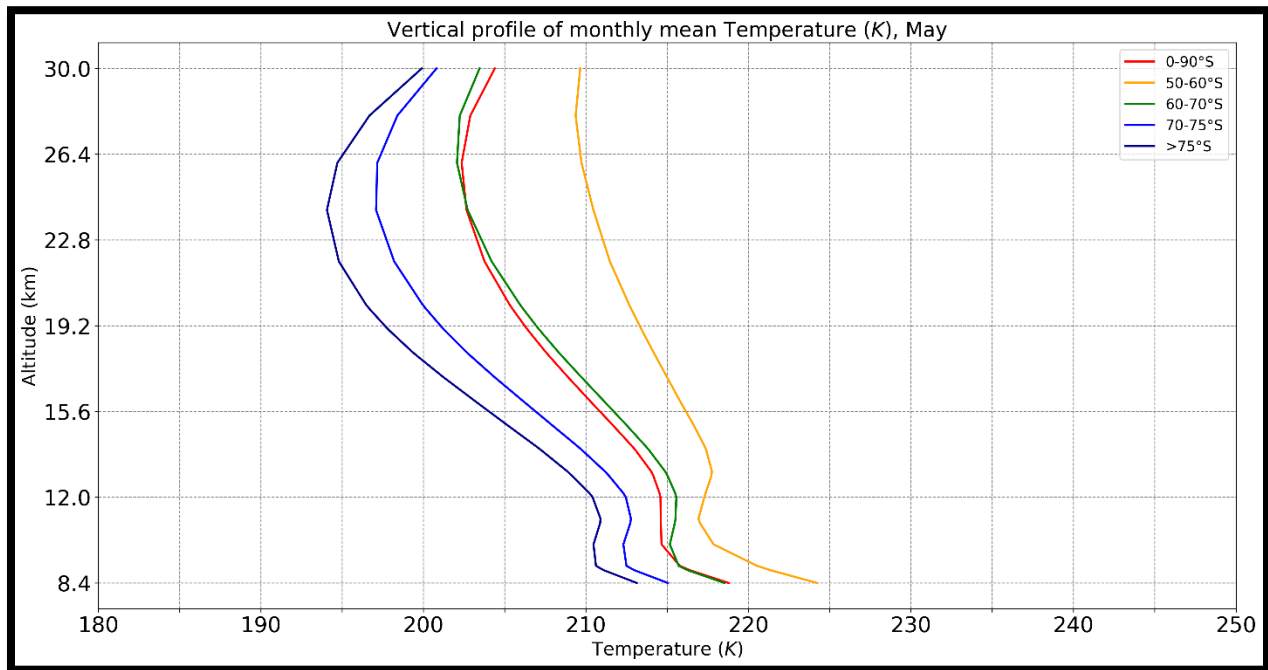
SOUTHERN HEMISPHERE
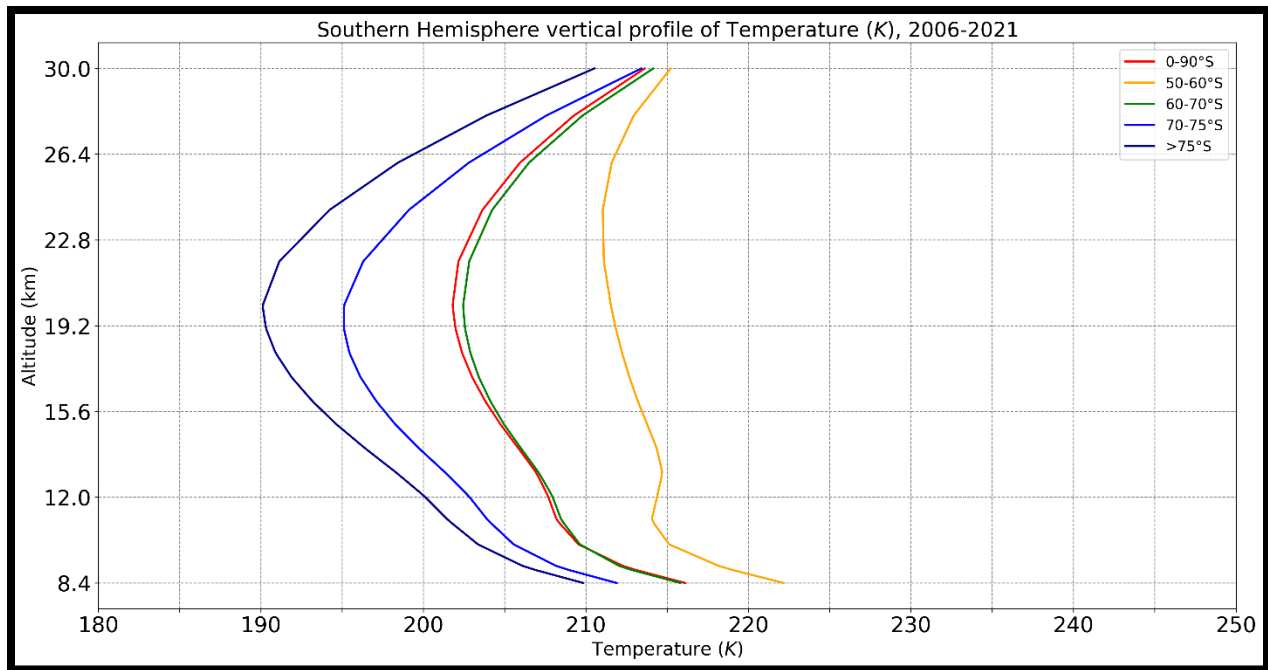
Figure 65: Vertical Profile of the Average Temperature of the Southern Hemisphere for the period 2006-2020.

The overall depiction of the vertical distribution of stratospheric temperatures over the Southern Hemisphere reveals a distinct pattern from that of the Northern Hemisphere. Unlike in the Northern Hemisphere, where a three-turnpoint pattern is observed across all latitudinal zones, this pattern is not present across the Southern Hemisphere, with the exception of the lower latitudinal zone of 50-60 degrees south. According to Figure 63, the coldest temperatures over Antarctica drop to 190K, whereas the lowest temperatures within the 50-60 degrees latitudinal zone approximate 211K. This results in a significant 21K difference between the coldest temperatures in higher versus lower altitudinal zones, a stark contrast to the 9K difference noted in the Northern Hemisphere. Additionally, the mean lowest temperature across the Southern

Hemisphere, denoted by the red line, is approximately 202K at an altitude of 21km. This mean lowest temperature is very similar to that observed for the latitudinal zone of 60-70 degrees South, at around 202K at 20km altitude, indicating a close alignment. The temperature discrepancies among the various latitudinal zones are markedly more pronounced than those in the Northern Hemisphere, with the 60-70 degrees latitudinal zone aligning most closely with the hemispheric average, showing a minimal mean difference of about 0.2K. The data for this analysis span from July 2006 to October 2020 covering 14 and a half Antarctic seasons.

Figure 66: Vertical Profile of the Average May Temperature for the Southern Hemisphere for the period 2007-2020.

In May, as depicted in Figure 64, the coldest temperatures recorded over the Antarctic reach down to 194K at an altitude of 24km, with the average hemispheric temperature approximately 202.5K at 26km. This value aligns closely with that observed in the latitudinal zone of 60-70 degrees. For the 50-60 degrees latitude zone, the lowest recorded temperature is 209.5K at an altitude of 28km. This marks a temperature difference of 15.5K between the coldest readings of the lowest and highest latitudinal zones, indicating significant thermal stratification. Additionally, the graph reveals an altitudinal difference of nearly 4km between these two latitudinal zones, representing the largest observed gap in the analysis so far.

In June, where PSCs have increased a lot in terms of areal coverage as detailed in Section 4.1, a significant shift in temperature and altitude measurements over the Antarctic is observed. The lowest recorded temperatures, as seen in figure 65, drop to 186.5K at an altitude of 22km, representing a decrease of 7.5K in temperature and a reduction of 2km in altitude compared to May. Within the 50-60 degrees latitudinal zone, the minimum temperatures are found to be approximately 203K at 28km, leading to a notable temperature disparity of 16.5K between the

coldest temperatures across the lowest and highest latitudinal zones. A comparative analysis of the mean hemispherical values for May and June reveals that, in May, the coldest temperatures are situated at 26km, reaching 202.5K, whereas in June, these temperatures shift to 24km, with a reduction to 196K. This delineates an average differential of the coldest temperatures to be approximately 6.5K between the two months, alongside an altitudinal discrepancy of 2km.

Despite the altitude of maximum PSC occurrence experiencing a smaller displacement of 1km, rather than the 2km observed in temperature shifts, and considering the nearly elevenfold increase in PSC areal coverage from May to June, the temperature difference of 6.5K emerges as a critical factor. However, it is imperative to recognize that this temperature variance, while significant, is not the sole influential factor in the dynamics of PSC formation and distribution.

The temperature difference indeed acts as a critical trigger for PSC formation, as it directly affects the saturation point of water vapor and other substances that compose PSCs. However, the physical processes involved in PSC formation, including nucleation and the growth of ice particles, are also dependent on the concentration of condensable gases and the presence of particulate matter in the stratosphere. Additionally, variations in stratospheric circulation can redistribute these constituents, further influencing PSC characteristics.
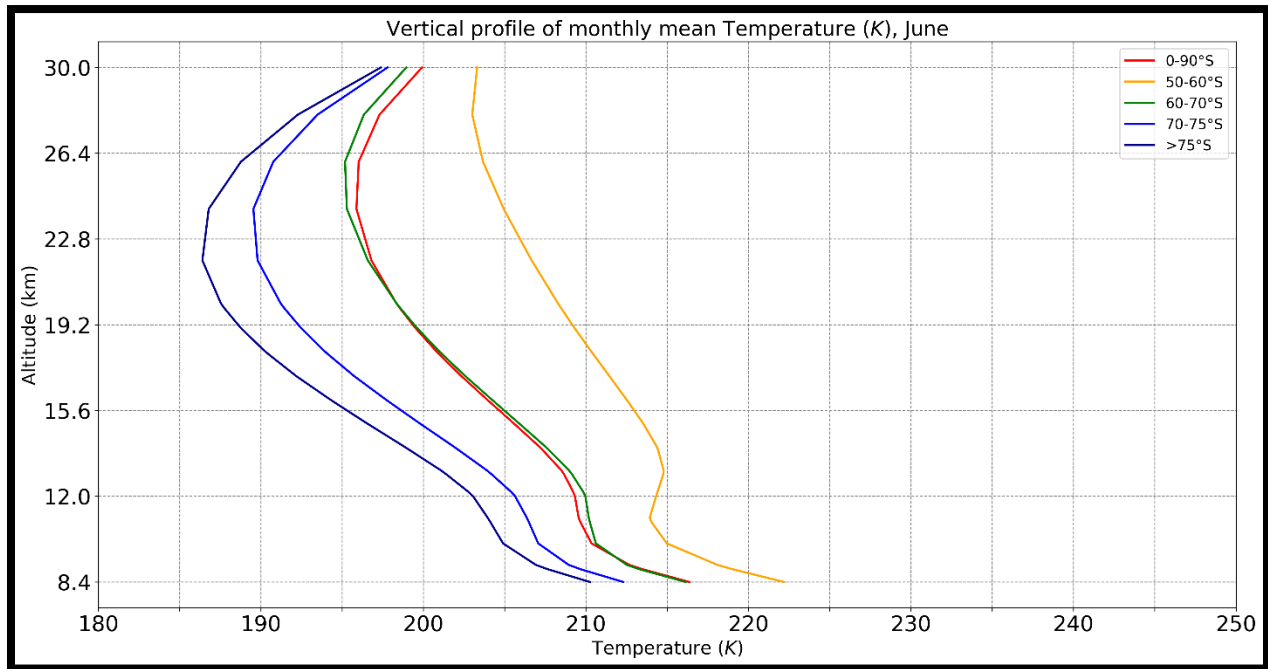

Figure 67: Vertical Profile of the Average June Temperature for the Southern Hemisphere for the period 2007-2020.

Delving into the peak of the Antarctic PSC season, July's temperatures (figure 66) are observed to be the coldest across all latitudinal zones when compared to May and June. Specifically, temperatures over the 75 degrees latitudinal zone plummet to approximately 183.5K at an altitude of 22km. In the 50-60 degrees latitudinal zone, temperatures reach 203K at an altitude of

26km. This marks a significant temperature disparity of around 19.5K, a wider gap than what was recorded in the preceding months.

When assessing the average hemispheric coldest temperatures, a notable finding is that these temperatures, observed at 24km, descend to 194K—almost 2K lower than the average in June and 8.5K below that of May. Additionally, the average hemispheric temperature profile, represented by the red line, demonstrates a close alignment with the temperature profile of the 60-70 degrees latitudinal zone from 8.4 to 15km. This alignment is one of the most substantial continuous correlations noted so far in the analysis after June's (from 14 to 21km). July's data signifies the core period of PSC activity in the Antarctic highlighting the extreme cold conditions that facilitate the expansive coverage of PSCs.
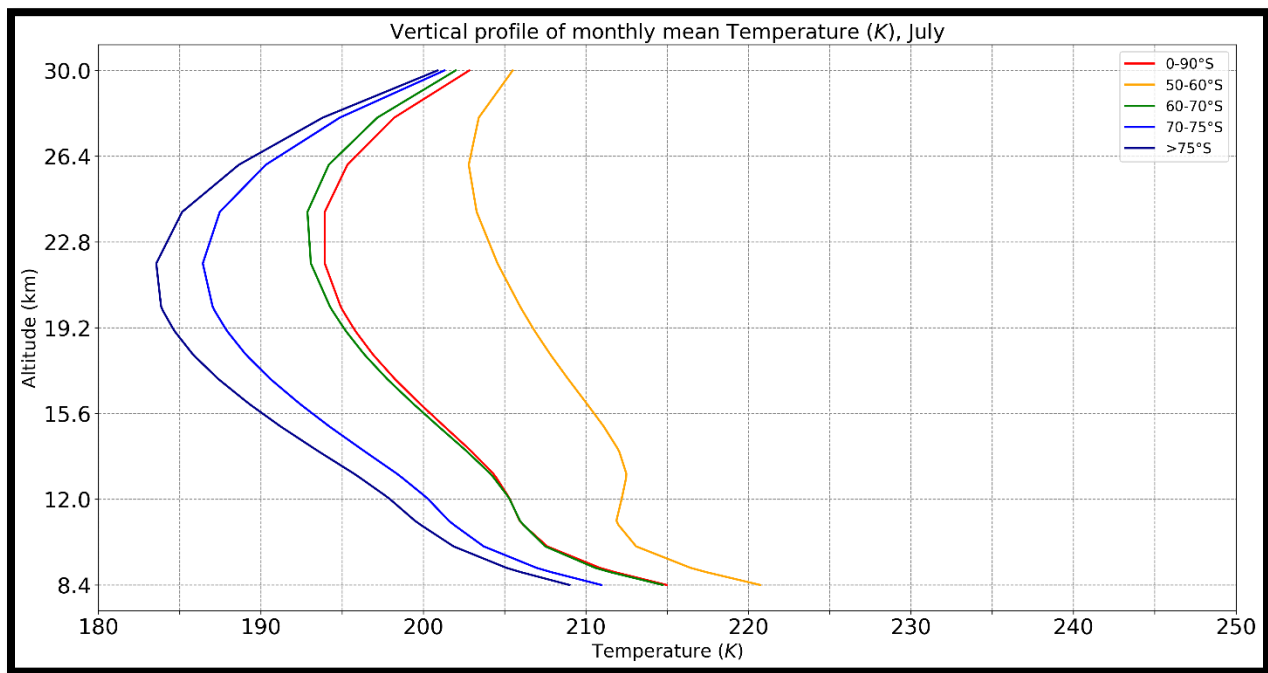
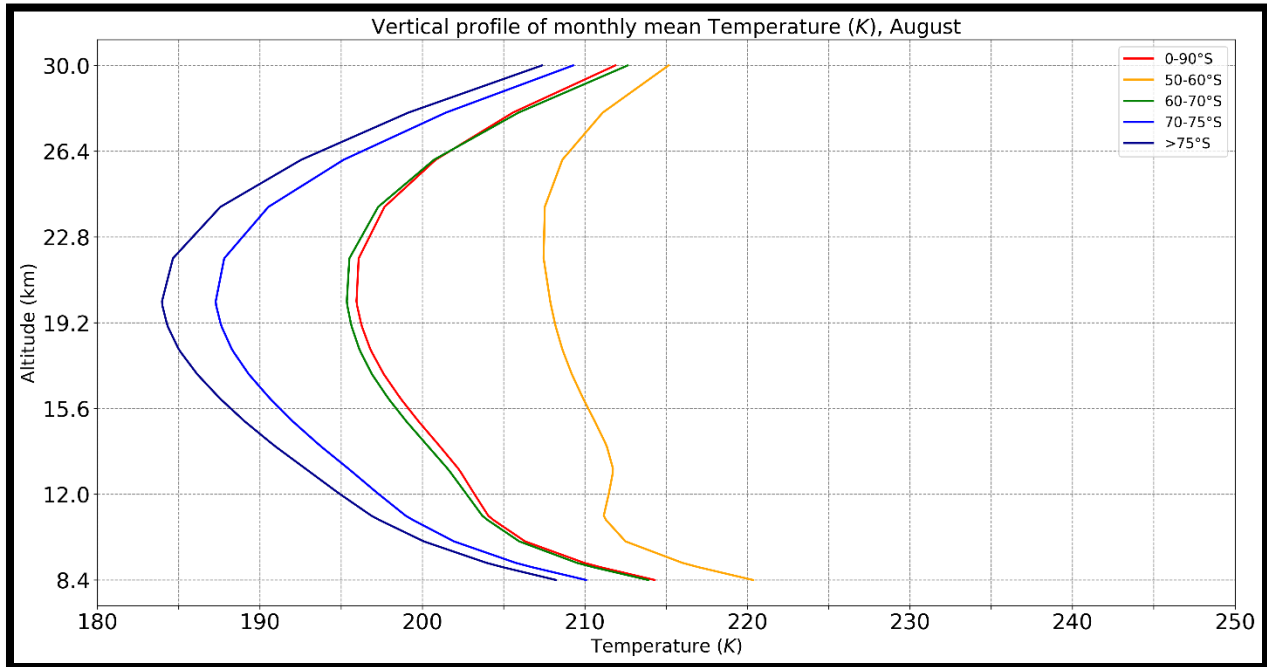*Figure 68: Vertical Profile of the Average July Temperature for the Southern Hemisphere for the period 2006-2020.*

August continues to display significant PSC areal coverage, surpassing that observed in May and June, with temperatures remaining at levels comparable to those of July. Specifically, as depicted in figure 67, the coldest temperatures for latitudes above 75 degrees are recorded at nearly 184K at an altitude of 20km—positioned almost 2km higher and approximately 0.5K colder than in July for the same latitudinal zone. For the 50-60 degrees latitudinal zone, the lowest recorded temperatures reach 207.5K at 23km, marking an increase of roughly 4.5K and a decrease in altitude of 3km from July's measurements in the same zone. Notably, the mean hemispherical profile of stratospheric temperatures in August reaches its minimum values at 20km and 196K, aligning with the lowest values of June, yet shifted 4km lower in altitude. In the 70-75 degrees latitudinal zone, temperatures are observed at 187.5K at 20km, slightly higher than the July figures, which showed the lowest temperatures at approximately 186.5K at 22km.

This analysis reveals that the temperature difference between the lowest and highest latitudinal zones in August widens to 23.5K, the most significant disparity noted throughout the study. This finding is particularly interesting when compared to the Northern Hemisphere, where the difference between the lowest temperatures decreases as the PSC season progresses from December through March. Conversely, in the Southern Hemisphere, this difference expands as the season advances from May to August. The expanding temperature disparity in the Southern Hemisphere's PSC season could suggest atmospheric conditions or processes at play, with implications for understanding global stratospheric behavior and its impact on climate patterns.

Figure 69: Vertical Profile of the Average August Temperature for the Southern Hemisphere for the period 2006-2020.

Reaching the end of Antarctic PSC season, in September (figure 68) a transition to higher temperatures begins, with the coldest ones observed to be at 190K at the altitude of 18km.

In September, the average hemispheric temperature is observed at its lowest point of 202K at 17km altitude, marking an increase of nearly 6K from August's average minimum temperature. The 50-60 degrees latitudinal zone records its lowest temperature at 16km, reaching 213K, which is remarkably close to the value at 11km—only 0.25K higher. Notably, this month presents a first in the observed data: for altitudes above 28km, the temperatures within the 50-60 degrees latitudinal zone are lower than those in the 70-75 and 60-70 degrees zones.
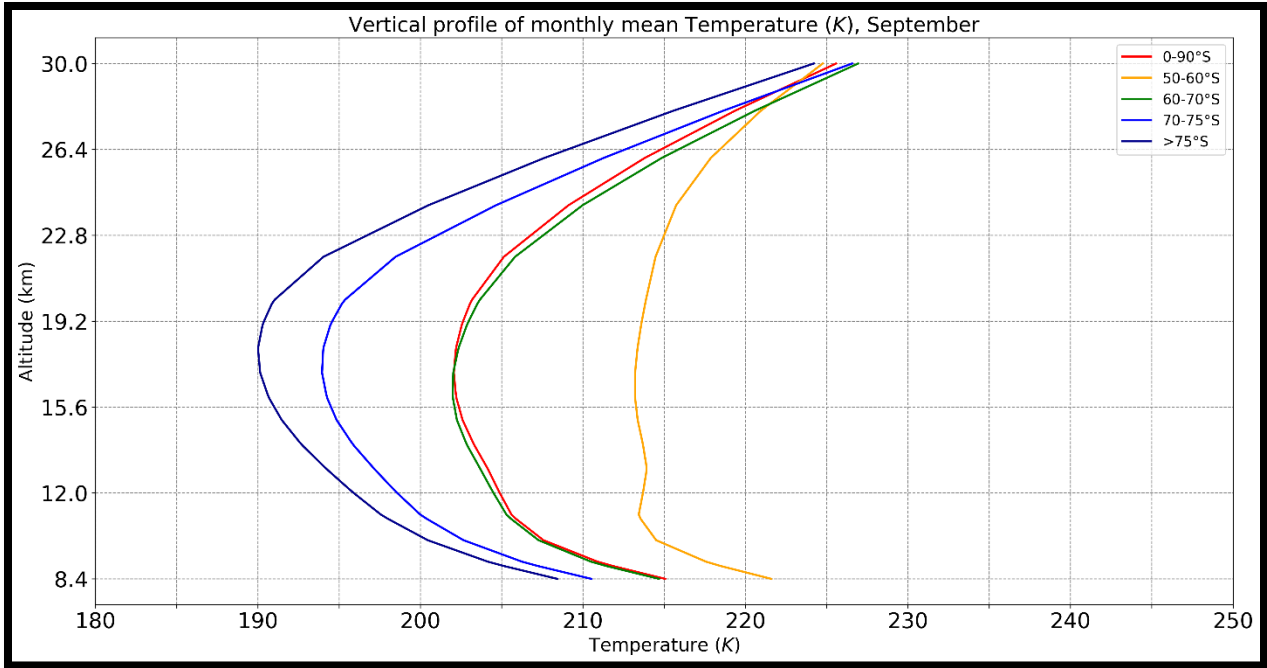
Figure 70: Vertical Profile of the Average September Temperature for the Southern Hemisphere for the period 2006-2020.
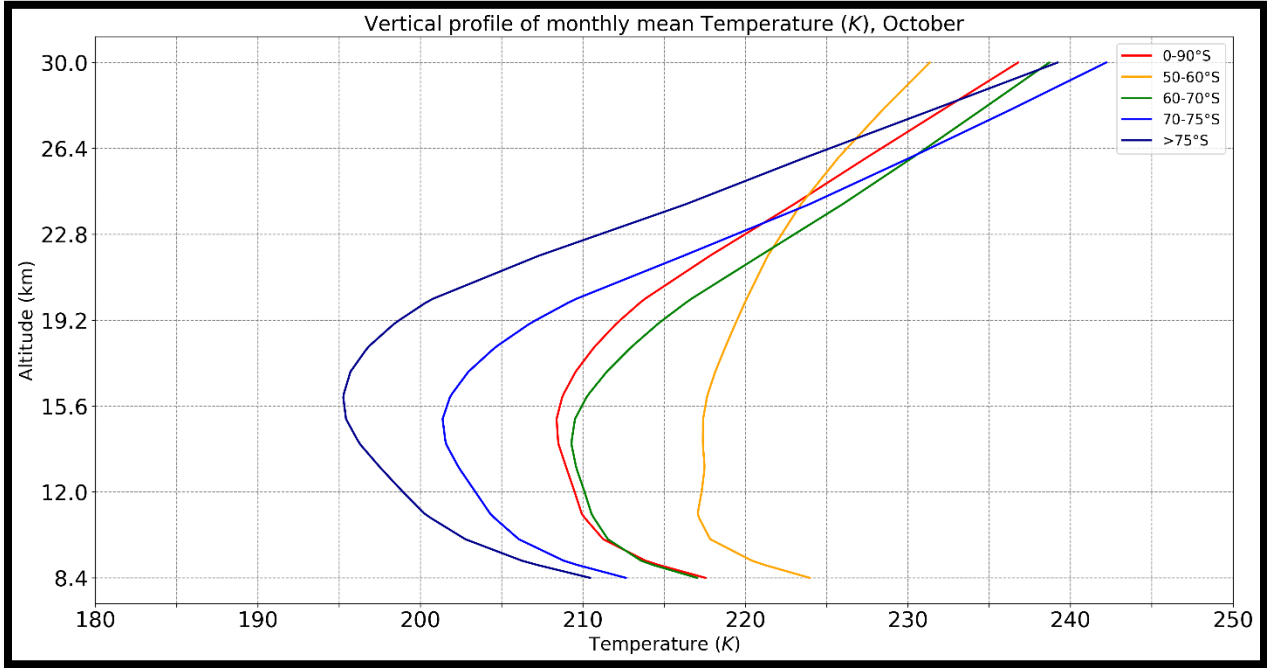

Figure 71: Vertical Profile of the Average October Temperature for the Southern Hemisphere for the period 2006-2020.

October, marking the conclusion of the Antarctic PSC season according to the dataset, sees the coldest temperatures dropping to about 195K at nearly 16km altitude. This month stands out for

recording the lowest temperatures at significantly lower altitudes compared to other months, both in the Northern and Southern Hemispheres, with these minimum temperatures observed at or below 16km. Notably, within the 50-60 degrees latitudinal zone, the lowest temperature observed is 217.5K at nearly 11km, aligning with the first turnpoint of the three-turnpoint pattern for this zone. This occurrence is unique to October. The average lowest temperature across the Southern Hemisphere for October is identified at 208.5K, noted at 15km altitude, highlighting a temperature difference of approximately 22.5K between the coldest temperatures of the lowest and highest latitudinal zones.

Additionally, October's temperature profile reveals significant warming at altitudes above 22km, especially within the lower latitudinal zone, contrasting with the higher zonal temperatures observed in other regions. This warming trend in higher altitudes aligns with the onset of spring in the Southern Hemisphere, which introduces increased solar radiation and, consequently, warmer temperatures.

Differences between Arctic and Antarctic

It has been clearly demonstrated that the Antarctic exhibits lower stratospheric temperatures than the Arctic, with variations in temperature differences not uniformly distributed across all altitudes. Focusing on the average hemispherical vertical profile of temperatures, the most significant discrepancies are observed at approximately 17 km in altitude. Conversely, the smallest differences are noted at both the lower and higher extremes of the dataset, indicating that as one moves away from 17 km, either higher or lower, the temperature difference between the Arctic and the Antarctic diminishes.

The alignment between the altitude of the average hemispheric lowest temperatures and the altitude of maximum PSC formation is more pronounced in the Southern Hemisphere than in the Northern Hemisphere. This closer alignment in the Southern Hemisphere could suggest a more direct correlation between the lowest stratospheric temperatures and the peak conditions for PSC formation, potentially due to the hemispheric differences in atmospheric circulation, land-sea distribution, and solar radiation receipt. The Southern Hemisphere's stratosphere is known for its strong polar vortex, as discussed before, which can isolate polar air more effectively, leading to colder temperatures and, consequently, a higher propensity for PSC formation. This isolation helps maintain the cold temperatures necessary for PSC formation closer to the altitude where these conditions are met more frequently.

The average temperature of the lower stratosphere in Antarctica is 6–7 degrees lower than in the Arctic, with the most significant difference observed in the altitudinal range between 13 and 21.5 km, where the average difference exceeds 9 degrees (figure 70). Against the background of a higher temperature of the lower stratosphere in the Arctic, according to Jakovlev et al. (2021), individual years with a stable polar vortex (1997 and 2011) stand out, when the temperature of the lower stratosphere is significantly lower than the average climatic temperature during the

winter-spring period, which led to the formation of ozone anomalies. In Antarctica, on the contrary, there are several years when the temperature is significantly higher than the average climatic, mainly as a result of the SSW, which was the strongest in 2002, as shown in the work of Jakovlev et al. (2019). It should be noted that during the last decade (2010–2020), the destruction of the polar vortex, leading to a sharp increase in the temperature of the lower stratosphere, occurs in Antarctica more often than in previous decades.
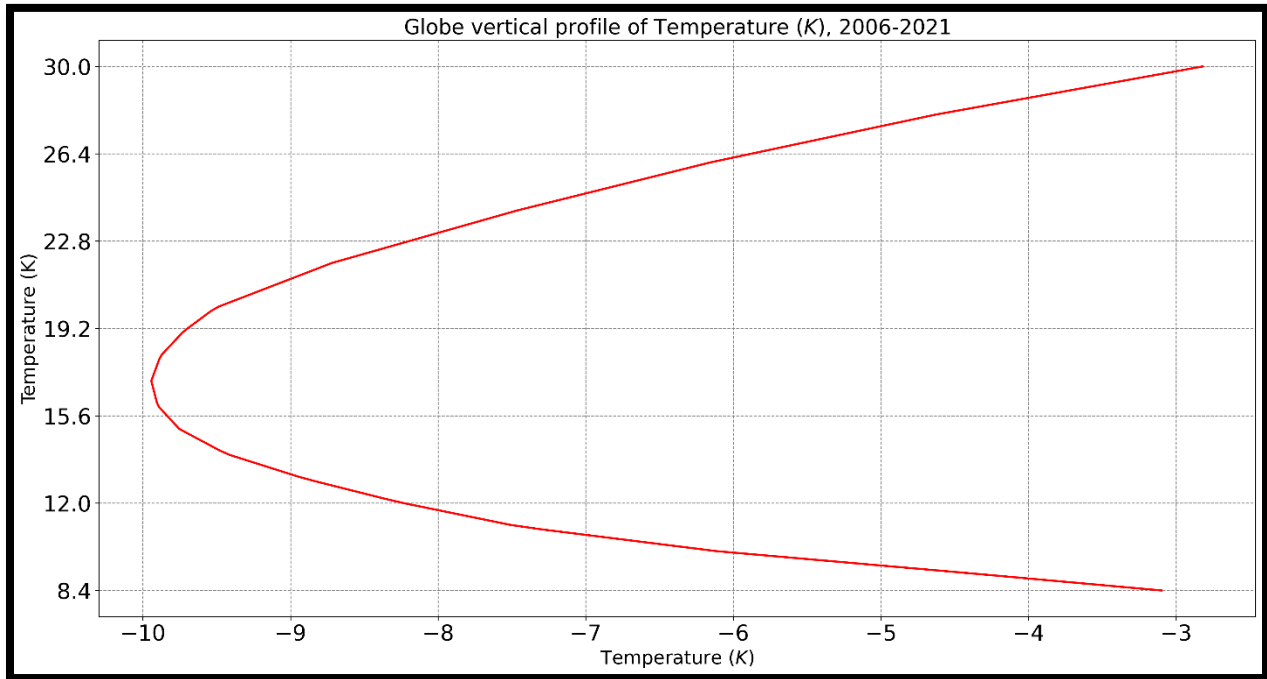
Figure 72: Vertical Profile of the Difference in Average Temperatures between the Southern and Northern Hemispheres.

4.3. Relationship between PSCs, Stratospheric Temperatures and Sunspots

Having examined the presence of PSCs vertically, horizontally, and over time, as well as the spatial and temporal distribution of stratospheric temperatures, we now shift our focus to exploring the correlation among PSC areal coverage, stratospheric temperatures, and the number of sunspots. To facilitate this analysis, all parameters have been evaluated using both monthly and yearly averages. It is crucial to clarify that the term "yearly" used in this analysis does not encompass all months of the year. Specifically, for the northern hemisphere, "yearly" calculations are based on data from only January, February, March, and December. Meanwhile, in the Southern Hemisphere, "yearly" refers to data from May through October. Therefore, whenever the term "yearly" is mentioned in this context, it pertains exclusively to the months specified above.

This analysis was conducted for both the northern and southern hemispheres, covering latitudes from 50° to 82°. Two distinct approaches were employed to calculate the vertical profiles of the

correlation coefficient between these parameters. The first approach involves calculating the hemispherical average, further analyzed into zonal averages at each of the 121 altitudes within each hemisphere, treating the data as a time series for each altitude layer. This method entails averaging the data across each month for each altitude layer and then calculating the correlation coefficient (r) for these averaged values. The second approach analyzes the correlation coefficient for each pixel between the parameters under investigation, thus retaining the spatial resolution of the data. An average correlation coefficient is then calculated for each altitude across different latitudinal zones. It is from the perspective of each method that the pixel-to-pixel approach can provide a more thorough analysis, as it maintains the integrity of spatial variability and thus enables the detection of local phenomena and patterns that may be obscured by averaging over larger areas.

The study focused on the zonal latitudinal distribution between 50-60 degrees, 60-70 degrees, 70-75 degrees, and greater than 75 degrees for both hemispheres. Although a focused pixel by pixel analysis could reveal more detailed information on these relationships for each specific region, the scope of this study does not extend to examining the correlation between our parameters in such fine detail, as the goal is to provide a general overview of the parameters under study. For each pair of parameters (PSCs – Temperature, Temperature – Sunspots, Sunspots – PSCs), the pixel-to-pixel approach is applied for both the Arctic and the Antarctic, where the best vertical correlation profiles between the yearly and monthly averages are presented. However, the remainder of the pixel-to-pixel profiles are presented in Appendix D, followed by all the crafted profiles of the averaged data in Appendix E.

Comparing the results between these two approaches, it appears that when calculating the correlation between sunspots and temperature over the Antarctic, both the monthly and yearly averages produce almost identical profiles, with only minor differences at lower altitudes. This consistency suggests that either method used to calculate the vertical profile of correlation (r) between these two parameters in the Antarctic yields similar results, potentially indicating a trend between them. An extended dataset, both in time and across altitudinal ranges, could likely reveal more significant insights. A similar pattern emerges in the Northern Hemisphere, although the latitudinal zone of 50-60 degrees exhibits a more distinct behavior for the yearly averaged values compared to other zones. Notably, the method detailed in Appendix E has yielded stronger correlations (or anticorrelations) for the parameters under study. Without delving further into the two methods, we encourage the reader to consult the appendix for a more comprehensive understanding of the vertical profiles of the correlations and the methodologies employed. Now, focusing on the pixel-to-pixel approach, the results presented below are:

4.3.1. PSCs – Stratospheric Temperatures

Starting with the vertical correlation profiles between PSCs and stratospheric temperatures, it has been observed that for the pixel-to-pixel analysis, the monthly values exhibited slightly stronger correlations than the yearly averages. This finding is consistent across both the Arctic and the

Antarctic, indicating that the monthly mean values better represent the vertical profiles of correlation between these two parameters. By "stronger" correlations, it is meant that the correlation provides a more robust physical explanation. In this context, we aim for correlation coefficients as close to -1 as possible, reflecting the inverse relationship where higher temperatures typically result in fewer clouds. This understanding is grounded in the physical processes involved, suggesting that a "good" profile is one which consistently shows such low r values, thereby aligning with our expectations based on atmospheric dynamics.

In the northern hemisphere's profile (Figure 73), it is evident that the higher latitudes exhibit the most representative vertical profile, compared to other zonal profiles. It is important to note that the sky-blue color line, indicating latitudes from 0-90 degrees, actually represents only latitudes ranging from 50 to 82 degrees. This representation was chosen for the graph to reflect the general data trends of the northern hemisphere, and it serves as a depiction of the hemisphere's behavior regarding PSCs, which start to appear at latitudes greater than 50 degrees. This was thoroughly examined and analyzed in section 4.1. Thus, going forward, this line will be used to represent each hemisphere's behavior, but it is important to keep in mind that it specifically calculates the discussed latitudes.
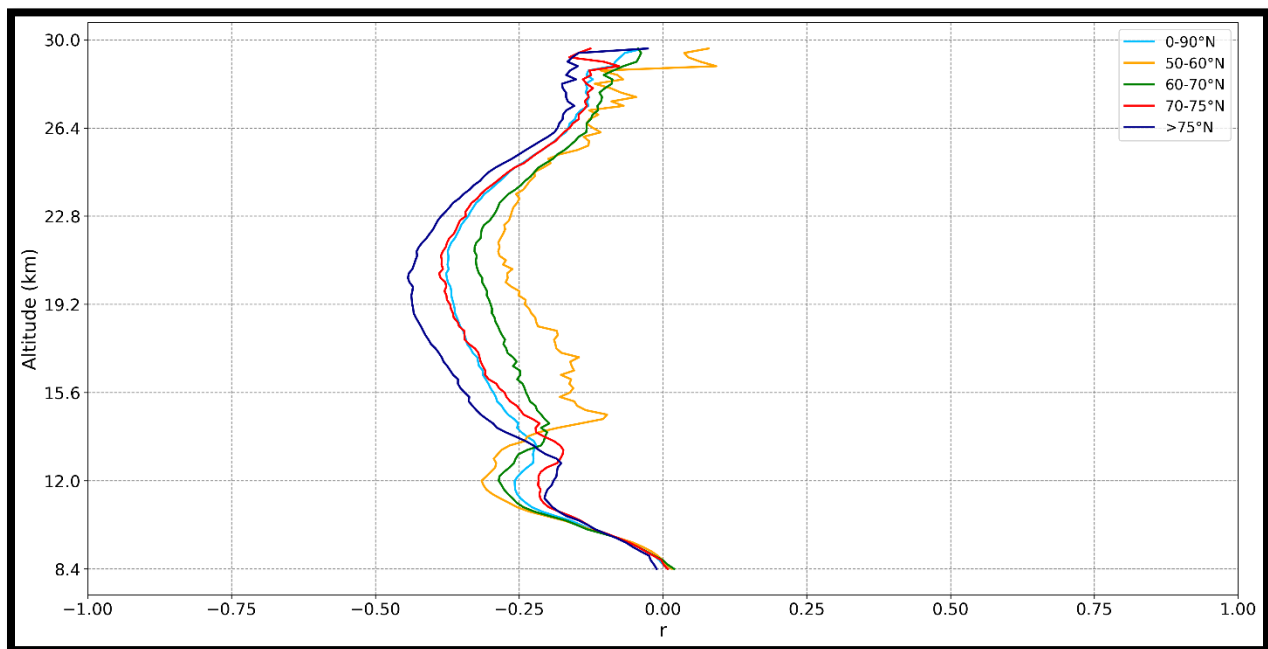

Figure 73: Vertical distribution of correlation coefficients between monthly mean values of PSCs and stratospheric temperatures across different latitudinal bands over the Arctic, from December 2006 to March 2021.

Analyzing the various profile zones, it appears that the strongest anticipated correlation occurs at altitudes above 75 degrees N, reaching a peak correlation coefficient of -0.44 at approximately 20.5 km above sea level. This region, spanning from 17.5 to 22.5 km, consistently presents the best r values, all lower than -0.4, a distinction not seen in the other latitudinal zones. The second

most significant vertical profile is observed in the latitudinal band between 70-75 degrees N, where the highest correlation value reaches -0.39 at 20.5 km. Within this band, correlation values below -0.35 are found in the altitudinal range of 18.5 to 22.5 km. Following this, the general behavior of the Northern Hemisphere shows the next best profile, with the strongest r value at -0.38 at 20.5 km, and values below -0.35 extending from 18.5 to approximately 22.5 km.

The latitudinal zone of 50-60 N reaches its optimal r value of -0.33 at 21.5 km, with correlation coefficients below -0.3 observed between 19 and 23 km in altitude. Notably, the behavior of the 50-60 N zone at lower altitudes is quite interesting; its best correlation coefficient of -0.32 is observed at 12 km above sea level. This zone maintains the strongest anticorrelation values up to 13.5 km in altitude, before the highest latitudinal zone begins to exhibit the best profiles. This observation aligns with the findings discussed in section 4.1, where it is noted that the most PSCs at low altitudes appear at small latitudes than those at higher altitudes.

However, it is important to remind that the identification of PSCs is not always straightforward due to the complexity of the term "PSCs." This complexity arises because it is possible that many of the observed in this zone may actually be a mixture of upper cirrus clouds and lower stratospheric clouds.
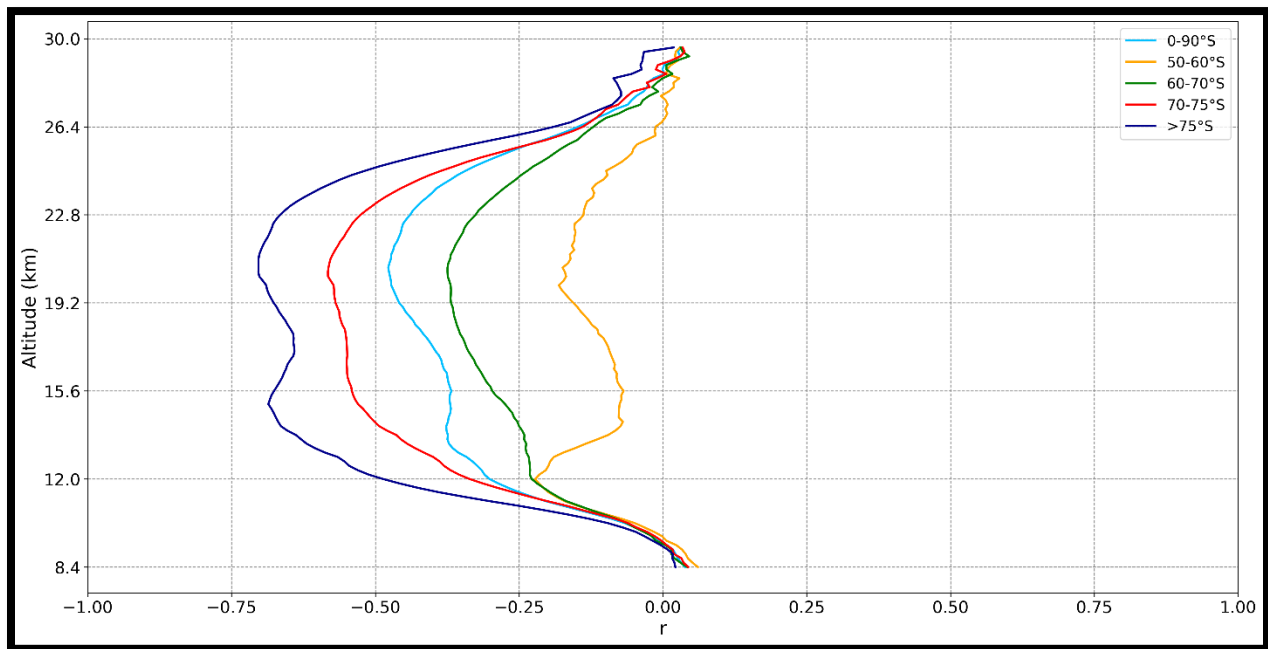

Figure 74: Vertical distribution of correlation coefficients between monthly mean values of PSCs and stratospheric temperatures across different latitudinal bands over the Antarctic, from July 2006 to October 2020.

Moving to the southern hemisphere's vertical profile of the correlation coefficient between temperature and PSCs (Figure 74), the analysis becomes more intriguing. The r values are significantly closer to -1 compared to those in the northern hemisphere, and the behavior of the profiles according to their latitude zones is much clearer. Unlike in the northern hemisphere

where various profiles crossed each other at altitudes both below and above 13.5km, in the southern hemisphere, each latitudinal zone presents a distinct profile that remains consistent over a substantial vertical extent—often across the entire vertical range—without intersecting with others.

Similar to the northern hemisphere, the most pronounced profile is observed at the highest latitudes (>75S), where there is a notable double peak in the correlation values. The first peak occurs at 20.5km above sea level with an r value reaching -0.7, and these strong correlation values persist, staying below -0.7 within the altitudinal range of 20.3 to 21.3 km. A secondary peak is observed at approximately 15km with a value of -0.69. Interestingly, the r values remain relatively low, staying below -0.6 across a wide altitudinal range from about 13.5 to 23.5km. No other latitudinal zone analyzed with this method achieves an r value greater than the absolute value of 0.6.

The second-best profile in the southern hemisphere belongs to the latitudinal zone of 70-75° S, where the highest correlation coefficient (r value) reaches -0.58. This zone maintains relatively low r values, staying below -0.55, within the altitudinal range of 16.5 to 22 km. Profiles for other latitudes show r values higher than -0.5, with the next most notable profile representing the general behavior of the southern hemisphere. Here, the best r value reaches -0.48, with consistently low values (below -0.45) from 19 to 22.5 km above sea level.

For the latitudinal zone of 60-70° S, the best r value is found at -0.38 at 20.5 km. In the lowest latitudinal zone, the best r value is observed at 12 km, reaching -0.22. It is noteworthy that above 12 km, the vertical profile of r for the zone of 50-60° S begins to rapidly approach zero, showing its largest discrepancy with the best profile at 15.2 km (absolute r value difference = 0.61).

Commenting on these findings, the results demonstrate a consistent pattern regarding the altitude at which maximum PSC occurrence and the lowest temperatures coincide—most PSCs over the Antarctic have been observed around 20.5 km, with the coldest temperatures typically recorded near 20 km.

4.3.2. Stratospheric Temperatures – Sunspots

The next correlation profile analyzed in this thesis turned out to be one of the most intriguing. Initially, it was hypothesized that a correlation between temperature and sunspots would be robust, particularly in comparison to the correlation between PSCs and sunspots. This assumption was based on the premise that changes in solar activity, particularly the increased ultraviolet radiation during periods of maximum sunspot activity, would impact stratospheric temperatures. This effect is mediated by the increase in stratospheric ozone, which leads to greater stratospheric heating by solar radiation, as noted by Garcia et al. (1984) and Brasseur and Solomon (1986). Further supporting this hypothesis, a study by Angell, J. K. (1991) analyzed the correlation between annual values of stratospheric temperature and sunspot numbers for the period 1972-1989 over the northern hemisphere. This analysis found a correlation coefficient of

approximately r = 0.25 at an altitude of 20 km, with correlations increasing with altitude up to the 46-55 km layer, which was the highest layer examined in that study.

However, the methodologies employed in this thesis differ significantly in terms of the time series used and the definition of "annual" or "yearly" data. In this analysis, the correlation between stratospheric temperature and the number of sunspots is specifically limited to the months during which PSCs are typically observed. An alternative approach that investigates the potential relationship using data from all months of each year could potentially reveal more distinct patterns or provide deeper insights into this relationship. This broader analysis might capture variations and influences over the entire annual cycle, which could significantly enhance our understanding of the interplay between solar activity and stratospheric temperature changes.
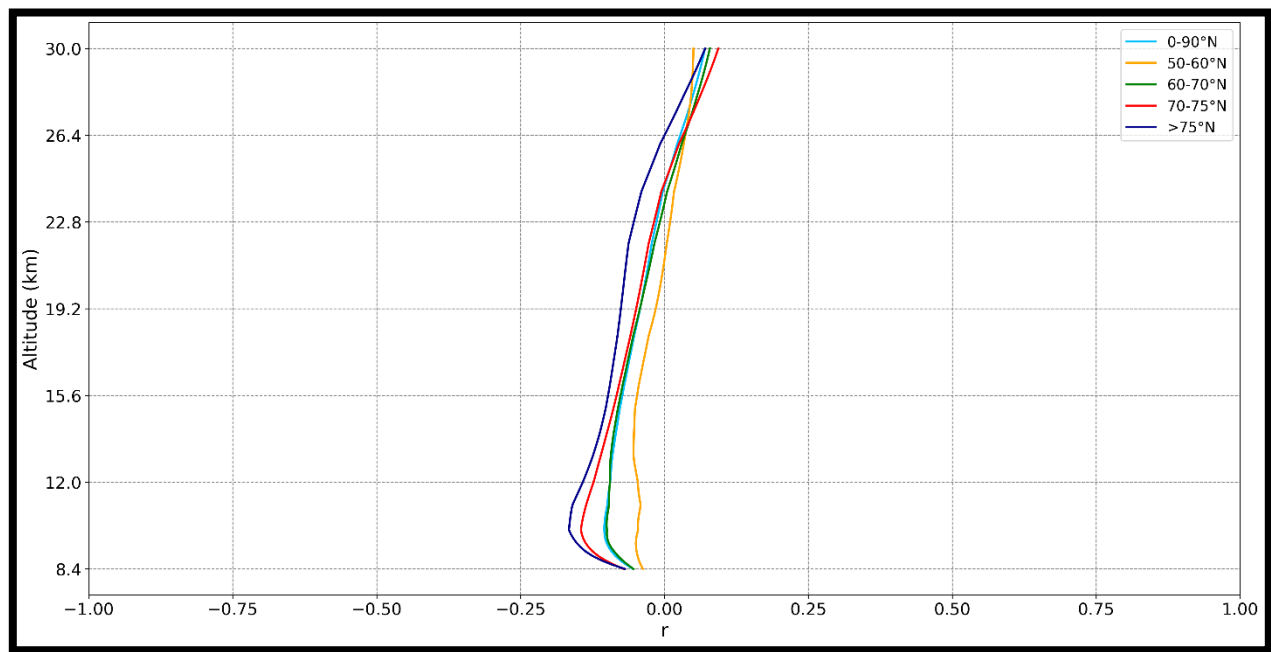
Figure 75: Vertical distribution of correlation coefficients between monthly mean values of stratospheric temperatures and the number of sunspots across different latitudinal bands over the Arctic, from December 2006 to March 2021.

Choosing the "best" vertical profile of the correlation coefficient (r) for temperature and the number of sunspots between the monthly and yearly values (pixel-to-pixel analysis) proved challenging, as the two profiles were somewhat similar and neither displayed the expectedly low r values between these two parameters. However, the monthly mean values demonstrated slightly better correlation coefficients than the annual data, achieving the highest correlation at the dataset's maximum altitude of 30 km in the latitudinal zone of 70-75N, where it approached nearly r=0.1. As shown in Figure 75, the r values start to rise above 10-12 km, with the lowest latitudinal zone of 50-60N showing "better" r values than the others, reaching positive r values first at 21 km and maintaining the highest r values until approximately 26.5 km.

126

Focusing more on this specific latitudinal zone, 50-60N, its r values appear to stabilize at r = 0.05 from 29 to 30 km, while the r values in the rest of the profiles continue to rise. What is particularly interesting here is that the lower latitudinal zone in the northern hemisphere receives more direct solar radiation compared to others, especially considering that the months constituting the northern hemisphere's PSC season—from December to March—are influenced by the Earth's axial tilt. This phenomenon also applies to the Southern Hemisphere, as illustrated in Figure 76, where the r values in the latitudinal zone 50-60S lead at higher altitudes. This likely occurs because the Antarctic PSC season lasts longer, thus encompassing more months in spring compared to the northern hemisphere.

As a final note on Figure 75, it is observed that at lower altitudes, most latitudinal zones experience a decrease in correlation coefficients to lower, or "worse," values until approximately 10km, except in the zone 50-60N. There isn't a clear explanation for why this pattern occurs, but an initial hypothesis might relate to the solar minima and maxima.

According to G. Tsiropoula (2003), the analysis of the temperature response of the stratosphere and mesosphere to the 11-year solar cycle—observed in recent decades by various instruments including radars, lidars, rockets, satellites, and radiosondes—indicates a solar signature. This signature is highly variable both in amplitude and sign and is influenced by latitude and altitude. Solar ultraviolet (UV) radiation plays a significant role in the temperature, dynamics, and photochemistry of the stratosphere. Between wavelengths of 120 and 300 nm, solar UV radiation is absorbed by ozone and molecular oxygen in Earth's outer atmosphere. The increased levels of UV radiation result in heating most of the middle stratosphere and mesosphere due to this absorption, with less pronounced effects in the lower stratosphere. These dynamics could be influencing the observed patterns in correlation values at various altitudes, potentially explaining the specific trends noted in the low stratosphere.

Another interesting finding relates to the influence of the 11-year solar cycle on stratospheric geopotentials and temperatures. Labitzke and van Loon (1992) reported a distinct correlation between the 30-hPa geopotential heights and temperatures in the lower stratosphere of the Northern Hemisphere and the 11-year solar cycle. Building on this, van Loon and Labitzke (1998) utilized global data from NCEP/NCAR re-analyses for the stratosphere at levels as high as the 10-hPa geopotential heights, demonstrating the presence of the 11-year solar signal in both hemispheres. They discovered that this signal is most pronounced during the northern summer, and interestingly, the highest correlations between the solar cycle signal and stratospheric temperatures shift from one summer hemisphere to the other depending on the time of year. Additionally, they observed that these correlations are weakest globally during the local winter months in both the Southern and Northern Hemispheres.

The southern hemisphere's vertical profile of the correlation coefficient (r) between monthly and annual values shows considerable variability in how r values change across different altitudes within each latitudinal zone—indicating an inconsistent rate of change vertically. Despite the

selection of yearly mean values (figure 76) to represent this profile, it is strongly recommended that the reader refer to Appendices D and E for a comprehensive comparison. Appendix D details the profiles obtained through the pixel-to-pixel method for both yearly and monthly values, while Appendix E provides the profiles derived from the other method. What is particularly interesting is that the vertical profiles of correlation coefficients (r) for both the monthly and yearly data are almost identical across these methods (e.g. the profile of the yearly mean values using the pixel-to-pixel method is almost identical to that profile of the other method), a phenomenon that remains under investigation as there is no clear explanation for this similarity. However, further analysis using the pixel-to-pixel approach will assist in understanding the potential behavior and underlying factors influencing these vertical profiles.
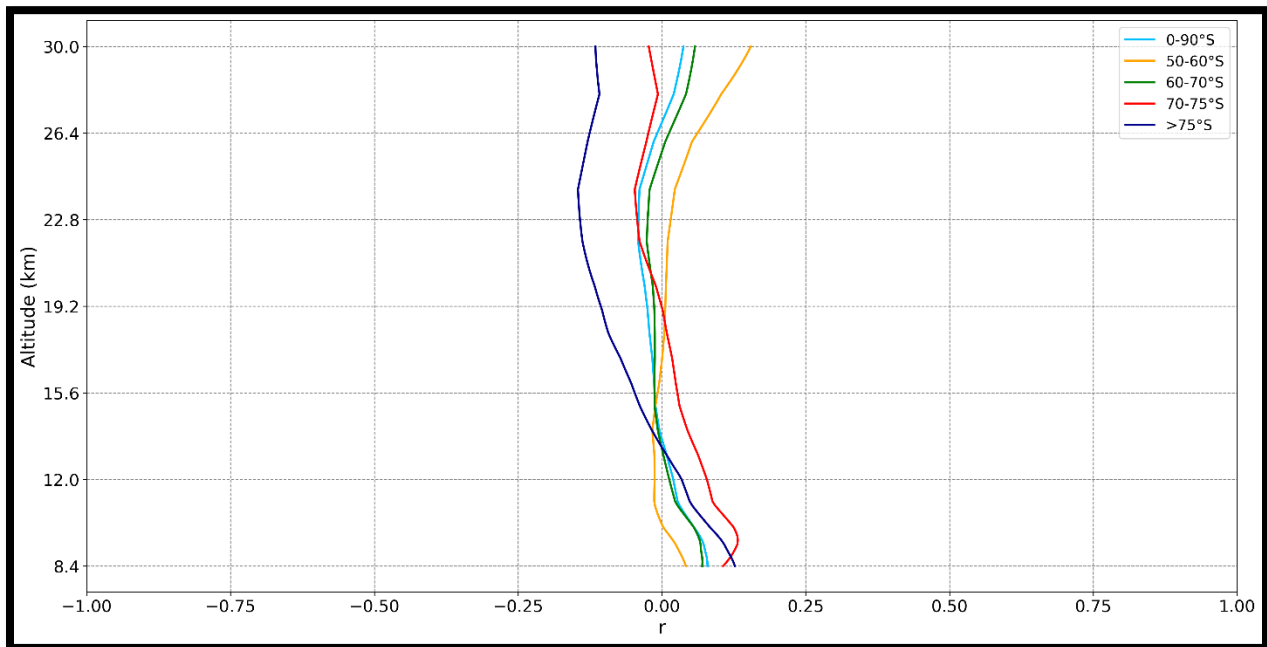
Figure 76: Vertical distribution of correlation coefficients between yearly mean values of stratospheric temperatures and the number of sunspots across different latitudinal bands over the Antarctic, from 2006 to 2020.

According to Figure 82 of appendix D, the highest r value occurs in the latitudinal zone of 50-60S, reaching nearly 0.08. This is followed by the 60-70S zone, with a maximum r value of 0.05, and then the 70-75S zone, where the maximum r value is 0.035 at approximately 28km. The least favorable profile is observed in the >75S latitudinal zone, nearly reaching 0.015 at the highest altitudes.

Figure 76 presents two key aspects of the correlation between stratospheric temperatures and the number of sunspots across various latitudinal zones in the Southern Hemisphere. The first point of interest is the vertical trend changes within the correlation profiles, and the second is the range of correlation coefficients, encapsulated by their maximum and minimum values within each zone.

For the entire Southern Hemisphere, represented by the blue line, a significant shift in trend is observed at an altitude of approximately 21.8 km. Within the 50-60°S latitudinal zone, a series of trend transitions are noticeable at altitudes of about 13.8 km, 12 km, and again at 11 km. Moving to the 60-70°S zone, a complex array of trend alterations emerges. Here, directional changes in correlation are marked at roughly 21.5 km, 17 km, and 16 km, with a conclusive shift occurring at the study's lowest measured altitude, between 8.4 and 8.6 km. The trend shifts in the 70-75°S zone manifest distinctly, occurring at altitudes of approximately 28 km, 24 km, and 9.5 km. Lastly, for the expanse above 75°S latitude, trend reversals are evident at higher altitudes, specifically around 28 km and 24 km.

These observations highlight the dynamic nature between solar activity and atmospheric temperatures, which manifests distinctly across various altitudinal layers and latitudinal zones. However, drawing definitive conclusions regarding these specific behaviors remains a challenge, particularly within the limited scope of this study. The data suggests a dependency of temperature correlations on both altitude and latitude, yet the underlying mechanisms driving these correlations necessitate further investigation.

Further analysis of the results reveals that from approximately 21 km upwards, the lower latitudinal zones exhibit higher correlation coefficients compared to the higher ones. This pattern indicates that the 50-60°S zone shows better correlation than the 60-70°S, which in turn is better than the 70-75°S, and so forth up to the >75°S zone. A plausible explanation for this phenomenon could be that the lower latitudes receive more direct solar radiation than the higher ones. This is particularly relevant considering that the data for this analysis were collected from May to October, spanning from the last month of the local autumn (May) through the local winter months (June, July, and August) in the southern hemisphere. During this period, the high latitudes (>70°S) receive only a minimal amount of direct solar radiation.

However, an intriguing question arises as to why this trend is observed specifically at altitudes above 21 km, while a different pattern may exist below this altitude. As mentioned in this study, several factors influence and contribute to changes in atmospheric parameters within the stratosphere. Notably, variations in the solar cycle, including the solar minima and maxima, predominantly affect the middle and upper stratosphere rather than the lower-middle stratosphere. This differentiation suggests that the solar cycle's impact on the upper levels of the stratosphere is a significant factor that could explain the observed correlation trends.

Another consideration is the vertical ozone profile. According to NOAA, based on the 21-year median from 1991 to 2012, the maximum concentration of ozone occurs at around 18 km. From this altitude upwards, there is a substantial presence of ozone, and at higher altitudes, there is also more solar radiation. This situation provides a robust explanatory framework based on well-understood stratospheric mechanisms that could influence the observed vertical correlation profile between stratospheric temperature and the number of sunspots.

A noteworthy observation in the analysis is the better relationship at lower altitudes for higher latitudinal zones compared to lower ones between these two parameters. While no other study

has directly examined this relationship between stratospheric temperature and the number of sunspots, it has been noted that PSCs are more prevalent at higher latitudes (>70°S) than at lower ones. The presence of more PSCs provides numerous surfaces that facilitate heterogeneous chemical reactions, producing compounds that catalyze ozone depletion. According to figure 36, the highest concentrations of PSCs over the Antarctic are found between 15-23 km above sea level. Consequently, as the ozone hole expands during spring, it allows more UV radiation to penetrate deeper into the lower stratosphere. This increased UV radiation at lower altitudes could be a critical factor in the observed correlations and is a significant aspect of stratospheric dynamics during the PSC season.

4.3.3. Sunspots – PSCs

The final stage of this thesis is presented in this subsection, outlining the correlation coefficient (r) vertical profiles between the presence of PSCs and the number of sunspots. These profiles are once again derived using the pixel-to-pixel analysis, with the yearly values producing "better" results compared to the monthly ones. However, it is observed that the yearly vertical profiles over the northern hemisphere somewhat resemble the monthly profiles; the primary difference being that the yearly profiles exhibit a wider range of r values. Specifically, the yearly profiles reach both lower and higher r values compared to the monthly (see appendix D for details). The results, shown in Figures 77 and 78, reveal interesting differences between the two hemispheres. This approach has not been examined previously in scientific literature, therefore, our results could not be directly compared with similar studies.
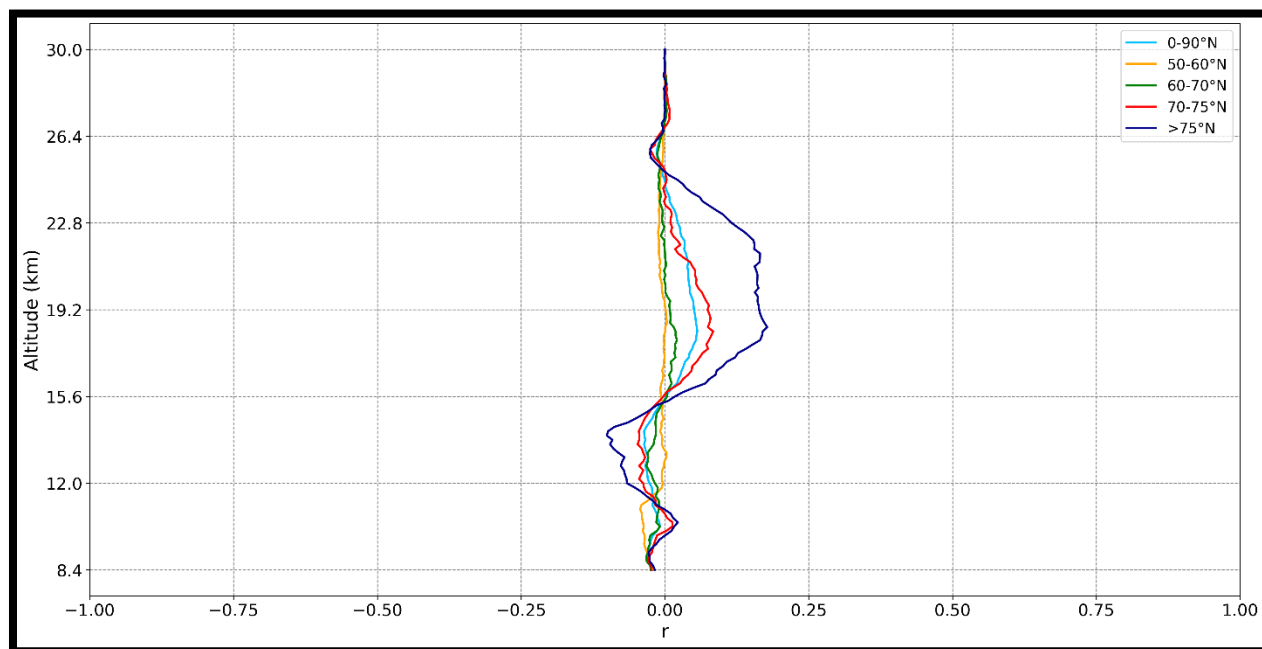
Figure 77: Vertical distribution of correlation coefficients between yearly mean values of PSCs and the number of sunspots across different latitudinal bands over the Arctic, from 2007 to 2021.

Over the northern hemisphere (Figure 77), the best and worst r values are observed in the highest latitudinal zone (>75N), with the best r value reaching -0.1 at 14 km and the worst recorded at 18.5 km with r = 0.18. When referencing "best" r values in this context, it is essential to note that these values should be negative. This negative correlation indicates an inverse relationship between the presence of PSCs and sunspots, grounded in the understanding that increased solar radiation leads to higher temperatures, which in turn results in a lower presence of clouds. This is particularly relevant for PSCs, which require significantly low temperatures to form in polar regions. Therefore, for these two parameters, the most desirable (best) r values are negative, indicating a stronger inverse relationship, and the least desirable (worst) r values are positive.

The next best r profile is found in the latitudinal zone 70-75N, with its best r value reaching -0.05 at approximately 13.5 km and its worst r value recorded at approximately 18.5 km. All other profiles generally display their best r values closer to zero. Specifically, the latitudinal zone 50-60N records its best r value at approximately 11 km, reaching roughly -0.045. Following this, the profile representing the northern hemisphere (indicated by the blue line) achieves an r value of -0.35 at 13.5 km in altitude. The last noteworthy profile is that of the latitudinal zone 60-70N, with an r value of approximately -0.35 at 9 km. However, these r values are too low to warrant a detailed exploration into the mechanisms producing them due to their lack of statistical significance. Despite this, there are several observations that can be made to enhance our understanding of how or why some of these r values were calculated. This reflection may aid in improving the methodologies or interpretations applied in studying these interactions.

Focusing on the altitudes above 28 km, it is evident that all the r values of the profiles approximate zero, indicating that there is no discernible relationship between the presence of PSCs and the number of sunspots. As shown in section 4.1, and specifically in Figure 30, PSCs at these altitudes have an extremely low areal coverage, distributed in sparse pixels over the Arctic (Figure 18a), resulting in a limited sample size. For an enhanced understanding of its correlation, a more thorough analysis could potentially yield different results (either better or worse) if focused solely on the "slices" (latitude-longitude areas) where PSCs most frequently occur at these altitudes, and then comparing these findings with the number of sunspots. In the context of this study, delving into this specific area goes beyond the core idea; however, for future research based on this thesis, investigating this particular aspect could provide valuable insights. Such an approach would allow for a more detailed examination of the interactions between high-altitude PSCs and solar activity.

Further analysis of the results clearly shows that all vertical r profiles display their worst values within a narrow vertical range of about 1 km, specifically extending from approximately 18 km to roughly 18.8 km. There is no clear explanation for why this occurs, especially considering that the altitude of the greatest PSC areal coverage over the northern hemisphere is about 21 km above sea level. Being 2-3 km lower than the initial peak of PSC areal coverage suggests the influence of another mechanism, which remains a topic for further investigation within the context of this study.

Another interesting observation is made concerning the altitudinal zone of 13-14 km, where most of the profiles display their best r values. Intriguingly, as seen in Figure 30, this zone represents the altitudinal zone of minimum PSC areal coverage, just a few kilometers above the secondary peak of PSC coverage at 11.5 km in the northern hemisphere. This altitude, within the low stratosphere, is where one would typically expect a lesser relationship between PSCs and the number of sunspots. However, a possible explanation could relate to the dynamics of the Arctic ozone hole, which, while less profound than in Southern Hemisphere, could play a significant role in this finding.

While a few insights have been derived from this analysis, the r values calculated are relatively low (in absolute terms) to conclusively demonstrate a strong relationship or anti relationship between these two parameters. Some explanations have been proposed based on the altitudes of maximum and minimum PSC areal coverage, but this analysis could be further refined by examining specific slices of latitude-longitude areas. Additionally, a correlation profile of ozone levels with both PSCs and sunspot numbers could yield results that might further clarify the connections between PSCs and solar activity.

Transitioning the analysis to the southern hemisphere (Figure 78), a significant observation emerges regarding the lower latitudinal zone of 50-60S, which displays the "worst" r profile. Here, the highest numerical positive correlation is observed at 15.6 km with an r value of 0.135. Comparatively, the next highest positive r value is 0.03, observed at 28.5 km in the latitudinal zone >75S. However, this same zone (>75S) also shows the most significant negative r values, achieving -0.18 at both lower and higher altitudes, specifically at 13.5 km and approximately 26 km, thus presenting a profile with two peaks.

A similar two-peak profile is observed in the latitudinal zone 70-75S, where the r values reach -0.17 at nearly 26 km and 14.5 km. The next notable negative r values are found in the 60-70S zone, with an r value of -0.12 at 22.5 km. Meanwhile, for the lowest latitudinal zone of 50-60S, the best r value is -0.02, occurring within the altitudinal range of 21.2 to 21.7 km. This distribution of r values across different latitudinal zones and altitudes in the southern hemisphere highlights varied interactions between solar activity and the presence of PSCs, as mentioned before, probably contributed to the distribution of PSCs both horizontally and vertically.

Focusing on the lower altitudes, most profiles exhibit their best r values within the altitudinal range of 13.5 to 15 km, a pattern that is also observed in the northern hemisphere. Notably, the two highest latitudinal zones (>75S and 70-75S) show quite similar behavior up to 22.8 km, beyond which the profiles begin to diverge significantly. For instance, at 24 km, the higher latitudinal zone (>75S) records an r value of -0.01, whereas the zone 70-75S shows a significantly lower r value of -0.1, indicating a tenfold difference in magnitude.

When summarizing the general profiles over the Antarctic by averaging all values across all altitudes, it is found that the best average r value belongs to the 70-75S zone, with an r value of -

0.08. This is followed by the >75S zone with an r value of -0.07, the 60-70S zone with -0.05, the averaged hemispherical value (0-90S) at -0.04, and finally, the 50-60S zone which exhibits a positive r value of 0.02. This distribution suggests that higher latitudes tend to exhibit a stronger anti-correlation compared to lower ones.
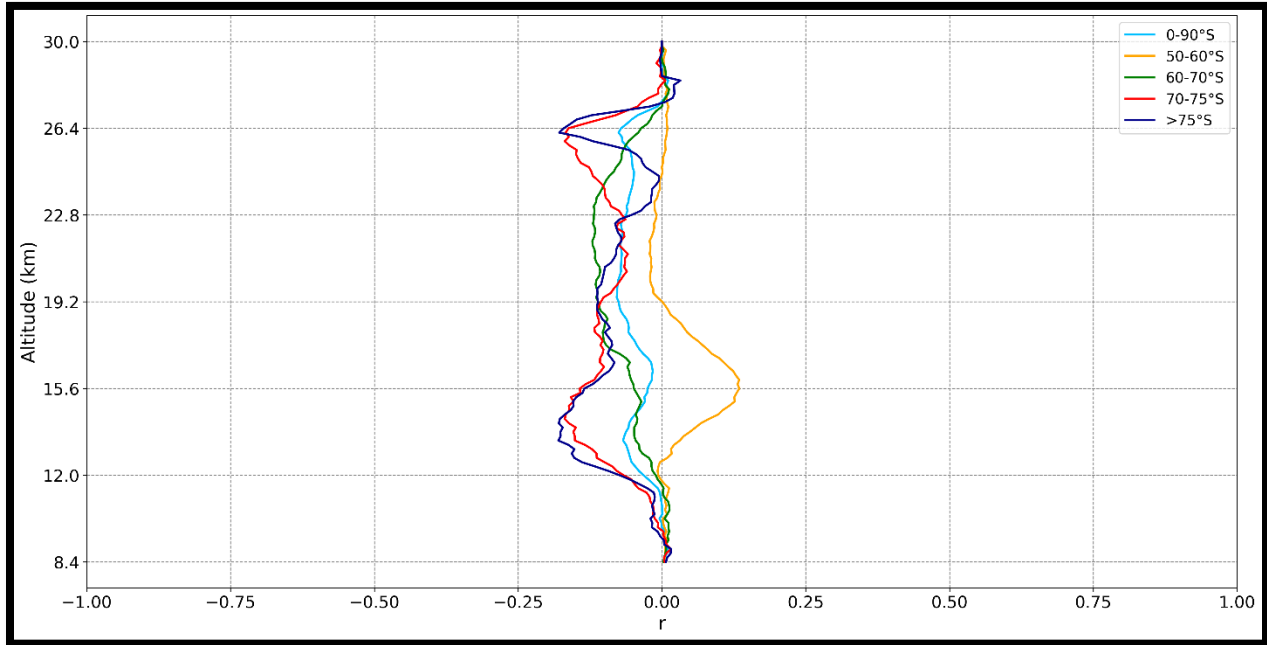

Figure 78: Vertical distribution of correlation coefficients between yearly mean values of PSCs and the number of sunspots across different latitudinal bands over the Antarctic, from 2006 to 2020.

In the context of this study, it is important to recognize that the most PSCs have been observed at these higher latitudes. Therefore, the better anti-correlation at higher latitudes could be linked to the prevalence of PSCs in these regions. This implies that solar activity, which impacts the formation and dynamics of PSCs, might be more pronounced at higher latitudes, leading to more significant interactions between sunspots and stratospheric temperatures.

However, the explanation of the relationship between PSCs and solar activity is not straightforward for either hemisphere. One major challenge arises from the fact that PSCs predominantly form during the local winter periods at high latitudes, where there is little to no direct solar radiation. Additionally, most PSCs are observed at altitudes below 25km in the low to middle stratosphere, where solar radiation is not only scarce but also varies across different wavelengths.

One significant factor is the polar stratospheric vortex. According to Svetlana Veretenenko's 2022 study, the polar vortex plays a crucial role in various atmospheric processes and significantly impacts how solar activity influences the lower atmosphere, from the middle troposphere up to the stratosphere. Variations in the intensity of the vortex are known to cause temporal variability in the correlation observed between atmospheric characteristics and solar

phenomena. As noted in Section 4.1, during periods when the polar vortex is particularly strong, stratospheric temperatures tend to be very low, which enhances the formation of PSCs. Therefore, a comprehensive study that investigates the behavior and link between the intensity of the polar vortices in both the southern and northern hemispheres, identifying their maxima and minima in relation to solar activity, would provide deeper insights.

Further enhancing such work, an analysis of ozone distribution within the stratosphere, alongside correlations among it, the vortex, and the solar cycle, could potentially shed light on the various mechanisms that might link PSCs with solar activity. The altitudes where PSCs and the number of sunspots display correlation values like -0.18, -0.17, and so on, are particularly noteworthy due to the indirect nature of the link between these two parameters. The results suggest that there is indeed a relationship between these parameters, although it is not particularly strong. This is attributed to the multitude of other factors that also influence their relationship.

5. Conclusions and Perspectives

The aim of this thesis was to develop a climatology of PSCs and investigate any potential relationship between their occurrence and the 11-year solar cycle from July 2006 to March 2021. The first step involved creating the climatology of PSCs for both hemispheres, locating them in space and time, observing their trends, their overall distribution, and obtaining a comprehensive picture of their areal coverage across the two hemispheres. Due to the relationship between PSCs and stratospheric temperatures, it was crucial to examine the stratospheric temperature profiles both vertically and horizontally to identify any patterns between the presence of PSCs and temperatures. This approach stemmed from the realization that solar activity could have a more direct effect on temperatures, which in turn affects the PSCs. With this in mind, the investigation of a potential relationship between PSCs and solar activity was divided into three profiles based on their correlation coefficients' vertical profiles. This included the profile of PSCs and temperatures, followed by the profile of temperatures and the solar cycle, and concluded with the profile of PSCs and the solar cycle. The core results derived from this analysis are summarized as follows:

PSCs

The study revealed distinct spatial patterns in the distribution of PSCs across both hemispheres.

- In the Southern Hemisphere, PSCs have a more uniform and extensive spread, particularly over Antarctica, due to the presence of a large, relatively axisymmetric stratospheric polar vortex. In contrast, the Arctic in the Northern Hemisphere shows more variability in PSC distribution because of irregular topography and stronger wave activities influencing the Arctic vortex. The spatial coverage of PSCs in the Southern Hemisphere peaks in July and August during the coldest phase of the vortex, whereas in the Northern Hemisphere, it varies more pronouncedly, with some seasons showing extensive coverage and others minimal, reflecting the dynamic nature of the Arctic atmosphere.
- In the Northern Hemisphere, PSCs are predominantly found between 60°W to 120°E, aligning with the preferred position of the Arctic vortex, which has been shifting towards Eurasia due to increased zonal wavenumber 1 activity. The highest frequency of occurrence is at 21 km, extending from 60°W to 120°E, with a secondary maximum at 11.5 km. In the Southern Hemisphere, PSCs show a specific longitudinal pattern, slightly displaced towards the Greenwich Meridian quadrant. The highest frequency is near the vortex edge at 20.3 km, typically located near the base of the Antarctic Peninsula, influenced by mountain wave events and upper tropospheric forcing.

In the Northern Hemisphere, PSCs predominantly occur at altitudes ranging from 13 to 24 km, exhibiting maximum frequency between 18 and 22 km. Conversely, in the Southern Hemisphere, PSCs are observed at altitudes from 12 to 26 km, with their peak frequency occurring between 16 to 22 km. The vertical distribution of PSCs presents notable differences between the hemispheres. In the Southern Hemisphere, PSCs are distributed across a broader range of

altitudes, with maximum coverage often found at high altitudes. This is attributed to the colder and more stable conditions of the Antarctic stratosphere.

Northern Hemisphere:

- **Altitude Range:** PSCs predominantly occur at 13 to 24 km, with maximum frequency between 18 and 22 km.

- **Seasonal and Altitudinal Variability:** The highest frequency and coverage peak at 21 km from December to March, with a secondary maximum at 11.5 km. PSC occurrences drop to nearly zero below 10 km. The altitude of maximum PSC occurrence shifts to lower altitudes as the season progresses.

- **Interannual Variability:** Significant fluctuations in coverage occur across different years, influenced by polar vortex strength and stratospheric temperature anomalies. Years with colder temperatures and a stable vortex (e.g., 2015 and 2016) show higher PSC occurrences, while warmer years (e.g., 2014) show reduced activity.

Southern Hemisphere:

- **Altitude Range:** PSCs occur at 12 to 26 km, with peak frequency between 16 and 22 km.

- **Seasonal and Altitudinal Patterns:** The highest frequency occurs at 20.3 km, with significant occurrences at lower altitudes, especially around 11.5 km. PSC occurrences decrease below 10 km. Peak occurrences are found during colder months (June to September), with highest concentrations in July and August.

- **Interannual Consistency:** The Southern Hemisphere shows a more consistent pattern of PSC occurrences from year to year, although there is still noticeable variability influenced by temperature and polar vortex conditions. Extensive coverage often occurs in July, aligned with the coldest stratospheric temperatures. Certain years (e.g., 2006, 2011, and 2016) saw peak PSC activities due to intense cold snaps and stable vortex conditions.

While both hemispheres show peak PSC occurrences at similar altitudes (around 20-21 km), the Southern Hemisphere has a slightly lower peak altitude. Both hemispheres exhibit strong seasonal dynamics: the Northern Hemisphere sees peak altitudes decrease from winter to early spring, while the Southern Hemisphere maintains a consistent peak altitude during its winter months and exhibits a longer period of PSC presence due to persistent cold conditions.

From 2006 to 2021, the Northern Hemisphere showed a slight, statistically insignificant upward trend in PSC coverage, while the Southern Hemisphere showed a slight downward trend, potentially aiding ozone recovery since 2000. These trends highlight the complex interplay between PSC formations and climatic phenomena such as sunspot activity, El Niño, and La Niña, warranting further investigation.

Stratospheric Temperatures

Transitioning from PSC climatologies to stratospheric temperatures, it has been observed that:

- Stratospheric temperatures at the critical altitude of 21 km are coldest across the Arctic, peaking between 30°W to 90°E, aligning with the highest frequencies of PSC occurrences.
- At 20.3 km, the coldest temperatures in Antarctica are observed in the latitudinal zone from 60°E to 90°W, which also corresponds to the highest PSC occurrence rates.
- Temperature trends over the period July 2006 to March 2021 are insignificant both for the 5% and 10% significance level and, at the same time, weakly negative for the Northern Hemisphere and positive for the Southern Hemisphere.

The vertical temperature profiles across different latitudinal zones, note the most pronounced temperature gradients occur at mid to high altitudes, where PSCs are most prevalent. For instance, in the Northern Hemisphere, temperatures range significantly with altitude, showing colder temperatures aloft that favor PSC formation. In the Southern Hemisphere, the coldest temperatures shift to higher altitudes as the season progresses, mirroring the movement and formation patterns of PSCs, suggesting a dynamic relationship between altitude, temperature, and PSC activities. The lowest stratospheric temperatures, which coincide with the peak PSC seasons in both hemispheres can highlight the sensitivity of PSC formation to temperature fluctuations. Years with colder temperatures tend to have more extensive PSC coverage, underlining the critical impact of temperature on PSC dynamics.

Relationships

PSCs - Temperatures

There is a robust correlation between the occurrence of PSCs and lower stratospheric temperatures, with both phenomena showing a strong seasonal and interannual linkage. This correlation is particularly evident during periods of significant cooling, which aligns with increased PSC activity. However, the correlations between PSCs and temperatures showed varying strengths across different latitudinal bands, with the strongest correlations over the Arctic typically found at latitudes above 75°N. The peak correlation coefficients reached values around -0.44 at altitudes around 20.5 km, where PSCs are most likely to form due to the coldest stratospheric temperatures. Over the Antarctic, the correlations were generally stronger and more consistent, with some latitudinal bands showing correlation coefficients of -0.7, especially at altitudes near 20km where PSC formation is most frequent, particularly at latitudes above 75°S.

Sunspots – Temperatures

Across both hemispheres, the study found no strong or consistent correlations between the number of sunspots and stratospheric temperatures. The correlation between the number of sunspots and stratospheric temperatures shows in general weak positive values, particularly at higher altitudes and lower latitudes. In the Northern Hemisphere, the zone 50-60°N showed the highest r-values between sunspots and temperatures, starting to increase at altitudes above 21 km.

- The correlation between sunspot numbers and stratospheric temperatures in the Arctic shows weak positive values at higher altitudes, above 25km, peaking at 0.1 at 30 km. At lower altitudes, particularly below 21 km, the correlations are negligible, further emphasizing the limited influence of sunspot activity on temperature variations in the stratosphere of the Arctic.

- In the Antarctic, the correlations between sunspot numbers and stratospheric temperatures are also weak, however stronger than those of the Arctic, yet with no clear or consistent pattern emerging across different altitudinal and latitudinal zones. The highest r-values have peaked at 30km, reaching almost 0.16. The weak correlations at various altitudes indicate that sunspots do not significantly affect stratospheric temperatures in the Antarctic, similar to observations in the Arctic, suggesting global consistency in the minimal impact of solar activity on stratospheric temperatures.

These findings suggest that the role of solar activity, as measured by sunspots, in directly influencing stratospheric temperatures is less significant than previously hypothesized. This is likely because the correlation was examined only for Arctic areas and not for the entire latitudinal band from -90 to 90 degrees. The correlation might be stronger in other latitudes, such as tropical or subtropical regions, where solar radiation is more consistent and direct than in higher latitudes. However, in our specific latitudinal zones above 50 degrees, it is observed that the higher the altitude, the higher the r-values between these two parameters. According to the literature (Angell, 1991), this is expected, although not to the desired extent.

Sunspots - PSCs

The relationship between sunspot numbers and PSC coverage is less clear and shows more variability. While some negative correlations are observed, they are not consistent or strong enough to suggest a direct or robust relationship. This indicates that while solar activity may have some influence on PSC formation, it is likely indirect and modulated by other atmospheric factors. Yearly data, which aggregates sunspot activity over the PSC season, does not show markedly stronger correlations compared to monthly data. This suggests that short-term solar variations (reflected in monthly data) are as indicative of trends as the longer-term seasonal aggregates. The study hints at geographical variability in the sunspot-PSC relationship, with different patterns observed in the Northern and Southern Hemispheres. However, the overall weak correlations suggest that other environmental and atmospheric conditions play a more significant role in PSC dynamics than solar activity alone.

The r-values were generally low, suggesting weak or no substantial relationship. In the Arctic region above 75°N, the yearly correlation coefficients vary, showing weak values with the best being -0.1 and the worst being +0.18. Similar to the Northern Hemisphere, the correlation between sunspot numbers and PSC coverage in the Antarctic is also weak. However, the relationship tends to show slightly more consistency at lower altitudes, although the r-values remain close to zero, suggesting no significant direct relationship. The minimal correlations

indicate that while solar activity might influence atmospheric conditions, its direct impact on PSC formation in the Antarctic is limited.

Perspectives for future research:

While relationships between PSCs and temperatures were generally significant, notable differences emerged in the two different approaches used for calculating correlation coefficients. It is strongly recommended that for a better and more enhanced construction of vertical profiles of the correlation coefficient, the analysis should be divided into specific latitude-longitude areas (rather than only latitude as was done in this study). This would involve identifying areas with higher PSC occurrence (as seen in section 4.1) and correlating these with the analogous regions with stratospheric temperatures. For a more comprehensive and detailed study, it is advisable to create these profiles based on each month, and then determine if there is any month that exhibits a stronger relationship or more distinct link between PSCs and stratospheric temperatures.

A more extensive dataset would assist in identifying patterns between solar cycles and PSCs or stratospheric temperatures, primarily due to the significant impact of solar cycle minima and maxima. These phases are crucial because they lead to variations in solar irradiance, which differentially influence the atmosphere. While our study includes almost one and a half solar cycles, it would be much more beneficial to extend the dataset to cover more than two 11-year solar cycles for a more comprehensive analysis.

Due to the altitudinal constraints previously discussed (refer also to Tsiropoula, 2003), the influence of solar radiation is primarily observed in the mid-upper stratosphere. Focusing on stratospheric temperatures, it is highly advisable to extend the altitude range beyond 30 km, encompassing the entire stratosphere up to approximately 50 km, aiming to seek a stronger correlation between temperatures and the number of sunspots.

To better comprehend the trends and interannual variability observed in PSCs, extending the dataset beyond the current periods could offer deeper insights into long-term climatic and atmospheric changes. This extension would also enhance the accuracy in assessing the impacts of climate change. Moreover, increasing the geographic coverage of data collection efforts to more than 80 degrees, particularly in under-studied regions of both hemispheres, would provide a more comprehensive global picture of stratospheric temperature dynamics and PSC distribution.

Exploring the relationship between ozone and temperatures, PSCs, and solar activity would significantly enhance this study, considering the formation and destruction mechanisms of ozone and its interactions with temperatures, PSCs, and sunspots. Additionally, examining major events such as volcanic eruptions and correlating them with specific years, as well as their connections to PSCs and temperatures, could reveal more detailed information about the lifecycle of PSCs.

6. References

Molina, M.J., and Rowland, F.S. (**1974**). "Stratospheric sink for chlorofluoromethanes: chlorine atom-catalysed destruction of ozone." Nature, 249, 810-812.

Eddy, J. A. (**1976**). The Maunder Minimum: The reign of Louis XIV appears to have been a time of real anomaly in the behavior of the sun. Science, 192(4245), 1189-1202.

Pittock, A. B., A critical look at long-term sun-weather relationships, Rev. Geophys., 16, 400-420, **1978**.

Penner, J. E., and J. S. Chang, Possible variations in atmospheric ozone related to the 11-year solar cycle, Geophys. Res. Lett., 5, 817-820, **1978**.

Brasseur, G., and P. C. Simon, Stratospheric chemical and thermal response to long-term variability in the solar UV irradiance, J. Geophys. Res., 86, 7343-7362, **1981**.

Brasseur, G., A- De Rudder, G. M. Keating and M. C. Pitts, Response of the middle atmosphere to short-term solar ultraviolet variations, 2, Theory, J. of Geophys. Res., 92, 903-914, **1987.**

Pittock, A- B., Solar variability, weather, and climate: An update, Q. j. R. Meteorol. Soc., 109, 23-55, **1983.**

Garcia, IL IL, S. Solomon, IL G. Robie, and D. W. Rusch, A numerical response of the middle atmosphere to the 11-year solar cycle, Planet. Space Sct., 32, 411-423, **1984**.

Solomon, S., Garcia, Rs. R., Rowland, F. S., and Wuebbles, D. J.: On the depletion of Antarctic ozone, Nature, 321, 755–758, **1986**.

Heath, D. and B. Schlesinger, The MG 280 nm doublet as a monitor of changes in solar ultraviolet irradiance, J. Geophys. Res., 91, 8672-8682, **1986**.

Angell, J. K., **1991**: Stratospheric Temperature Change as a Function of Height and Sunspot Number during 1972–89 Based on Rocketsonde and Radiosonde Data. *J. Climate*, **4**, 1170–1180, https://doi.org/10.1175/1520-0442(1991)004<1170:STCAAF>2.0.CO;2.

Labitzke, K., van Loon, H., **1992**. Association between the 11-year solar cycle and the atmosphere. Part V: Summer. Journal of Climatology 5, 240–251.

Crutzen, P. J., Müller, R., Brühl, C., and Peter, T.: On the potential importance of the gas phase reaction CH3O2 + ClO → ClOO + CH3O and the heterogeneous reaction HOCl+HCl → H2O+Cl2 in "ozone hole" chemistry, Geophys. Res. Lett., 19, 1113–1116, https://doi.org/10.1029/92GL01172, **1992**.

Huang T. Y. W., and G. Brasseur, Effect of long-term solar variability in a two-dimensional interactive model of the atmosphere, d. Geophys. Res., 98, 20,413-20,427, **1993**.

Chandra, S., and IL D. McPeters, The solar cycle variation of ozone in the stratosphere inferred from Nimbus 7 and NOAA 11 satellites, d. Geophys. Res., 99, 20,665-20,671, **1994**.

Poole, L. R., & Pitts, M. C. (**1994**). *Polar stratospheric cloud climatology based on Stratospheric Aerosol Measurement II observations from 1978 to 1989*. Journal of Geophysical Research, 99(D12), 13083-13089.

Labitzke, IC and H. van Loon, Connection between the troposphere and stratosphere on a decadal scale, Tellus, 47A, 275-286, **1995**.

Lean, J., Beer, J., & Bradley, R. (**1995**). Reconstruction of solar irradiance since 1610: Implications for climate change. Geophysical Research Letters, 22(23), 3195-3198.

Haigh, J. D. (**1996**). The impact of solar variability on climate. Science, 272(5264), 981-984.

Carslaw, K. S., Wirth, M., Tsias, A., Luo, B. P., Dörnbrack, A., Leutbecher, M., ... & Peter, T. (**1997**). Increased stratospheric ozone depletion due to mountain-induced atmospheric waves. Nature, 390(6655), 556-560.

Zerefos, C. S. and H. T. Mantis, Climatic fluctuations in the northern hemisphere stratosphere, Arch. Meteorol. Geophys., Ser. B., 25, 33-39, **1977**.

Lean, J., & Rind, D. (**1998**). Climate forcing by changing solar radiation. Journal of Climate, 11(12), 3069-3094.

Solomon, S. (**1999**). Stratospheric ozone depletion: A review of concepts and history. Reviews of Geophysics, 37(3), 275-316.

Fligge, M., and Solanki, S. K. (**2000**). Properties of flux tubes and the relation with solar irradiance variability. *J. Astrophysics Astronomy* 21, 275–282. doi:10.1007/bf02702409

Highwood, E. J., Hoskins, B. J., and Berrisford, P.: Properties of the arctic tropopause, Q. J. Roy. Meteorol. Soc., 126, 1515–1532, https://doi.org/10.1002/qj.49712656515, **2000**.

Shindell, D. T.: Climate and ozone response to increased stratospheric water vapor, Geophys. Res. Lett., 28, 1551–1554, https://doi.org/10.1029/1999GL011197, **2001**.

Ramaswamy, V., et al. (**2001**), Stratospheric temperature trends: Observations and model simulations, *Rev. Geophys.*, **39**(1), 71–122, doi:10.1029/1999RG000065.

Mitchell, J. F. (**2001**). Detection of climate change and attribution of causes. Climate change 2001: the scientific basis.

Fahey, D. W., Gao, R. S., Carslaw, K. S., Kettleborough, J., Popp, P. J., Northway, M. J., Holecek, J. C., Ciciora, S. C., McLaughlin, R. J., Baumgardner, D. G., Gandrud, B., Wennberg, P. O., Dhaniyala, S., McKinney, K., Peter, T., Salawitch, R. J., Bui, T. P., Elkins, J. W., Webster, C. R., Atlas, E. L., Jost, H., Wilson, J. C., Herman, R. L., and Kleinbohl, A.: The detection of

large HNO3-containing particles in the winter Arctic stratosphere, Science, 291, 1026–1031, **2001**.

G. Tsiropoula, Signatures of solar activity variability in meteorological parameters, Journal of Atmospheric and Solar-Terrestrial Physics, Volume 65, Issue 4, **2003**, ISSN 1364-6826, https://doi.org/10.1016/S1364-6826(02)00295-X.

Folland, C. K., Karl, T. R., Christy, J. R., Clarke, R. A., Gruza, G. V., Jouzel, J., ... & Zhai, P. (**2001**). Observed climate variability and change. Climate change 2001: the scientific basis, Intergovernmental panel on climate change.

Northway, M. J., Gao, R. S., Popp, P. J., Holecek, J. C., Fahey, D. W., Carslaw, K. S., Tolbert, M. A., Lait, L. R., Dhaniyala, S., Flagan, R. C., Wennberg, P. O., Mahoney, M. J., Herman, R. L., Toon, G. C., and Bui, T. P.: An analysis of large HNO3- containing particles sampled in the Arctic stratosphere during the winter of 1999 /2000, J. Geophys. Res., 107, 8289, https://doi.org/10.1029/2001JD001079, **2002**.

Stephens, G. L., Vane, D. G., Boain, R. J., Mace, G. G., Sassen, K., Wang, Z., Illingworth, A. J., O'Connor, E. J., Rossow, W. B., Durden, S. L., Miller, S. D., Austin, R. T., Benedetti, A., Mitrescu, C., and the CloudSat Science Team: The CloudSat mission and the A-Train: A new dimension of space-based observations of clouds and precipitation, B. Am. Meteorol. Soc., 83, 1771–1790, https://doi.org/10.1175/BAMS-83-12-1771, **2002**.

Manzini, E., B. Steil, C. Bruhl, M. A. Giorgetta, and K. Kruger (**2003**), A new interactive chemistry-climate model: 2. Sensitivity of the middle atmosphere to ozone depletion and increase in greenhouse gases and implications for recent stratospheric cooling, *J. Geophys. Res.*, 108(D14), 4429, doi:10.1029/2002JD002977.

Rex, M., R. J. Salawitch, P. von der Gathen, N. P. R. Harris, M. P. Chipperfield, and B. Naujokat (**2004**), Arctic ozone loss and climate change, *Geophys. Res. Lett.*, **31**, L04116, doi:10.1029/2003GL018844.

Rex, M., Salawitch, R. J., Von Der Gathen, P., Harris, N. R., Chipperfield, M. P., & Naujokat, B. (**2004**). Arctic ozone loss and climate change. Geophysical Research Letters, 31(4).

Yashiro, S., Gopalswamy, N., Michalek, G., St. Cyr, O. C., Plunkett, S. P., Rich, N. B., et al. (**2004**). A catalog of white light coronal mass ejections observed by the SOHO spacecraft. *J. Geophys. Res.* 109 (A7), A07105. doi:10.1029/2003ja010282.

Newman, P. A., & Nash, E. R. (**2005**). Quantifying the wave driving of the stratosphere. Journal of the Atmospheric Sciences, 62(9), 2934-2940.

Voigt, C., Schlager, H., Luo, B., Dörnbrack, A., Roiger, A., Stock, P., ... & Peter, T. (**2005**). Nitric acid trihydrate (NAT) formation at low NAT supersaturation in polar stratospheric clouds (PSCs). Atmospheric Chemistry and Physics, 5(5), 1371-1376.

Ramaswamy, V., et al. (**2006**), Anthropogenic and natural influences in the evolution of lower stratospheric cooling, *Science*, **311**, 1138–1141.

Rex, M., et al. (**2006**), Arctic winter 2005: Implications for stratospheric ozone loss and climate change, *Geophys. Res. Lett.*, **33**, L23808, doi:10.1029/2006GL026731.

Seinfeld, J. H., & Pandis, S. N. (**2006**). Atmospheric Chemistry and Physics: From Air Pollution to Climate Change. Wiley.

Hostetler, C. A., Liu, Z., Reagan, J., Vaughan, M., Winker, D., Osborn, M., Hunt, W. H., Powell, K. A., and Trepte, C.: CALIOP Algorithm Theoretical Basis Document- Part 1: Calibration and Level 1 Data Products, PC-SCI-201, available at: http://www-calipso.larc.nasa.gov/ resources/project_ documentation.php, NASA Langley Research Center, Hampton, VA, **2006**.

Braesicke, P., M. M. Hurwitz, and J. A. Pyle (**2006**), The stratospheric response to changes in ozone and carbon dioxide as modeled with a GCM including parameterized ozone chemistry, *Meteorol. Z.*, **15**, 343–354.

Winker, D. M., McGill, M., and Hunt, W. H.: Initial performance assessment of CALIOP, Geophys. Res. Lett., 34, L19803, https://doi.org/10.1029/2007GL030135, **2007**.

Manney, G.L., Pickett, H.M., Pumphrey, H.C., …, Webster, C.R., Weinstock, E.M. and Wu, D.L.: Aura Microwave Limb Sounder upper tropospheric and lower stratospheric H2O and relative humidity with respect to ice validation, J. Geophys. Res., 112, D24S35, https://doi.org/10.1029/2007JD008752, **2007**.

Thomas, J. H., & Weiss, N. O. (**2008**). *Sunspots and Starspots*. Cambridge University Press.

Lowe, D. and MacKenzie, A. R.: Polar stratospheric cloud microphysics and chemistry, J. Atmos. Sol.-Terr. Phy., 70, 13–40, https://doi.org/10.1016/j.jastp.2007.09.011, **2008**.

Newman, P. A., et al. (**2009**), What would have happened to the ozone layer if CFCs had not been regulated? *Atmos. Chem. Phys.*, **9**, 2113–2128.

Randel, W. J., et al. (**2009**), An update of observed stratospheric temperature trends, *J. Geophys. Res.*, **114**, D02107, doi:10.1029/2008JD010421.

Akiyoshi, H., L. B. Zhou, Y. Yamashita, K. Sakamoto, T. Nagashima, M. Takahashi, J. Kurokawa, M. Takigawa, T. Imamura (**2009**), A CCM simulation of the breakup of the Antarctic polar vortex in the years 1980–2004 under the CCMVal scenarios, *J. Geophys. Res.*, **114**, D03103, doi:10.1029/2007JD009261.

Winker, D. M., Vaughan, M. A., Omar, A. H., Hu, Y., Powell, K. A., Liu, Z., Hunt, W. H., and Young, S. A.: Overview of the CALIPSO Mission and CALIOP Data Processing Algorithms, J. Atmos. Ocean. Tech., 26, 2310–2323, https://doi.org/10.1175/2009 JTECHA1281.1, **2009**.

Randel, W. J., et al. (**2009**). *An update on the observed and simulated variability in the stratosphere*. Reviews of Geophysics, 47(4).

Hunt, W. H., Winker, D. M., Vaughan, M. A., Powell, K. A., Lucker, P. L., & Weimer, C. (**2009**). *CALIPSO Lidar Description and Performance Assessment*. Journal of Atmospheric and Oceanic Technology, 26(7), 1214-1228.

Solomon, S., Rosenlof, K. H., Portmann, R. W., Daniel, J. S., Davis, S. M., Sanford, T. J., & Plattner, G. K. (**2010**). *Contributions of stratospheric water vapor to decadal changes in the rate of global warming*. Science, 327(5970), 1219-1223.

Waugh, D. W., & Polvani, L. M. (**2010**). *Stratospheric polar vortices*. In The Stratosphere: Dynamics, Transport, and Chemistry. American Geophysical Union.

Frame, T. H. A., & Gray, L. J. (**2010**). The 11-year solar cycle in ERA-40 data: An update to 2008. Journal of Climate, 23(8), 2213-2222.

Charbonneau, P. (**2010**). *Dynamo models of the solar cycle*. Living Reviews in Solar Physics, 7(1), 3.

Winker, D. M., Vaughan, M. A., Omar, A., Hu, Y., Powell, K. A., Liu, Z., ... & Young, S. A. (**2010**). *Overview of the CALIPSO mission and CALIOP data processing algorithms*. Journal of Atmospheric and Oceanic Technology, 26(11), 2310-2323.

Alexander, S. P., Klekociuk, A. R., Pitts, M. C., McDonald, A. J., and Arevalo-Torres, A.: The effect of orographic gravity waves on Antarctic polar stratospheric cloud occurrence and composition, J. Geophys. Res.-Atmos., 116, D06109, https://doi.org/10.1029/2010JD015184, **2011**.

World Meteorological Organization. (**2011**). Scientific assessment of ozone depletion: 2010. Global Ozone Research and Monitoring Project-Report No. 52.

Peter, T., & Grooß, J. U. (**2012**). Polar Stratospheric Clouds and Sulfate Aerosol Particles: Microphysics, Denitrification and Heterogeneous Chemistry. Surveys in Geophysics, 33, 573-613.

Lockwood, M. (**2012**). *Solar influence on global and regional climates*. Surveys in Geophysics, 33(3-4), 503-534.

Kohma, M. and Sato, K.: Simultaneous occurrence of polar stratospheric clouds and upper-tropospheric clouds caused by blocking anticyclones in the Southern Hemisphere, Atmos. Chem. Phys., 13, 3849–3864, https://doi.org/10.5194/acp-13- 3849-2013, **2013**.

Omar, A. H., Winker, D. M., Tackett, J. L., Giles, D. M., Kar, J., Liu, Z., ... & Trepte, C. R. (**2013**). *CALIOP and AERONET aerosol optical depth comparisons: One size fits none*. Journal of Geophysical Research: Atmospheres, 118(10), 4748-4766.

Jinyou Liang, Chemical composition of the atmosphere of the Earth, Chemical Modeling for Air Resources, Academic Press, **2013**, Pages 3-20, ISBN 9780124081352, https://doi.org/10.1016/B978-0-12-408135-2.00001-X.

Molleker, S., Borrmann, S., Schlager, H., Luo, B., Frey, W., Klingebiel, M., Weigel, R., Ebert, M., Mitev, V., Matthey, R., Woiwode, W., Oelhaf, H., Dörnbrack, A., Stratmann, G., Grooß, J.-U., Günther, G., Vogel, B., Müller, R., Krämer, M., Meyer, J., and Cairo, F.: Microphysical properties of synoptic-scale polar stratospheric clouds: in situ measurements of unexpectedly large HNO3-containing particles in the Arctic vortex, Atmos. Chem. Phys., 14, 10785–10801, https://doi.org/10.5194/acp-14-10785-2014, **2014**.

Hathaway, D. H. (**2015**). *The solar cycle*. Living Reviews in Solar Physics, 12(1), 4.

Seinfeld, J. H., & Pandis, S. N. (**2016**). *Atmospheric Chemistry and Physics: From Air Pollution to Climate Change*. John Wiley & Sons.

Zhang, J., Tian, W., Chipperfield, M., Xie, F., and Huang, J.: Persistent shift of the Arctic polar vortex towards the Eurasian continent in recent decades, Nat. Clim. Change, 6, 1094–1099, https://doi.org/10.1038/nclimate3136, **2016**.

Bosilovich, M. G., Lucchesi, R., and Suarez, M.: MERRA-2: File Specification, GMAO Office Note No. 9 (Version 1.1), 73 p., available at: https://gmao.gsfc.nasa.gov/GMAO_products/reanalysis_products.php, **2016**.

Smyshlyaev, S.P.; Pogoreltsev, A.I.; Galin, V.J. Influence of wave activity on gaseous composition of stratosphere of polar regions. *Geomagn. Aeron.* **2016**, *56*, 102–116.

Ott, L. E., Duncan, B. N., Thompson, A. M., Diskin, G., Fasnacht, Z., Langford, A. O., Lin, M., Molod, A. M., Nielsen, J. E., Pusede, S. E., Wargan, K., Weinheimer, A. J., and Yoshida, Y.: Frequency and impact of summertime stratospheric intrusions over Maryland during DISCOVER-AQ (2011): New evidence from NASA's GEOS-5 simulations, J. Geophys. Res.-Atmos., 121, 3687–3706, https://doi.org/10.1002/2015JD024052, **2016**.

Gelaro, R., McCarty, W., Suárez, M. J., Todling, R., Molod, A., Takacs, L., and Zhao, B.: The Modern-Era Retrospective Analysis for Research and Applications, version 2 (MERRA-2), J. Climate, 30, 5419–5454, https://doi.org/10.1175/JCLI-D-16-0758.1, **2017**.

Hoffmann, L., Hertzog, A., Rößler, T., Stein, O., and Wu, X.: Intercomparison of meteorological analyses and trajectories in the Antarctic lower stratosphere with Concordiasi super pressure balloon observations, Atmos. Chem. Phys., 17, 8045–8061, https://doi.org/10.5194/acp-17-8045-**2017**, 2017a.

Morgenstern, O., Hegglin, M. I., Rozanov, E., O'Connor, F. M., Abraham, N. L., Akiyoshi, H., Archibald, A. T., Bekki, S., Butchart, N., Chipperfield, M. P., Deushi, M., Dhomse, S. S., Garcia, R. R., Hardiman, S. C., Horowitz, L. W., Jöckel, P., Josse, B., Kinnison, D., Lin, M., Mancini, E., Manyin, M. E., Marchand, M., Marécal, V., Michou, M., Oman, L. D., Pitari, G., Plummer, D. A., Revell, L. E., Saint-Martin, D., Schofield, R., Stenke, A., Stone, K., Sudo, K., Tanaka, T. Y., Tilmes, S., Yamashita, Y., Yoshida, K., and Zeng, G.: Review of the global models used within phase 1 of the Chemistry–Climate Model Initiative (CCMI), Geosci. Model Dev., 10, 639–671, https://doi.org/10.5194/gmd-10-639-2017, **2017**.

World Meteorological Organization (WMO). (**2018**). "Scientific Assessment of Ozone Depletion: 2018." Global Ozone Research and Monitoring Project-Report No. 58.

Pitts, M.C.; Poole, L.R.; Gonzalez, R. Polar stratospheric cloud climatology based on CALIPSO spaceborne lidar measurements from 2006 to 2017. *Atmos. Chem. Phys.* **2018**, *18*, 10881–10913.

Pitts, M. C., Poole, L. R., Lambert, A., & Thomason, L. W. (**2018**). *The 2015–2016 Arctic winter: Impacts of interannual variability in dynamic and chemical forcing on polar processing and springtime ozone*. Journal of Geophysical Research: Atmospheres, 123(1), 681-700.

Kar, J., Vaughan, M. A., Lee, K.-P., Tackett, J. L., Avery, M. A., Garnier, A., Getzewich, B. J., Hunt, W. H., Josset, D., Liu, Z., Lucker, P. L., Magill, B., Omar, A. H., Pelon, J., Rogers, R. R., Toth, T. D., Trepte, C. R., Vernier, J.-P., Winker, D. M., and Young, S. A.: CALIPSO lidar calibration at 532 nm: version 4 nighttime algorithm, Atmos. Meas. Tech., 11, 1459–1479, https://doi.org/10.5194/amt-11-1459-2018, **2018**.

M.L. Brusseau, A.D. Matthias, S.A. Musil, H.L. Bohn, Chapter 4 - Physical-Chemical Characteristics of the Atmosphere, Environmental and Pollution Science (Third Edition), Academic Press, **2019**, Pages 47-59, ISBN 9780128147191, https://doi.org/10.1016/B978-0-12-814719-1.00004-5.

Jakovlev, A.R.; Smyshlyaev, S.P. Impact of the Southern Oscillation on Arctic Stratospheric Dynamics and Ozone Layer. *Izv. Atmos. Ocean. Phys.* **2019**, *55*, 86–99.

Jakovlev, A.R.; Smyshlyaev, S.P.; Galin, V.Y. Interannual Variability and Trends in Sea Surface Temperature, Lower and Middle Atmosphere Temperature at Different Latitudes for 1980–2019. *Atmosphere* **2021**, *12*, 454. https://doi.org/10.3390/atmos12040454.

Tritscher, I., Pitts, M. C., Poole, L. R., Alexander, S. P., Cairo, F., Chipperfield, M. P., et al. (**2021**). Polar stratospheric clouds: Satellite observations, processes, and role in ozone depletion. *Reviews of Geophysics*, 59, e2020RG000702. https://doi.org/10.1029/2020RG000702.

Georgieva K and Veretenenko S (**2023**) Solar influences on the Earth's atmosphere: solved and unsolved questions. *Front. Astron. Space Sci.* 10:1244402. doi:10.3389/fspas.2023.1244402.

7. Appendix

Appendix A: Polar plots of PSC areal coverage over the Arctic and the Antarctic
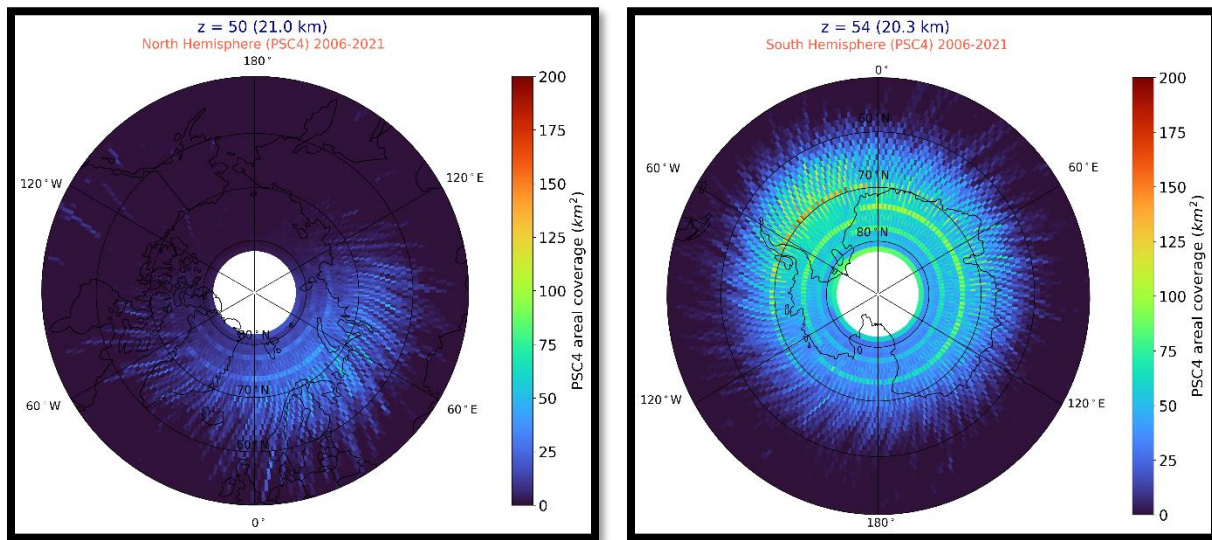
Figure 79: Polar plots of PSC areal coverage (km²) spatial distribution at a) z=21km, over the Arctic and b) z=20.3, over the Antarctic.

Appendix B: Interannual variability and vertical distribution of PSC areal coverage for each month of the dataset
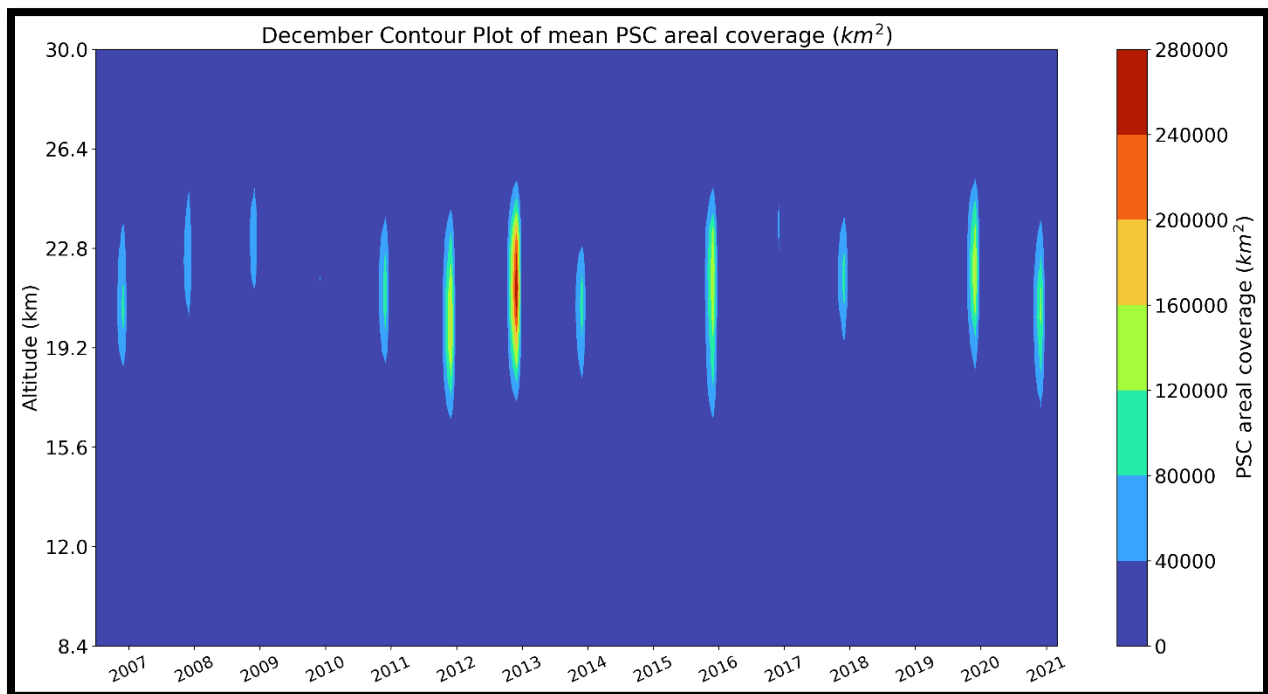
Figure 80: Mean Monthly Interannual Variability and Vertical Distribution of PSC Areal Coverage (km²) in the Northern Hemisphere during December for the period 2006-2020.
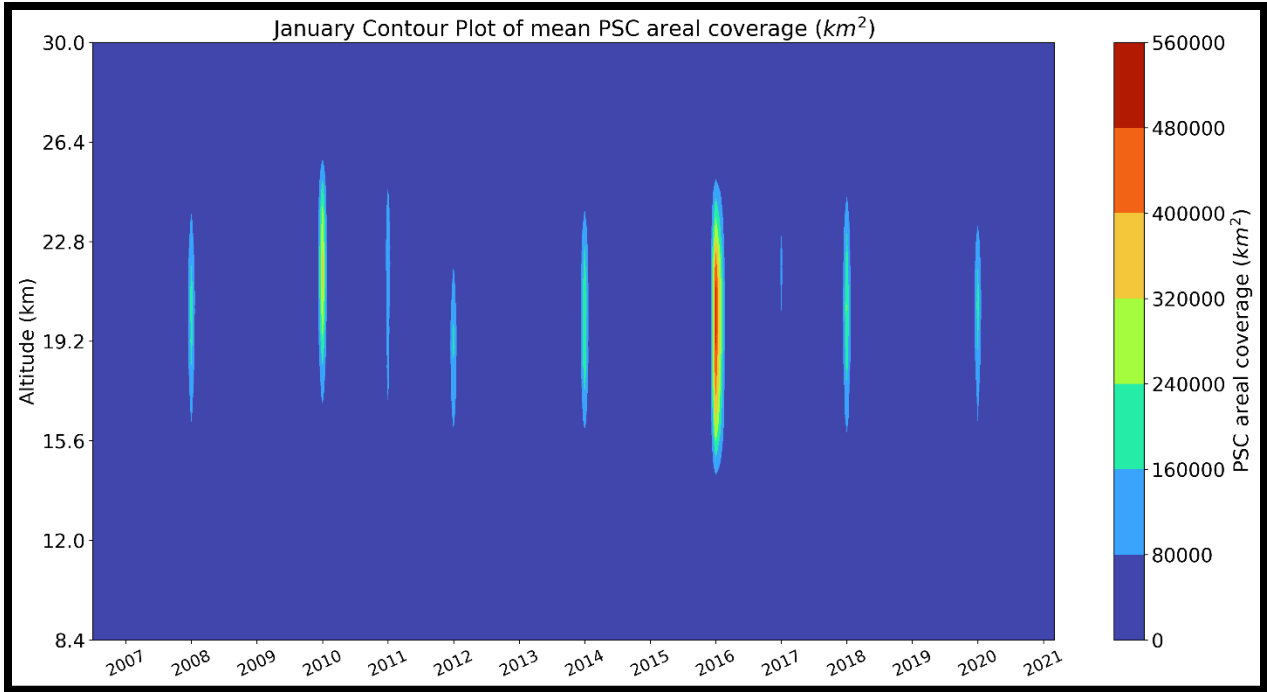
Figure 81: Mean monthly interannual variability and vertical distribution of PSC areal coverage (km²) in the Northern Hemisphere during January for the period 2007-2021.
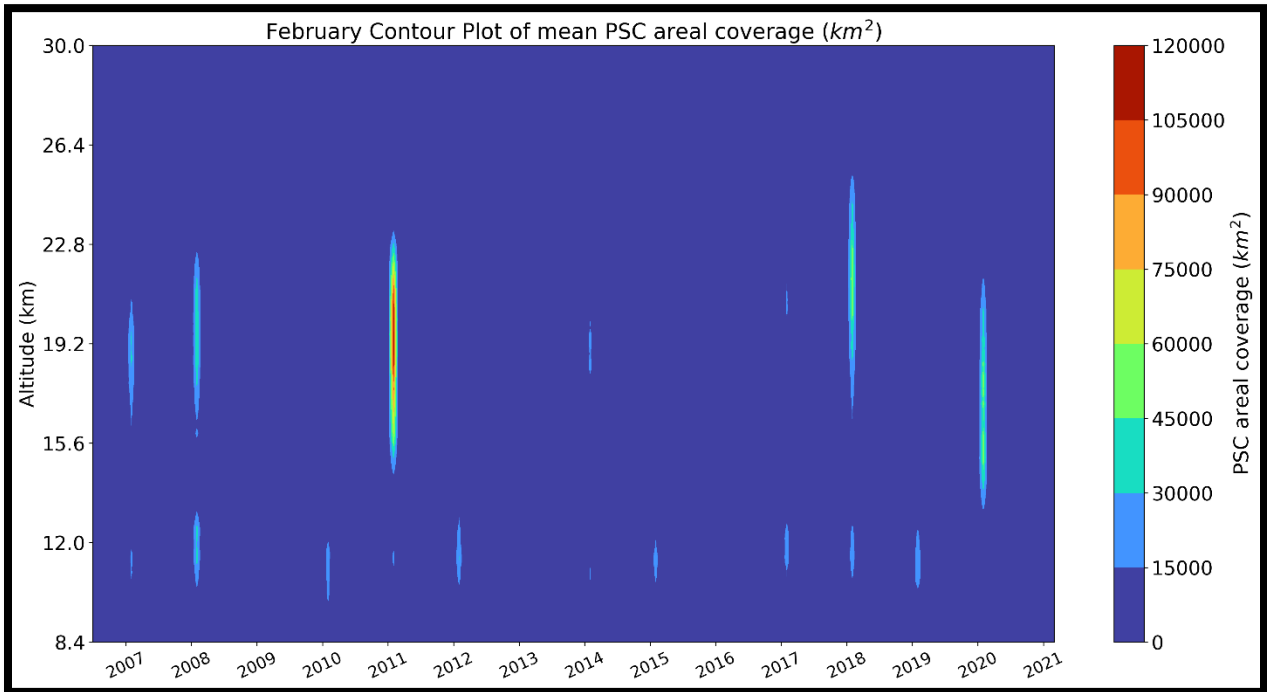
Figure 82: Mean monthly interannual variability and vertical distribution of PSC areal coverage (km²) in the Northern Hemisphere during February for the period 2007-2021.
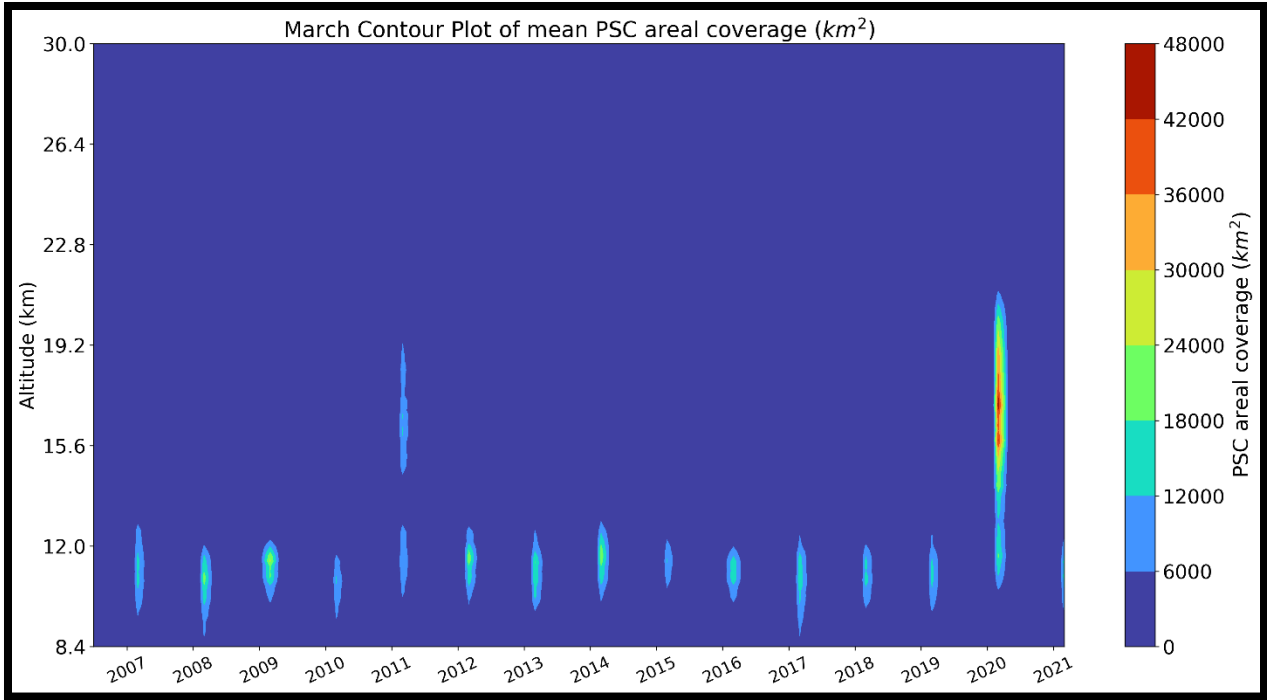
Figure 83: Mean monthly interannual variability and vertical distribution of PSC areal coverage (km²) in the Northern Hemisphere during March for the period 2007-2021.
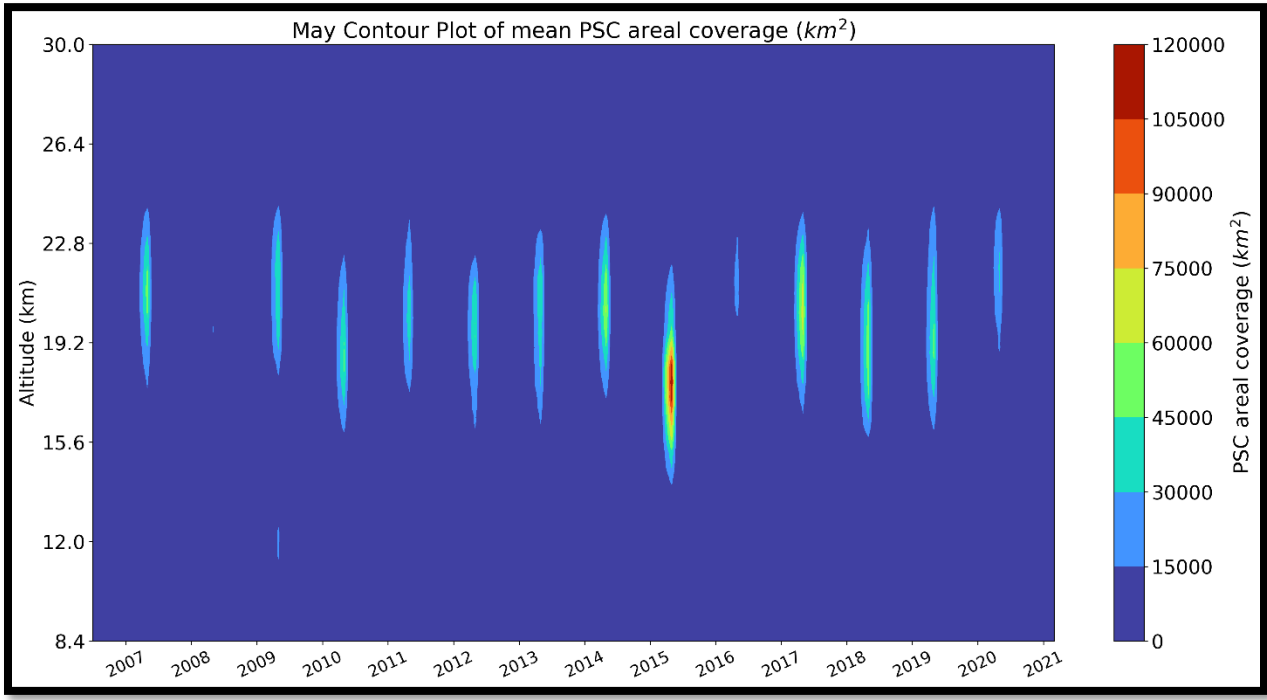
Figure 84: Mean monthly interannual variability and vertical distribution of PSC areal coverage (km²) in the Southern Hemisphere during May for the period 2007-2020.
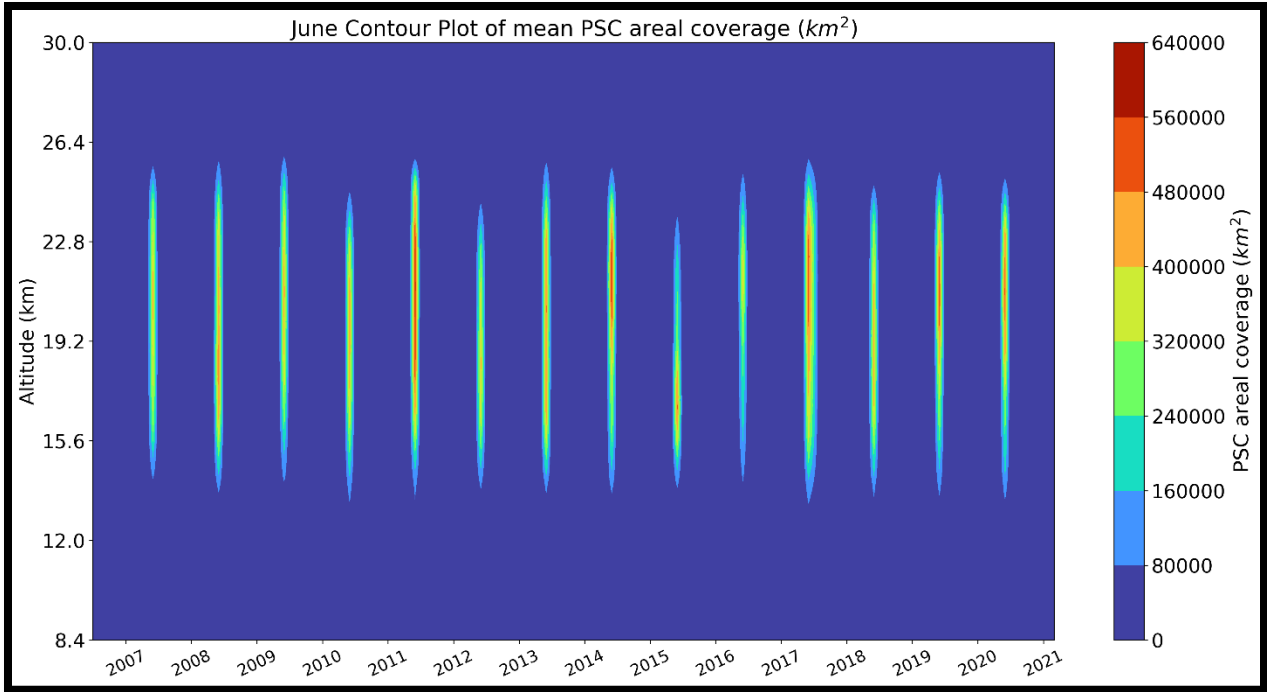
Figure 85: Mean monthly interannual variability and vertical distribution of PSC areal coverage (km²) in the Southern Hemisphere during June for the period 2007-2020.
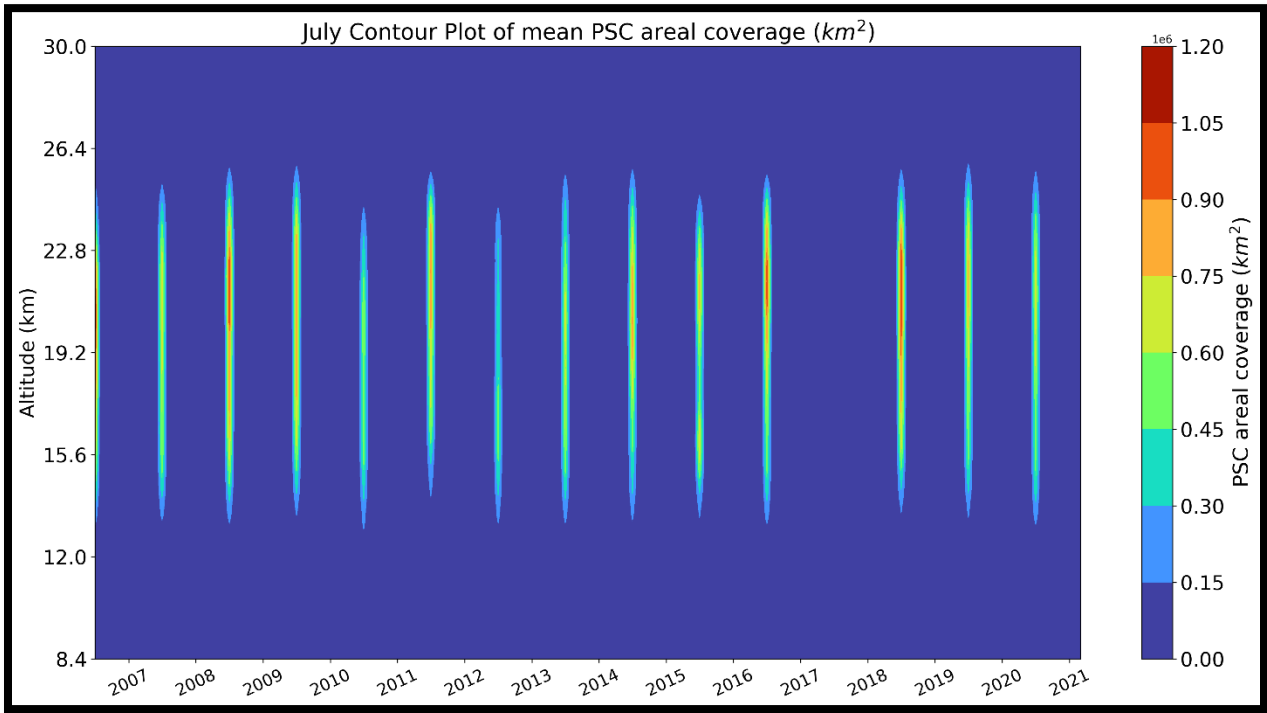
Figure 86: Mean monthly interannual variability and vertical distribution of PSC areal coverage (km²) in the Southern Hemisphere during July for the period 2006-2020.
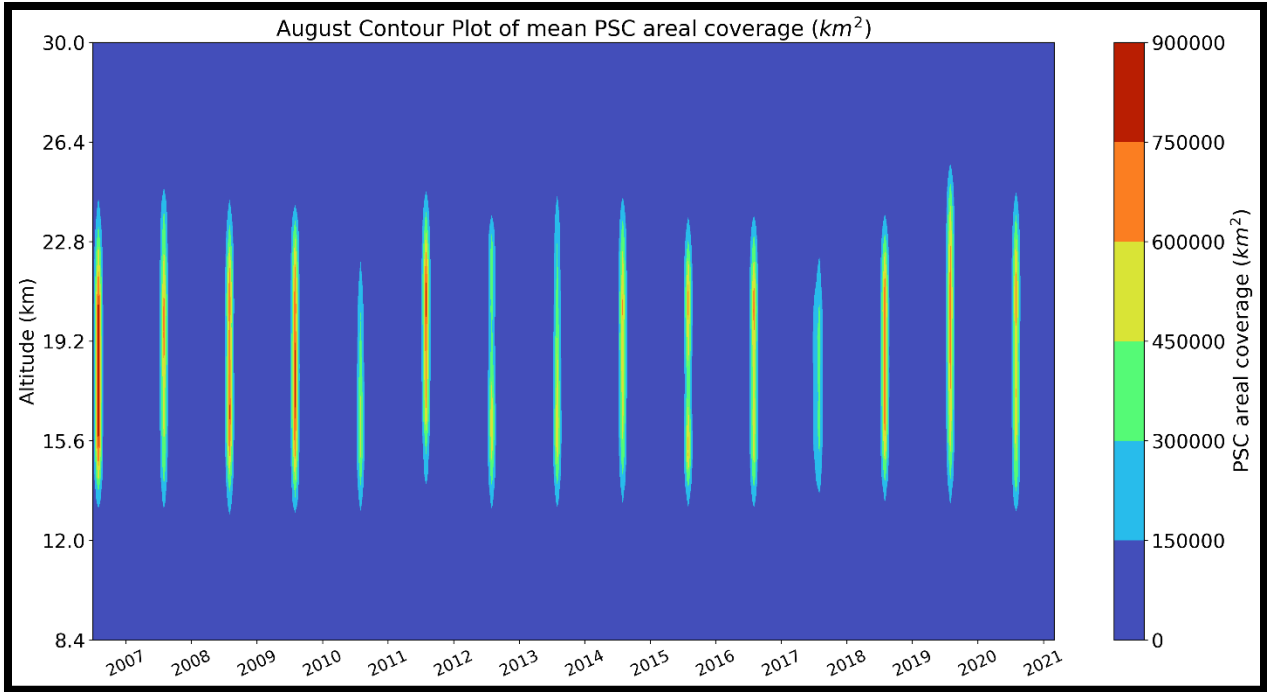
Figure 87: Mean monthly interannual variability and vertical distribution of PSC areal coverage (km²) in the Southern Hemisphere during August for the period 2006-2020.
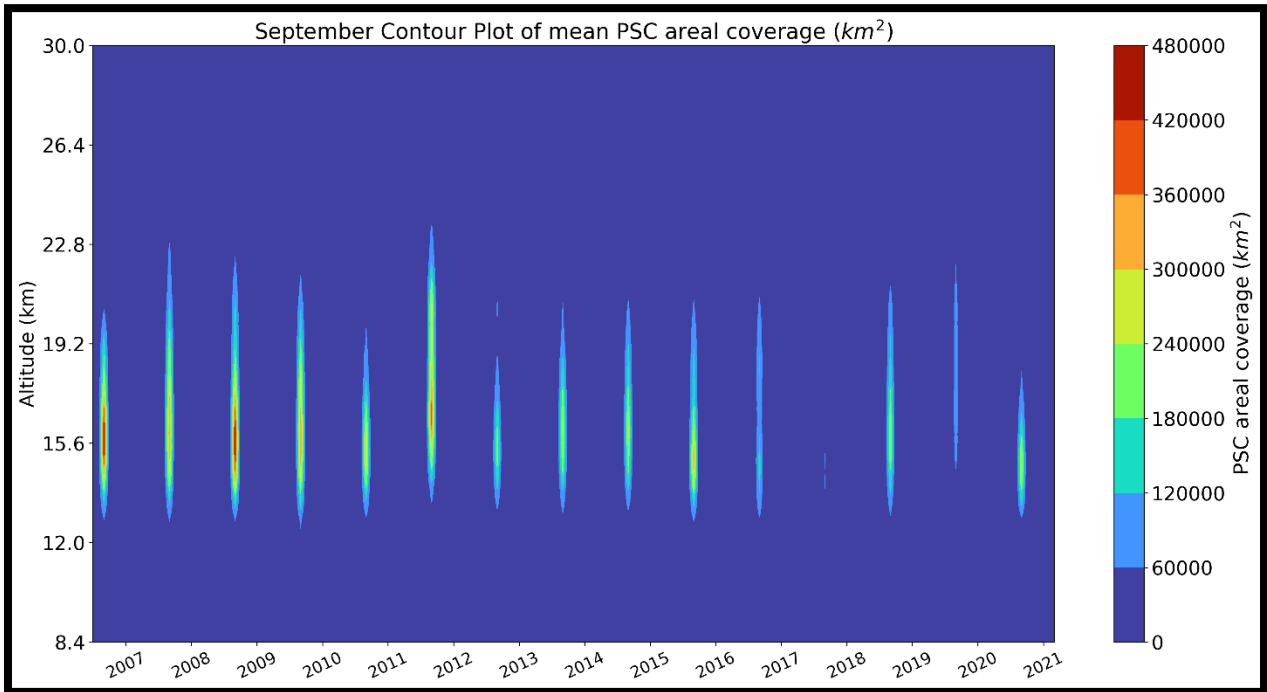
Figure 88: Mean monthly interannual variability and vertical distribution of PSC areal coverage (km²) in the Southern Hemisphere during September for the period 2006-2020.
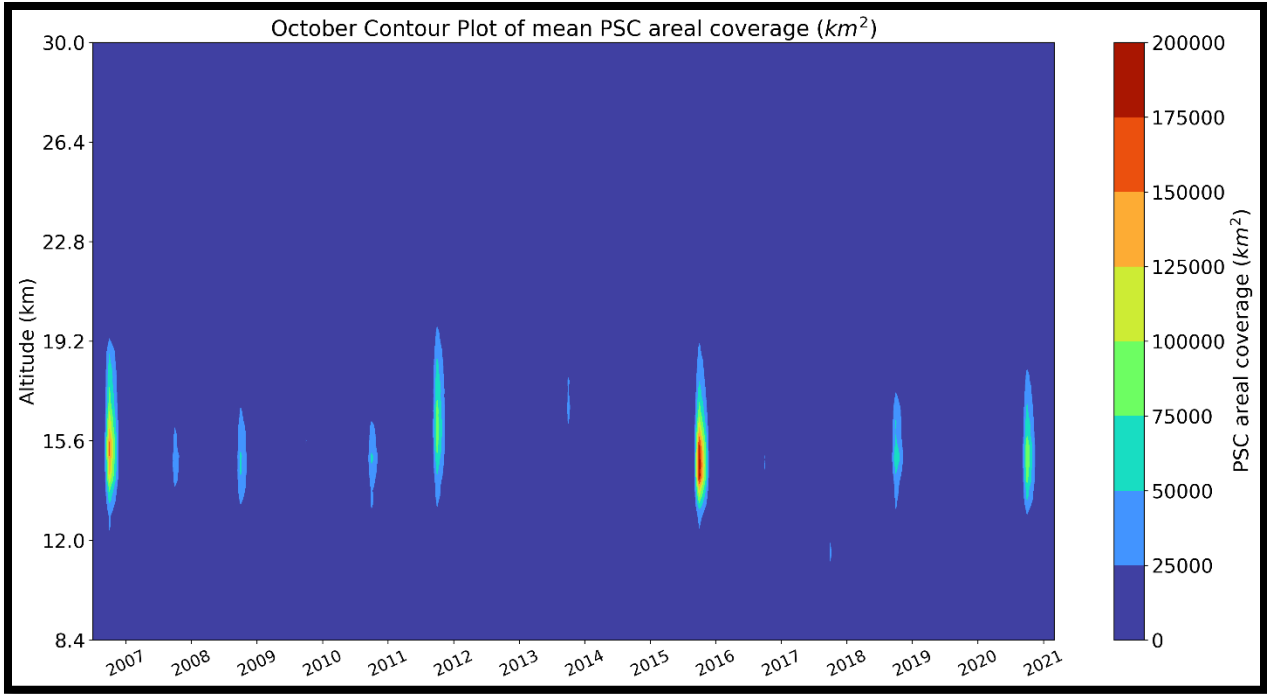
Figure 89: Mean monthly interannual variability and vertical distribution of PSC areal coverage (km²) in the Southern Hemisphere during October for the period 2006-2020.

Appendix C: Pixel to Pixel method of correlation coefficient computation
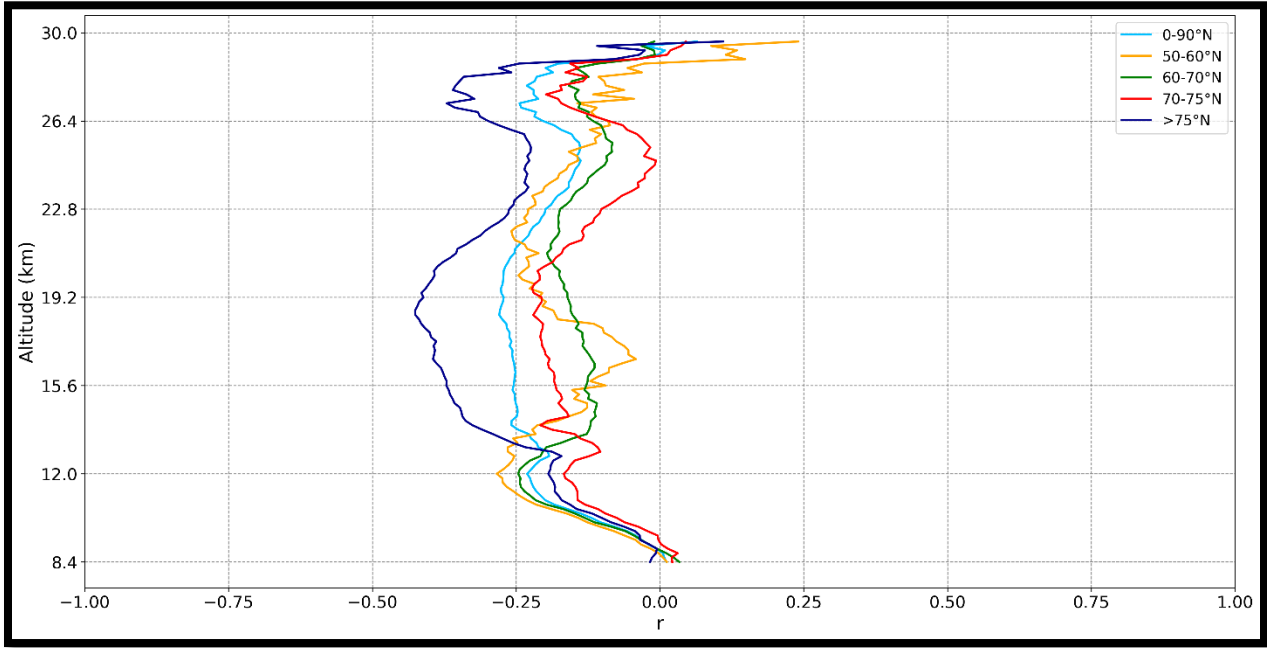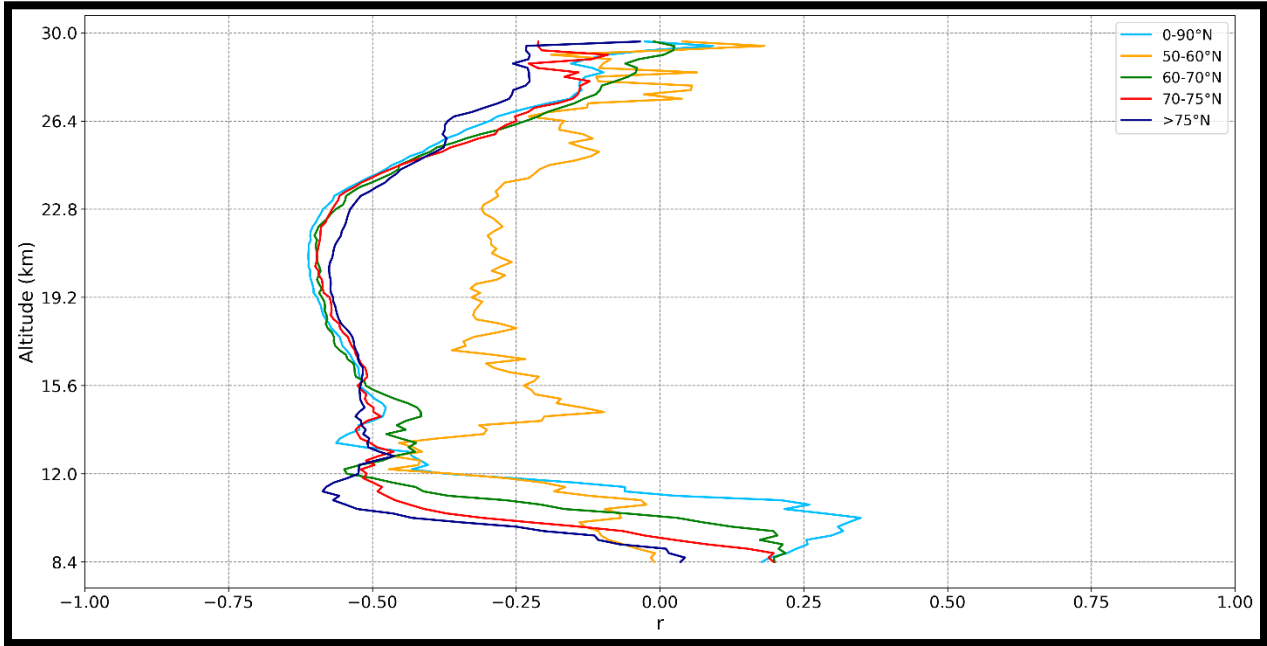
Temperature - PSCs

Figure 90: Vertical distribution of correlation coefficients between yearly mean values of PSCs and stratospheric temperatures across different latitudinal bands over the Arctic, from 2007 to 2021.
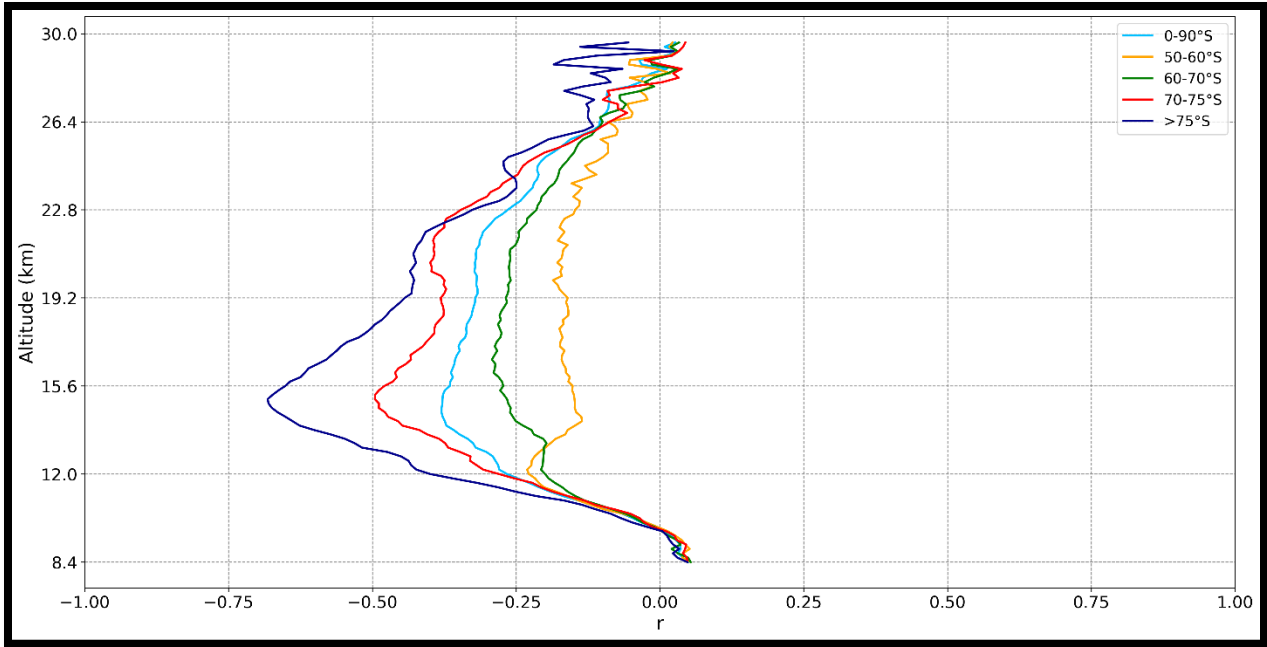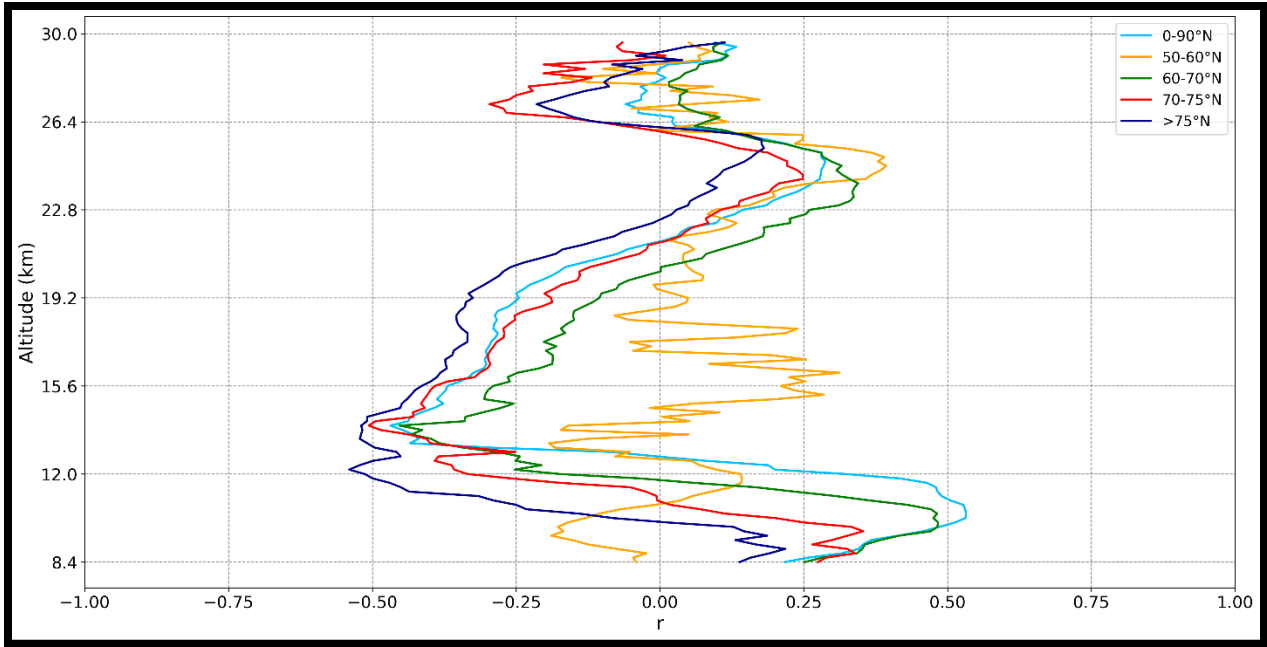
Figure 91: Vertical distribution of correlation coefficients between yearly mean values of PSCs and stratospheric temperatures across different latitudinal bands over the Antarctic, from 2006 to 2020.
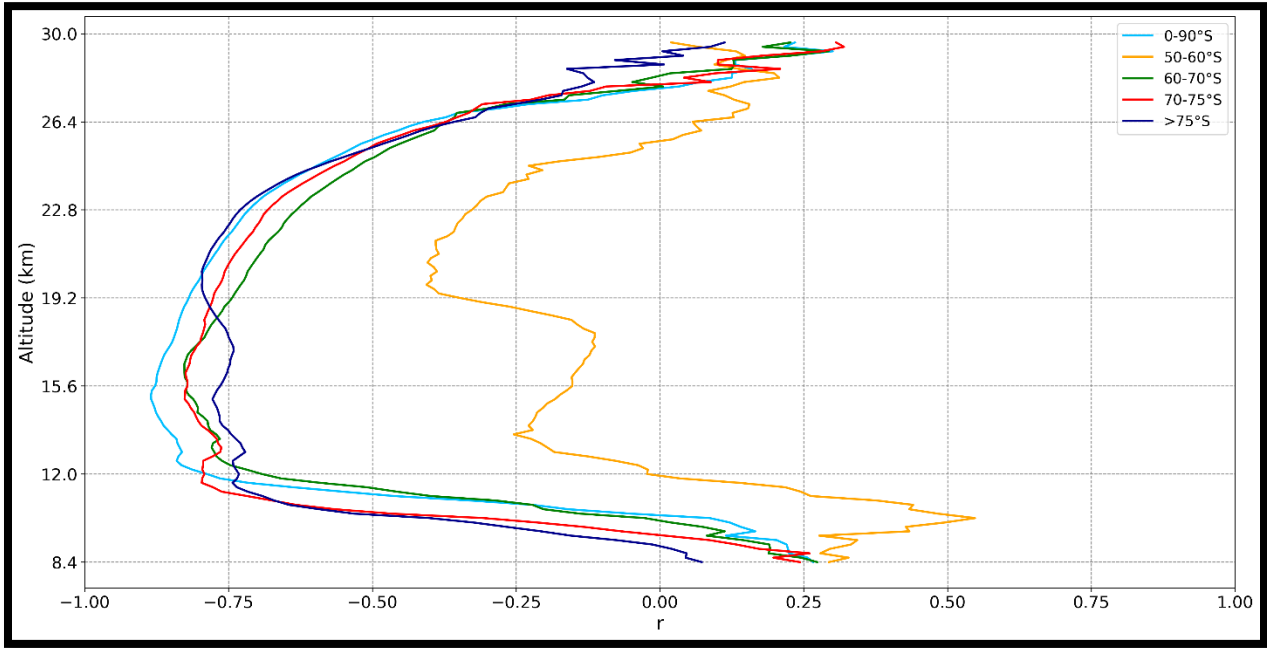
Sunspots - Temperature
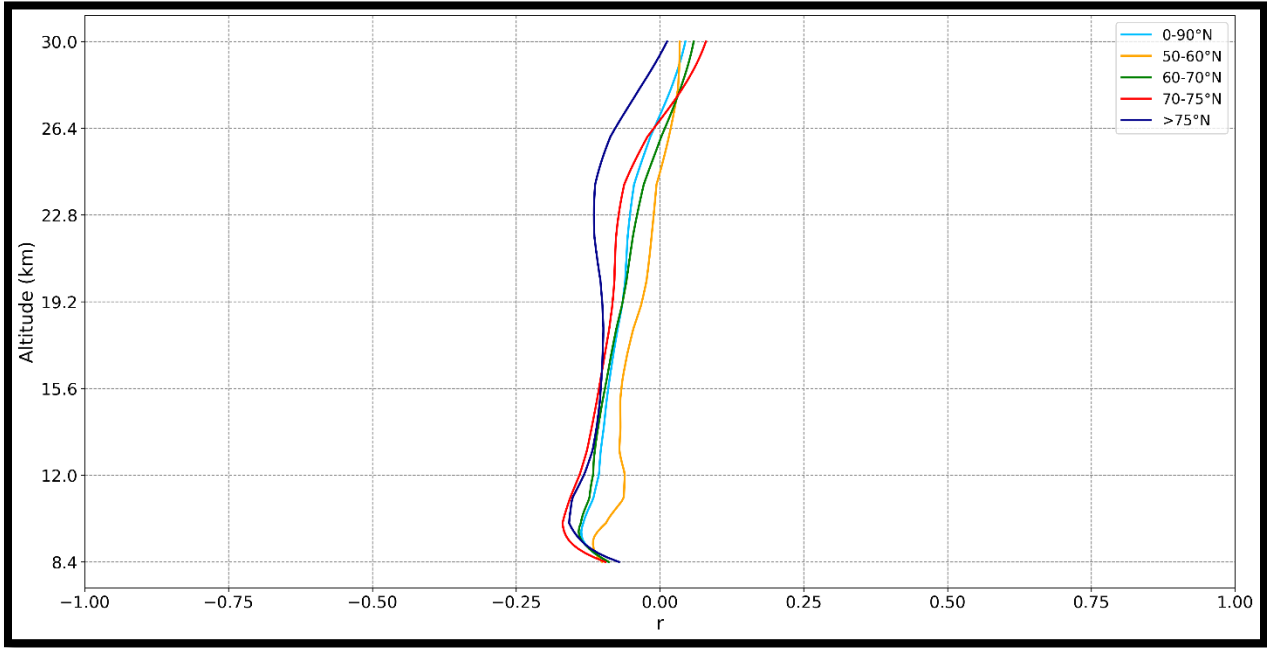
Figure 92: Vertical distribution of correlation coefficients between monthly mean values of stratospheric temperatures and the number of sunspots across different latitudinal bands over the Arctic, from December 2006 to March 2021.
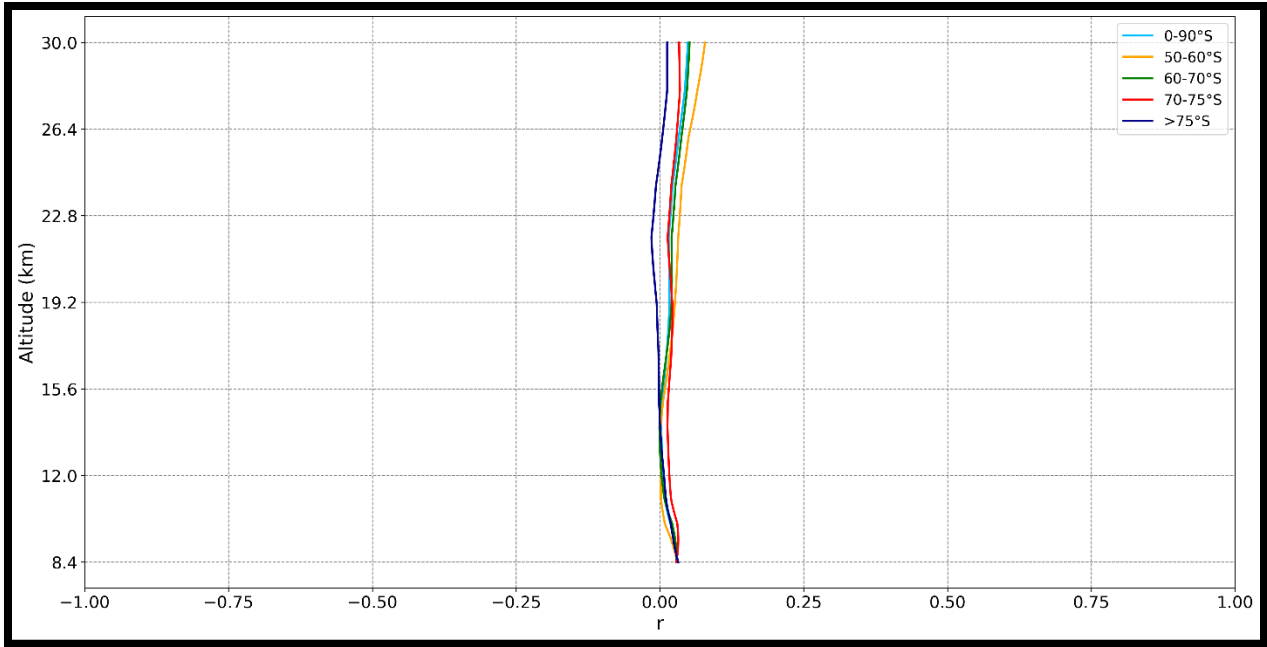
Figure 93: Vertical distribution of correlation coefficients between monthly mean values of stratospheric temperatures and the number of sunspots across different latitudinal bands over the Antarctic, from July 2006 to October 2020.

Sunspots - PSCs
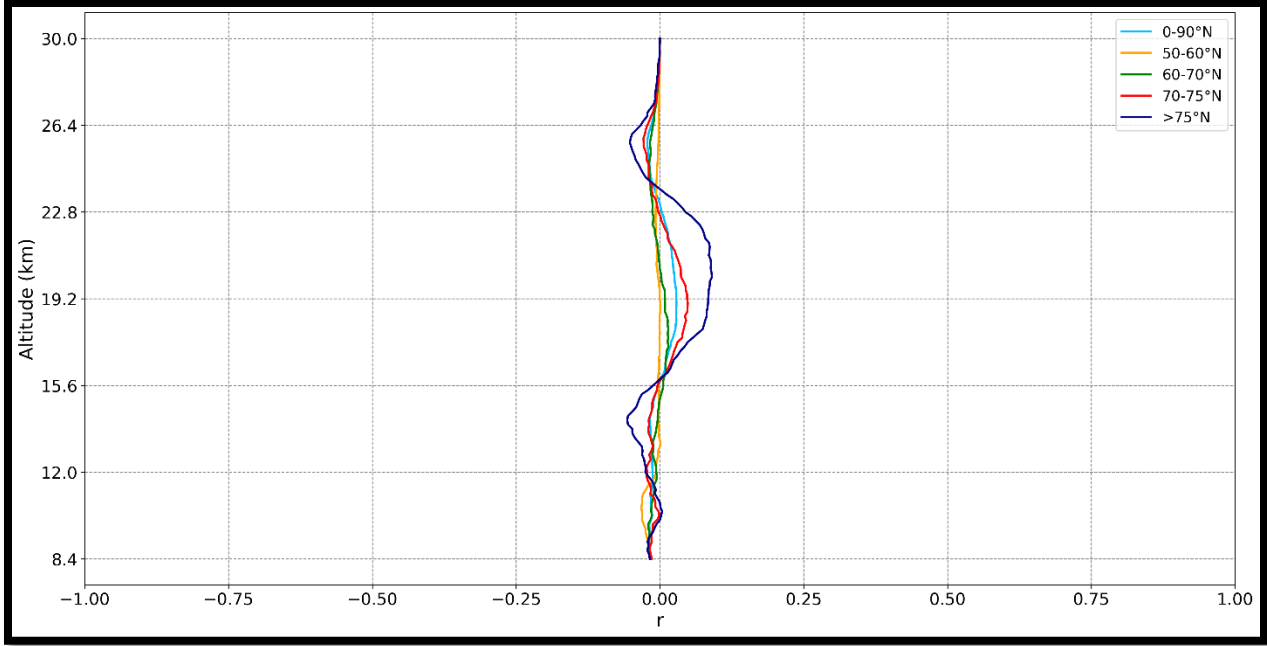
Figure 94: Vertical distribution of correlation coefficients between monthly mean values of PSCs and the number of sunspots across different latitudinal bands over the Arctic, from December 2006 to March 2021.

154
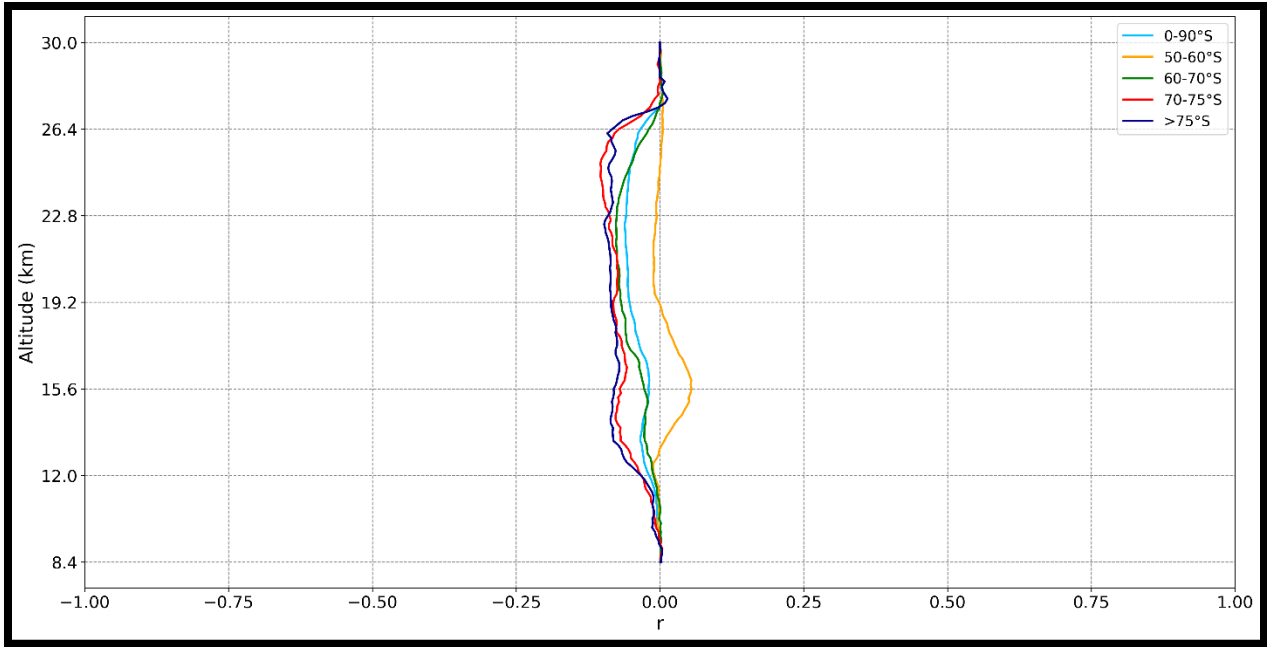
Figure 95: Vertical distribution of correlation coefficients between monthly mean values of PSCs and the number of sunspots across different latitudinal bands over the Antarctic, from July 2006 to October 2020.
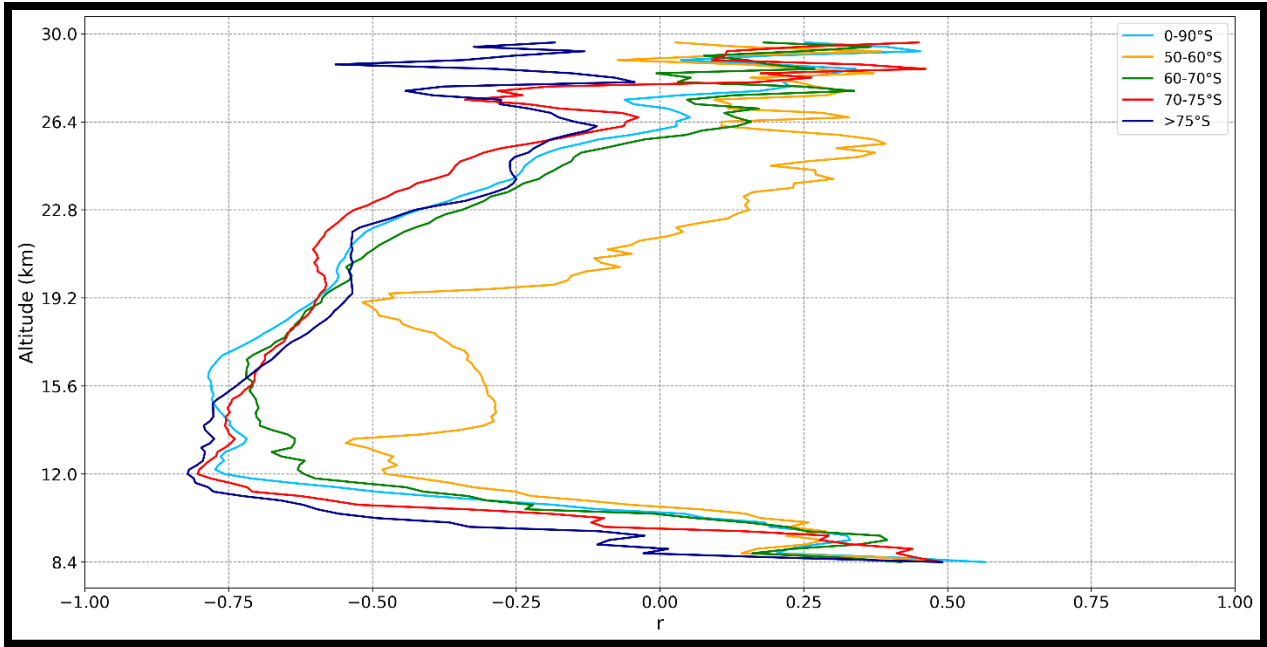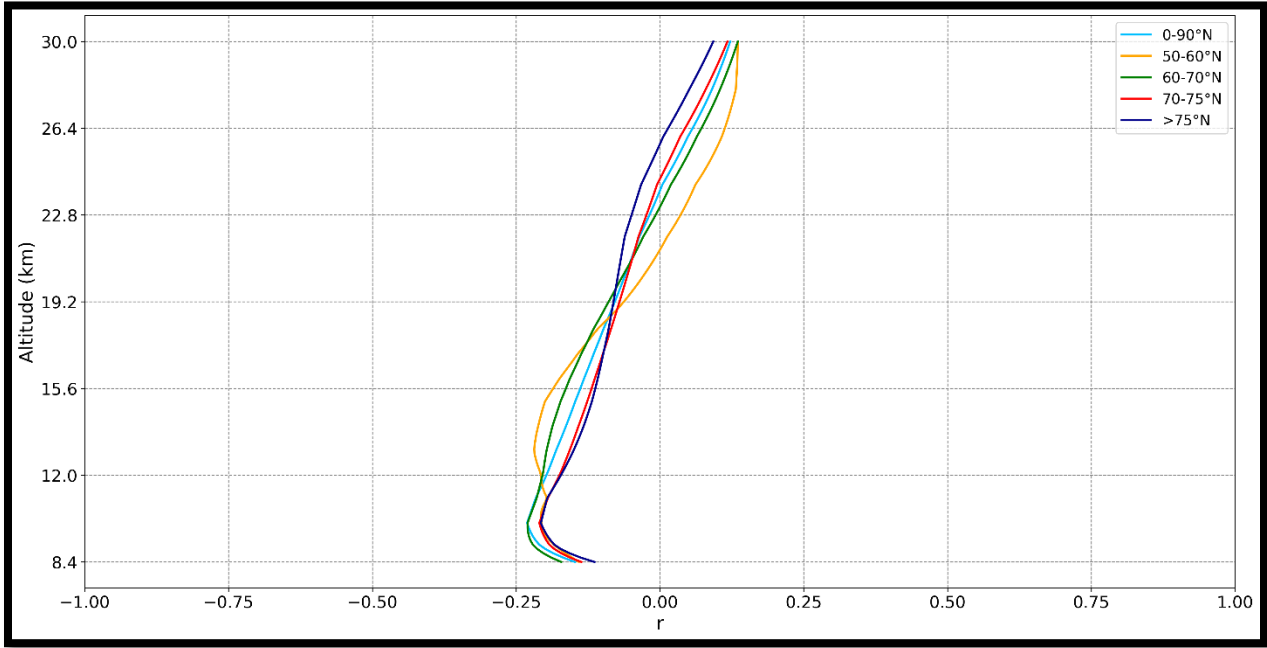
Appendix D: Latitudinal averaged method of correlation coefficient computation

<u>Temperature - PSCs</u>

Figure 96: Vertical distribution of correlation coefficients between monthly mean values of PSCs and stratospheric temperatures across different latitudinal bands over the Arctic, from December 2006 to March 2021.

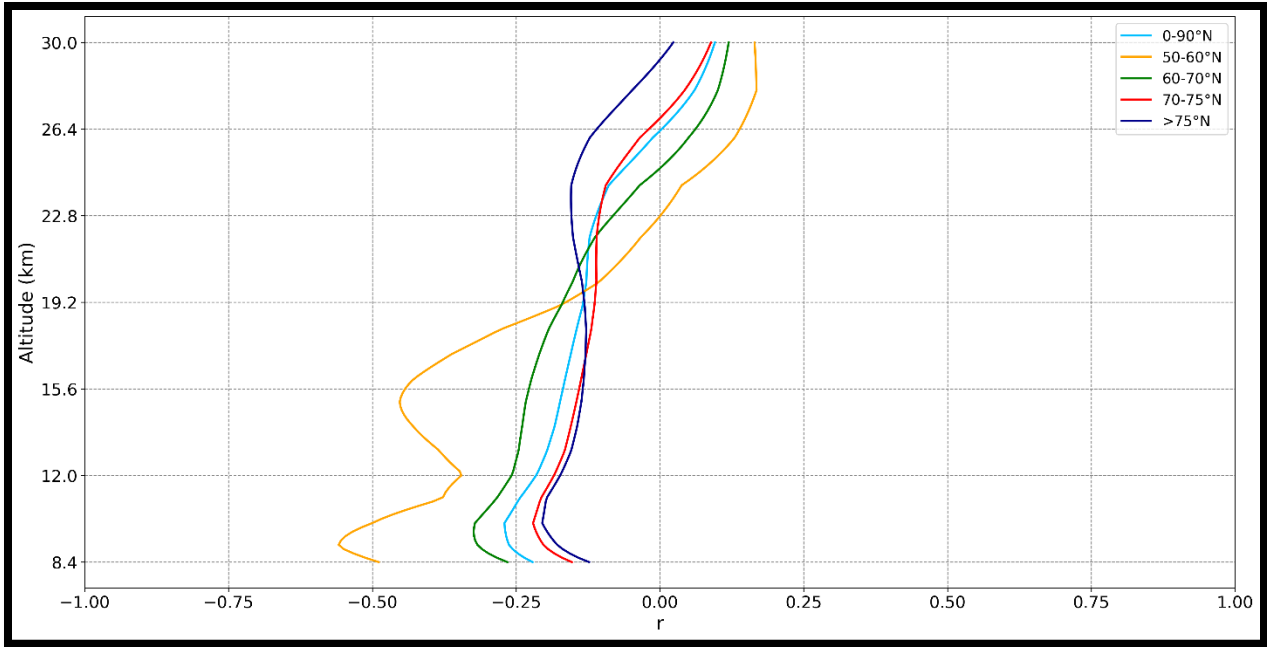*Figure 97: Vertical distribution of correlation coefficients between yearly mean values of PSCs and stratospheric temperatures across different latitudinal bands over the Arctic, from 2007 to 2021.*

Figure 98: Vertical distribution of correlation coefficients between monthly mean values of PSCs and stratospheric temperatures across different latitudinal bands over the Antarctic, from July 2006 to October 2020.

Figure 99: Vertical distribution of correlation coefficients between yearly mean values of PSCs and stratospheric temperatures across different latitudinal bands over the Antarctic, from 2006 to 2020.
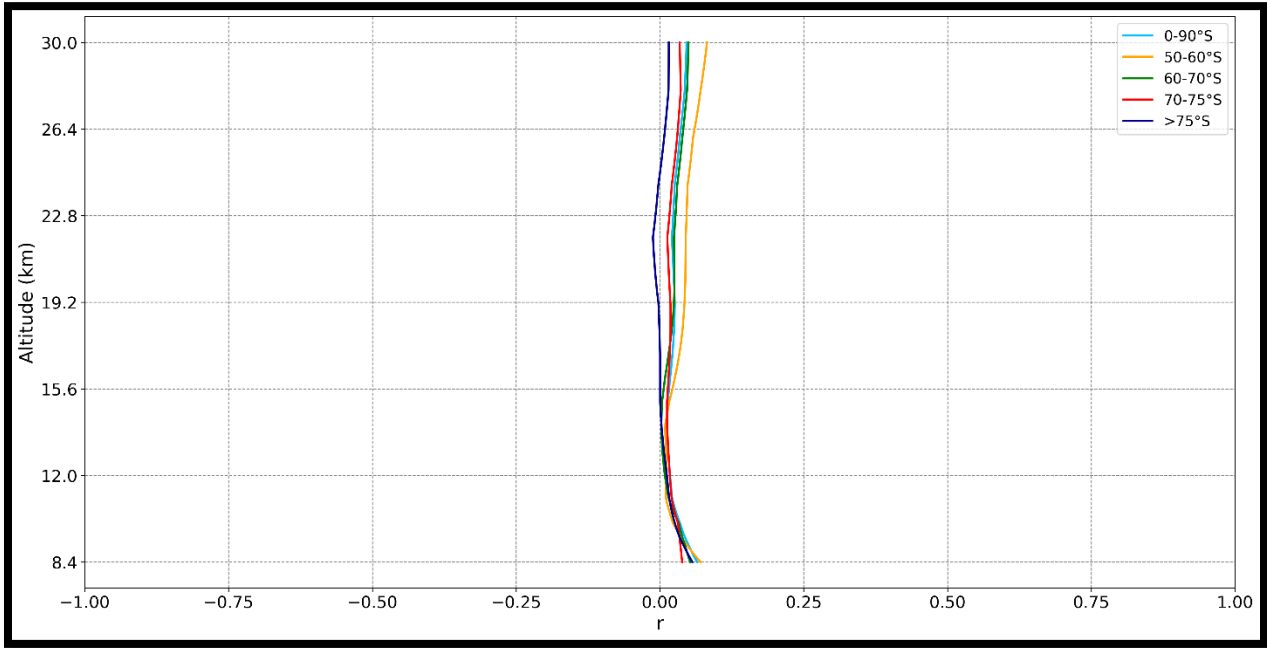
Sunspots - Temperature

Figure 100: Vertical distribution of correlation coefficients between monthly mean values of stratospheric temperatures and the number of sunspots across different latitudinal bands over the Arctic, from December 2006 to March 2021.

Figure 101: Vertical distribution of correlation coefficients between yearly mean values of stratospheric temperatures and the number of sunspots across different latitudinal bands over the Antarctic, from 2007 to 2021.

Figure 102: Vertical distribution of correlation coefficients between monthly mean values of stratospheric temperatures and the number of sunspots across different latitudinal bands over the Antarctic, from July 2006 to October 2020.
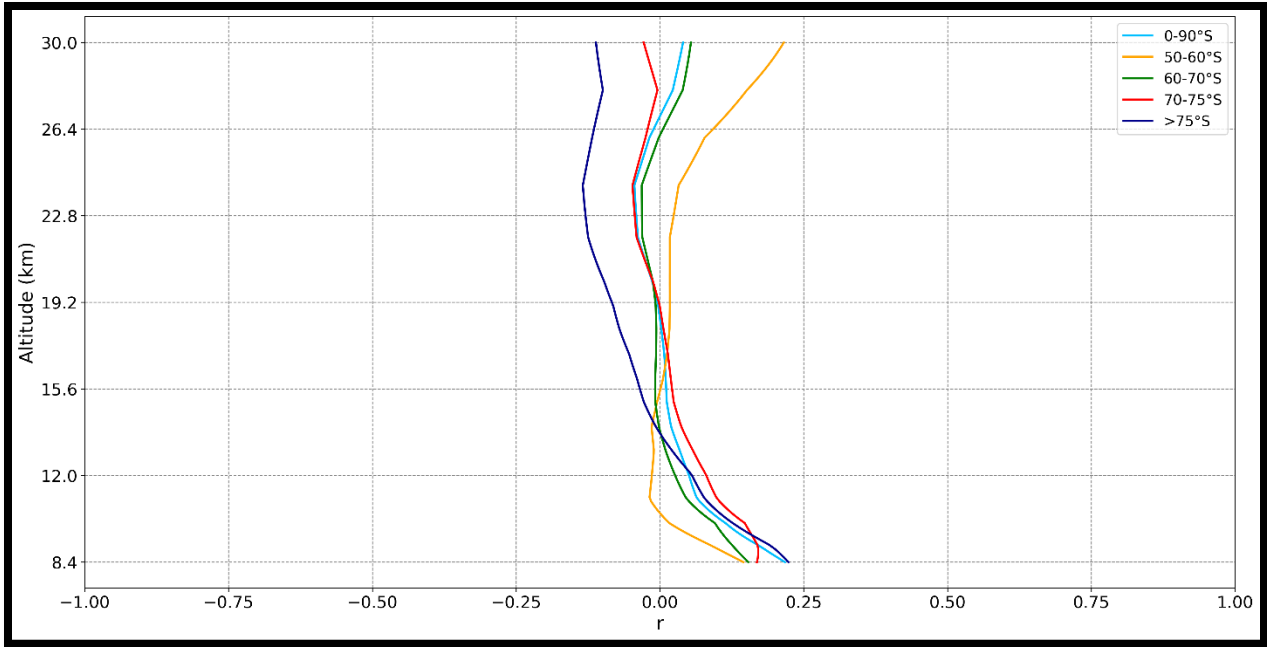
158

Figure 103: Vertical distribution of correlation coefficients between yearly mean values of stratospheric temperatures and the number of sunspots across different latitudinal bands over the Antarctic, from 2006 to 2020.
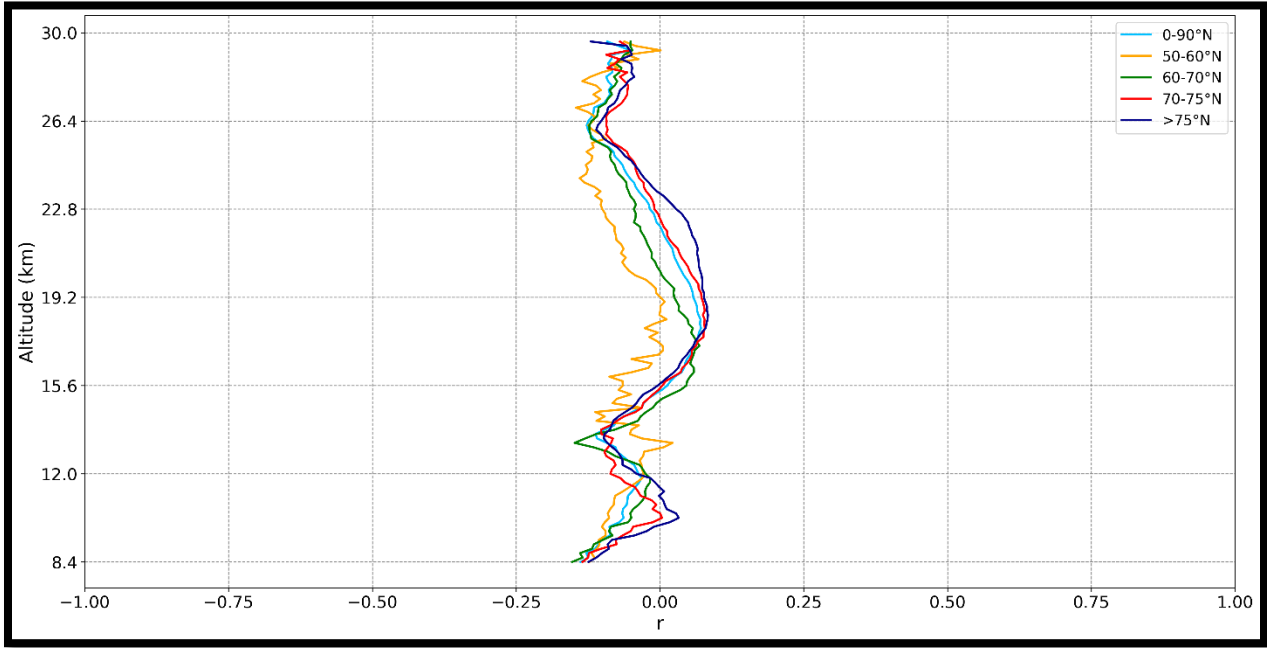
Sunspots – PSCs

Figure 104: Vertical distribution of correlation coefficients between monthly mean values of PSCs and the number of sunspots across different latitudinal bands over the Arctic, from December 2006 to March 2021.
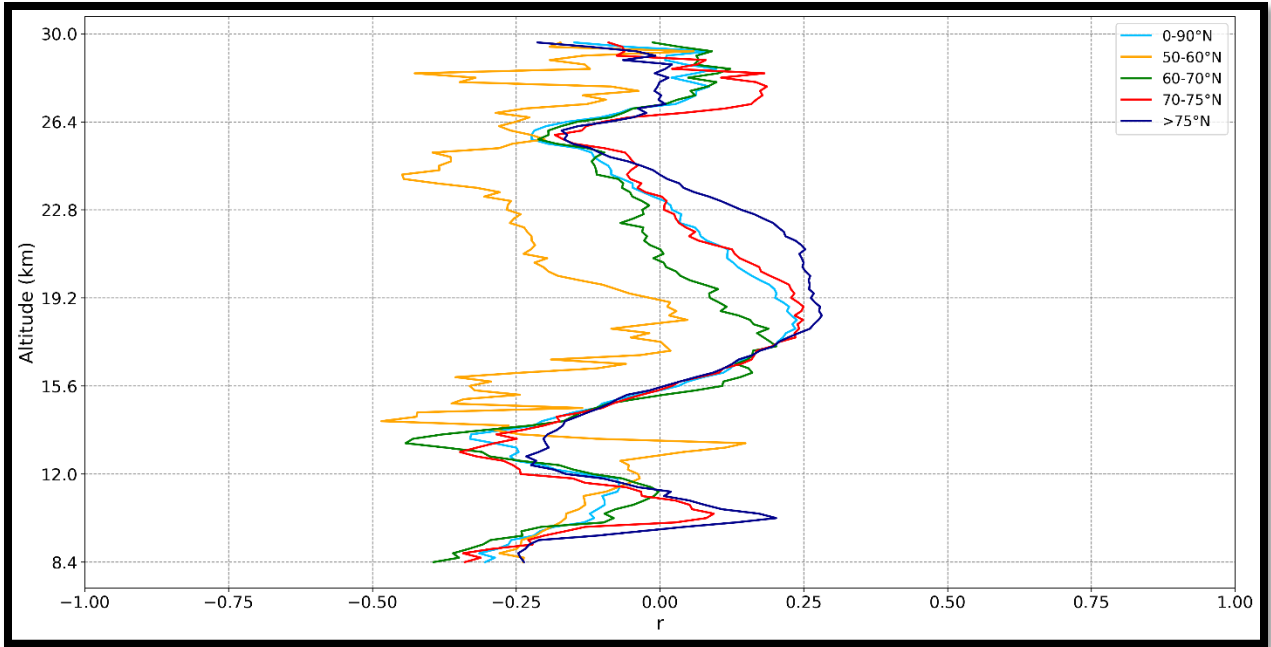
Figure 105: Vertical distribution of correlation coefficients between yearly mean values of PSCs and the number of sunspots across different latitudinal bands over the Arctic, from 2007 to 2021.
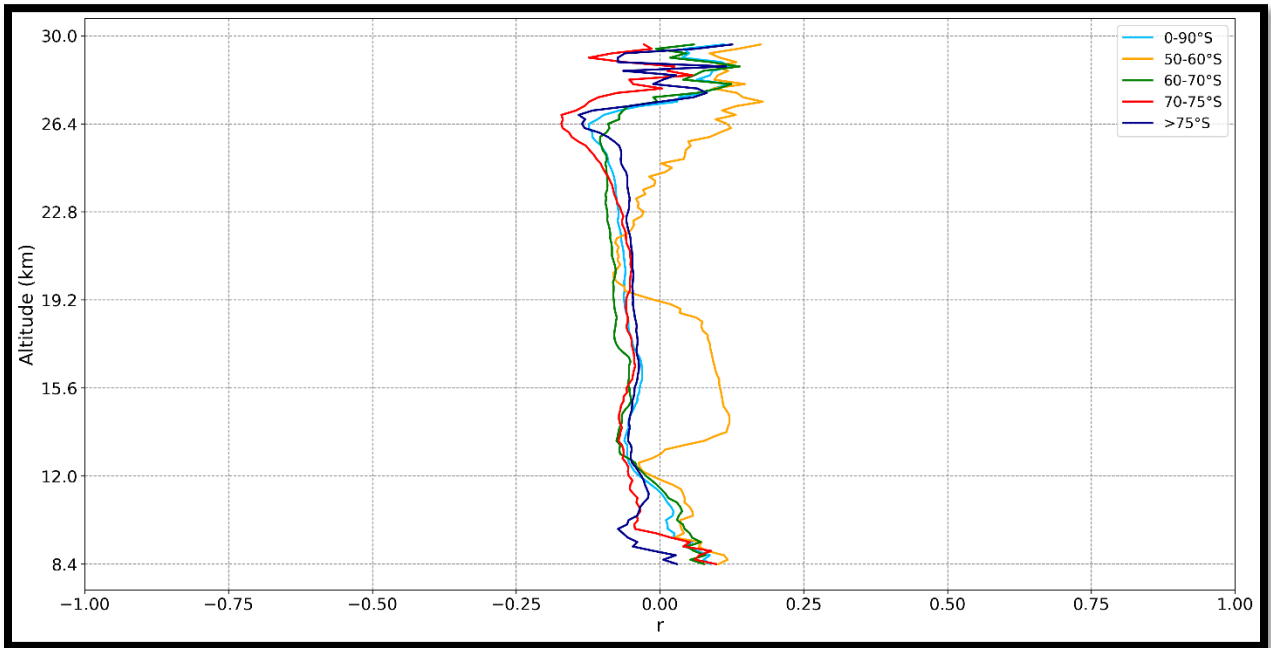

Figure 106: Vertical distribution of correlation coefficients between monthly mean values of PSCs and the number of sunspots across different latitudinal bands over the Antarctic, from July 2006 to October 2020.
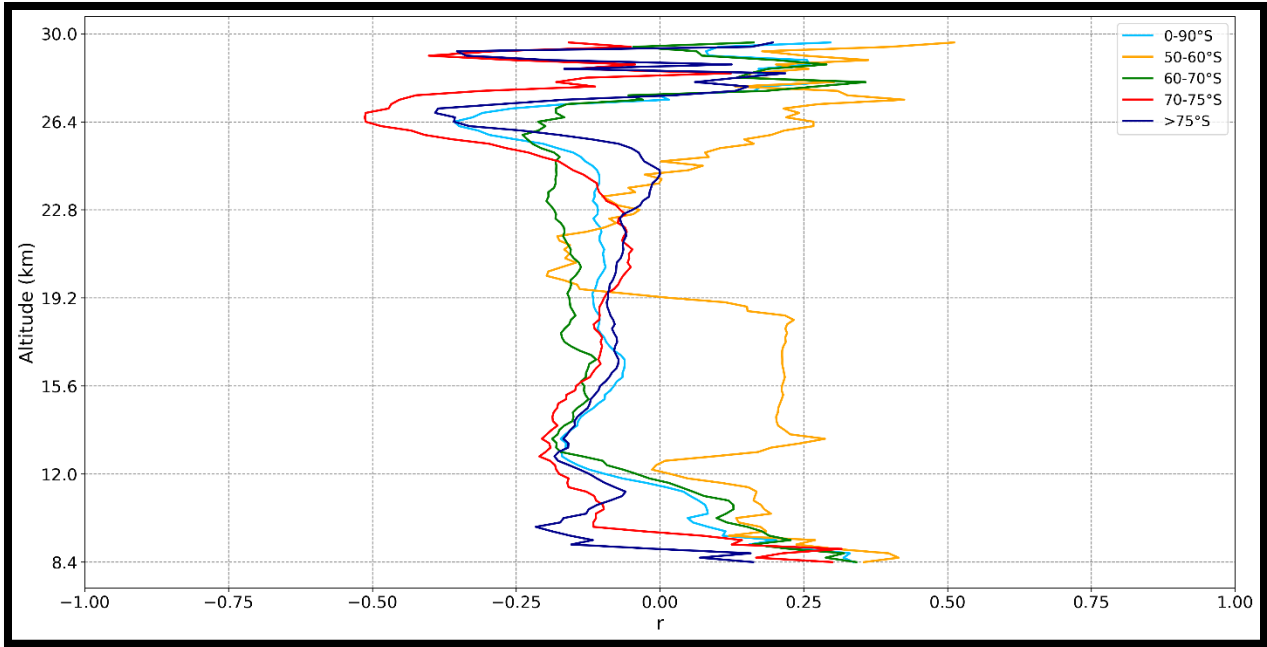
Figure 107: Vertical distribution of correlation coefficients between yearly mean values of PSCs and the number of sunspots across different latitudinal bands over the Antarctic, from 2006 to 2020.